Investigations into the Gas-Phase Rearrangements of Some Transition Metal β-Diketonate Complexes

by

Jordan O. Lerach

Submitted in Partial Fulfillment of the Requirements

for the Degree of

Master of Science

in the

Chemistry

Program

YOUNGSTOWN STATE UNIVERSITY

July, 2008

Investigations into the Gas-Phase Rearrangements of Some Transition Metal

β-Diketonate Complexes

Jordan O. Lerach

I hereby release this thesis to the public. I understand that this thesis will be made available from the OhioLINK ETD Center and the Maag Library Circulation Desk for public access. I also authorize the University or other individuals to make copies of this thesis as needed for scholarly research

Signature:

Jordan O. Lerach, Student Date

Approvals:

Dr. Brian D. Leskiw, Thesis Advisor Date

Dr. Larry S. Curtin, Committee Member Date

Dr. Howard D. Mettee, Committee Member Date

Dr. Peter J. Kasvinsky, Dean of Graduate Studies & Research Date

ABSTRACT

A series of gas-phase reactions between various transition metal β-diketonate complexes were observed *in situ* using a double sector mass spectrometer. Co, Ni, Cu, Zn and Al complexes with the ligands 2,4-pentanedione, 1,1,1,5,5,5-hexafluoro-2,4-pentanedione and 1,1,1-trifluoro-5,5-dimethyl-2,4-hexanedione were used. Metal center and ligand effects are investigated. Ligand exchange reactions were observed to occur readily between binary combinations of most complexes and an ion-neutral reaction mechanism is proposed.

Heteroleptic species were also synthesized through ligand exchange reactions *in solvo* to yield monomeric and dimeric structures of heteroleptic nickel species with the ligands 2,4-pentanedione and 1,1,1,5,5,5-hexafluoroacetylacetonate.

ACKNOWLEDGEMENTS

First and foremost, I would like to thank my family for their love and support throughout this, and many other ventures. I would specifically like to extend my appreciation to my parents, who have made many sacrifices in order to help their children achieve their goals.

Next, I would like to thank Dr. Brian Leskiw for ushering me into this project and allowing me the freedom to use my knowledge and love of the chemical sciences to explore other tangents of this work. Dr. Leskiw was more than willing to work with me during any problems I encountered with the research, and was also more than willing to sit down and converse when I needed a break.

Special thanks are extended to Dr. Matthias Zeller and Ray Hoff. Dr. Zeller has helped me greatly with X-ray analyses, and also with the myriad of other questions I would pester him with, though rather than just giving me a quick explanation he would help make sure I actually understood the answers to my questions. Ray Hoff helped me fix and re-fix the hi-res and GCQ mass spectrometers *ad nauseam*. He has helped me learn quite a lot about the functions of a mass spectrometer, and many other instruments, through both conversation and hands-on experience.

My thanks go out to the faculty of the YSU Chemistry Department, especially Dr. Larry Curtin and Dr. Howard Mettee, the two other members of my committee.

The Cushwa Family is acknowledged for their financial support through the Cushwa/Shearing Commercial Graduate Fellowship, and affording me the opportunity to work in an industrial setting. On that note, I would also like to thank Mark Peters from Fireline TCON, Inc. for giving me an internship which I really enjoyed.

My former undergraduate advisor Dr. Jen Aitken of Duquesne University also deserves recognition. She has provided me, and still continues to provide, support and has helped me realize my potential to become a great scientist.

My colleagues in the YSU Chemistry Department have also helped out greatly. Calvin Austin and Jon Milo have helped me through many chemistry related, and non-chemistry related, problems and have been good friends to me. Daryl Mains taught me how to use the hi-res mass spectrometer and paved the way for this research project. Tara Cruickshank was an undergraduate who was also assigned to this project. She performed quite a lot of the syntheses which allowed me more time to research. Many of the other graduate students have helped me along the way and my thanks goes out to them.

TABLE OF CONTENTS

LIST OF TABLES

LIST OF EQUATIONS

LIST OF FIGURES

Chapter 1: Introduction and Literature Review

1.1 Introduction

Metal β-diketonate complexes are used in a vast array of applications including trace analysis[1], catalysis[2] and also play a significant role in chemical vapor deposition processes[3,4]. While, metal β-diketonate complexes may not technically be classified as organometallic compounds, since they lack a direct metal-carbon bond, they can certainly be classified as coordination compounds, with their utility being facilitated by their ease of preparation[5-8] and increased volatility through functionalization[9].

Coordination compounds, in general, can be described by having a metal atom bound to molecules or even ions. Those species surrounding the metal center are known as ligands and act as Lewis bases, or electron donors while, in turn, the metal centers behaves as Lewis acids, or electron acceptors. The metal center and accompanying ligands need not have balanced charges, though, if this is the case, they will require a counterion on the outside of the coordination sphere to balance the charge.

In the study presented herein the stability and reactivity of a series of bis and tris metal β-diketone complexes are examined. The specific β-diketone complexing agents include 2,4-pentanedione (Hacac), 1,1,1,5,5,5-hexafluoro-2,4-pentanedoine (Hhfac) and 1,1,1-trifluoro-5,5-dimethylhexanedione (Htftm).

These bidentate molecules exhibit interesting characteristics both before and after chelation. The β-diketone ligand, before ionization, exists as a keto-enol tautomer; as shown in Fig. 1.1.

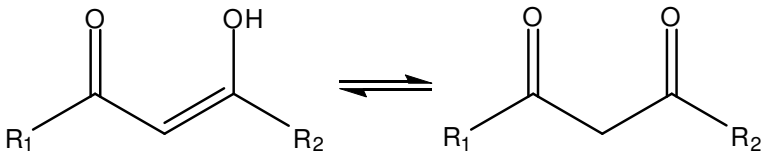

Fig. 1.1 The keto-enol tautomerism of a β-diketone

On the right side of Fig. 1.1, which is the keto form, each oxygen atom, both at the primary and β position, exists as a carbonyl. The α-carbon is sp^3 hybridized, as it is bound to two carbon atoms and two hydrogens. Whereas, in the enol form shown on the left of Fig. 1.1, the oxygen bound to the β-position exists as an alcohol. The hydrogen that was previously bound to the α-carbon is now attached to the oxygen bound to the β-carbon. A double bond now exists between the α and β carbons. Allen & Dwek[11] and others[11-15] have reported the rate of tautomerization for 2,4-pentanedione as well as some fluorinated derivatives.

Upon the introduction of a β-diketone into a basic media, the acidic proton involved in the above described tautomerism will be stripped from the β-diketone, resulting in the stable β-diketonate ion. Resonance is an important factor in the bidentate character of the β-diketonate ion, were the resonance structures shown in Fig. 1.2, llustrate the delocalization of the charge between the two oxygen atoms. This characteristic is what allows this ligand to maintain a -1 charge, yet still bind through two sites on the metal center.

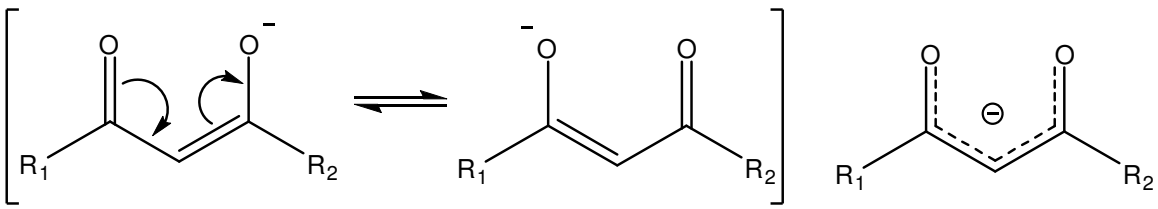

Fig. 1.2 The resonance structures of a β-diketonate ligand and its charge delocalization.

The five carbon backbone of the β-diketone creates an ideal place for functionalization. The α-carbon and the terminal carbons (R_1 & R_2 in Figs. 1.1 & 1.2) can readily be substituted with functional groups.

Perhaps one of the most exploited substituents are those which affect volatility. Many acetylacetonates sublime under moderate temperatures and low pressures and through the functionalization by addition of fluorinated moieties, the volatility of these compounds becomes variable[9].

The chemical industry has taken advantage of the ease of the addition/substitution for β-diketonate complexes where much work has focused on metal-organic chemical vapor deposition (MOCVD) processes. Researchers have been able to chelate specific metals and vaporize them accordingly for deposition as thin films for a multitude of applications[2,3,16-19] thus adding to the breadth of research applications these complexes are used for.

1.2 Literature Review

Not only has industry embraced the tunability of β-diketonate complexes, but mass spectrometrists have as well, with literature dating as far back as 1966[20]. Needless to say, much work has been done since then. For practically every ionization technique of mass spectrometry (MS), one or more research groups have used it to examine metal β-diketonate complexes in detail. Electron impact[23,24,27] (EI), chemical ionization (CI)[20], liquid secondary-ion mass spectrometry[39] (LSIMS) and now even matrix-assisted laser desorption/ionization[41,42] (MALDI) have been employed to investigate this class of compounds with mass spectrometry.

MS has been used not just as an analytical tool with these compounds, but can be applied to all other disciplines of chemistry to shed light on fundamental concepts, namely bond energetics[21,22], reaction mechanisms[23-25], structure and stability. Such data is often backed up with further theoretical and other experimental findings. The complementary nature of MS allows for this technique to be applied to a variety of scientific fields.

Much of the MS work focusing on metal β-diketonate complexes was nicely summarized in a review paper by Westmore[26]. In this review, Westmore examines ionization, fragmentation, appearance potentials and other aspects of the mass spectrometry of metal β-diketonate complexes. This review provides a thorough background of the work conducted on these compounds, and a brief summary of some key points central to the studies is presented in the following paragraphs.

Since the studies presented herein involve positive ion mass spectrometry, it is particularly important to understand the mechanisms of ionization for these compounds. Where we use complexes of the form $M(L)_n$ where n=2 or 3, understanding the method by which ionization occurs is particularly important. Unlike a simple organic compound, it is hard to show specifically where the charge may be localized on these metal β-diketonates. These organometallic complexes are composed of organic components, metal-oxygen bonds with aromatic characteristics such as pi-bonding, as well as the possibility of valence changes on the metal center. The generation of the positive molecular ion using electron impact ionization can be expressed by the following equation;

$$ML_n + e^-_{(70eV)} \rightarrow [ML_n]^+ + 2e^- \qquad \text{Eqn. 1.1}$$

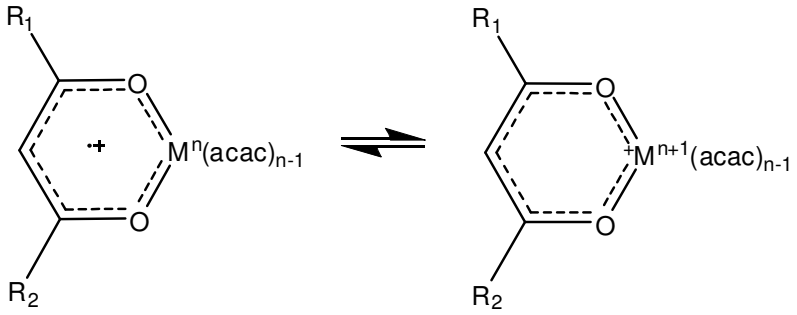

Fig. 1.3 Charge location over the $[ML_n]^+$ complex.

In Fig. 1.3, the structure on the left side shows the delocalization of the charge over the pi-bound system while the structure on the right shows the charge centralized on the metal, accompanied by its oxidation. These two species are not necessarily in equilibrium with each other and, depending on the metal, one structure may be so unfavorable that its contribution is negligible. For example, consider a Zn complex, which possesses a full d-shell. Ionization of the metal center would cost much more energy than ionization of the ligand, thus making it unlikely for the metal center to lose an electron. The structure on the left in Fig. 1.3 would be the likely scenario for a Zn complex. A compound containing Fe could exist as either a high or low-spin complex, making either resonance structure likely with the charge distributed over the metal or the ligand.

The identity of the R-groups associated with the β-diketonate ligand also has a great influence on the charge localization. Fluorination of these complexes is common, especially in the work presented herein. Replacing the methyl groups of the acetylacetonate ligand with trifluoro-methyl (CF_3) groups creates a more electron withdrawing environment, which would lead to an increase in the charge localization over the ligand.

The ionization of these fluorinated complexes may be acyclic due to the heavily electron withdrawing capabilities of the CF_3 groups, as recapitulated by Westmore in the review. The possible acyclic structures are displayed below in Fig. 1.4.

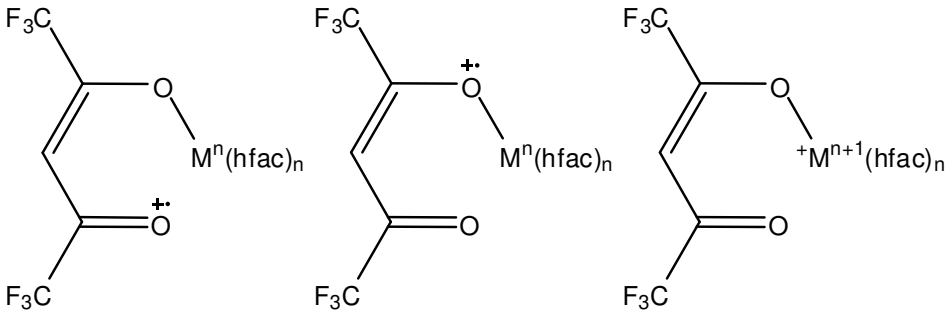

Fig. 1.4 Charge localization with the 1,1,1,5,5,5-hexafluoro-2,4-pentanedionato ligand complex.

Of the structures illustrated in Fig. 1.4, the left and center structures describe how two species would share the charge localization when the metal is difficult to oxidize. The structure on the right would likely be suitable only for a metal center that can easily adopt different valancies. With these possible molecular ions in mind, one must now consider the fragmentation of these compounds. Compounds regularly undergo fragmentation, which is especially dependent on the terminal groups of the ligand. As is the case with the molecular ion, the actual location of the charge varies with differing ligands and metals.

Mass spectrometry can also provide insight about structural information, but only to a certain extent. One cannot determine characteristics of space-group or bond-lengths in the gas phase through mass spectrometry, though one can infer possible structural motifs.

Following the loss of an R group, which is the preferred loss channel for many metal β-diketonates, three possible structures illustrating charge delocalization are displayed below in Fig. 1.5.

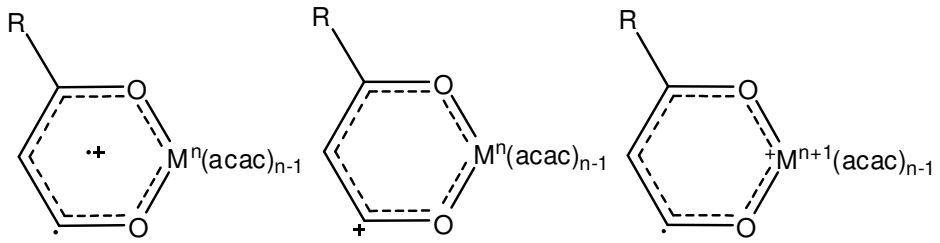

Fig. 1.5 Charge localization of a fragmented β-diketonate complex

While the actual delocalization of charge will ultimately depend on the identity of the ligand and metal center, the rightmost structure is likely to describe the ensuing charge delocalization of a complex containing a metal center that can be readily oxidized. The structure on the left shows delocalization of the charge over the ring system, with a lone electron on the carbon from which the fragment was removed. The central structure has the charge on the carbon from which the fragment was removed and is an even electron species. The above species all require the bidentate nature of these structures to remain intact upon ionization. With complexes containing electron withdrawing groups, however, this may not be the case, as shown below with the fragmentation of $M(hfac)_n$ in Fig. 1.6.

While all of the resonance structures in Fig. 1.6 would probably exist in some complex equilibrium, the preferred structure is likely the top figure, (Fig. 1.6a) given its resonance capabilities. The structure on the bottom (Fig. 1.6b) lacks rational resonance structures making it less favorable.

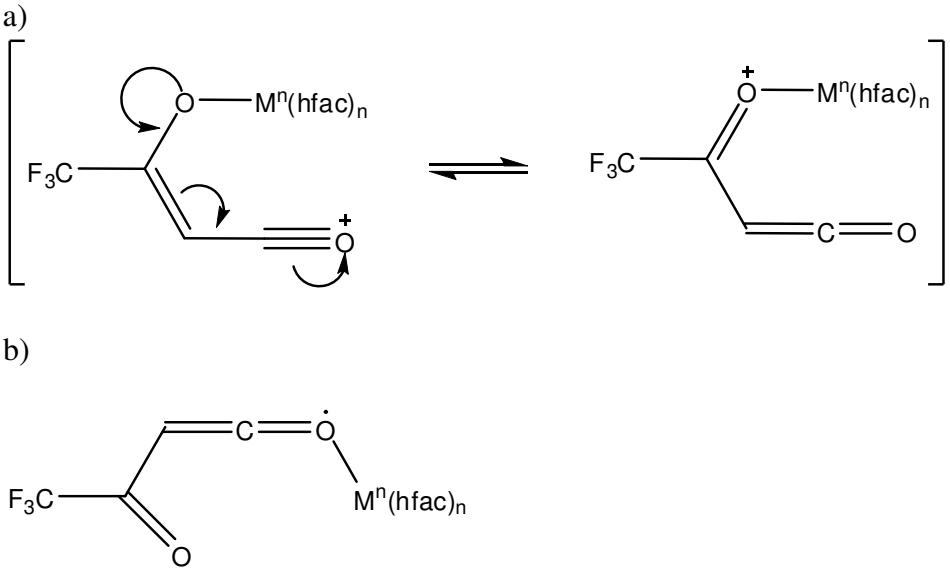

Fig. 1.6 Structure and charge localization for a fragmented complex with electron withdrawing groups a) Two possible resonance structures can be seen for a fragmented complex with the remaining group attached to the carbon adjacent to the bridging oxygen makes this arrangement more favorable. b) Lack of resonance stabilization for the fragment removed from the carbon adjacent to the bridging oxygen makes this structure less favorable.

The structures contained in Fig's 1.1 to 1.6 were all adapted from Westmore's review, and in the context of the research presented herein, ie: $M(acac)_n$ and $M(hfac)_n$, the above structures should represent these structural variants of these compounds quite accurately. For the 1,1,1-trifluoro-5,5-dimethyl-2,4-hexanedione (Htftm) analogs, different structures for the positive ions will arise since complexes with this ligand are both structurally asymmetric and asymmetric with respect to the electron withdrawing capabilities of the ligand itself. As previously mentioned, the structure of the ion depends heavily on the electron withdrawing (or donating) characteristics of the ligand.

Prior to Westmore's review, it is important to acknowledge the previous work in the broad area of metal β-diketonate complexes. Early literature focusing on these compounds was relegated mostly to positive ion electron impact (EI) and chemical ionization (CI) studies.

Literature describing this dates first back to Macdonald and Shannon in 1966[20]. They used chemical ionization methods (with CH_4) with different metal complexes of acac's and bzac's. This was a very thorough study probing varied metal valency, ligand effects and even the shifting of the R-groups associated to the dione backbone. They were also the first to report heteroleptic, or mixed ligand, species as the result of a gas phase reaction. This initial work will be vital to the continuing mass spectral studies of this class of compounds, as many other groups would begin investigating these compounds.

Shortly after MacDonald and Shannon, a series of papers appeared in the literature focusing on the mass spectra of metal β-diketonates. The corresponding appearance energies, ionization potentials and fragmentation patterns were shown for various transition metal complexes, both divalent and trivalent[27-30]. This concerted effort was an attempt to thoroughly assign appearance energies to this class of complexes.

Other papers followed, with one in particular describing the loss of the first ligand from the $Al(hfac)_3$ species. The authors stated that the loss of one hfac ligand is actually a two step process, first involving the loss of a CF_3 group, then the subsequent loss of the remaining portion ($OCCHCOCF_3$) of the ligand[23]. They used metastable analysis to support their observations and also showed just how advantageous the use of metastable peaks to follow the mechanisms of fragmentation would become.

The EI mass spectra of a variety of asymmetric β-diketonate complexes soon followed. Each analog in this study had a CF_3 group in common, while the other R-group could be another CF_3 group or one of a variety of alkyl, aryl or sulfur-bound cyclic structures[24], with another groups reporting on further asymmetric work as well[30].

Other work investigated the role the metal center played during fragmentation as displayed in the resulting mass spectrum[23], with a subsequent review detailing the role of valence-change of the metal in this class of compounds[31].

It is important to note that Macdonald and Shannon's paper[20] reports the first case of gas phase ligand exchange, which they showed as having occurred between acac and bzac complexes of iron. Majer and Perry reported some mixed ligand compounds[32], though the heteroleptic species were not both β-diketonates. Various perfluorinated derivatives were used in conjunction with metal hydroxyquinolinates to produce gas phase heteroleptic species. While they attempted to form clustered compounds with two metal centers and varying amounts of ligands, they were successful in forming several mixed metal species, both homoleptic and heteroleptic with various metal and ligand combinations.

After the initial surge of papers regarding the basics of the mass spectral properties of this class of compounds, papers were subsequently published with a focus on the clustering capabilities of these compounds. Schildcrout showed that higher pressures may be more conducive to the generation of clustered compounds using metal β-diketonates as precursors[33]. The study concluded that the resulting species were being formed from ion-neutral reactions, given the effect the repeller potential had on the product distribution[33]. At higher pressures, collisions occur more frequently, thus favoring cluster formation over fragmentation. Dean and co-workers were able to examine more compounds with EI, as well as using CI techniques with CH_4 and NH_3 to create clustered compounds[34].

Heteroleptic and clustered compounds were not the only secondary species being reported. The presence of fluorine-migration in many of these spectra led Morris and Koob to explore this process with the application of hard/soft acid base theory[35].

All the while, many groups were determining ionization potentials for these complexes[36,37] though, as stated by Westmore[26], multiple discrepancies were evident between reports.

More groups would be inclined to test different ionization techniques of these compounds where, for example, Secondary Ion Mass Spectrometry (SIMS)[38,39], Fast Atom Bombardment (FAB)[40] and Matrix Assisted Laser Desorption/Ionization (MALDI)[41,42] techniques would be employed to investigate these complexes.

What most of these groups' findings have in common is a lack of evidence for the gas-phase rearrangement of these compounds, or a reason for refuting it. The scope of the project presented herein is to show that these rearrangements occur readily in the gas phase.

Chapter 2: Instrumentation

2.1 Mass Spectrometry

Mass spectrometry (MS) is a very common analytical technique found in many branches of science. MS is a powerful tool that can yield information where one can begin to infer the structure of compounds by determining the mass to charge ratio (m/z) of the analyte. A charged species must be used in mass spectrometry in which the analyte can be in the form of either molecules or an atom. The m/z obtained is a ratio between the molecular mass (m) of the analyte and its charge (z). For example, methanol, which has the molecular formula CH_3OH, has a nominal molecular weight of 32. A methanol ion with a 1+ charge will have an m/z value of 32/1 or 32. If it has a 2+ charge, it will have an m/z value of 32/2 or 16.

Nominal (integer) masses are used for mass spectrometry, except during high-resolution experiments. By adding up the number of protons and neutrons of an isotope of an element, one obtains the nominal mass, as shown above for methanol. Isotopes of certain elements can actually be very useful in identifying certain samples. For example, chlorine has two common isotopes, ^{35}Cl and ^{37}Cl. These two isotopes exist at 75.78(4)% ^{35}Cl and 24.22(4)% ^{37}Cl and in a mass spectrum the ^{37}Cl peak will be roughly 1/3 the height of the ^{35}Cl peak. A compound such as chlorobenzene C_6H_5Cl will have two predominant peaks in a mass spectrum at the m/z values of 100 and 102 due to the two different isotopes of chlorine. A mass spectrometrist faced with identifying an unknown in a sample can use isotope ratios to accurately determine the composition of a compound.

As stated before, mass spectrometry can also be used to determine structural information. Ionization of an analyte will yield the molecular ion (MI), which is the ionized form of the un-fragmented analyte. In itself, this will only yield a m/z value, and will not be able to distinguish between certain species such as propanol and isopropanol, which both have the same nominal mass. However, the fragmentation of these species is will yield a different spectrum which will be indicative of their respective structures.

The main concept of mass spectrometry is to take the analyte, ionize it and then pass it through a mass analyzer. A multitude of ionization techniques and mass analyzers have allowed this technique to be widely used for a variety of different applications ranging from forensic analysis[43,44], determination of contaminants in wine[45,46] and as far reaching as outer space[47]!

Ionization techniques include electron impact ionization, a hard technique which leads to much fragmentation to softer techniques such as chemically induced dissociation. More modern techniques such as matrix assisted laser desorption/ionization (MALDI) use a laser as an energy source which energizes a substrate to which the analyte is bound causing a charge transfer, thus ionizing the sample.

Mass analyzers are just as diverse as the ionization techniques. Magnetic sector instruments are among the oldest analyzers. These use a magnetic field to change the flight path of an ion. Electric sector instruments are similar, though they use an electrical field instead of a magnetic field to discriminate between ions. More modern techiniques include time-of-flight (TOF) instruments which have no theoretical upper limit on the mass range of the sample being analyzed.

The widespread use of MS is easy to understand when one considers the versatility of the technique. Much could be said about each part of this technique, but only descriptions of those used in this study are detailed in the following sections of this chapter.

MS is the primary tool used in this body of work for many reasons. It is perhaps one of the best suited techniques for gas-phase ion chemistry, which will be monitored. The gas-phase rearrangements of these complexes can easily be observed through mass spectrometry, since many steps in these reactions involve gaseous ions. We can observe the reactions *in situ* with this technique, with no need to isolate a certain species for further analysis. Small sample quantities are needed since this is a trace-analysis technique as well. Quality assurance is always a concern with any reaction, and MS affords the ability of observing any contaminants, by-products or any other concerns directly in chemical reactions. Ionization and subsequent reactions of various metal β-diketonate complexes will be primarily observed using MS.

2.1.1 Ionization Techniques: Electron Impact Ionization

Electron impact (EI) ionization is a common technique employed in mass spectrometry where ionization is caused by the bombardment of the gaseous analyte with high energy electrons. The typical energy of the incident electron is 70 eV (6.8×10^3 kJ/mol) and is maintained by the potential difference between an anode and a positively charged filament. The ionization energy of most analytes is far below 70 eV, so this form of ionization is very energetic. The large energy difference causes more than just the molecular ion to be formed as shown by extensive fragmentation of the molecular ion.

Softer techniques such as chemical induced dissocation (where a gaseous species such as CH_4 is ionized by EI to CH_5^+ and typically transfers a proton to the analyte resulting in a positively charged species) tend not to fragment species as much as EI does.

2.1.2 Mass analyzers

2.1.2.1 The Double Focusing Mass Analyzer

Most measurements were taken on a Finnigan MAT 8430 double focusing MS. This specific instrument has a reverse geometry configuration where the magnetic sector (B) precedes the electric sector (E). These two distinct regions are separated by a region with no field, hence the title; field free region, as shown in Fig. 2.1. This geometry is very convenient for other MS techniques such as molecular ion kinetic energy spectrometry (MIKES) and the study of metastable ions[48,49].

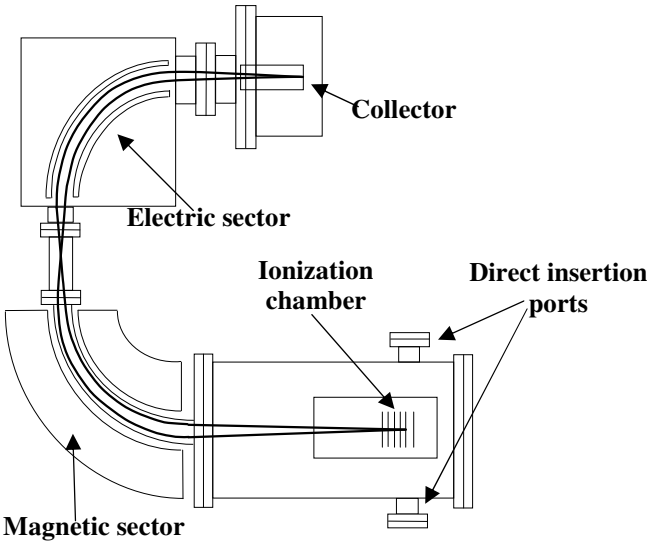

Fig. 2.1 Schematic diagram of the double sector instrument

A distinct advantage of the double focusing MS is its high-resolution capabilities. Resolutions of up to 100,000 are capable with this type of instrument where resolution is given by the equation

$$R = m/\Delta m \qquad \text{Eqn. 2.1}$$

Where R is the resolution, m is the mass in question, and Δm is the difference in mass to charge ratio between two species. The resolution method used with this instrument is the 10% valley method where, at a given resolution, two nearby peaks will overlap at only 10% of the total height of the peak.

2.1.2.1.1 The Magnetic Sector

The magnetic sector is governed by the following equation;

$$zevB = (mv^2)/r \qquad \text{Eqn. 2.2}$$

Where z is the charge on the ion, e is the elementary charge, m is the mass of the ion, v is the velocity of the ion, B is the strength of the magnetic field in which the ion is passing through and r is the radius of the flight path which is a semi-circle.

As ions are accelerated into the magnetic field, where the field's force acts upon the ion perpendicularly, their trajectories will follow a curved path, related to the field's direction and strength.

Equation 2.3 represents the behavior of an ion within the magnetic field.

$$m/z = eB^2r^22V \qquad \text{Eqn. 2.3}$$

With this equation one can see that the mass to charge ratio is proportional to either B^2 or V. Scanning through a range of either B or V will allow the user to gain a spectrum of ions based on their respective m/z ratios. Scanning through varying B's is preferable since a low V may not accelerate enough ions through to the detector, while a higher fixed V and varied B will allow more ions, with potentially lower V values, to pass through to the detector[48,49].

2.1.2.1.2 The Electric Sector

The electric sector of the double sector instrument discriminates between different ions based on charge. The electric sector is composed of two plates of opposite charges arranged in a semi-circle with radius R. An ion entering this field will be repelled by a force F, given by the equation

$$F = zE \qquad \text{Eqn. 2.4}$$

Where z is the charge on the species and E is the strength of the electric field between the plates. Since the plates are arranged in a semicircle one, can rearrange the equation to be in terms of a centripetal force acting upon the flight path of an ion as the following equation

$$zE = mv^2/R \qquad \text{Eqn. 2.5}$$

Where m is the mass of the ion and v is its velocity through an electric sector with radius R. Relating kinetic energy to charge and potential, the equation for the electric sector is obtained.

$$mv^2 = 2zV = zER \qquad \text{Eqn. 2.6}$$

Canceling the z value shows that

$$R = 2V/E \qquad \text{Eqn. 2.7}$$

This demonstrates that for a fixed radius, the trajectory will be affected by the potential by which the ions were accelerated into this mass analyzer, as well as the strength of the electric field in the electric sector. This is the means by which the electric sector discriminates between ions[49,49].

2.1.2.2 The Quadrupole Ion Trap

Quadrupole ion traps (QIT) are very versatile mass analyzers with many advantages, yet significant disadvantages. The main feature of the QIT is its ability to trap and store ions then selectively eject them. One can eject all masses and obtain the overall mass spectrum, or one can eject all ions except one mass then perform tandem mass spectrometry (MS^n) on the sample. This is a great advantage since the ion trap quite literally traps the ions, so no second mass analyzer is needed for subsequent MS analysis on the sample. The theoretical limit to how many times one can run MS is dependent on how many times the analyte(s) can fragment. Though, more practical limits take precedence usually. The trap can only hold a certain number of ions, and each time analyte is ejected some of the trapped analyte may also escape. When MS^n is operated not all analyte species are fragmented, so some of the parent ion can remain, thus drastically limiting the extent to which MS^n can be run[50].

The limitations of QIT MS are few, but substantial. One of the largest problems is the amount of sample able to be trapped at a given time. The ion trap has a finite size, and can only hold so many ions, before repulsion forces between the ions start affecting the experiments. Also, QIT MS has limited resolution. This is related to the rf field used to eject ions, as well as the time between ejections. Typical instruments run near 1000, giving integer mass resolution up to 1000 a.m.u..

2.2 Powder X-ray Diffraction

Powder X-ray diffraction (PXRD) can be used as an incredibly powerful analytical tool, as well as being capable of elucidating structural information from exceptional data. PXRD can be used to analyze solid microcrystalline compounds.

The intent of this study is primarily to observe and investigate the gas phase rearrangements of metal β-diketonate complexes, though formation of mixed ligand species as stable products in solid and liquid phases is also being investigated. PXRD is used to analyze reactions with synthesis of these products as the goal. PXRD coupled with single-crystal X-ray analyses give concise information as to what has taken place in these reactions.

This technique utilizes high energy X-ray electromagnetic radiation typically created by molybdenum or copper sources with averaged wavelengths of 0.71069Å and 1.54178 Å respectively. X-ray radiation is used since its wavelength is along the same order of magnitude as lattices between the crystal planes. A longer wavelength would not provide the resolution needed for this type of work.

The conditions that must be met for diffraction to take place can be expressed by the Bragg Equation, shown as Eqn. 2.8.

$$n\lambda = 2d(\sin\theta) \qquad \text{Eqn. 2.8}$$

Where n is the order of the diffraction, λ is the wavelength of the radiation, d is the distance between the diffracting planes, and θ is the angle of the incident radiation relative to the plane of the sample

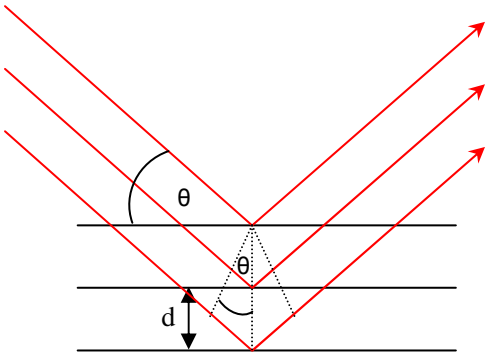

Fig. 2.2 Schematic of the Bragg equation

The diffracted radiation generates a spectrum specific to the analyte with relatively high resolution, depending on the sample quality. The diffraction patterns can be compared to other known patterns, or be used for further structural analyses.

Chapter 3: Experimental

3.1 Preparation of Various Homoleptic Metal β-diketonates

Aqueous preparation of $M(acac)_n$ and $M(tftm)_n$ compounds was adapted from the procedures outlined by Watson & Lin[51]. A small amount of the metal chloride would be dissolved in 50-100 mL of room temperature de-ionized H_2O which was being stirred with a magnetic stir plate and a PTFE coated stir bar.

Many of the complexes that were purchased, as well as synthesized, were hydrates. This is not of great concern for studies in the gas phase since Zheng *et al*[52] showed that whether such compounds were hydrated, or associated to other similar species through a hydroxyl group (MeOH, EtOH) they would become uncoordinated upon sublimation, or conditions near those necessary for sublimation. The study presented herein utilizes sublimation as the introduction method into the gas phase, and the results agree with Zheng and co-workers' findings.

After the metal chloride was added to the stirring H_2O, two or three molar equivalents of the free ligand 2,4-pentanedione (Hacac) or 1,1,1-trifluoro-5,5-dimethyl-2,4-hexanedione (Htftm) would then be added to the solution. The water and ligand were immiscible. Over time the free metal (from the metal salt) may have been able to coordinate to the ligand, but to increase the rate of coordination, a base was added to deprotonate one of the acidic H's from the free ligand. A basic solution, typically 1:1 (v/v) H_2O:NH_4OH, was added slowly. In most cases, precipitate would form almost immediately. To ensure completion of the reaction, a few more drops of the basic solution were added and the solution was allowed to stir typically between one-half to two hours, and sometimes overnight.

The precipitate was then separated from the rest of the solution via vacuum filtration on either a no. 1 qualitative or a no. 42 ashless filter paper. In the case of iron, cobalt and manganese more than one phase was present in the precipitate, as shown by different colored phases present in the precipitate. Extraction with MeOH or toluene was used to separate the phases. The phase which was soluble in the organic solvent was the desired phase and the solvent was removed *in vacuo*.

It should be noted that the $M(tftm)_n$ species were synthesized since no commercial source could be found. However, the $Cu(acac)_2$ and $Ni(acac)_2$ compounds are readily available from many commercial sources. The acac complexes were made for comparative purposes with the goal of creating heteroleptic and heterometal complexes under similar reactions conditions. This was done in the event that the commercial sources of the complexes were a different phase, or in case we were creating a different product altogether. As stated earlier, these considerations are less important in the gas phase. However, the possibility of the hydrates and different crystalline phases of the same complexes becomes important only when analyzing solid phases through powder X-ray diffraction.

3.1.1 $Mn(tftm)_2$ Synthesis

Addition the $MnCl_2$ yielded no color change in the H_2O, nor did the addition of the ligand. Addition of the base caused the solution to turn brownish yellow. The precipitate collected was a mixture of yellow and brown powders. The products were extracted according to the methods described by Fay & Piper. Extraction with acetone was used to separate the $Mn(tftm)_2$ complex from any residual starting material. If the Mn(II) starting material was oxidized to Mn(III) in the synthesis both phases would be extracted into the acetone.

The part of the precipitate which was insoluble in acetone was a dark brown powder. The acetone was removed *in vacuo* to reveal a mixture of yellow and brown powders. The next step was to extract the binary phase from the ternary with benzene. The insoluble portion was the brown powder, and the soluble was the yellow portion. The benzene was extracted *in vacuo*.

Another subsequent reaction followed the same synthetic pathway, but the yellow phase was separated from the brown by extracting the yellow phase into MeOH and filtering off the insoluble brown phase.

The structure of this compound was validated through Mass Spectrometry. Also, exact amounts of the reactants used for this, and all other reactions can be found in Appendix D.

3.1.2 $Co(tftm)_2$ Synthesis

Addition of $CoCl_2$ to H_2O turned the water a light red color. Addition of the ligand caused the solution to take on a blueish hue. Addition of the base caused the blue color to intensify. Over a few minutes, the solution started to turn green and a brown powder was formed on the bottom of the flask. Filtration yielded two products: a red powder and a brown-yellow powder. Extraction with benzene caused the red powder do dissolve, leaving behind the brown-yellow powder.

The red product was able to be re-crystallized by slow evaporation from a MeOH solution. The structure of this compound was analyzed and confirmed using mass spectrometry and single crystal analysis.

3.1.3 $Ni(tftm)_2$ Synthesis

Upon addition the $NiCl_2$ to water, the solution turned a light green color. Addition of the ligand yielded no color changes. The addition of the base caused some light green precipitate to form and turned the solution from green to blueish green. Vacuum filtration through a no. 1 qualitative filter yielded a light green powder. No further purification was needed. The structure was verified by mass spectrometry and single crystal X-ray analysis.

3.1.4 $Cu(tftm)_2$ Synthesis

Upon addition of $CuCl_2$ to water, the solution turned blue. Addition of the ligand would cause blue hydrophobic pockets to form. Addition of the base caused the blue color of the solution to intensify, and resulted in a light blue precipitate. The precipitate was vacuum filtered through a no. 1 qualitative filter. No further purification was needed. The structure was verified by mass spectrometry and single crystal X-ray analysis.

3.1.5 $Zn(tftm)_2$ Synthesis

Addition of $ZnCl_2$ to H_2O yielded no change in color, nor did the addition of the ligand to the solution. Upon addition of the base, the solution turned a cloudy white color and a white precipitate formed. The precipitate was vacuum filtered with a no. 1 qualitative filter. No further purification was needed. The structure was validated by mass spectrometry only, since no crystals suitable for single crystal X-ray analysis were able to be grown.

3.1.6 $Al(tftm)_3$ Synthesis

Addition of $AlCl_3$ into H_2O yielded no change in color, nor did the addition of the ligand. Upon addition of the base to the solution, a very pale green precipitate formed. The precipitate was then filtered on a no. 42 ashless filter yielding a white powder with a green hue. No further purification steps were taken. This sample was analyzed using PXRD.

3.1.7 $Al(acac)_3$ Synthesis

Addition of $AlCl_3$ to H_2O yielded no color change, nor did the addition of the free ligand. Upon addition of the base, the solution turned yellow. Eventually the solution evolved a cloudy white precipitate, yet retained its yellow hue. The precipitate was filtered on a no. 42 ashless filter. No further purification steps were taken. The sample was analyzed using PXRD.

3.1.8 $Ni(acac)_2$ Synthesis

Addition of $NiCl_2$ to H_2O yielded a light green solution. No further changes were noted upon addition of the ligand. Addition of the base caused the solution to turn a cloudy blue. Filtration of the solution on a no. 1 qualitative filter yielded a light blue powder. No further purification steps were taken. The sample was analyzed using PXRD.

3.1.9 $Cu(acac)_2$ Synthesis

Addition of $CuCl_2$ to H_2O yielded a light blue solution. Addition of the ligand caused the solution to turn to green, with some blue particles on the top of the solution. Upon addition of the base, the solution turned dark blue and cloudy.

The solution was filtered on a no. 1 qualitative filter to yield a dark blue powder. No further purification steps were taken, and the sample was analyzed using PXRD.

3.2 Non-Aqueous Synthesis of Homoleptic Metal β-diketonates

3.2.1 $Al(tftm)_3$

The preparation of $Al(tftm)_3$ followed a modification in the synthesis described by Fay & Piper[53] where benzene or toluene was used as the solvent instead of H_2O. Aluminum isopropoxide was added to the organic solvent. Htftm was added at three times the molar amount of the aluminum present in the solution.

The reaction was allowed sufficient time to stir, between two hours to overnight, on a stir-plate with a PTFE stir bar inside the reaction vessel with subsequent removal of the solvent *in vacuo*. This yielded a white highly viscous liquid. Dissolving the product in MeOH and removing the solvent *in vacuo* three to five times turned the product into a fine white powder. No further purification steps were taken. The structure was validated with mass spectrometry.

3.3 Synthesis of Some Heteroleptic Metal β-diketonates

This series of reactions was performed to see if heteroleptic species could be created from a process similar to the aqueous synthesis reactions used to create the homoleptic species. Using NMR, research groups have shown that, under the right conditions, certain species will exchange ligands in solution from whole complexes, with the heteroleptic species actually being quite favorable[54,55]. Our approach was different, however, since we did not use pre-synthesized complexes. Rather we attempted to synthesize a heteroleptic species by introducing both ligands to an aqueous solution of the metal chlorides.

T. Cruickshank synthesized these mixed ligand complexes. Attempts were made to create the species $Ni(acac)_1(tftm)_1$ and $Cu(acac)_1(tftm)_1$. The procedure used for each was similar to the other synthetic procedures for the homoleptic species which were adapted from Watson & Lin[51]. The difference with these specific reactions was the addition of an extra ligand. While the other reactions with Ni and Cu had the ratio of metal to free ligand of 1:2, this set of reactions had the addition of another ligand in a 1:1:1 ratio of metal to Hacac to Htftm. The expected products of the reaction can be expressed by the following equation.

$$MCl_2 + Hacac + Htftm \rightarrow M(acac)_2 + M(tftm)_2 + M(acac)_1(tftm)_1 + NH_4Cl \quad \text{Eqn. 3.1}$$

Note: this is an unbalanced equation since the actual rates of formation have not been determined. It is expected that once thermodynamic equilibrium is achieved the three metal-complex products exist in a specific ratio with respect to each other.

3.3.1 $Ni(acac)_1(tftm)_1$ Aqueous Synthesis

A 1:1:1 molar ratio of Ni:Hacac:Htftm was used for this reaction. This was intended to synthesize the product $Ni(acac)_1(tftm)_1$, though byproducts in the form of $Ni(acac)_2$ and $Ni(tftm)_2$ were expected in some equilibrium.

Upon addition of $NiCl_2$ to de-ionized water the solution turned pale green. This was followed by the subsequent addition of the two ligands. The first dropwise additions of the base yielded an "oily" precipitate. The "oily" description is used to describe a thin film of precipitate. that appeared to be hydrophobic, as it forms on the surface of the solution. Addition of more base yielded a noticeable vapor evolved above the solution. Over time the solution turned blue and cloudy and a white precipitate gradually formed.

After an hour of stirring, the solution was filtered on a no. 1 qualitative filter yielding a light blue/green precipitate. The products of these reactions were investigated with PXRD.

3.3.2 $Cu(acac)_1(tftm)_1$ Aqueous Synthesis

Much like in the $Ni(acac)_1(tftm)_1$ reaction, a 1:1:1 Cu:Hacac:Htftm molar ratio was used. Addition of $CuCl_2$ to H_2O yielded a pale blue solution. Addition of the Hacac caused the solution to turn greenish, while the addition of Htftm yielded no color change. As the solution began to stir some, "oily" blue/dark blue particles formed on the surface. Addition of NH_4OH yielded more dark blue particles, as well as a teal colored precipitate. The filtered precipitate. included both the teal and dark blue powder. Powder X-ray diffraction (PXRD) was employed to study the composition of both products.

3.3.3 $Al(acac)_x(tftm)_{3-x}$ Aqueous Synthesis

The goal of this reaction was to create a heteroleptic aluminum complex by following the aqueous synthetic route of $Al(tftm)_3$ but with two ligands. Solutions of 1:1:2 and 1.2.1 Al:Hacac:tftm were used.

In both cases the addition of the $AlCl_3$ to the solution had no effect on the color of the H_2O, nor did adding the ligands. 1-TMC-31 (1:1:2) showed no changes upon addition of the base either. After vacuum filtration on a no. 42 ashless filter a very small amount of precipitate was collected. 1-TMC-33 (1:2:1) appeared slightly yellow and slightly cloudy upon addition of the base. Vacuum filtration on a no. 42 ashless filter yielded a very small amount of white powder which was analyzed with PXRD.

3.4 Synthesis of Some Mixed Metal β-diketonates

It has been shown that stable heterometal, homoleptic complexes can be created[56]. This group, however did not create these compounds in the liquid phase, rather they used a successful elevated temperature solid state approach.

Some attempts to make similar compounds in the liquid phase are presented below, using the synthetic approaches outlined above, but with the inclusion of two metals instead of one in the synthetic process.

3.4.1 Ni + Cu + Hacac + acid synthesis

This reaction was done as a counterpart to the next reaction (in the presence of base) in order to verify that the presence of an acid would shift the equilibrium towards the reactants before proceeding to the next reaction. A molar ratio of 1:1:1:2.5 of Ni:Cu:L:acid where L = Hacac and the acid was the strong acid HCl was employed.

The Ni and Cu were added to the H_2O as their MCl_2 forms, and an extra molar equivalent of $NiCl_2$ was added accidentally. This attempt was a modified version of what other groups had done, as an attempt to see which metal the samples would prefer, in the presence of a strong acid. $NiCl_2$ was added first to the water. The solution turned green. $CuCl_2$ was added and caused the solution to turn teal/blue. Upon addition of the Hacac, blue particles began to form. This could indicate the existence of $Cu(acac)_2$ species in solution, since this is in accordance with previous work done by T. Cruickshank. Upon addition of the acid though, the particles disappeared. This was probably due to the acac being protonated, and subsequently removed from the metal complex. The products were collected, and PXRD analysis was performed.

3.4.2 Ni + Cu + Hacac + Base Aqueous Synthesis

A 1:1:2, and a 1:1:4 molar ratio of Ni:Cu:Hacac was used for these reactions. For both reactions, the addition of $NiCl_2$ to DI H_2O caused a green solution to form. Addition of $CuCl_2$ to the solution caused it to turn a blueish green. Addition of ligand had no effect on the color of the solution. The addition of the base turned the solution deeper green, then changed to a deep blue color as a blue precipitate formed. PXRD analysis was performed on these samples.

3.4.3 Ni + Al + Hacac + Base Aqueous Synthesis

A 1:1:3, and a 1:1:5 molar ratio of Ni:Al:Hacac was used for these reactions. For both solutions, addition of $NiCl_2$ turned the solution green, while addition of $AlCl_3$ and the ligand yielded no color change. Upon addition of the base, the solutions turned a more intense green, though no further color changes were observed.

The solutions were stirred overnight, and the precipitate formed was collected from the samples in the morning by filtering on a no. 42 ashless filter. The 1:1:3 sample yielded a mixture of darker green and white powders. For the 1:1:5 ratio a light green color sample was recovered. PXRD analyses were performed on these samples.

3.5 Solution Ligand Exchange Reactions

A series of reactions was performed with the intent of creating heteroleptic species via ligand exchange in solution from the homoleptic precursors, as opposed to the ground-up synthetic approach adapted from Watson & Lin[51] used in the previous experiments. The approach taken here would rely on the kinetics of the exchange itself, rather than the rates associated to chelation of the metal. This type of work has been reported already, and it shows that, for some complexes, the heteroleptic species are actually quite favorable[54,55].

The approach outlined here exploits the fact that, in a certain solvents such as benzene and CCl_4, these thermodynamically stable heteroleptic complexes do exist. The formation of this species should be independent of the rates of formation for the aqueous synthesis steps outlined in prior paragraphs, rather it should be dominated by the mechanisms of exchange for these compounds.

The setup of this reaction was quite simple. An equimolar solution of $Ni(acac)_2$ with $Ni(hfac)_2$, $Ni(hfac)_2$ with $Ni(tftm)_2$, or $Ni(tftm)_2$ with $Ni(acac)_2$ in MeOH was heated to reflux, at a rate of about one drop per 30 seconds, and stirred with a cold-water reflux condenser attached to the top of the reaction vessel.

The solutions were refluxed for roughly two days to ensure completion. The MeOH solvent was then removed *in vacuo*.

Sublimation was employed as the separation method. This was done so to prevent any product obtained, especially the heteroleptic species, from reverting back to the thermodynamically stable products. For example, the generic reaction taking place can be represented by Eqn. 3.2.

$$aML_2 + aML'_2 \rightarrow bML_2 + cML'_2 + dMLL' \qquad \text{Eqn. 3.2}$$

Given a method of separating the target compound MLL' from the rest of the products, the problem arises from placing the MLL' product into solution again and it reverting back to the products, represented by Eqn. 3.3.

$$dMLL' \rightarrow b'ML_2 + c'ML'_2 + d'MLL' \qquad \text{Eqn. 3.3}$$

where the thermodynamically stable product is represented by the ratio b':c':d' which will have the same ratio as b:c:d.

Sublimation would, presumably, eliminate this worry since it has been shown that heightened F-content increases volatility of these compounds. Thus, these compounds, and their fluorinated derivatives, should be easily separated through sublimation.

The sublimation apparatus was set up with a liquid cooled condenser which was able to be connected to a vacuum line. The vacuum line was connected to a mechanical pump which typically maintains pressure between 10^{-2} to 10^{-3} torr. Temperatures were maintained with a heated bath of silicone oil. A roundbottom flask was submerged only slightly above the sample (1 to 2 cm), and the condenser was roughly 1-1.5 cm from the sample itself. Fractions were collected at varying temperatures, until no more sublimate was formed on the condenser. Initially samples were collected by manually scraping the sublimate off of the condenser, though in some cases, such little sample was present, it was collected by dissolution in MeOH, which was then removed by evaporation in atmosphere.

Samples were examined using PXRD and single crystal X-ray analysis (where applicable).

3.5.1 Refluxing of $Ni(acac)_2$ with $Ni(hfac)_2$

Equimolar amounts of $Ni(acac)_2$ and $Ni(hfac)_2$ were allowed to react in refluxing MeOH, at a rate of ~one drop per 30 seconds, for 48 hours. Initially, this was done under reduced pressure using the in-house vacuum line, but the pressure was unpredictable and often led to spikes of reduced pressure which would cause brief periods of uncontrolled boiling of the solution. The vacuum line was subsequently removed, and the apparatus exposed to atmosphere. Negligible MeOH was lost since the reflux condenser performed so efficiently.

Overall four fractions were collected, with some product, still a green powder, left behind. Samples from these fractions were recrystallized by vapor diffusion of hexanes into a solution of the product and Et_2O. Crystals formed during this process were analyzed using single crystal X-ray analysis.

3.5.2 Refluxing of $Ni(tftm)_2$ with $Ni(acac)_2$

Equimolar amounts of $Ni(tftm)_2$ and $Ni(acac)_2$ were allowed to react in refluxing MeOH for 44 hours. This reaction's water line was set up in parallel with the $Ni(hfac)_2$ and $Ni(tftm)_2$ reaction (described below), with this specific receiving the cooling water second. This led to the reflux condenser being slightly warmer, thus less efficient. Some MeOH was lost, and some light green product formed around the round-bottom flask just above the solvent line, but more MeOH was added to dissolve it on two occasions. After removal of the MeOH *in vacuo*, a light green powder was present.

3.5.3 Refluxing of $Ni(hfac)_2$ with $Ni(tftm)_2$

Equimolar amounts of $Ni(hfac)_2$ and $Ni(tftm)_2$ were allowed to react in refluxing MeOH for 44 hours. This water line in this reaction was set up in parallel with the reaction described in 3.5.2 with this setup receiving the cooling water first, leading to negligible MeOH loss. After removal of the solvent *in vacuo* a homogenous light green powder was present.

3.6 Mass Spectrometry

Mass spectrometry was used for sample analysis as well as for the observation of gas phase reactions of various metal β-diketonate complexes. Gas phase reactions between multiple metal β-diketonate complexes were performed *in situ*, with the goal of understanding by what mechanism these reactions are proceeding. It was also desired to investigate the role of the metal center and ligand effects on the reactivity of these specific species. All mixed reactions were observed *in situ* with the Finnigan MAT 8430 double focusing mass spectrometer.

All samples were introduced as solutions in MeOH. Concentrations were held constant at 0.025 M, except for the less soluble $Cu(acac)_2$ complex, which had to be diluted to 0.0125 M. The samples were introduced into the mass spectrometer through a direct insertion (DI) probe. For single compound analysis, the sample was injected into the sample cup, allowed time to dry, then inserted into the MS via the DI probe. For mixed compound reactions, one sample would first be injected into a sample cup, and allowed to dry. The second reactant would then either be injected into the cup directly on top of the dried sample, or laced around the rim of the sample cup.

It was not believed that any of the observed products were due to liquid-phase reactions prior to sublimation, because the low concentrations, and the general high-heat of the sample-preparation would cause the MeOH to evaporate quickly, leaving very little time for potential liquid-phase reactions.

The DI probe was inserted into the MS, and subsequently heated to a known temperature, between 300 and 600 K. The recorded mass spectra were typically taken by magnetic sector sweeping with scan rates of between 2 and 3 seconds per decade. Resolution was typically 1000 by the 10% valley method. Pressures inside the MS were maintained between 10^{-6} and 10^{-5} torr, and electron energy was a constant 70 eV.

Chapter 4: Results and Discussion

4.1 Mass Spectrometry

In this study mass spectrometry was used for sample analysis and observation of gas phase reactions *in situ*. All proposed molecular formulae have been confirmed using isotope ratios, except where otherwise stated.

4.1.1 Fragmentation of $M(tftm)_n$ Complexes in the Double Sector Instrument

Multiple $M(tftm)_n$ complexes were synthesized for this study, and their fragmentation patterns are discussed below. Reactions between these synthesized compounds and various acac and hfac complexes will be presented in later sections. The fragmentation patterns of these acac and hfac complexes have been reported previously in many bodies of work, as stated in the literature review, and more recently by D. Mains[57]. However, the fragmentation of these $M(tftm)_n$ complexes described herein has not been previously reported.

The following sections detail the fragmentation of four synthesized $M(tftm)_2$ complexes and one $M(tftm)_3$ complex in the double sector mass spectrometer using a 70 eV EI source, while monitoring positive ions. Table 4.1 shows a comparison of relative abundances between the four $M(tftm)_2$ complexes investigated. This was made to elucidate the possible mechanisms by which these compounds fragment, and also to give a point of reference for comparison with other gas-phase reactions, namely those involving different ligands.

	$Co(tftm)_2$	$Ni(tftm)_2$	$Cu(tftm)_2$	$Zn(tftm)_2$
Species Present	Rel. Ab.	Rel. Ab.	Rel. Ab.	Rel. Ab
$M(tftm)_1$-CF_3	0	0	3	0
$M(tftm)_1$-^{t}Bu	0	9	46	1
$M(tftm)_1$-CF_2	17	13	0	5
$M(tftm)_1$	22	42	28	8
$M(tftm)_2$-$2(CF_3)$	18	22	9	0
$M(tftm)_2$-CF_3,^{t}Bu	0	0	2	0
$M(tftm)_2$-$2(^t$Bu)	0	0	100	0
$M(tftm)_2$-CF_3	1	1	0	0
$M(tftm)_2$-^{t}Bu	100	100	72	100
$M(tftm)_2$-CF_2	0	0	0	0
$M(tftm)_2$	46	71	47	13

Table 4.1 Relative ion intensities (normalized to their own respective base peaks) of the positive 70 eV EI msas spectra at 373 K

The molecular ion is visible for all species, though it is not observed as the base peak for any spectra. The loss of one tftm ligand is also visible for each compound and all four $M(tftm)_2$ complexes show the loss of one *tertiary*-butyl (^{t}Bu) group at very high intensities (most are the base peak) for all four species.

Some fragments may be observed in some spectra and not others, though it should be noted that a limit of one count was the minimum signal cutoff for analysis and the sensitivity of the instrument may not have been high enough to pick up certain species. Also, these values are representative of their respective spectrum shown below. All datum were confirmed using averaged spectra and comparing relative isotope ratios with their next highest isotope. The presented abundances are consistent with the averaged spectra.

$Cu(tftm)_2$ exhibits unique behavior since two successive losses of ^{t}Bu groups are observed for it, and not for any other complexes. This also happens to be the base peak of the spectrum, and is a singly charged species. Single charges are also observed for all species where the loss of two groups is observed.

The spectra were analyzed for any doubly charged species, but none were present. F-migration is observed for cobalt, nickel and zinc, though it only is shown after the initial loss of a tftm group which is in accordance with other findings[35].

By comparing the relative abundances displayed in Table 4.1, fragmentation pathways were proposed and shown in Fig. 4.1. The pathways in this figure are representative of all possible pathways observed for these substituted β-diketonate complexes. It does not, however, guarantee that these positive ions will be observed for a certain complex, since the fragmentation pattern heavily relies on the interaction between the electron withdrawing capabilities of the ligand and the ability of the metal to change valence states.

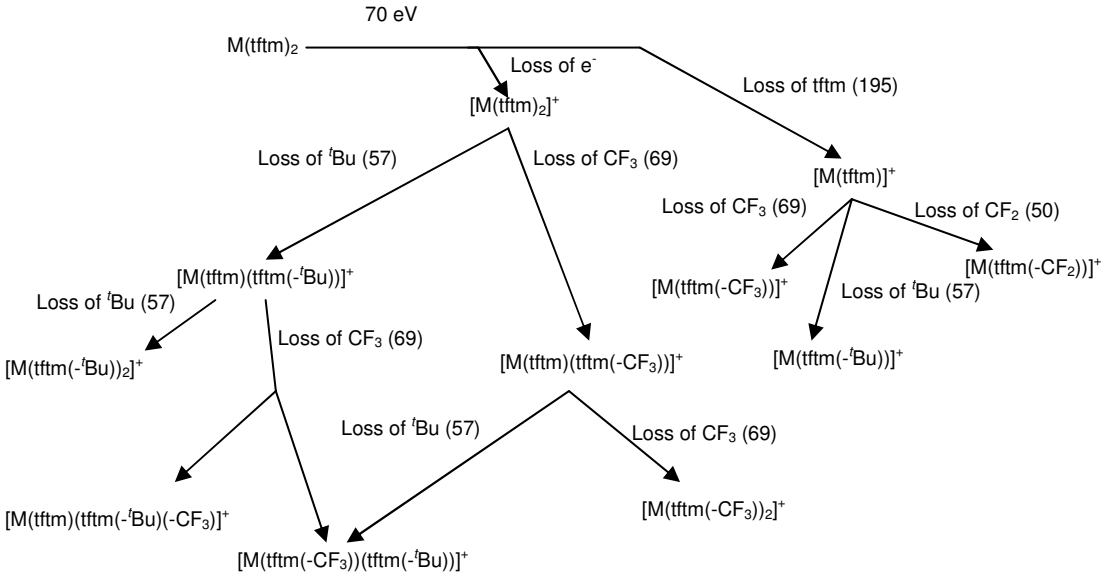

Fig. 4.1 Typical fragmentation routes of the $M(tfm)_2$ compounds. Note: This is a generic diagram, and not all $M(tftm)_2$ complexes will not show all of these fragments.

As shown in Table 4.1 the losses of CF_3 groups and, much more-so, ^{t}Bu groups are common fragmentation pathways for this class of compounds.

The products of these fragments are peculiar since the $^{t}Bu^{+}$ and CF_3^{+} groups are also visible in the positive EI mass spectrum as well as the positive ion of the metal fragment. Equation 4.1 shows the products as having the charge localized on the metal complex, not the ^{t}Bu fragment.

$$[M(tftm)_2]^{+} \rightarrow [M(tftm)_2(-{}^{t}Bu)]^{+} + [{}^{t}Bu]^{0} \qquad \text{Eqn. 4.1}$$

One would expect the ^{t}Bu group to be an odd electron neutral, by the N-rule, but it appears as an even electron positive ion. A competing reaction must be occurring, as shown in Eqn. 4.2 where the charge is localized over the ^{t}Bu fragment.

$$[M(tftm)_2]^{+} \rightarrow [M(tftm)_2(-{}^{t}Bu)]^{0} + [{}^{t}Bu]^{+} \qquad \text{Eqn. 4.2}$$

By Eqn. 4.2, the fragment $M(tftm)_2(-{}^{t}Bu)$ must also be present as a neutral species, though the high abundance of the singly charged ion $[M(tftm)_2\text{-}({}^{t}Bu)]^{+}$ makes one wonder if the peak at m/z 57 might also be due to a secondary reaction and not just a competing reaction meaning the process outlined in Eqn. 4.2 may not be very favorable. It is known that secondary collisions can lead to further fragmentation. It is also known that the loss of an entire tftm ligand exists as a neutral, thus making it possible for further ionization of this neutral ligand to yield the very stable positive ^{t}Bu ion.

A similar treatment of the data regarding the presence of positive ions for both the CF_3^{+} ion and the fragmented complex cation can be asserted, though these ions are observed in low abundances and only for certain $M(tftm)_2$ parent species.

4.1.1.1 $Co(tftm)_2$

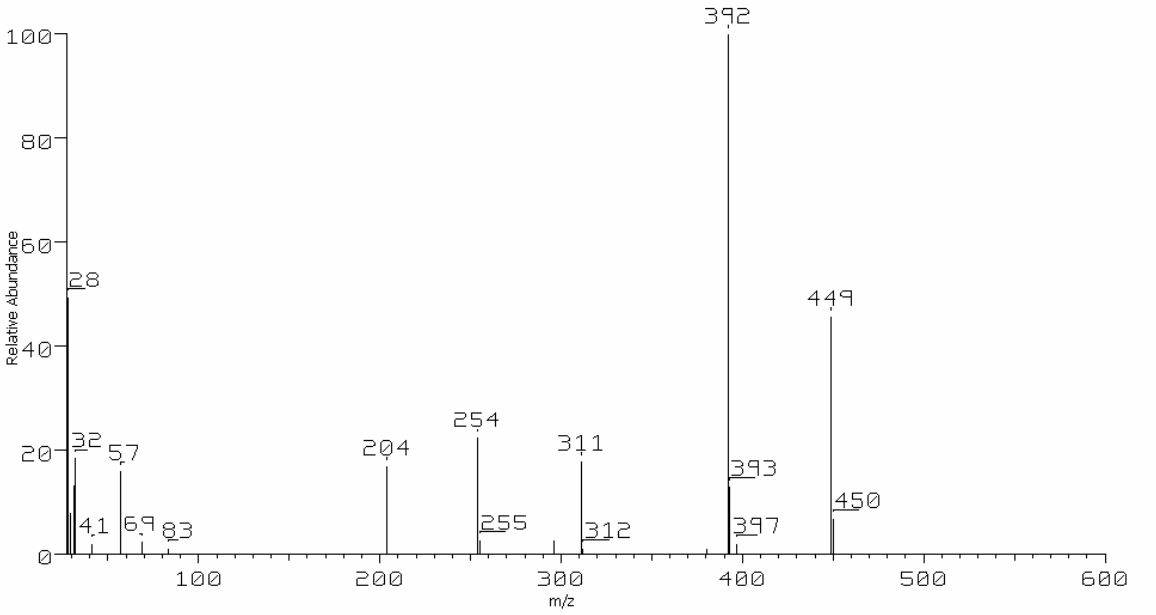

Fig. 4.2 The 70 eV positive EI mass spectrum of $Co(tftm)_2$

m/z	Species Present	Rel. Ab.
204	$Co(tftm)_1$-CF_2	17
254	$Co(tftm)_1$	22
311	$Co(tftm)_2$-2(CF_3)	18
380	$Co(tftm)_2$-CF_3	1
392	$Co(tftm)_2$-^{t}Bu	100
449	$Co(tftm)_2$	46

Table 4.2 Relative ion abundances of the Co species present upon ionization of $Co(tftm)_2$

The above spectrum is representative of a typical EI mass spectrum of $Co(tftm)_2$. As with nickel and zinc, the preferential loss of a ^{t}Bu group is preferred over the formation of the molecular ion. F-migration is visible at m/z 204.

Cobalt and nickel are the only two samples to show an ion due to the loss of a CF_3 group, albeit observed at extremely low abundance relative to their respective base peaks.

The observed fragmentation pathways of the $Co(tftm)_2$ complex is represented in Fig. 4.3. Comparing Fig.'s 4.1 and 4.3 one can clearly see the differences between the possible and observed pathways.

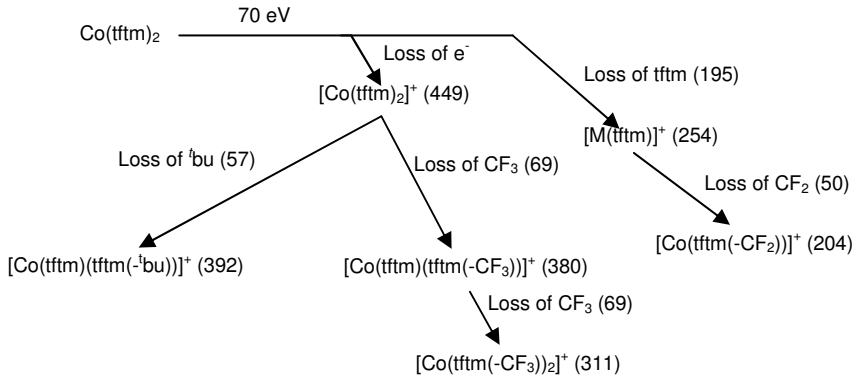

Fig. 4.3 The favored fragmentation pathways observed for the 70 eV positive EI spectrum of $Co(tftm)_2$

4.1.1.2. $Ni(tftm)_2$

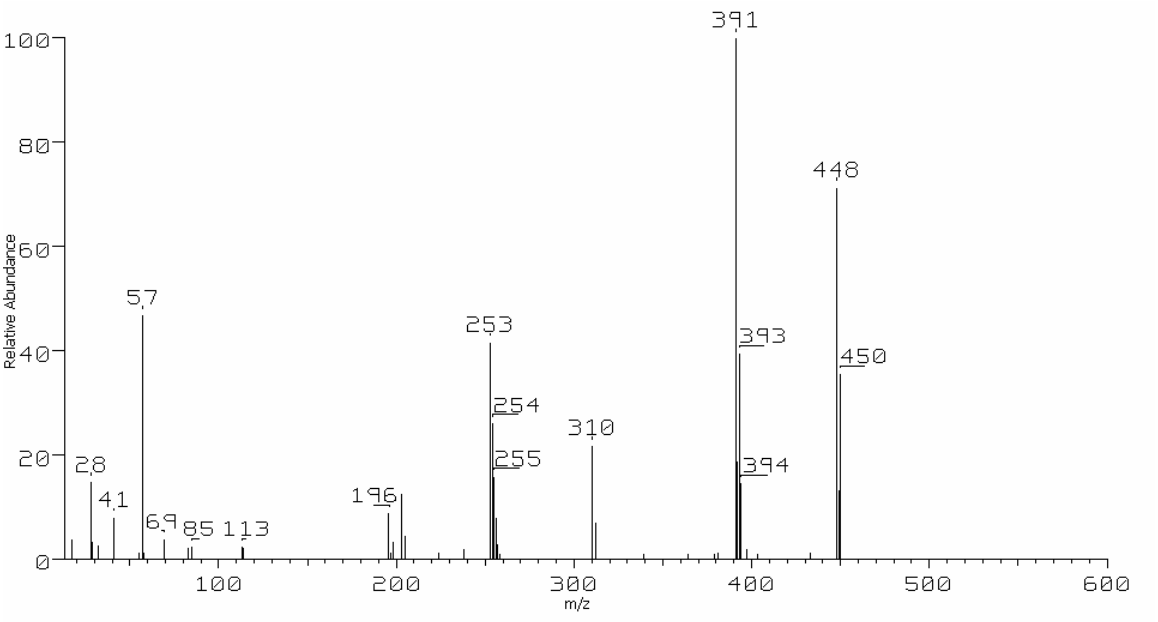

Fig. 4.4 The 70 eV positive EI mass spectrum of $Ni(tftm)_2$

The mass spectrum in Fig. 4.4 is representative of the typical fragmentation pattern observed for $Ni(tftm)_2$. Note the preferential loss of the ^{t}Bu group from the molecular ion. Unlike the copper analog of this compound, which is presented in section 4.1.1.3, a second ^{t}Bu group is not removed to yield a positive ion.

m/z	Species Present	Rel. Ab.
196	$Ni(tftm)_1$-^{t}Bu	9
203	$Ni(tftm)_1$-CF_2	13
253	$Ni(tftm)_1$	42
310	$Ni(tftm)_2$-2(CF_3)	22
379	$Ni(tftm)_2$-CF_3	1
391	$Ni(tftm)_2$-^{t}Bu	100
448	$Ni(tftm)_2$	71

Table 4.3 Relative ion abundances of the Ni species present upon the ionization of $Ni(tftm)_2$

The loss of CF_3 at m/z 379 can barely be seen, much like the scenario observed with the analogous cobalt compound. F-migration is visible at m/z 203 as evident by the loss of a CF_2 group.

4.1.1.3 Cu(tftm)$_2$

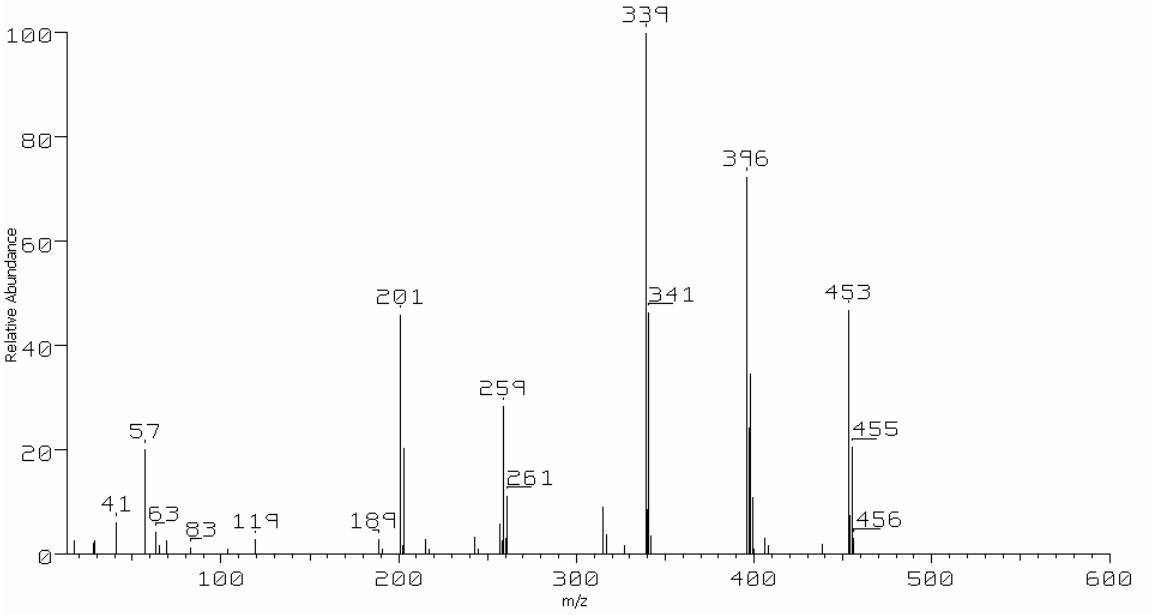

Fig. 4.5 The 70 eV positive EI mass spectrum of Cu(tftm)$_2$

The mass spectrum in Fig. 4.5 is representative of the typical fragmentation pattern for Cu(tftm)$_2$. Note that the base peak is not due to the molecular ion, rather it is due to the subsequent loss of two ^{t}Bu groups. This fragmentation pathway presents a major inconsistency when comparing the data since neither the cobalt, nickel nor zinc complexes exhibit the analogous ion. The other inconsistency would be the lack of an ion due to F-migration.

m/z	Species Present	Rel. Ab.
189	Cu(tftm)$_1$-CF_3	3
201	Cu(tftm)$_1$-^{t}Bu	46
259	CuH(tftm)$_1$	28
315	Cu(tftm)$_2$-2(CF_3)	9
327	Cu(tftm)$_2$-CF_3,^{t}Bu	2
339	Cu(tftm)$_2$-2(^{t}Bu)	100
396	Cu(tftm)$_2$-^{t}Bu	72
453	Cu(tftm)$_2$	47

Table 4.4 Relative ion abundances of the Cu species present upon ionization of Cu(tftm)$_2$

An important finding was observed from the lack of F-migration and other data. The subsequent losses of the ^{t}Bu groups, and the loss of CF_3 groups observed for the other complexes, shows that fragmentation from both ligands are possible, and still yield singly charged positive ions. It remains unclear whether symmetric ligands can yield this same data without first performing isotopic enrichment experiments.

4.1.1.4 Zn(tftm)$_2$

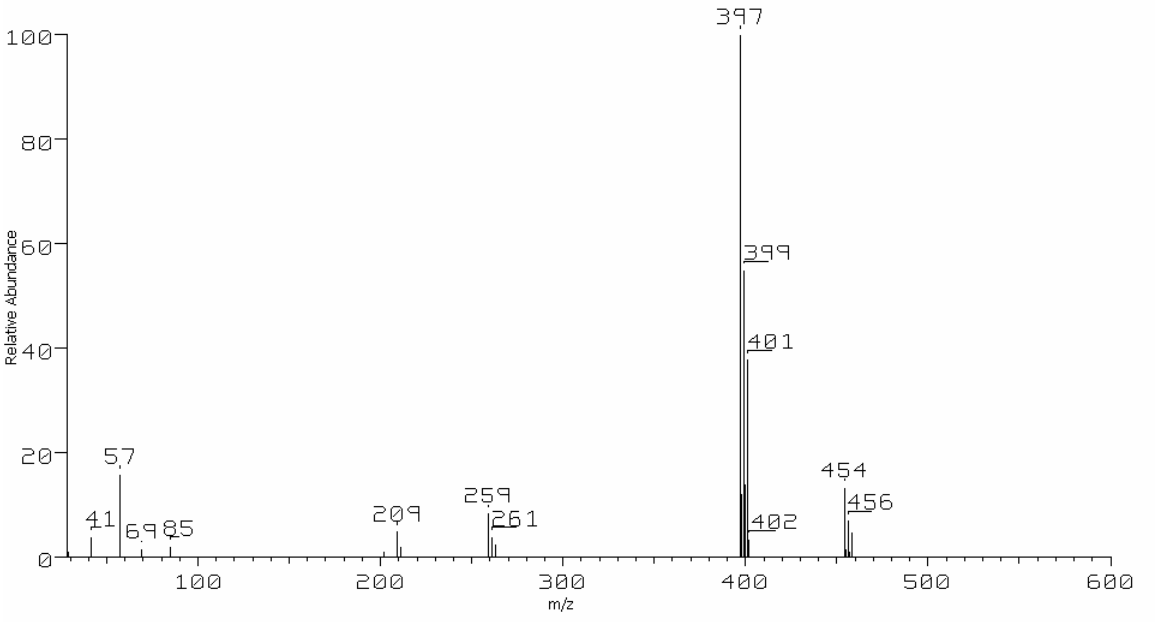

Fig 4.6 The 70 eV positive EI mass spectrum of Zn(tftm)$_2$

Fig. 4.6 is representative of a typical EI mass spectrum of Zn(tftm)$_2$. As with the nickel and cobalt analogs, the preferential loss of a ^{t}Bu group is observed as the base peak, as opposed to the molecular ion. Such high intensities of the base peak seem to swamp out the intensities of the rest of the smaller peaks, though they still remain visible. This zinc complex is yet another example which shows evidence for F-migration as evidenced by the peak observed at m/z 209.

m/z	Species Present	Rel. Ab.
202	Zn(tftm)$_1$-^{t}Bu	1
209	Zn(tftm)$_1$-CF_2	5
259	Zn(tftm)$_1$	8
397	Zn(tftm)$_2$-^{t}Bu	100
454	Zn(tftm)$_2$	13

Table 4.5 Relative ion abundances of the species present upon the ionization of Zn(tftm)$_2$

This zinc complex illustrates, most predominantly, the preferred ^{t}Bu loss pathway. The relative abundance of this fragment compared to the molecular ion supplies sufficient evidence for this claim.

4.1.1.5 Al(tftm)$_3$

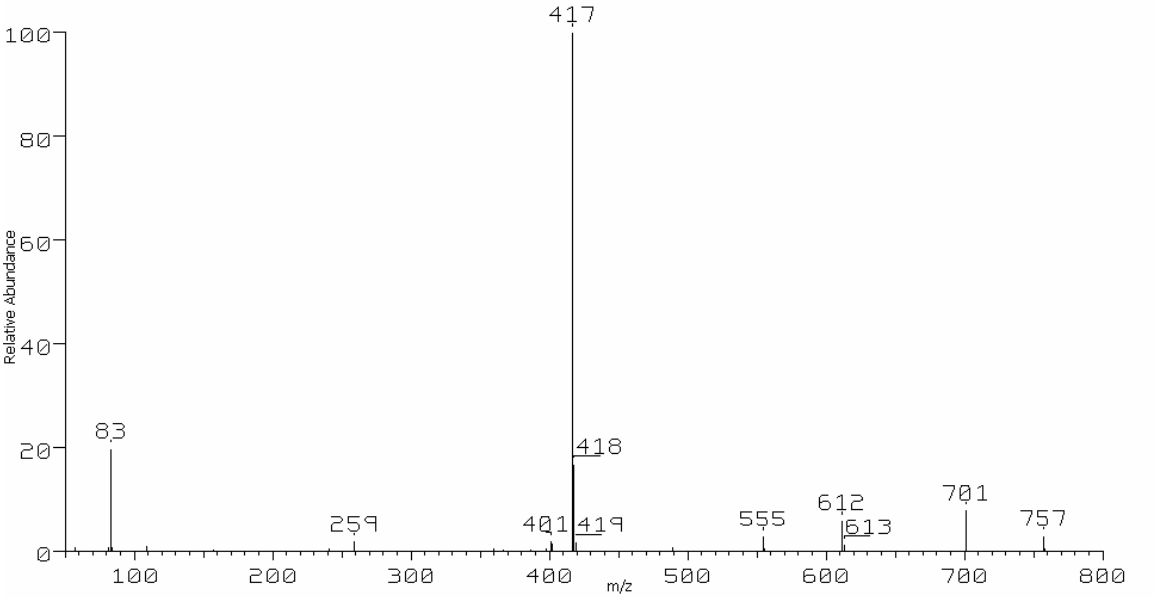

Fig. 4.7 The 70 eV positive EI mass spectrum of Al(tftm)$_3$

The fragmentation of Al(tftm)$_3$ is represented by the mass spectrum shown in Fig. 4.7. This complex was not included in the earlier comparisons since it is the only tris complex, while the other four were bis complexes, though it does follow a similar fragmentation pathway when compared to the rest of the other complexes.

The molecular ion is present in the spectrum at m/z 612, though the most common fragment observed is the loss of a single ligand to yield [Al(tftm)$_2$]$^+$ at m/z 417. The loss of a single ligand is especially common for the aluminum β-diketonate complexes as shown by D. Mains and others[57].

m/z	Species Present	Rel. Ab.
417	Al(tftm)$_2$	100
555	Al(tftm)$_3$-^{t}Bu	3
612	Al(tftm)$_3$	6
701	Al$_2$(tftm)$_4$-(F, 2^{t}Bu)	8
757	Al$_2$(tftm)$_4$-(HF, ^{t}Bu)	3

Table 4.6 Relative ion abundances present during the ionization of Al(tftm)$_3$

The loss of a ^{t}Bu group from the molecular ion is not surprising, given the previous experiments with the $M(tftm)_2$ analogs also exhibit this behavior. Clustered compounds are also present in this reaction, and have been formulated using nominal masses and verified by comparing predicted with observed isotope ratios. These complexes are different from the common M_xL_y form, where the ligands are intact, and not fragmented, as seen with some acac and hfac complexes. A mechanism for these clustered compounds has not been provided by any research group, but it is expected that these aluminum clusters follow a different mechanism due to their fragmented nature.

4.1.2 Fragmentation of Some Nickel β-diketonate Complexes in the QIT

The fragmentation patterns of a select group of complexes were also investigated using a quadrupole ion trap (QIT) mass analyzer. For comparative purposes with the data collected from the double sector instrument, the potential of the ionization source was held consistently for both instruments at 70V, thus the incident electron for both ion sources has an ionizing energy of 70 eV.

The main difference noted with the data from the QIT versus the data from the BE sector instrument was the association of water or methanol to the complexes. Zheng *et al* stated that upon sublimation and ionization, metal β-diketonate complexes will lose any coordinated solvent[52]. They showed this with a quadrupole analyzer. Our own results with a BE sector analyzer also agree with this. However, the use of the QIT shows different results. It is believed that the statements from Zheng *et al*'s findings remain accurate, and that the results we have found in the QIT are not necessarily due directly to the ionization of a species coordinated to solvent, rather they are due to secondary ion-ion reactions in the ion trap itself.

The QIT functions by trapping all ions created in the ion source and selectively ejects them based off of an R_f frequency. The instrument will only record values it is programmed to, even though all ions formed during ionization are being trapped and ejected. The typical range for the Finnigan MAT GCQ used in this experiment was from m/z 50-800. Even though the ions for MeOH and H_2O may not be visible in the spectra shown, they are still common fragments upon ionization. The presence of these solvent species leads to a mixture of the molecular ion and its fragments, as well as solvent ions in the QIT. Helium is also present in the QIT to help act as a buffer between the ions to help diminish ion-ion interaction. However, these reactions still persist even though general physics will tell us that, since these ions all possess positive charges they are likely to repel each other. High concentrations of ions in the trap lead to more collisions and subsequent reactions.

The following mass spectra are representative of the nickel complexes with the ligands acac, hfac and tftm. Electron energy was held constant at 70 eV, and all samples were introduced as solutions of MeOH and analyte. The possibility of coordination to H_2O vs. MeOH is summarized by Zheng *et al*[52].

4.1.2.1 $Ni(acac)_2$ in the QIT

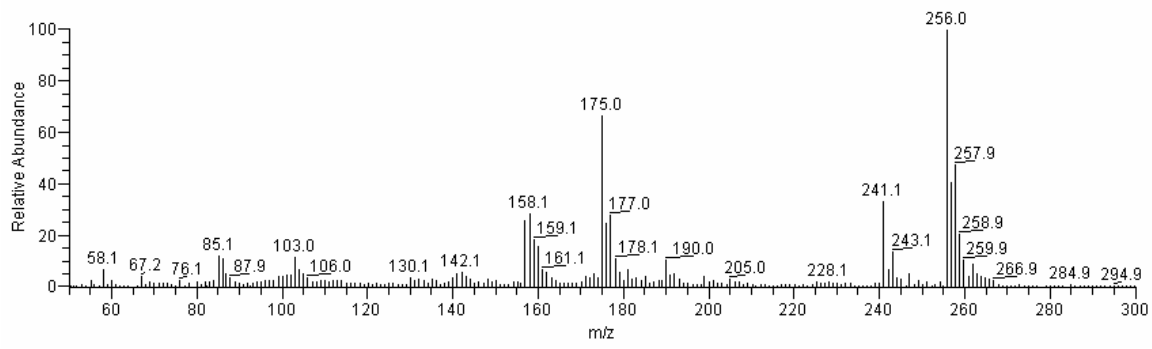

Fig 4.8 The 70 eV positive EI mass spectrum obtained for $Ni(acac)_2$ in the QIT

Fig. 4.8 shows the mass spectrum obtained for $Ni(acac)_2$ using the QIT mass analyzer. The peaks at m/z 256 and 157 are due to $[Ni(acac)_2]^+$ and the fragment $[Ni(acac)_1]^+$, respectively. The peak at m/z 158 is due to the protonated fragment $[Ni(acac)_1H]^+$. Association of H_2O to the fragment is visible at m/z 175 to form the species $[Ni(acac)_1H_2O]^+$.

m/z	Species Present	Rel. Ab.
157	$Ni(acac)_1$	25
158	$Ni(acac)_1H$	30
175	$Ni(acac)_1H_2O$	62
241	$Ni(acac)_2$-CH_3	36
258	$Ni(acac)_2$	100

Table 4.7 Relative ion abundances of the species present in the mass spectrum of $Ni(acac)_2$ in the QIT

4.1.2.2 $Ni(hfac)_2$ in the QIT

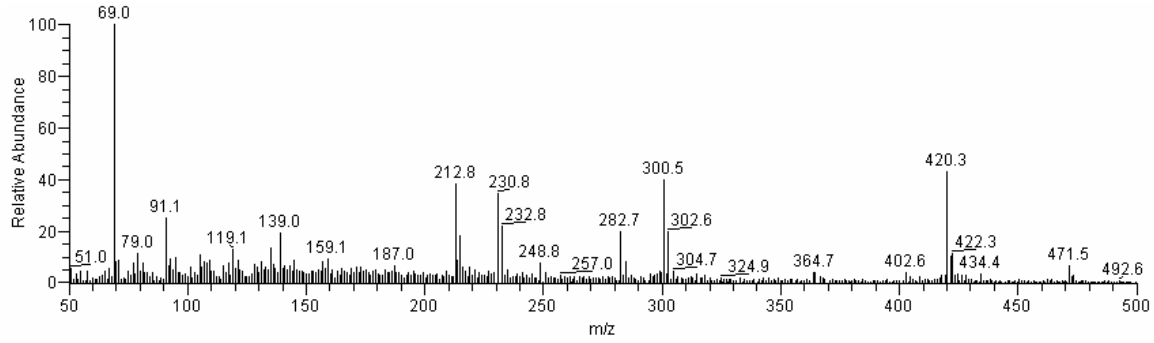

Fig 4.9 The 70 eV positive EI mass spectrum obtained for $Ni(hfac)_2$ in the QIT

The spectrum of $Ni(hfac)_2$, shown in Fig. 4.9, shows association of H_2O at a few sites. The ions $[Ni(hfac)_1(H_2O)_1]^+$ and $[Ni(hfac)_1(H_2O)_2]^+$ are visible at m/z 283 and 301 respectively. Loss of CF_3 groups followed by the addition of OH is observed for $[Ni(hfac)_1OH\text{-}CF_3]^+$ and $[Ni(hfac)_2OH\text{-}CF_3]^+$ at m/z 213 and 420, respectively. The addition of H_2O molecules to the complex observed at m/z 213 are responsible for the peaks at m/z 231 and 249.

m/z	Species Present	Rel. Ab.
213	$Ni(hfac)_1OH\text{-}CF_3$	38
231	$Ni(hfac)_1(OH)(H_2O)\text{-}CF_3$	35
249	$Ni(hfac)_1(OH)(H_2O)_2\text{-}CF_3$	7
283	$Ni(hfac)_1H_2O$	20
301	$Ni(hfac)_1(H_2O)_2$	40
420	$Ni(hfac)_2OH\text{-}CF_3$	43
472	$Ni(hfac)_2$	7

Table 4.8 Relative ion abundances of the species present in the mass spectrum of $Ni(hfac)_2$ in the QIT

4.1.2.3 $Ni(tftm)_2$ in the QIT

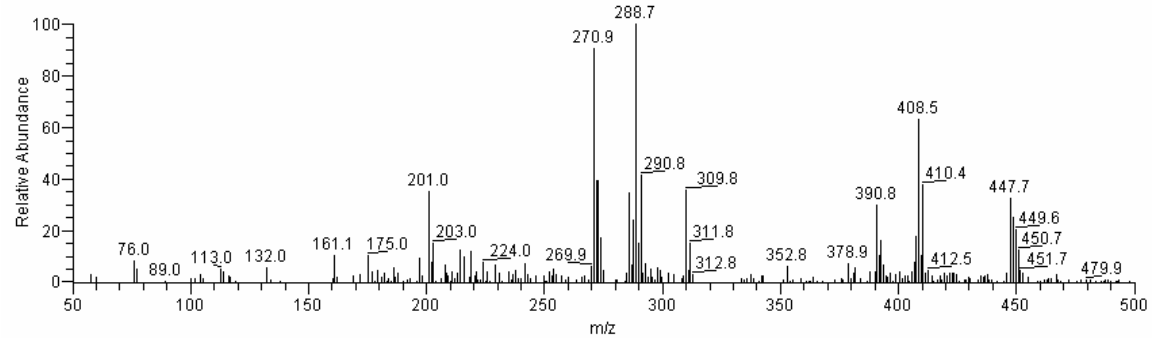

Fig 4.10 The 70 eV positive EI mass spectrum obtained for $Ni(tftm)_2$ in the QIT

The spectrum of $Ni(tftm)_2$, shown in Fig. 4.10, shows the addition of H_2O to multiple fragments. The ion $[Ni(tftm)_1H_2O]^+$ is observed at m/z 271, while $[Ni(tftm)_2H_2O\text{-}^tBu]^+$ is observed at m/z 409. MeOH is shown associated by the species $[Ni(tftm)_1MeOH]^+$ at m/z 286.

Though not much work was done in this study with the QIT mass analyzer, the results are quite profound. The findings from the QIT led this group to relegate most other work to the BE sector instrument. The BE sector instrument was chosen over the QIT due to the complications that were found with the QIT, namely the secondary reactions in the mass analyzer. The intent is to initially find out by what mechanism heteroleptic complexes can be formed in the gas phase. In order to do so, secondary reactions and by-products must be diminished. The BE sector instrument allows for minimization of the secondary reactions in our studies.

m/z	Species Present	Rel. Ab.
201	$Ni(tftm)_1H_2O\text{-}HCF_3$	35
271	$Ni(tftm)_1H_2O$	91
289	$Ni(tftm)_2(H_2O)_2$	100
310	$Ni(tftm)_2\text{-}2(CF_3)$	36
353		6
379	$Ni(tftm)_2\text{-}CF_3$	7
391	$Ni(tftm)_2\text{-}^tBu$	10
409	$Ni(tftm)_2H_2O\text{-}^tBu$	63
448	$Ni(tftm)_2$	33

Table 4.9 Relative ion abundances of the species present in the mass spectrum of $Ni(tftm)_2$ in the QIT

Perhaps when more work has been done in this field, and it is wished to explore these secondary reactions more, the QIT may become an asset. However, at this point, the BE sector instrument is the logical choice.

4.1.3 Heteroleptic Gas-Phase Reactions with Homometal Precursors

The following reactions were executed with the intent of creating heteroleptic complexes from precursors which share the same metal center. We chose these conditions with the hope of determining whether specific ligands would be observed in gas phase rearrangements while keeping the metal center constant. The following paragraphs describe the mechanism by which these reactions took place.

The mechanism by which the rearrangements occur has not been reported in any journal to date. Our investigation is the first to propose a mechanism which we believe to be an ion-neutral process. We extend this concept not only to mixed heteroleptic species, $Ni(hfac)_1(acac)_1$ for example, but also to homoleptic species which are the result of substitution. Consider the reaction between $Ni(acac)_2$ and $Cu(hfac)_2$ whose products are, among others, $[Ni(hfac)_1]^+$ and $[Ni(hfac)_2]^+$. These newly formed species are the direct result of gas phase ion-neutral reactions.

Ionization of free acetylacetone, as shown by D. Mains[57], shows the positive molecular ion at m/z 100. Ionization of $M(acac)_n$ complexes, however, yields no positive ion pertaining to an intact acac fragment. Granted, we cannot directly observe neutral species in the mass spectrometer, it is still assumed that these fragments are in fact neutral species. We commonly see the molecular ions of the metal complexes, as well as fragments due to the loss of one or more whole ligands.

It is also worth noting that these species are observed as having a 1+ charge, since change in valence state can be seen for many of the transition metal complexes we have used in this study. The mechanism for the formation of heteroleptic species is summarized in the following equations using the generic homometllic precursors ML_2 and $M'L'_2$.

$$[M'L'_2]^+ \rightarrow [M'L']^+ + L'^0 \qquad \text{Eqn. 4.3}$$

$$[ML_2]^+ \rightarrow [ML]^+ + L^0 \qquad \text{Eqn. 4.4}$$

$$[M'L']^+ + L^0 \rightarrow [M'L'L]^+ \qquad \text{Eqn. 4.5}$$

$$[ML]^+ + L'^0 \rightarrow [MLL']^+ \qquad \text{Eqn. 4.6}$$

The above equations show the necessary steps involved for the target heteroleptic complexes $[MLL']^+$ and $[M'L'L]^+$. Notice that if the metals share the same identity Eqn's 4.5 and 4.6 both lead to the same heteroleptic compound.

The steps shown in Eqn's 4.3 and 4.4 illustrate the first necessary step in the reaction, which is the loss of a ligand as a neutral from the ionized complex. This leaves a positively charged fragment of the complex and a neutral ligand, both of which are parts of subsequent reactions. The free neutral ligand, L^0, from Eqn. 4.3 is able to come in contact with the other positively charged fragments, $[ML]^+$ from Eqn. 4.4 and form a new heteroleptic species. This process is shown in Eqn. 4.6 to form the heteroleptic species $[MLL']^+$. The other possible heteroleptic complex $[M'L'L]^+$ shown by Eqn. 4.5 follows a similar mechanism using the unused fragments $[M'L']^+$ and L^0 from Eqn's 4.3 and 4.4 respectively.

Heteroleptic species are observed in most reactions, as shown later, but homoleptic products, that are due to gas-phase rearrangements, are also observed.

These reactions are secondary reactions generated after the decomposition of their heteroleptic precursors. Consider the decomposition of the heteroleptic positive ion $[MLL']^+$ in Eqn. 4.7.

$$[MLL']^+ \rightarrow [ML']^+ + L^0 \qquad \text{Eqn. 4.7}$$

Recall that the initial reacant was ML_2, but a homoleptic ion with different ligand identity is observed as $[ML']^+$. It is possible that a competing reaction is also taking place for the $[ML']^+$ product where the initial complex may lose all of its ligands and exist as an ion, then be chelated to a neutral ligand again, yielding the same product. Evidence for a bare metal ion to be chelated is limited only to copper since that is the only metal ion observed in our studies.

The presence a metal ion also lends itself to further substitution. If a neutral ligand can associate to this ion and form a heteroleptic complex, its formation pathway would be indistinguishable from that shown in Eqn. 4.7, or further homoleptic complexation as shown in Eqn. 4.8.

$$[ML']^+ + L'^0 \rightarrow [ML'_2]^+ \qquad \text{Eqn. 4.8}$$

The species $M'L_2$ is also formed by the same mechanism. This mechanism accounts for the gas phase rearrangements to form heteroleptic and homoleptic products. A similar mechanism may also be applied to tris complexes of the form ML_3. The general mechanism is still involves the loss of ligands as neutrals and association of non-native neutral ligands. In addition the ML_3 complexes may lose one, two or all three native ligands, and subsequently gain the appropriate number of non-native ligands. However, it should be noted that other mechanisms may be possible.

A few characteristics of this study have been manipulated to intentionally create conditions which would maximize gas-phase reactions.

Multiple reactions were performed with the samples separated from each other, so competing reactions would be minimized and effectively negated. This was done to eliminate solution exchange, where pressure would effect the formation of clusters, or competing reactions. The double sector instrument was chosen over the ion-trap to minimize ion-ion reactions which were shown to occur in the QIT instrument in section 4.1.2. It has been shown that ligand exchange occurs in solution as a concerted reaction between two complexes[54,55], but these types of reactions depend heavily on solvent, temperature and other factors. Gas-phase investigations simplify some of these variables. The mechanism is proposed as such an ion-neutral reaction is the most feasible process with other potential processes being minimized.

The species included in the equations above were observed in multiple spectra. The presence of these species, both as products and intermediates, puts forth a compelling case for the process as described, though more work is needed before any firm conclusive mechanisms can be proposed.

To further examine possible mechanisms, additional experimentation is necessary. One such experiment may focus on the time spent in the ionization chamber, since this is presumably where these reactions are taking place. The ionization chamber itself consists of the electron source, as well as the acceleration hardware to propel the ions into the mass analyzer. Regular adjustment of the ionization and acceleration hardware was necessary to tune for optimum performance, meaning the voltage on the repeller was not

constant. By not maintaining a static acceleration, residence times could have varied within the ionization chamber between different reactions.

The more time the ions spend in the presence of the neutrals, the more reactions would occur, and the same can be said for the secondary ionization needed for the non-native homoleptic species.

Much work can be also be done with metastable ions. Since it is proposed that some of the species present in the mass spectra are intermediates, it may be possible to analyze their metastable peaks. Also, this may help to eliminate other possible mechanistic routes by which these could be formed, one of which being the formation of clustered compounds, then subsequent fragmentation of the cluster to yield heteroleptic species.

4.1.3.1 Heteroleptic Co reactions

Gas-phase reactions between various Co β-diketonate complexes are presented.

4.1.3.1.1 $Co(tftm)_2$ with $Co(acac)_2$

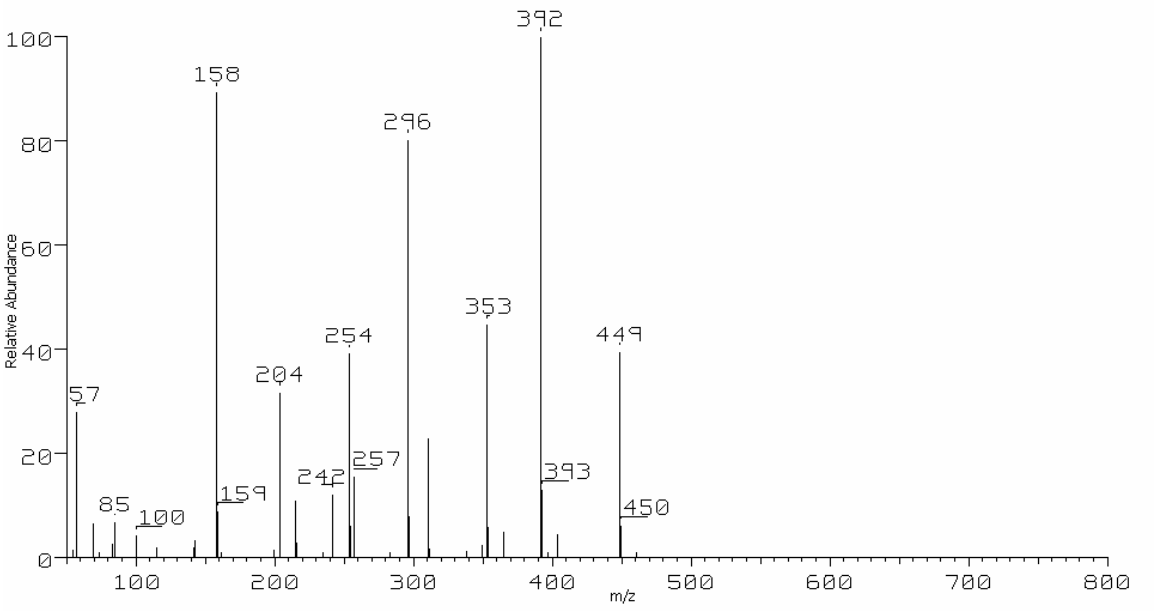

Fig 4.11 The 70 eV positive EI mass spectrum for the reaction of $Co(tftm)_2$ with $Co(acac)_2$

Heteroleptic species are present in the reaction of $Co(tftm)_2$ with $Co(acac)_2$ as shown in Fig. 4.11. The species $[Co(tftm)_1(acac)_1]^+$ is present at m/z 353 in relatively high abundance with fragments visible from both the acac and tftm ligands from this heteroleptic species. Loss of a ^{t}Bu group is a highly favored fragmentation channel for the heteroleptic species, especially when considering the loss of CH_3 from the same is essentially negligible at an abundance of 1% relative to the base peak. F-migration is visible from the $[Co(tftm)_1]^+$ fragment to form $[Co(tftm)_1\text{-}CF_2]^+$ yielding the relocation of a F atom from a CF_3 fragment onto the metal center. This was shown to occur previously in section 4.1.1.1.

m/z	Species present	Rel. Ab.
143	$Co(acac)_1\text{-}CH_3$	3
158	$Co(acac)_1$	89
204	$Co(tftm)_1\text{-}CF_2$	32
242	$Co(acac)_2\text{-}CH_3$	12
254	$Co(tftm)_1$	39
257	$Co(acac)_2$	16
296	$Co(tftm)_1(acac)_1\text{-}^t Bu$	80
311	$Co(tftm)_2\text{-}2(CF_3)$	23
338	$Co(tftm)_1(acac)_1\text{-}CH_3$	1
353	$Co(tftm)_1(acac)_1$	45
392	$Co(tftm)_2\text{-}^t Bu$	100
449	$Co(tftm)_2$	40

Table 4.10 Relative ion abundances of the Co species present in the reaction of $Co(tftm)_2$ with $Co(acac)_2$

4.1.3.1.2 $Co(tftm)_2$ with $Co(acac)_3$

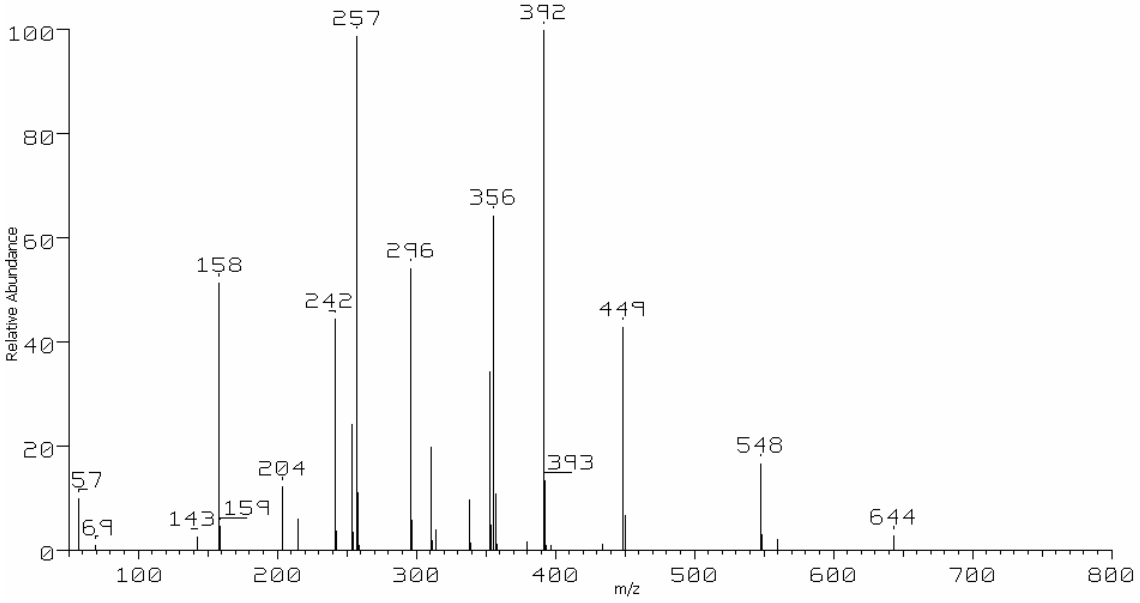

Fig. 4.12 The 70 eV positive EI mass spectrum for the reaction of $Co(tftm)_2$ with $Co(acac)_3$

Multiple heteroleptic species are present in the reaction of $Cu(tftm)_2$ with $Co(acac)_3$ as seen in the mass spectrum in Fig. 4.12. The ion $[Co(tftm)_1(acac)_1]^+$ can be seen at m/z 353. A fragment of this species due to the loss of a ^{t}Bu group is observed at m/z 296. This ion has greater intensity than that of its parent ion, but this is expected since the loss of a ^{t}Bu group for the $Co(tftm)_2$ species is also a very favorable process as seen in section 4.1.1.1. F-migration is also observed to occur for $[Co(tftm)_1]^+$ species by the formation of $[Co(tftm)_1\text{-}CF_2]^+$ at m/z 204.

m/z	Species present	Rel. Ab.
143	$Co(acac)_1\text{-}CH_3$	3
158	$Co(acac)_1$	52
204	$Co(tftm)_1\text{-}CF_2$	12
242	$Co(acac)_2\text{-}CH_3$	45
254	$Co(tftm)_1$	24
257	$Co(acac)_2$	98
296	$Co(tftm)_1(acac)_1\text{-}^t$Bu	54
311	$Co(tftm)_2\text{-}2(CF_3)$	20
353	$Co(tftm)_1(acac)_1$	34
356	$Co(acac)_3$	65
392	$Co(tftm)_2\text{-}^t$Bu	100
449	$Co(tftm)_2$	43
452	$Co(tftm)_1(acac)_2$	0
548	$Co(tftm)_2(acac)_1$	17
644	$Co(tftm)_3$	3

Table 4.11 Relative ion abundances of the Co species present in the reaction between $Co(tftm)_2$ with $Co(acac)_3$

A higher mass heteroleptic species is also present at m/z 548 and can be assigned $[Co(tftm)_2(acac)_1]^+$. This is an interesting peak since the tris cobalt complex can be accredited to the $Co(acac)_3$ reactant, with respect to the metal center's trivalent identity. The presence of $[Co(tftm)_2(acac)_1]^+$ would require two subsequent losses of acac neutrals and association of tftm neutrals. This is especially true since the abundance of the $[Co(acac)_2]^+$ ion is much greater than the $[Co(acac)_1]^+$ ion.

$$[Co(acac)_3]^+ \rightarrow [Co(acac)_1]^+ + 2acac^0 \qquad \text{Eqn. 4.9}$$

$$[Co(acac)_1]^+ + tftm^0 \rightarrow [Co(acac)_1(tftm)_1]^+ \qquad \text{Eqn. 4.10}$$

$$[Co(acac)_1(tftm)_1]^+ + tftm^0 \rightarrow [Co(acac)_1(tftm)_2]^+ \qquad \text{Eqn. 4.11}$$

Eqn. 4.9 is not intended to represent the loss of the acac neutral as a one step process. The products in Eqn's 4.10 and 4.11 show two products which are readily observed. It is believed that the product of Eqn. 4.10 is an intermediate of the product in Eqn. 4.11.

4.1.3.1.3 $Co(tftm)_2$ with $Co(hfac)_2$

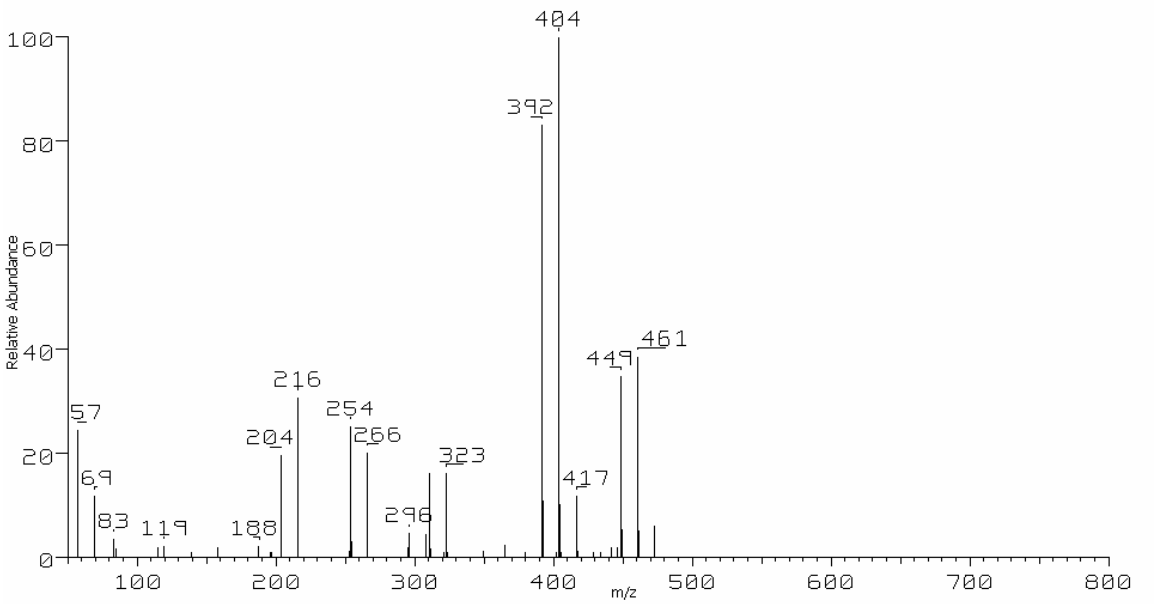

Fig. 4.13 The 70 eV positive EI mass spectrum for the reaction of $Co(tftm)_2$ with $Co(hfac)_2$

Heteroleptic species are observed for the reaction of $Cu(tftm)_2$ with $Co(hfac)_2$ shown in Fig. 4.13. The ion $[Co(tftm)_1(hfac)_1]^+$ is present at m/z 449 while the preferred loss channel of a ^{t}Bu group from this heteroleptic species is observed at m/z 404 which is also the base peak of this spectrum. F-migration is an observed pathway for both $[Co(tftm)_1]^+$ and $[Co(hfac)_1]^+$ precursors at m/z 204 and 216 respectively.

m/z	Species present	Rel. Ab.
204	$Co(tftm)_1$-CF_2	20
216	$Co(hfac)_1$-CF_2	31
254	$Co(tftm)_1$	25
266	$Co(hfac)_1$	20
311	$Co(tftm)_2$-2(CF_3)	16
323	$Co(tftm)_2$-CF_3,^{t}Bu	16
392	$Co(tftm)_2$-^{t}Bu	83
404	$Co(hfac)_1(tftm)_1$-^{t}Bu	100
449	$Co(tftm)_2$	35
461	$Co(tftm)_1(hfac)_1$	39
473	$Co(hfac)_2$	6

Table 4.12 Relative ion abundances of the species present in the reaction between $Co(tftm)_2$ and $Co(hfac)_2$

4.1.3.1.4 $Co(acac)_2$ with $Co(hfac)_2$

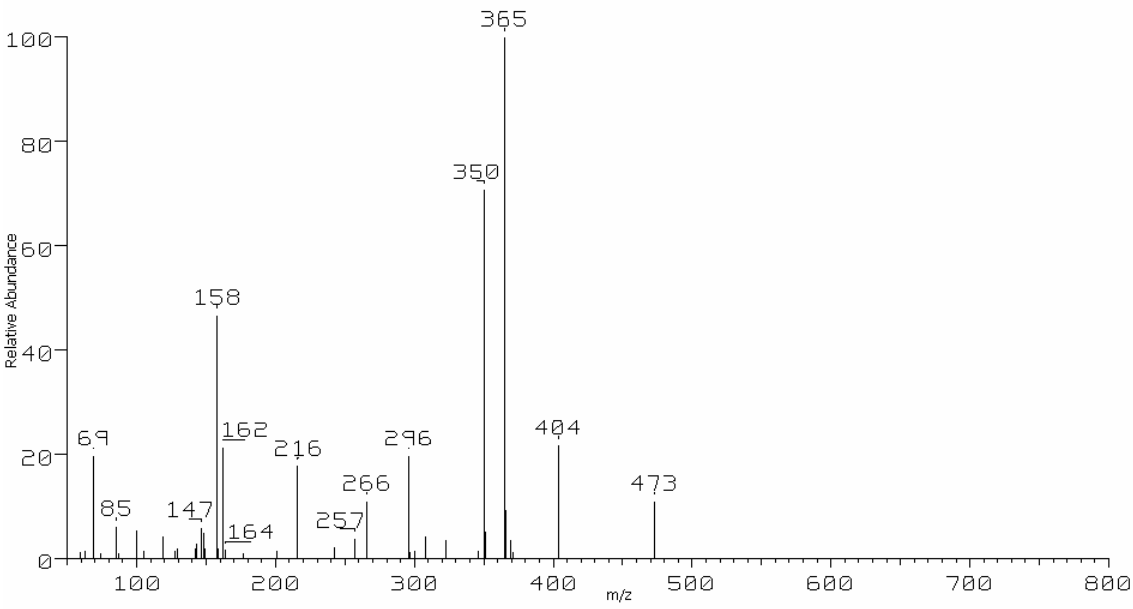

Fig. 4.14 The 70 eV positive EI mass spectrum for the reaction of $Co(acac)_2$ with $Co(hfac)_2$

Heteroleptic species are present in the reaction of $Co(acac)_2$ with $Co(hfac)_2$ as shown in Fig. 4.14. The heteroleptic species $[Co(acac)_1(hfac)_1]^+$ at m/z 365 is the base peak of this spectrum while losses of methyl and CF_3 groups at m/z 350 and 296 respectively are also present. F-migration is observed for the $Co(hfac)_1$ species to form $Co(hfac)_1$-CF_2 at m/z 216.

The reactions between the different cobalt species have shown the propensity of cobalt to form heteroleptic species. These reactions have also led to some interesting results, as shown with the mechanistic implications observed for the reactions with the $Co(acac)_3$ complex, as presented in section 4.1.3.1.2

m/z	Species Present	Rel. Ab.
147	$Co(acac)_1$-CH_3	6
158	$Co(acac)_1$	47
216	$Co(hfac)_1$-CF_2	18
257	$Co(acac)_2$	4
266	$Co(hfac)_1$	11
296	$Co(acac)_1(hfac)_1$-CF_3	20
350	$Co(acac)_1(hfac)_1$-CH_3	70
365	$Co(acac)_1(hfac)_1$	100
404	$Co(hfac)_2$-CF_3	22
473	$Co(hfac)_2$	11

Table 4.13 Relative ion abundances of the species present in the reaction of $Co(acac)_2$ with $Co(hfac)_2$

4.1.3.2 Homometal Ni reactions

Gas-phase reactions between various Ni β-diketonate complexes are presented.

4.1.3.2.1 $Ni(acac)_2$ with $Ni(hfac)_2$

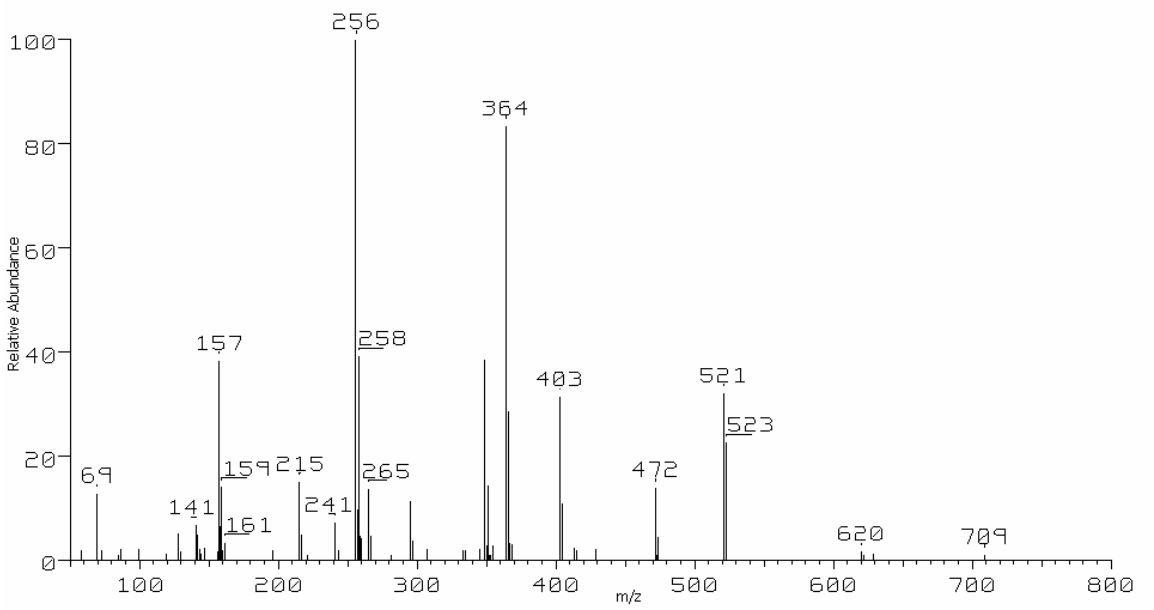

Fig 4.15 The 70 eV positive EI mass spectrum during the reaction of $Ni(acac)_2$ with $Ni(hfac)_2$

Heteroleptic species are observed for the reaction between $Ni(acac)_2$ and $Ni(hfac)_2$ and are shown in Fig. 4.15. The heteroleptic species is seen at m/z 364 and fragments of it are also visible, though in much lower abundances. The formation of larger compounds is also observed in this spectrum. The identity of the $[Ni_2(acac)_2(hfac)_1]^+$ ion at m/z 521 can be confirmed on the basis of isotope ratios. The identity of the other associated species is cautionary given their low abundance and the inability to validate through isotope ratios.

m/z	Species	Rel. Ab.
141	$Ni(acac)_1$-CH_3,H	7
157	$Ni(acac)_1$	38
196	$Ni(hfac)_1$-CF_3	2
215	$Ni(hfac)_1$-CF_2	15
241	$Ni(acac)_2$-CH_3	7
256	$Ni(acac)_2$	100
265	$Ni(hfac)_1$	14
295	$Ni(acac)_1(hfac)_1$-CF_3	12
333	$Ni(acac)_1(hfac)_1$-2(CH_3),H	2
349	$Ni(acac)_1(hfac)_1$-CH_3	39
364	$Ni(acac)_1(hfac)_1$	84
403	$Ni(hfac)_2$-CF_3	31
472	$Ni(hfac)_2$	14
521	$Ni_2(acac)_2(hfac)_1$	32
620	$Ni_2(acac)_3(hfac)_1$*	2
709	$Ni_2(acac)_2(hfac)_1$-F*	1

Table 4.14 Relative ion abundances of the Ni species present during the reaction of $Ni(acac)_2$ with $Ni(hfac)_2$
*denotes nominal mass verification only

4.1.3.3 Homometal Cu reactions

Gas-phase reactions between various Cu β-diketonate complexes are presented.

4.1.3.3.1 $Cu(tftm)_2$ with $Cu(hfac)_2$

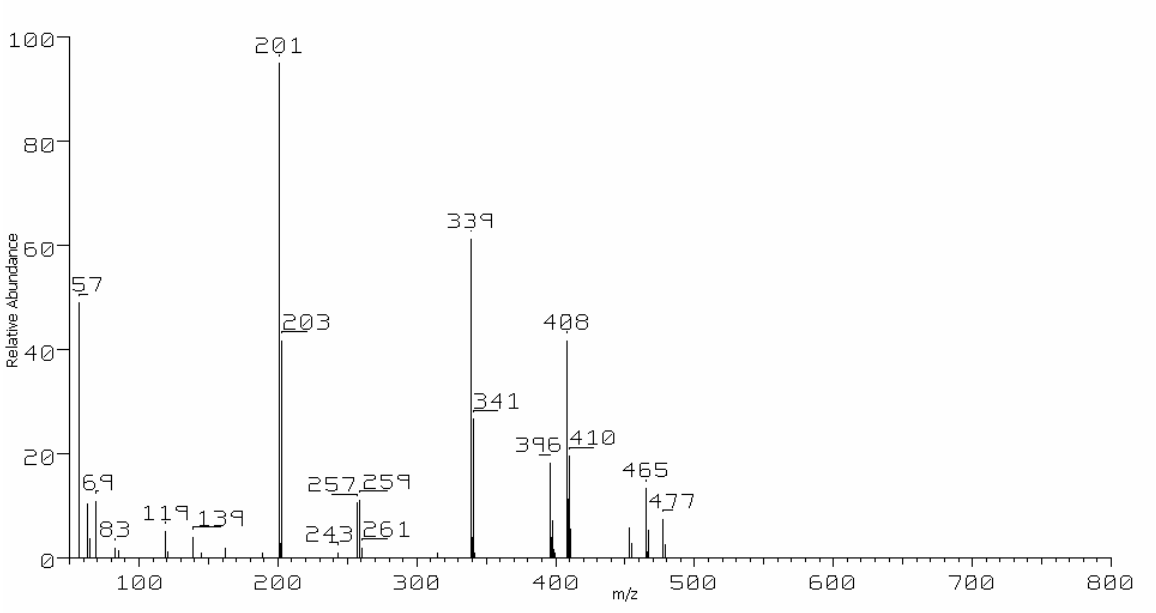

Fig. 4.16 The 70 eV positive EI mass spectrum during the reaction of $Cu(tftm)_2$ with $Cu(hfac)_2$

Evidence for the reaction between $Cu(tftm)_2$ and $Cu(hfac)_2$ is shown in the mass spectrum presented in Fig. 4.16 where evidence for the formation of mixed ligand species at m/z 465, namely the mixed species $[Cu(tftm)_1(hfac)_1]^+$ is observed. This heteroleptic species shows a higher abundance than the molecular ions for both reactants. Fragments of this species are also present, as described in Table 4.15, though some ambiguity remains when determining the fragmentation pathway. Specifically when the tftm (195 amu) ligand loses a ^{t}Bu (57 amu) group, and the hfac (207 amu) loses a CF_3 (69 amu) the remaining fragments have the same nominal mass of 138 amu.

m/z	Cu Species Present	Rel. Ab.
63	Cu	11
189	$Cu(tftm)_1$-CF_3	1
201	$Cu(tftm)_1$-^{t}Bu	100
258	$Cu(tftm)_1$	12
315	$Cu(tftm)_2$-2(CF_3)	1
339	$Cu(tftn)_2$-2(^{t}Bu)	64
396	$Cu(tftm)_2$-^{t}Bu	19
408	$Cu(hfac)_2$-CF_3	44
453	$Cu(tftm)_2$	6
465	$Cu(tftm)_1(hfac)_1$	14
477	$Cu(hfac)_2$	8

Table 4.15 Relative ion abundances of the species present during the reactions of $Cu(tftm)_2$ with $Cu(hfac)_2$

This isobaric ambiguity cannot be overcome by comparing isotope ratios since the isobaric peaks are due to fragments with the same atomic composition. Isotopic labeling or high-resolution techniques would have to be used to differentiate between species of this sort.

4.1.3.3.2 $Cu(hfac)_2$ with $Cu(acac)_2$

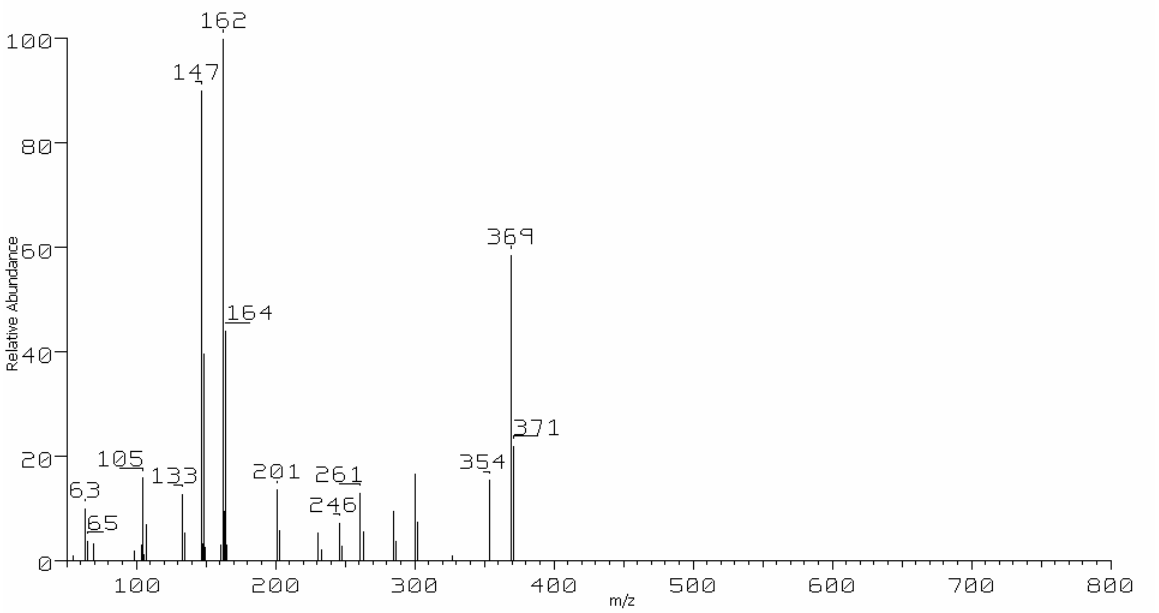

Fig. 4.17 The spectrum taken during the reaction of $Cu(hfac)_2$ with $Cu(acac)_2$

The results for the reaction between $Cu(hfac)_2$ and $Cu(acac)_2$ are shown in Fig. 4.17 where mixed ligand peaks are very abundant. The highest mass peak, at m/z 369, is due to the mixed ligand species $[Cu(hfac)_1(acac)_1]^+$. This peak is rather abundant too since the only peaks with higher intensities are due to the $[Cu(acac)_1]^+$ peak and its fragment due to the loss of a methyl group.

m/z	Species	Rel. Ab.
133	$Cu(acac)_1H\text{-}2(CH_3)$	13
147	$Cu(acac)_1\text{-}CH_3$	90
162	$Cu(acac)_1$	100
201	$Cu(hfac)_1\text{-}CF_3$	14
231	$Cu(acac)_1(hfac)_1\text{-}2(CF_3)$	5
246	$Cu(acac)_2\text{-}CH_3$	7
261	$Cu(acac)_2$	13
285	$Cu(acac)_1(hfac)_1\text{-}CF_3,CH_3$	10
300	$Cu(acac)_1(hfac)_1\text{-}CF_3$	17
354	$Cu(acac)_1(hfac)_1\text{-}CH_3$	16
369	$Cu(acac)_1(hfac)_1$	59

Table 4.16 Relative ion abundances of the Cu species present in the reaction of $Cu(hfac)_2$ with $Cu(acac)_2$

The absence of the molecular ion peak could arise from the fact that copper may form a more stable ion as the mixed ligand species.

4.1.3.4 Homometal Zn reactions

Gas-phase reactions between various Zn β-diketonate complexes are presented.

4.1.3.4.1 $Zn(tftm)_2$ with $Zn(acac)_2$

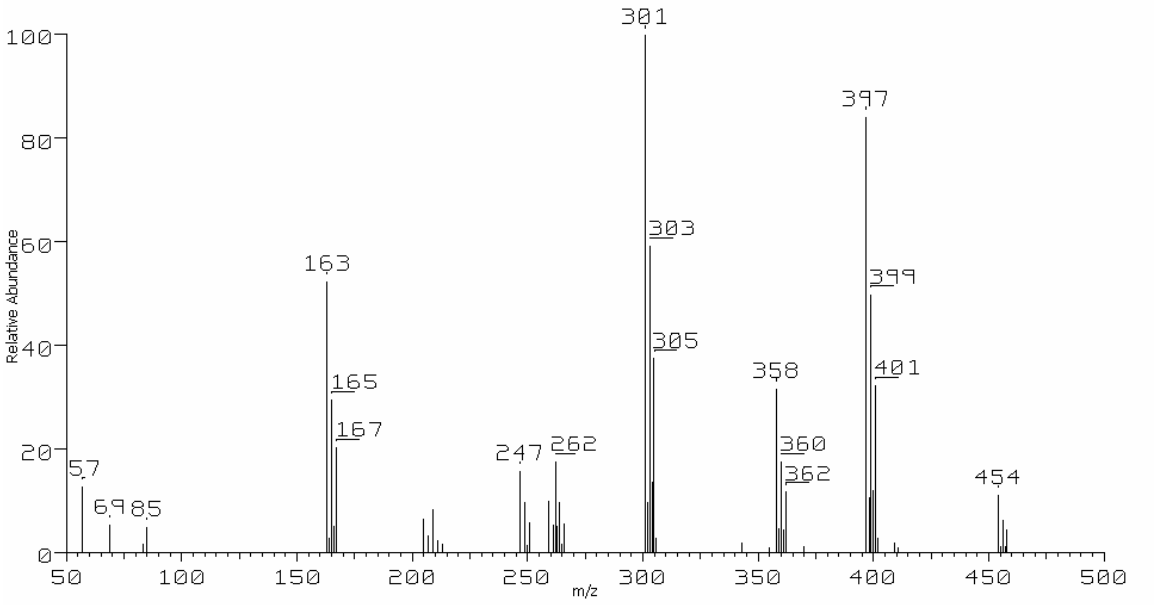

Fig. 4.18 The 70 eV positive EI mass spectrum during the reaction of $Zn(tftm)_2$ with $Zn(acac)_2$

Heteroleptic species are observed for the reaction of $Zn(tftm)_2$ with $Zn(acac)_2$ and is displayed in Fig. 4.18. The species $[Zn(tftm)_1(acac)_1]^+$ is present at m/z 358, where the fragment of this species is actually the base peak at m/z 301. The loss of a ^{t}Bu group is highly favored with the $Zn(tftm)_2$ complex, as shown in section 4.1.1.4, so it is no surprise that the heteroleptic zinc complex readily loses the ^{t}Bu group.

m/z	Species Present	Rel. Ab.
163	$Zn(acac)_1$	52
209	$Zn(tftm)_1$-CF_2	8
247	$Zn(acac)_2$-CH_3	16
259	$Zn(tftm)_1$	10
262	$Zn(acac)_2$	18
301	$Zn(tftm)_1(acac)_1$-^{t}Bu	100
343	$Zn(tftm)_1(acac)_1$-CH_3	3
358	$Zn(tftm)_1(acac)_1$	32
397	$Zn(tftm)_2$-^{t}Bu	84
454	$Zn(tftm)_2$	11

Table 4.17 Relative ion abundances of the ions present in the reaction of $Zn(tftm)_2$ with $Zn(acac)_2$

Another fragment of the heteroleptic species is observed, albeit at low intensity, at m/z 343 due to the loss of a methyl group. The loss of a methyl group is much less stable than the ^{t}Bu ion, thus its loss is generally not as favorable, as evidenced by its low intensity.

4.1.3.5 Homometal Al reactions

Gas-phase reactions between various Al β-diketonate complexes are presented.

4.1.3.5.1 $Al(tftm)_3$ with $Al(acac)_3$

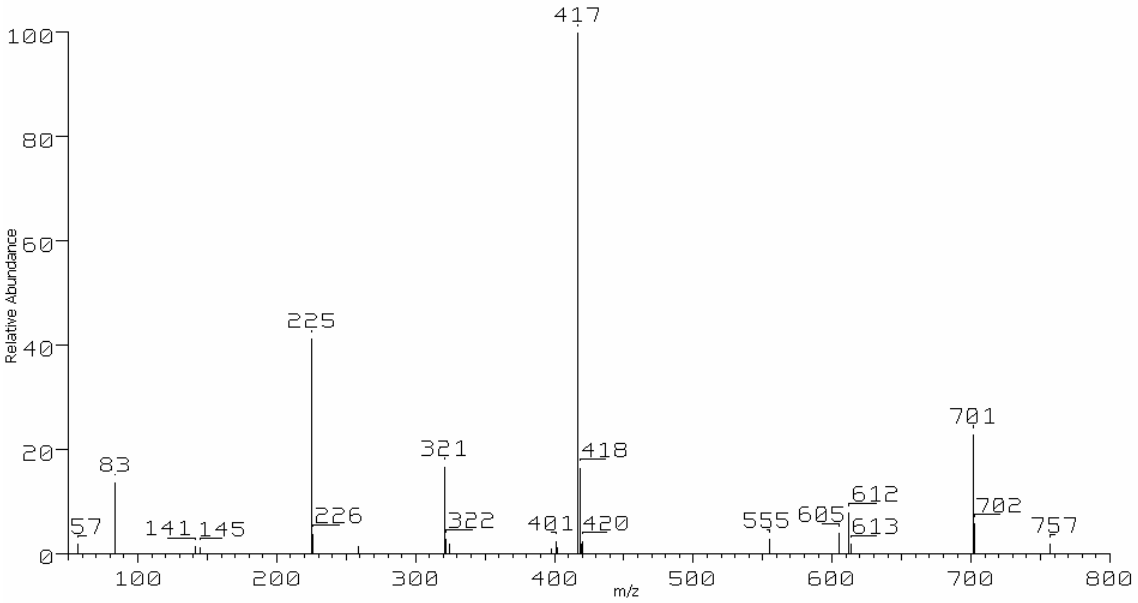

Fig. 4.19 The 70 eV positive EI mass spectrum during the reaction of $Al(tftm)_3$ with $Al(acac)_3$

Multiple heteroleptic species are observed for the reaction of $Al(tftm)_3$ with $Al(acac)_3$ as seen in Fig. 4.19. The most abundant heteroleptic species, $[Al(tftm)_1(acac)_1]^+$, is visible at m/z 321. It is expected that this bis complex is more prevalent than the tris analogs, since aluminum β-diketonate complexes generally prefer the bis arrangement, as our results have shown in section 4.1.1.5.

m/z	Species Present	Rel. Ab.
225	$Al(acac)_2$	41
321	$Al(tftm)_1(acac)_1$	17
324	$Al(acac)_3$	2
417	$Al(tftm)_2$	100
420	$Al(tftm)_1(acac)_2$	3
555	$Al(tftm)_3$-^{t}Bu	3
612	$Al(tftm)_3$	8
701	$Al_2(tftm)_4$-(F, 2^{t}Bu)	23
757	$Al_2(tftm)_4$-(HF, ^{t}Bu)	2

Table 4.18 Relative ion abundances of the species present in the reaction of $Al(tftm)_3$ with $Al(acac)_3$

These results are also concurrent with D. Mains's findings[57]. The only tris species present in the spectrum, $[Al(tftm)_1(acac)_2]^+$, is present at m/z 420, though in low abundance relative to the base peak. The tris arrangement of the complex allows us to assert that the tftm neutral fragment is associating to the $Al(acac)_2$ ion, which is more feasible than two acac neutrals associating to the $Al(tftm)_1$ ion, though this was not the case as shown in 4.1.3.1.2 with the cobalt species.

$$[Al(acac)_3]^+ \rightarrow Al(acac)_2]^+ + acac^0 \qquad \text{Eqn. 4.12}$$

$$[Al(acac)_2]^+ + tftm^0 \rightarrow [Al(acac)_2(tftm)_1]^+ \qquad \text{Eqn. 4.13}$$

Eqn's 4.12 and 4.13 show the mechanism by which the aluminum heteroleptic complex is likely to form. The other heteroleptic species $[Al(acac)_1(tftm)_1]^+$ is expected to form by the process in equation 4.14.

$$[Al(acac)_2(tftm)_1]^+ \rightarrow [Al(acac)_1(tftm)_1]^+ + acac^0 \qquad \text{Eqn. 4.14}$$

Larger aluminum clusters are also observed, thought these have already been reported with the $Al(tftm)_3$ species in section 4.1.1.5.

4.1.3.5.2 $Al(acac)_3$ with $Al(hfac)_3$

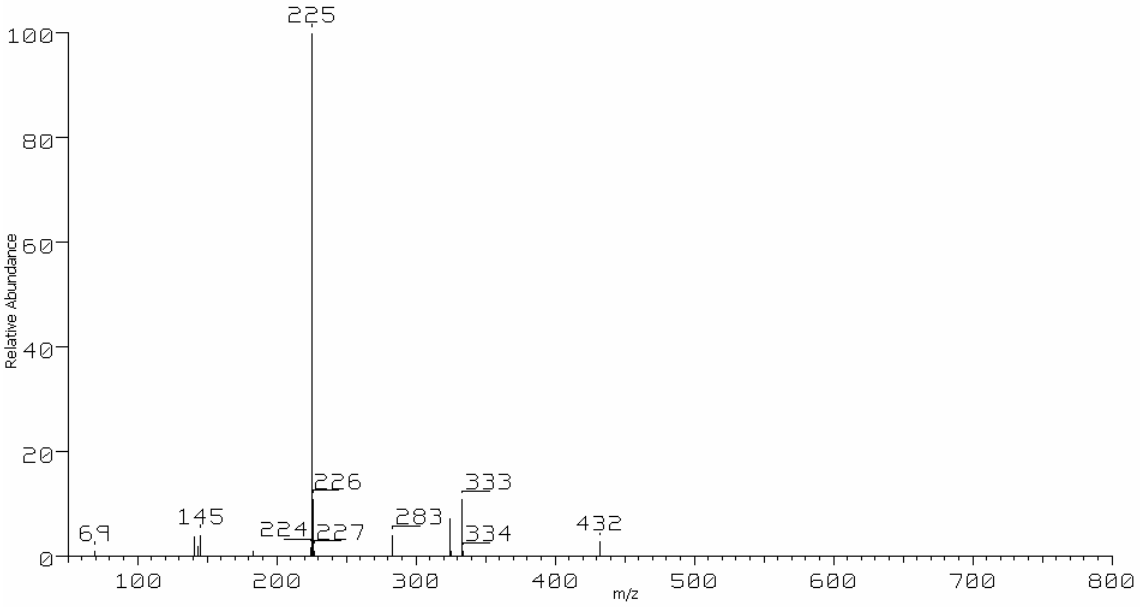

Fig 4.20 The 70 eV positive EI mass spectrum from the reaction of $Al(acac)_3$ with $Al(hfac)_3$

Heteroleptic species are observed for the reaction of $Al(acac)_3$ with $Al(hfac)_3$ as seen in Fig. 4.20. The two heteroleptic species present are $[Al(acac)_1(hfac)_1]^+$ at m/z 333 and $[Al(acac)_2(hfac)_1]^+$ at m/z 432. The tris species, having two acac ligands and one hfac, shows a similar trend observed with the reaction of $Al(tftm)_3$ and $Al(acac)_3$ where the $Al(acac)_n$ species is believed to act as the acceptor for the neutral ligand.

m/z	Species Present	Rel. Ab.
225	$Al(acac)_2$	100
283	$Al(acac)(hfac)_1$-CF_2	4
324	$Al(acac)_3$	7
333	$Al(acac)_1(hfac)_1$	11
432	$Al(acac)_2(hfac)_1$	3

Table 4.19 Relative ion abundances obtained from the reaction of $Al(acac)_3$ with $Al(hfac)_3$

This reaction is the first and only, in this study, to observe F-migration for a species chelated to more than one ligand. The species $[Al(acac)_1(hfac)_1\text{-}CF_2]^+$ present at m/z 283 is both heteroleptic, and has F-migration present. We have observed no other similar species in the homometallic reactions. Also, no clustered complexes were observed for this reaction.

4.1.4 Hetero-metallic gas phase reactions

Two surveys of reactions were performed in the following sections. The first of which was to compare and contrast the differences between the six nickel and copper acac, hfac and tftm complexes. A bilateral approach was used here, where the different metal center was kept constant during each reaction while varying ligand composition. For example, consider the reaction of $Ni(acac)_2$ and $Cu(hfac)_2$, we would also compare the reaction of $Ni(hfac)_2$ and $Cu(hfac)_2$ in order to see if any processes were favored in one reaction over the other, with respect to the reactants. This is a more focused approach than the larger subsequent survey between strictly $M(tftm)_n$ with $M(acac)_n$ and $M(hfac)_n$ complexes.

The second survey consisted of reactions between the five $M(tftm)_2$ compounds synthesized in the lab and a variety of commercially obtained $M(acac)_n$ and $M(hfac)_n$ compounds. The reaction conditions of these reactions were slightly different from those previously stated, where both samples were added to the sample cup as methanolic solutions. It is not believed that much, if any ligand exchange occurred due to the dilute nature of these samples, and the quickness of the evaporation of MeOH.

A similar study was performed by D. Mains concerning only $M(acac)_n$ and $M(hfac)_n$ compounds[57]. We wished to broaden this previous work by the addition of the $M(tftm)_n$ product into the series of reactions in order to compare results with Mains's findings and elucidate any trends present.

The addition of a different metal may help determine the extent to which a specific metal may or may not exchange ligands with other complexes. The addition of another metal center also allows us to observe partially mixed-ligand species, without having to isotopically label parts of the complexes. We knowingly reacted a specific $M(acac)_n$ or $M(hfac)_n$ complex with a $M(tftm)_n$ complex. It is possible for one of the ligands to partially or fully coordinate to the other metal in the reaction. These are not mixed ligand species, but are the result of mixed ligand reactions. It is believed that these species are not created by full ligand loss and then coordination by the neutral species, since no metal ion is present in the spectra other than for copper, but due to subsequent exchange reactions of the ligands to yield fully substituted species, or by ligand exchange followed by loss of initial ligand, to yield partial substitution as stated previously in section 4.1.3.

A spectrum for each reaction is located in the Appendix in section A, though for comparative purposes, multiple tables were constructed to show a side-by-side comparison of the reaction products.

4.1.4.1 Gas phase reactions with Ni and Cu acac, hfac and tftm complexes

This specific set of reactions was done with extra caution taken during preparation to ensure the samples were not in contact with each other. This co-sublimation technique ensures that all reactions should occur strictly in the gas phase.

4.1.4.1.1 Cu and Ni acac and hfac complexes

The following spectra in Fig. 4.21 and data in tables 4.20 and 4.23 describe the heteroleptic products of the reaction of $Ni(acac)_2$ with $Cu(hfac)_2$ and also $Ni(hfac)_2$ with $Cu(acac)_2$. An extensive amount of ligand exchange is occurring in these reactions.

4.21a) $Ni(acac)_2$ and $Cu(hfac)_2$

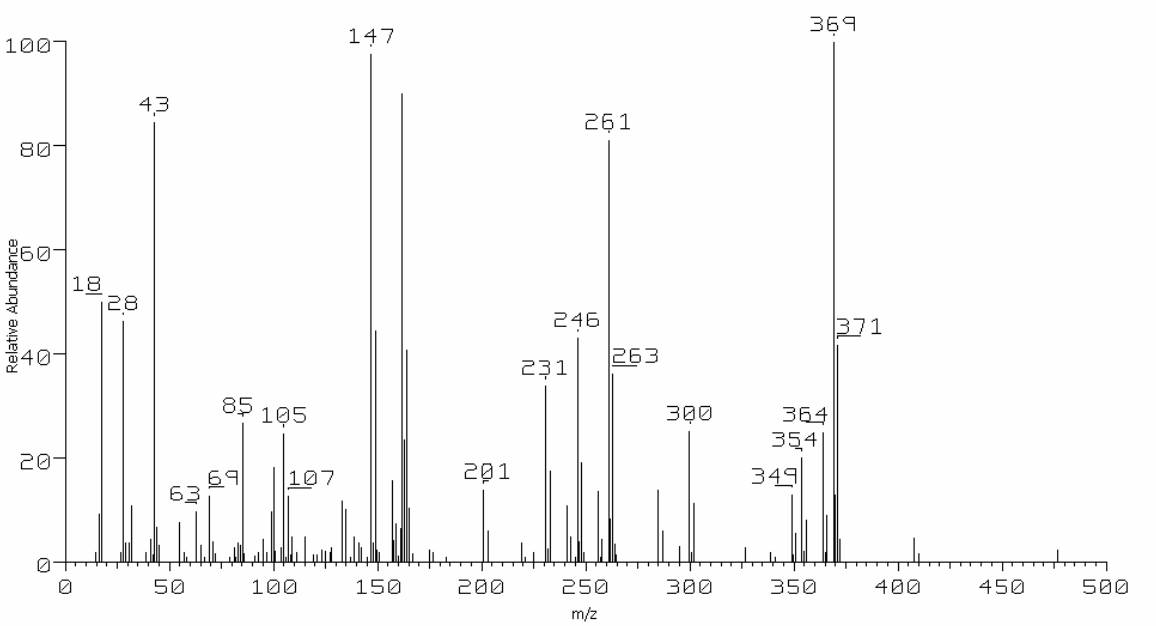

4.21b) $Ni(hfac)_2$ and $Cu(acac)_2$

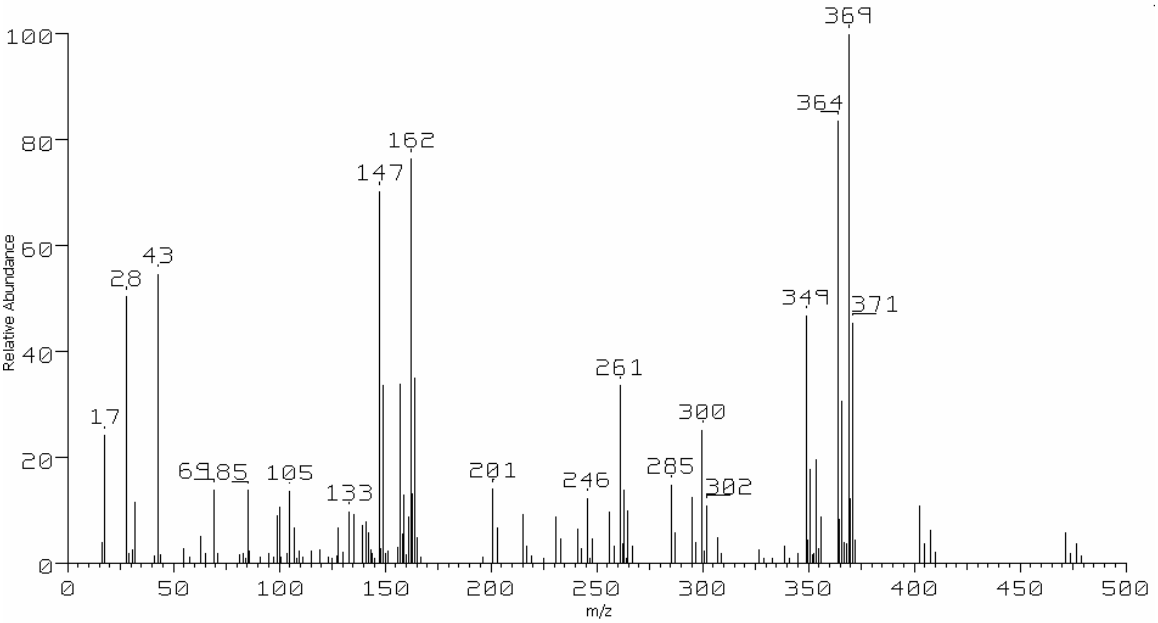

Fig 4.21 The 70 eV positive EI mass spectrum obtained from the reactions of a) $Ni(acac)_2$ with $Cu(hfac)_2$ and b) $Ni(hfac)_2$ and $Cu(acac)_2$

m/z	Species Present	Rel. Ab.	m/z	Species Present	Rel. ab.
369	$Cu(acac)_1(hfac)_1$	100	364	$Ni(acac)_1(hfac)_1$	25
354	$Cu(acac)_1(hfac)_1$-CH_3	20	349	$Ni(acac)_1(hfac)_1$-CH_3	13
339	$Cu(acac)_1(hfac)_1$-2(CH_3)	2	334	$Ni(acac)_1(hfac)_1$-2(CH_3)	0
300	$Cu(acac)_1(hfac)_1$-CF_3	25	295	$Ni(acac)_1(hfac)_1$-CF_3	3
285	$Cu(acac)_1(hfac)_1$-CH_3,CF_3	14	280	$Ni(acac)_1(hfac)_1$-CH_3,CF_3	0
231	$Cu(acac)_1(hfac)_1$-2(CF_3)	34	226	$Ni(acac)_1(hfac)_1$-2(CF_3)	0

Table 4.20 Relative ion abundances abundances of the heteroleptic species obtained during the reaction of of $Ni(acac)_2$ with $Cu(hfac)_2$

m/z	Species Present	Rel. Ab.	m/z	Species Present	Rel. Ab.
369	$Cu(acac)_1(hfac)_1$	100	364	$Ni(acac)_1(hfac)_1$	84
354	$Cu(acac)_1(hfac)_1$-CH_3	20	349	$Ni(acac)_1(hfac)_1$-CH_3	47
339	$Cu(acac)_1(hfac)_1$-2(CH_3)	3	334	$Ni(acac)_1(hfac)_1$-2(CH_3)	0
300	$Cu(acac)_1(hfac)_1$-CF_3	25	295	$Ni(acac)_1(hfac)_1$-CF_3	13
285	$Cu(acac)_1(hfac)_1$-CH_3,CF_3	15	280	$Ni(acac)_1(hfac)_1$-CH_3,CF_3	0
231	$Cu(acac)_1(hfac)_1$-2(CF_3)	9	226	$Ni(acac)_1(hfac)_1$-2(CF_3)	0

Table 4.21 Relative ion abundances abundances of the heteroleptic species obtained during the reaction of of $Ni(hfac)_2$ and $Cu(acac)_2$

The data reported above is clear evidence for ligand exchange. The mixed ligand species, in the case of Cu for both reactions, is the base peak in each spectrum. This shows a high degree of exchange while the high abundance of this species shows that it is quite stable. The Ni analog of the heteroleptic species is also intense, again leading us to believe these are quite stable complexes.

The fragments of these complexes are also routinely prominent in the spectra. These fragments are typical to their respective homoleptic species though, and are expected. The loss of a methyl group or a CF_3 group is a again observed as a common loss channel.

Considering both reactions, it appears that the same products are formed for each reaction. It would appear that, with this combination of metals and ligands, that the pathways taken to form the products are not reactant dependent.

4.1.4.1.2 Cu and Ni hfac and tftm complexes

4.22a) $Ni(hfac)_2$ & $Cu(tftm)_2$

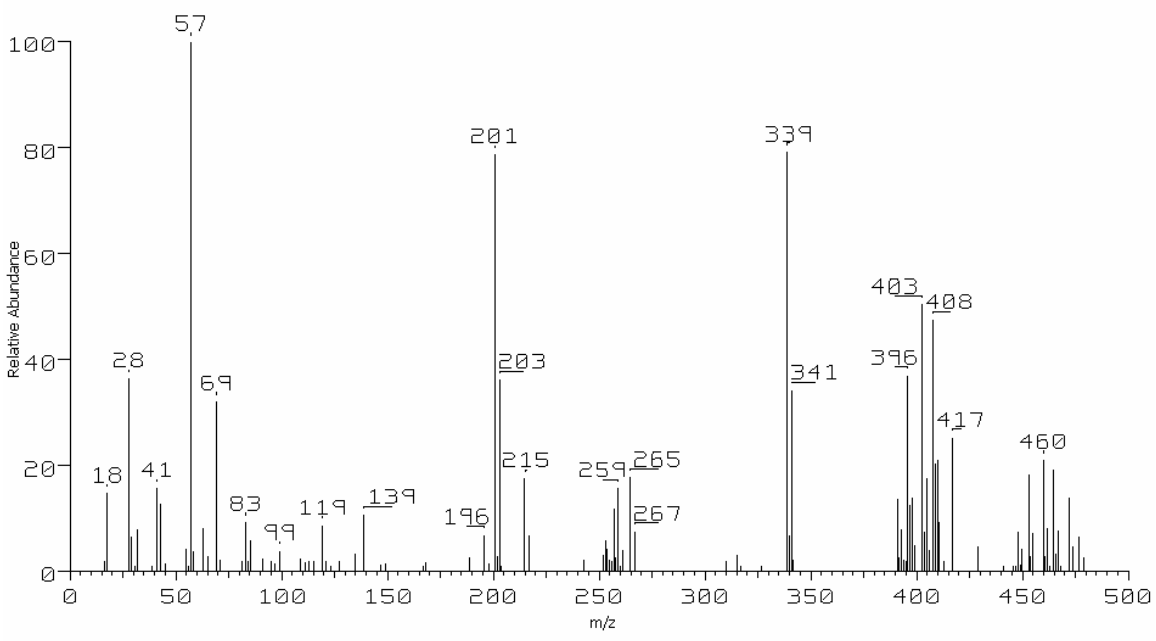

4.22b) $Ni(tftm)_2$ & $Cu(hfac)_2$

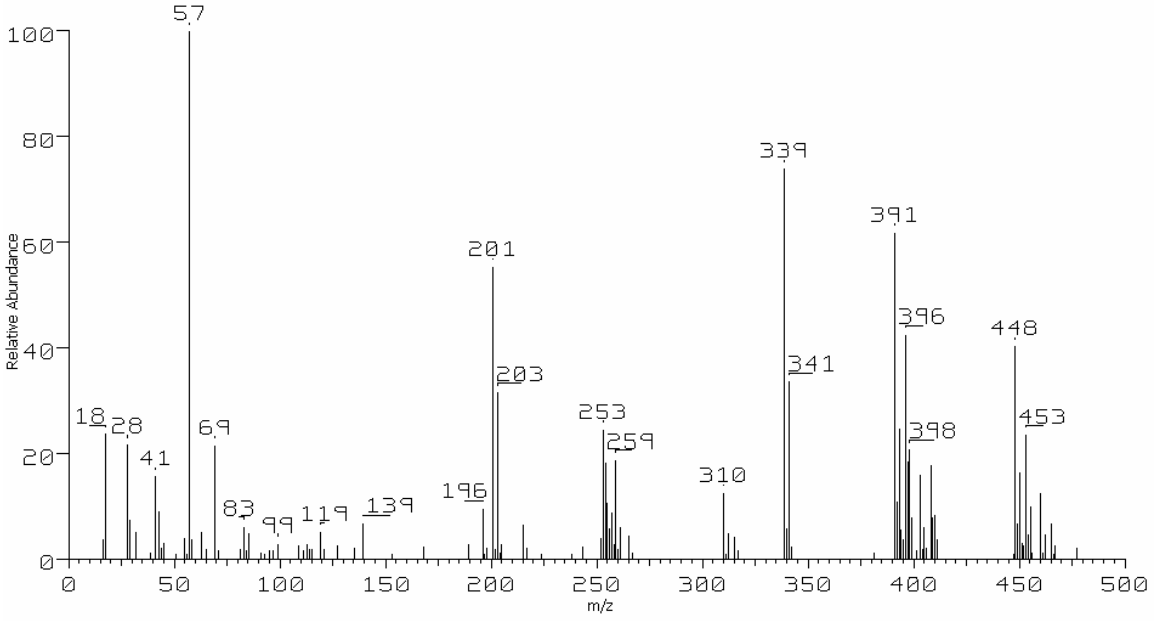

Fig. 4.22 The 70 eV positive EI mass spectrum obtained from the reactions of a) $Ni(hfac)_2$ with $Cu(tftm)_2$ and b) $Ni(tftm)_2$ and $Cu(hfac)_2$

m/z	Species	Rel. Ab.	m/z	Species	Rel. Ab.
465	$Cu(hfac)_1(tftm)_1$	19	460	$Ni(hfac)_1(tftm)_1$	21
408	$Cu(hfac)_1(tftm)_1$-^{t}Bu	47	403	$Ni(hfac)_1(tftm)_1$-^{t}Bu	50
396	$Cu(hfac)_1(tftm)_1$-CF_3	37	391	$Ni(hfac)_1(tftm)_1$-CF_3	14
351	$Cu(hfac)_1(tftm)_1$-2(^{t}Bu)	0	346	$Ni(hfac)_1(tftm)_1$-2(^{t}Bu)	0
339	$Cu(hfac)_1(tftm)_1$-CF_3,^{t}Bu	79	334	$Ni(hfac)_1(tftm)_1$-CF_3,^{t}Bu	0
327	$Cu(hfac)_1(tftm)_1$-2(CF_3)	1	322	$Ni(hfac)_1(tftm)_1$-2(CF_3)	0

Table 4.22 Relative ion abundances abundances of the heteroleptic species obtained during the reaction of $Ni(hfac)_2$ and $Cu(tftm)_2$

m/z	Species	Rel. Ab.	m/z	Species	Rel. Ab.
465	$Cu(hfac)_1(tftm)_1$	7	460	$Ni(hfac)_1(tftm)_1$	13
408	$Cu(hfac)_1(tftm)_1$-^{t}Bu	18	403	$Ni(hfac)_1(tftm)_1$-^{t}Bu	16
396	$Cu(hfac)_1(tftm)_1$-CF_3	43	391	$Ni(hfac)_1(tftm)_1$-CF_3	62
351	$Cu(hfac)_1(tftm)_1$-2(^{t}Bu)	0	346	$Ni(hfac)_1(tftm)_1$-2(^{t}Bu)	0
339	$Cu(hfac)_1(tftm)_1$-CF_3,^{t}Bu	74	334	$Ni(hfac)_1(tftm)_1$-CF_3,^{t}Bu	0
327	$Cu(hfac)_1(tftm)_1$-2(CF_3)	0	322	$Ni(hfac)_1(tftm)_1$-2(CF_3)	0

Table 4.23 Relative ion abundances abundances of the heteroleptic species obtained during the reaction of $Ni(tftm)_2$ and $Cu(hfac)_2$

The spectra shown in Fig. 4.22, coupled with the data presented in tables 4.22 and 4.23 describe the heteroleptic products of the reaction of $Ni(hfac)_2$ with $Cu(tftm)_2$ and $Ni(tftm)_2$ with $Cu(hfac)_2$. According to this data, ligand exchange reactions are prevalent in this reaction.

From these results, one can clearly see that ligand exchange is occurring between the copper and nickel hfac and tftm complexes. The intensities of the non-fragmented heteroleptic species are not as high as the fragmented forms, though this is analogous to the homoleptic species fragmentation. The ^{t}Bu and CF_3 groups are common fragments. As was the case in section 4.1.2.1.1, all of the observed heteroleptic products are not dependent upon the starting material composition, meaning these reactions are occurring bilaterally.

4.1.4.1.3 Cu and Ni acac and tftm complexes

4.23a) $Ni(tftm)_2$ & $Cu(acac)_2$

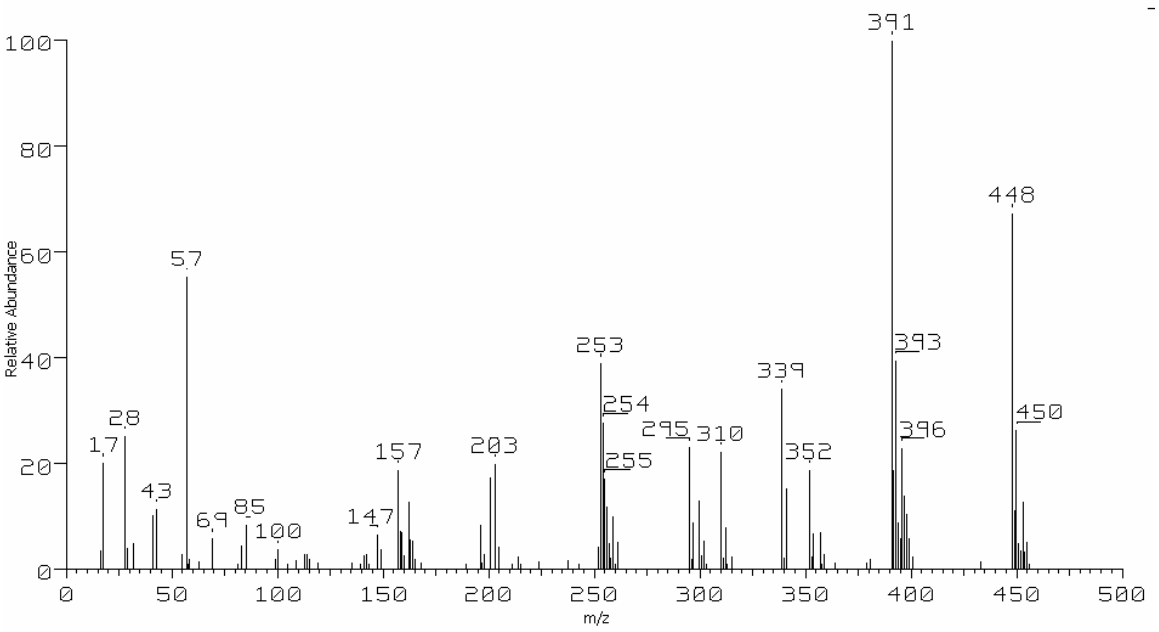

4.23b) $Ni(acac)_2$ & $Cu(tftm)_2$

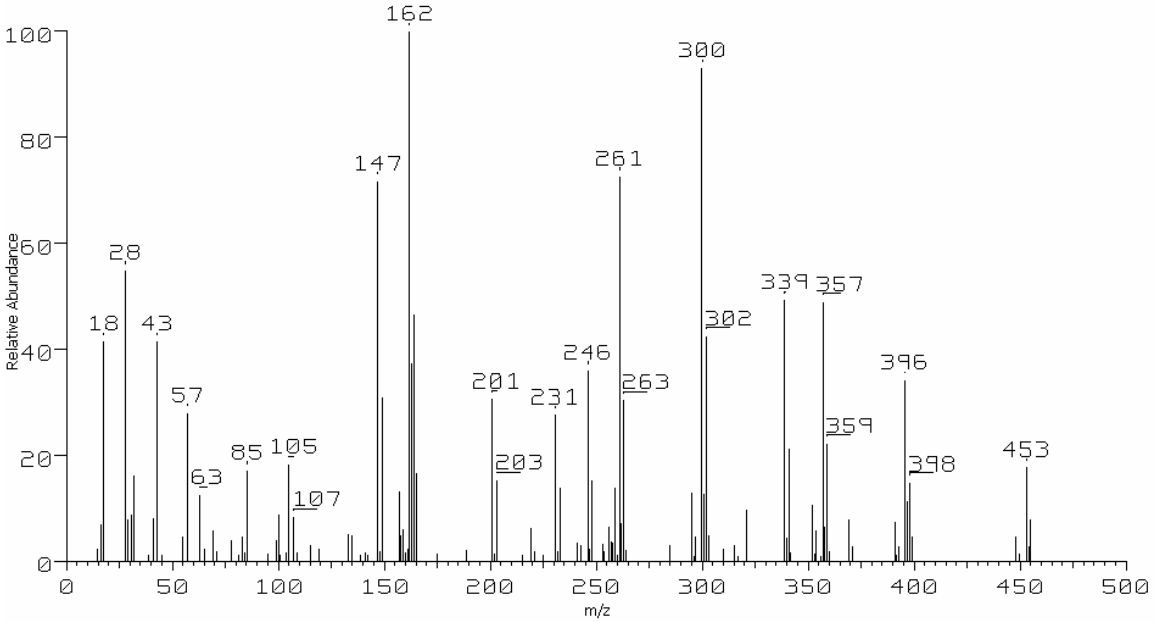

Fig. 4.23 The 70 eV positive EI mass spectrum obtained from the reactions of a) $Ni(tftm)_2$ with $Cu(acac)_2$ and b) $Ni(acac)_2$ and $Cu(tftm)_2$

m/z	Species Present	Rel. Ab.	m/z	Species Present	Rel. Ab.
357	$Cu(acac)_1(tftm)_1$	7	352	$Ni(acac)_1(tftm)_1$	19
342	$Cu(acac)_1(tftm)_1$-CH_3	0	337	$Ni(acac)_1(tftm)_1$-CH_3	0
300	$Cu(acac)_1(tftm)_1$-^{t}Bu	13	295	$Ni(acac)_1(tftm)_1$-^{t}Bu	23
288	$Cu(acac)_1(tftm)_1$-CF_3	0	283	$Ni(acac)_1(tftm)_1$-CF_3	0
285	$Cu(acac)_1(tftm)_1$-CH_3,^{t}Bu	0	280	$Ni(acac)_1(tftm)_1$-CH_3,^{t}Bu	0
273	$Cu(acac)_1(tftm)_1$-CH_3,CF_3	0	268	$Ni(acac)_1(tftm)_1$-CH_3,CF_3	0
231	$Cu(acac)_1(tftm)_1$-CF_3,^{t}Bu	0	226	$Ni(acac)_1(tftm)_1$-CF_3,^{t}Bu	0

Table 4.24 Relative ion abundances abundances of the heteroleptic species obtained during the reaction of $Ni(tftm)_2$ & $Cu(acac)_2$

m/z	Species Present	Rel. Ab.	m/z	Species Present	Rel. Ab.
357	$Cu(acac)_1(tftm)_1$	49	352	$Ni(acac)_1(tftm)_1$	11
342	$Cu(acac)_1(tftm)_1$-CH_3	2	337	$Ni(acac)_1(tftm)_1$-CH_3	0
300	$Cu(acac)_1(tftm)_1$-^{t}Bu	93	295	$Ni(acac)_1(tftm)_1$-^{t}Bu	13
288	$Cu(acac)_1(tftm)_1$-CF_3	0	283	$Ni(acac)_1(tftm)_1$-CF_3	0
285	$Cu(acac)_1(tftm)_1$-CH_3,^{t}Bu	3	280	$Ni(acac)_1(tftm)_1$-CH_3,^{t}Bu	0
273	$Cu(acac)_1(tftm)_1$-CH_3,CF_3	0	268	$Ni(acac)_1(tftm)_1$-CH_3,CF_3	0
231	$Cu(acac)_1(tftm)_1$-CF_3,^{t}Bu	28	226	$Ni(acac)_1(tftm)_1$-CF_3,^{t}Bu	0

Table 4.25 Relative ion abundances abundances of the heteroleptic species obtained during the reaction of $Ni(acac)_2$ & $Cu(tftm)_2$

The spectra in Fig. 4.23 coupled with the data presented in tables 4.24 and 4.25 present the heteroleptic products observed during the reactions of $Ni(acac)_2$ with $Cu(tftm)_2$ and $Ni(tftm)_2$ with $Cu(acac)_2$. The data presented suggests ligand exchange reactions are occurring.

The tables shown above illustrate that heteroleptic species are prevalent products in these reactions between acac and tftm complexes. Again, common fragments are exhibited for all heteroleptic species. However, this set of reactions gives us the first case of mixed products only being formed for one of two reactions. For example, the species $[Cu(acac)_1(tftm)_1(-CF_3)(-^tBu)]^+$ present at m/z 231 at relatively high abundance, is only observed for the reaction of $Ni(acac)_2$ with $Cu(tftm)_2$ and not the reverse. Two other species, due to the loss of a methyl group and the other due to the loss of a methyl and ^{t}Bu group are also observed, but due to their low abundances, they are not considered to be a dominant pathway.

It is unknown why this species at m/z 231 is only present unilaterally, especially since this is a fragmented species which, by our mechanism stated in section 4.1.4, should be present in both.

4.1.4.2 $M(tftm)_n$ with $M(acac)_n$ reactions

4.1.4.2.1 $Co(tftm)_2$ with $M(acac)_n$

Species Present	$Cr(acac)_3$	$Mn(acac)_2$	$Fe(acac)_3$	$Ni(acac)_2$	$Zn(acac)_2$	$Al(acac)_3$
$Co(acac)_1$-CH_3		p		p		p
$Co(acac)_1$		p	p	p	p	p
$Co(acac)_2$-CH_3			p	p	p	
$Co(tftm)_1$	p	p	p*	p	p	p
$Co(acac)_2$		p	p	p	p	
$Co(tftm)_1(acac)_1$-^{t}Bu	p	p	p	p	p	p
$Co(tftm)_2$-2(CF_3)	p	p		p	p	
$Co(tftm)_1(acac)_1$		P	p*	p	p	p
$Co(tftm)_2$-^{t}Bu	p	p	p	p	p	p
$Co(tftm)_2$	p	p	p*	p	p	p
$M(acac)_1$	p	p	p	p	p	
$M(acac)_2$-CH_3	p		p	p	p	
$M(tftm)_1$		p	p*	p	p	
$M(acac)_2$	p		p*	p	p	p
$M(tftn)_1(acac)_1$-^{t}Bu		p	p	p	p	
$M(tftm)_2$-2(CF_3)			p	p		
$M(tftm)_1(acac)_1$		p	p	p	p	p
$M(acac)_3$	p		p*			p
$M(tftm)_2$-^{t}Bu		p	p	p	p	
$M(tftm)_2$		p	p	p	p	p
$M(tftm)_1(acac)_2$			p*			p
$M(tftm)_2(acac)_1$						p

Table 4.26 Positive identification of species present in the reaction of $Co(tftm)_2$ with various $M(acac)_n$ complexes is denoted with a p. Note M = the other metal involved in the reaction (Cr, Mn, Fe, Ni, Zn or Al) *denotes isobaric species

Table 4.26, shown above, shows a summary of the products present in the reaction between $Co(tftm)_2$ and various $M(acac)_n$ species as observed using mass spectrometry over a variety of temperatures. Regarding the cobalt metal center, mixed ligand species are present for all reactions except with $Cr(acac)_3$, though a fragment of the mixed ligand species, $[Co(tftm)_1(acac)_1$-^{t}Bu$]^+$, is present in the reaction with $Cr(acac)_3$.

The presence of this species is likely to stem from the fragmentation of a complex formed from the ion-neutral reaction between the neutral acac ligand, and the $[Co(tftm)_1]^+$ ion, followed by fragmentation of the ^{t}Bu group. The loss of a ^{t}Bu group is a very common occurance, as was shown in section 4.1.1. The ion $[Co(acac)_1(tftm)_1]^+$ may just not be present in great enough abundance to be visible in the mass spectrometer, or the fragmented species may be much more highly favored, as is commonly observed in the homo-metal reactions.

Full substitution of the tftm ligand on the cobalt center to yield $[Co(acac)_2]^+$ is observed for all species except chromium and aluminum. Though, partial substitution to form the species $[Co(acac)_1]^+$ is observed for all reactions except with $Cr(acac)_3$.

Regarding the other metal involved in the reaction, the mixed ligand species $[M(acac)_1(tftm)_1]^+$ was observed for all reactions except with $Cr(acac)_3$. Tris-chelated heteroleptic species are observed for reactions with the tris-acac species $Fe(acac)_3$ and $Al(acac)_3$. Each of these reactions yielded the primary substitution product $[M(acac)_2(tftm)_1]^+$, while only the reaction with Al yielded the secondary product $[Al(acac)_1(tftm)_2]^+$. No reactions yielded the $[M(tftm)_3]^+$ complex.

The partially substituted species $[M(tftm)_1]^+$ was observed for all reactions except for those with $Cr(acac)_3$ and $Al(acac)_3$, though the bis-species $[M(tftm)_2]^+$ was present for all reactions except with chromium.

4.1.4.2.2 $Ni(tftm)_2$ with $M(acac)_n$

Species Present	$Cr(acac)_3$	$Mn(acac)_2$	$Co(acac)_3$	$Zn(acac)_2$	$Al(acac)_3$
$Ni(acac)_1$-CH_3			p		p
$Ni(acac)_1$		p	p	p	p
$Ni(tftm)_1$-CF_3		p			
$Ni(tftm)_1$-^{t}Bu		p	p		
$Ni(acac)_2$-CH_3				p	
$Ni(tftm)_1$	p	p	p	p	p
$Ni(acac)_2$		p	p	p	p
$Ni(tftm)_1(acac)_1$-^{t}Bu	p	p	p	p	p
$Ni(tftm)_2$-2(CF_3)	p	p	p	p	p
$Ni(tftm)_1(acac)_1$	p	p	p	p	p
$Ni(tftm)_2$-^{t}Bu	p	p	p	p	p
$Ni(tftm)_2$	p	p	p	p	p
$M(acac)_1$-CH_3			p		
$M(acac)_1$	p		p	p	
$M(acac)_2$-CH_3			p	p	
$M(tftm)_1$	p	p	p	p	
$M(acac)_2$	p	p	p	p	p
$M(tftm)_1(acac)_1$-^{t}Bu		p	p	p	
$M(tftm)_2$-2(CF_3)			p		
$M(tftm)_1(acac)_1$	p		p	p	p
$M(acac)_3$	p	p	p		
$M(tftm)_2$-^{t}Bu		p	p	p	
$M(tftm)_2$	p	p	p	p	p
$M(tftm)_1(acac)_2$	p	p	p		p
$M(tftm)_2(acac)_1$	p		p		p

Table 4.27 Positive identification of species present in the reaction of $Ni(tftm)_2$ with various $M(acac)_n$ complexes. Note M = the other metal involved in the reaction

Table 4.27 shows a summary of the gas phase reactions between $Ni(tftm)_2$ and various metal-acetylacetonates. The mixed ligand species $[Ni(tftm)_1(acac)_1]^+$ is present for all reactions and the partial substitution to yield $[Ni(acac)_1]^+$ is observed for all reactions except for with $Cr(acac)_3$, and the same result is observed for the full substitution of $Ni(tftm)_2$ to yield the species $[Ni(acac)_2]^+$.

The other metal involved in the reactions, in the form of an acetylacetonate complex, is observed as a mixed ligand product for all reactions except with $Mn(acac)_2$, though a fragment of $[Mn(tftm)_1(acac)_1$-^{t}Bu$]^+$ is observed.

Consequently, this leads us to believe that all reactions between $Ni(tftm)_2$ and the $M(acac)_n$ complexes listed above create mixed ligand species.

$$[M(acac)_1(tftm)_1]^+ \rightarrow [M(acac)_1(tftm)_1\text{-}{}^t\!Bu]^+ + {}^t\!Bu^0 \qquad \text{Eqn. 4.15}$$

The mechanism by which we propose the fragmented bis-heteroleptic complex is formed is described in Eqn. 4.15, while the formation of that heteroleptic species was discussed earlier in section 4.1.3. By the mechanism in Eqn. 4.15, the intact heteroleptic species must form, followed by subsequent loss of a ^{t}Bu group. As stated previously, the loss of a ^{t}Bu group is highly favored in most of these complexes, and in 4.1.1.2, it is seen that for the $Ni(tftm)_2$ complex, the loss of a ^{t}Bu group is favored over the molecular ion.

Tris-chelated heteroleptic complexes were observed for each reaction with a tris-acetylacetonate complex, specifically for $Cr(acac)_3$, $Co(acac)_3$ and $Al(acac)_3$. Each of these three reactions show evidence for both possible arrangements of the tris-heteroleptic complex in the forms of $[M(tftm)_1(acac)_2]^+$ and $[M(tftm)_2(acac)_1]^+$, though full substitution to yield $[M(tftm)_3]^+$ is not observed.

The partially substituted species $[M(tftm)_1]^+$ is observed for all reactions except with $Al(acac)_3$, though $[M(tftm)_2]^+$ is observed for all reactions.

4.1.4.2.3 $Cu(tftm)_2$ with $M(acac)_n$

Species Present	$Cr(acac)_3$	$Fe(acac)_3$	$Co(acac)_2$	$Co(acac)_3$	$Zn(acac)_2$	$Al(acac)_3$
Cu	p		p	p	p	
$Cu(acac)_1$-CH_3		p	p	p	p	p
$Cu(acac)_1$		p	p	p	p	p
$Cu(tftm)_1$-CF_3	p			p		
$Cu(tftm)_1$-^{t}Bu	p	p	p	p	p	p
$Cu(acac)_2$-2(CH_3)		p	p		p	p
$Cu(acac)_2$-CH_3		p	p		p	p
$Cu(acac)_2$		p	p		p	p
$Cu(tftm)_1(acac)_1$-CF_3		p	p	p	p	p
$Cu(tftm)_2$-2(CF_3)	p			p	p	
$Cu(tftm)_2$-2(^{t}Bu)	p	p	p	p	p	p
$Cu(tftm)_1(acac)_1$		p	p	p	p	p
$Cu(tftm)_2$-^{t}Bu	p	p	p	p	p	p
$Cu(tftm)_2$	p	p	p	p	p	p
$Cu(tftm)_1(acac)_2$					p	
$M(acac)_1$	p	p	p	p	p	
$M(tftm)_1$-^{t}Bu					p	
$M(acac)_2$-CH_3			p	p	p	
$M(tftm)_1$		p	p		p	
$M(acac)_2$	p	p	p	p	p	p
$M(tftm)_1(acac)_1$-^{t}Bu		p	p	p	p	
$M(tftm)_2$-2(CF_3)			p			
$M(tftm)_2$-2(^{t}Bu)					p	
$M(tftm)_1(acac)_1$	p	p	p		p	p
$M(acac)_3$	p		p	p		p
$M(tftm)_2$-^{t}Bu		p	p		p	
$M(tftm)_2$		p	p		p	p
$M(tftm)_1(acac)_2$		p				p
$M(tftm)_2(acac)_1$		p				

Table 4.28 Positive identification of species present in the reaction of $Cu(tftm)_2$ with various $M(acac)_n$ complexes. Note M = the other metal involved in the reaction

Table 4.28, shown above, shows a summary of the species present upon the reaction of $Cu(tftm)_2$ with various metal-acetylacetonates. The mixed ligand complex $[Cu(tftm)_1(acac)_1]^+$ and the partially substituted complex $[Cu(acac)_1]^+$ are present for all reactions except with $Cr(acac)_3$. $[Cu(acac)_2]^+$ is observed for all reactions except with $Cr(acac)_3$ and $Co(acac)_3$.

The other metal involved in the reaction yields the mixed ligand product $[M(tftm)_1(acac)_1]^+$ and is believed to form for all reactions, even though that specific species is not present itself for the reaction with $Co(acac)_3$ since a fragment due to the loss of a ^{t}Bu group is present in that reaction. Higher order heteroleptic species are present for the reactions with $Fe(acac)_3$ and $Al(acac)_3$. The primary substitution of the $M(acac)_3$ is observed for both, while the secondary substitution is only observed for the reaction with $Fe(acac)_3$.

Partial substitution to yield the $[M(tftm)_1]^+$ species is observed for reactions with $Fe(acac)_3$, $Co(acac)_3$ and $Zn(acac)_2$, with the same result observed for the species $[M(tftm)_2]^+$.

4.1.4.2.4 $Zn(tftm)_2$ with $M(acac)_n$

Species Present	$Cr(acac)_3$	$Mn(acac)_2$	$Fe(acac)_3$	$Co(acac)_2$	$Co(acac)_3$	$Ni(acac)_2$	$Al(acac)_3$
$Zn(acac)_1$		p	p	p	p	p	p
$Zn(tftm)_1$-^{t}Bu	p	p		p	p		
$Zn(acac)_2$-CH_3			p	p		p	
$Zn(tftm)_1$	p	p		p	p	p	p
$Zn(acac)_2$			p	p		p	
$Zn(tftm)_1(acac)_1$-^{t}Bu		p	p	p	p	p	p
$Zn(tftm)_1(acac)_1$			p	p	p	p	
$Zn(tftm)_2$-^{t}Bu	p	p	p	p	p	p	p
$Zn(tftm)_2$	p	p		p	p	p	p
$M(acac)_1$-CH_3						p	
$M(acac)_1$	p		p	p	p	p	
$M(acac)_2$-CH_3			p	p	p	p	
$M(tftm)_1$		p	p	p		p	
$M(acac)_2$	p		p	p	p	p	p
$M(tftm)_1(acac)_1$-^{t}Bu			p	p	p	p	
$M(tftm)_2$-2(CF_3)						p	
$M(tftm)_2$-2(^{t}Bu)							p
$M(tftm)_1(acac)_1$	p		p	p		p	p
$M(acac)_3$	p		p		p	p	p
$M(tftm)_2$-^{t}Bu		p		p	p	p	
$M_2(acac)_3$	p						
$M(tftm)_2$		p	p	p		p	
$M(tftm)_1(acac)_2$	p		p				
$M(tftm)_2(acac)_1$			p				

Table 4.29 Positive identification of species present in the reaction of $Zn(tftm)_2$ with various $M(acac)_n$ complexes. Note M = the other metal involved in the reaction

Table 4.29 shows the results of reactions of $Zn(tftm)_2$ with various $M(acac)_n$ complexes. Mixed ligand species are present for all reactions except with $Cr(acac)_3$, though $Mn(acac)_2$ and $Al(acac)_3$ only show fragments of this species. $[Zn(acac)_1]^+$ is present for all reactions except with $Cr(acac)_3$. The fully substituted $[Zn(acac)_2]^+$ species is only present in reactions with $Fe(acac)_3$, $Co(acac)_2$ and $Ni(acac)_2$.

The other metal involved in the reaction yields the mixed ligand species $[M(tftm)_1(acac)_1]^+$ for all reactions except with $Mn(acac)_2$, though it is only present as a fragment for $Co(acac)_3$.

The tris heteroleptic species are observed only for the reaction with $Fe(acac)_3$ and is present as both primary and secondary substitution of the molecular ion.

Partial substitution to yield $[M(tftm)_1]^+$ and $[M(tftm)_2]^+$ is observed for $Fe(acac)_3$, $Mn(acac)_2$, $Co(acac)_2$ and $Ni(acac)_2$, yet no $[M(tftm)_3]^+$ is observed for any reaction.

4.1.4.2.5 $Al(tftm)_3$ with $M(acac)_n$

Species Present	$Cr(acac)_3$	$Mn(acac)_2$	$Co(acac)_2$	$Co(acac)_3$	$Ni(acac)_2$	$Zn(acac)_2$
$Al(acac)_2$	p	p	p		p	p
$Al(tftm)_1(acac)_1$-CF_3	p					
$Al(tftm)_1(acac)_1$	p	p	p		p	p
$Al(tftm)_2$-CF_3					p*	
$Al(tftm)_2$	p	p	p	p	p	p
$Al(tftm)_1(acac)_2$			p		p*	p*
$Al(tftm)_2(acac)_1$		p*	p		p*	p*
$Al(tftm)_3$-^{t}Bu			p		p	
$Al(tftm)_3$	p	p	p	p*	p	p
$M(acac)_1$-CH_3			p			
$M(acac)_1$	p	p*	p	p	p	p
$M(tftm)_1$-^{t}Bu						
$M(acac)_2$-CH_3	p		p	p	p	p
$M(tftm)_1$		p*	p		p	p
$M(acac)_2$	p	p*	p	p	p	p
$M(tftm)_1(acac)_1$-^{t}Bu		p*	p	p*	p	p
$M(tftm)_2$-$2(CF_3)$			p*		p	
$M(tftm)_1(acac)_1$	p	p*	p		p	p
$M(acac)_3$	p			p		
$M(tftm)_2$-^{t}Bu		p*	p		p	p
$M_2(acac)_3$			p			
$M(tftm)_2$		p*	p*		p	p*
$M(tftm)_1(acac)_2$	p					

Table 4.30 Positive identification of species present in the reaction of $Al(tftm)_3$ with various $M(acac)_n$ complexes. Note M = the other metal involved in the reaction. *denotes nominal mass assurance only

Table 4.30 shows a summary of the reactions of $Al(tftm)_3$ with various $M(acac)_n$ complexes. This specific set of reactions had particularly low intensities of some species, so nominal mass assurance was used in conjunction with the previous data regarding the formation and fragmentation to determine the identity of these compounds.

The mixed ligand species $[Al(tftm)_1(acac)_1]^+$ is present for all reactions except with $Co(acac)_3$. Tris-chelated heteroleptic species are observed for reactions with $Mn(acac)_2$, $Co(acac)_2$, $Ni(acac)_2$ and $Zn(acac)_2$. The primary substitution, to yield $[Al(tftm)_1(acac)_2]^+$, occurs for each of the four species except $Mn(acac)_2$, and the species $[Al(tftm)_2(acac)_1]^+$ is present for all four. It is unknown why the reaction with $Mn(acac)_3$ yielded the secondary substitution product, and not the primary.

Partial substitution of the aluminum center to yield $[Al(acac)_2]^+$ is present for all reactions except with $Co(acac)_3$. No $[Al(acac)_3]^+$ is observed.

The other metal center involved in the reaction yields the heteroleptic species $[M(tftm)_1(acac)_1]^+$ for all reactions except for $Co(acac)_3$, where it is observed as a fragment with the loss of a ^{t}Bu group. Only one tris-chelated heteroleptic species is observed, and that species is $[Cr(tftm)_1(acac)_2]^+$.

Partial substitution to yield the species $[M(tftm)_1]^+$ and $[M(tftm)_2]^+$ follow the same pattern, where they are observed for all reactions other than with $Cr(acac)_3$ and $Co(acac)_3$ and no $[M(tftm)_3]^+$ is observed.

4.1.4.3 $M(tftm)_n$ with $M(hfac)_n$ reactions

4.1.4.3.1 $Co(tftm)_2$ with $M(hfac)_n$

Species Present	$Mn(hfac)_2$	$Fe(hfac)_2$	$Ni(hfac)_2$	$Cu(hfac)_2$	$Al(hfac)_3$
$Co(tftm)_1$	p	p	p	p	p
$Co(hfac)_1$	p	p	p	p	p
$Co(tftm)_2$-CF_3	p	p	p		p
$Co(tftm)_1$-^{t}Bu	p	p	p	p	p
$Co(hfac)_2$-CF_3 or $Co(tftm)_1(hfac)_1$-^{t}Bu	p	p	p	p	p
$Co(tftm)_1$	p	p	p	p	p
$Co(tftm)_1(hfac)_1$	p	p	p	p	p
$Co(hfac)_2$	p	p	p	p	
M				p	
$M(tftm)_1$-^{t}Bu or $M(hfac)_1$-CF_3			p	p	
$M(tftm)_1$	p	p	p	p	
$M(hfac)_1$	p	p	p		
$M(tftm)_2$-2(CF_3)			p		
$M(tftm)_2$-2(^{t}Bu) or $M(hfac)_2$-2(CF_3)				p	
$M(tftm)_2$-^{t}Bu	p	p	p	p	
$M(hfac)_2$-CF_3 $M(hfac)_1(tftm)_1$-^{t}Bu	p	p	p	p	
$M(tftm)_2$	p	p	p	p	p
$M(tftm)_1(hfac)_1$	p	p	p	p	p
$M(hfac)_2$	p	p	p	p	p
$M(tftm)_3$		p			p
$M(tftm)_2(hfac)_1$		p			p

Table 4.31 Positive identification of species present in the reaction of $Co(tftm)_2$ with various $M(hfac)_n$ complexes. Note M = the other metal involved in the reaction

Table 4.31 shows a summary of the species present during the reaction of $Co(tftm)_2$ with various $M(hfac)_n$ complexes. The mixed ligand species $[Co(tftm)_1(hfac)_1]^+$ is present for all reactions, as is the partially substituted fragment $[Co(hfac)_1]^+$. The fully substituted species $[Co(hfac)_2]^+$ is present for all reactions except with $Al(hfac)_3$.

The other metal involved in the reaction also yields the mixed ligand species, $[M(tftm)_1(hfac)_1]^+$ for each reaction. Tris-chelated heteroleptic species are observed for the reactions with $Fe(hfac)_2$ and $Al(hfac)_3$.

Other reactions yield the product $[M(tftm)_2(hfac)_1]^+$, but this must mean iron must undergo a valence change as well. This is also interesting since neither show the primary substitution $[M(tftm)_1(hfac)_2]^+$. Another interesting note about this reaction is that both metals with the higher order heteroleptic species exhibit full substitution to yield $[M(tftm)_3]^+$.

4.1.4.3.2 $Ni(tftm)_2$ with $M(hfac)_n$

Species Presnet	$Mn(hfac)_2$	$Fe(hfac)_2$	$Co(hfac)_2$	$Cu(hfac)_2$	$Al(hfac)_3$
$Ni(tftm)_1$-^{t}Bu or $Ni(hfac)_1$-CF_3	p	p	p	p	p
$Ni(tftm)_1$	p	p	p	p	p
$Ni(hfac)_1$	p	p	p	p	p
$Ni(tftm)_2$-2(CF_3)	p	p	p		p
$Ni(tftm)_2$-^{t}Bu	p	p	p	p	p
$Ni(hfac)_2$-CF_3 or $Ni(hfac)_1(tftm)_1$-^{t}Bu	p	p	p	p	p
$Ni(tftm)_2$	p	p	p	p	p
$Ni(tftm)_1(hfac)_1$	p	p	p	p	p
$Ni(hfac)_2$			p	p	
M				p	
$M(tftm)_1$-^{t}Bu			p	p	
$M(tftm)_1$			p	p	
$M(hfac)_1$			p		
$M(tftm)_2$-2(CF_3)			p		
$M(hfac)_2$-2(CF_3) or $M(hfac)_1(tftm)_1$-^{t}Bu,CF_3				p	
$M(tftm)_2$-^{t}Bu	p		p	p	
$M(hfac)_2$-CF_3	p	p	p	p	
$M(tftm)_2$	p	p	p	p	p
$M(tftm)_1(hfac)_1$	p	p	p	p	p
$M(hfac)_2$	p	p	p	p	
$M(tftm)_3$		p			p

Table 4.32 Positive identification of species present in the reaction of $Ni(tftm)_2$ with various $M(hfac)_n$ complexes. Note M = the other metal involved in the reaction

Table 4.32 shows a summary of results obtained during the reaction of $Ni(tftm)_2$ with various $M(hfac)_n$ complexes. The mixed ligand species $[Ni(tftm)_1(hfac)_1]^+$ is present for all reactions.

The partially substituted fragment $[Ni(hfac)_1]^+$ is also present for all reactions, while the fully substituted species $[Ni(hfac)_2]^+$ is only present for reactions with $Co(hfac)_2$ and $Cu(hfac)_2$.

The other metal involved in the reaction also shows the bis-heteroleptic species $[M(tftm)_1(hfac)_1]^+$ for all reactions. The partially substituted fragment $[M(tftm)_1]^+$ is only observed for the reactions with $Co(hfac)_2$ and $Cu(hfac)_2$, while the fully substituted species $[M(tftm)_2]^+$ is present during all reactions. An unexplainable result for these reactions is the presence of $[M(tftm)_3]^+$ species for these metals, specifically for the $Fe(hfac)_2$ and $Al(hfac)_3$ reactions, yet no $[M(tftm)_{3-x}(hfac)_x]^+$ species were present while the $[M(tftm)_3]^+$ ion was. This may mean the scavenging process of the tftm neutral onto the $M(hfac)_n$ complexes acts remarkably quick.

4.1.4.3.3 $Cu(tftm)_2$ with $M(hfac)_n$

Species Present	$Mn(hfac)_2$	$Fe(hfac)_2$	$Co(hfac)_2$	$Ni(hfac)_2$	$Al(hfac)_3$
Cu	p	p	p	p	p
$Cu(tftm)_1$-CF_3			p	p	p
$Cu(tftm)_1$-^{t}Bu Or $Cu(hfac)_1$-CF_3	p	p	p	p	p
$Cu(tftm)_1$				p	p
$Cu(tftm)_2$-2(CF_3)	p		p	p	p
$Cu(tftm)_2$-2(^{t}Bu)	p	p	p	p	p
$Cu(tftm)_2$-^{t}Bu	p	p	p	p	p
$Cu(hfac)_2$-CF_3 or $Cu(hfac)_1(tftm)_1$-^{t}Bu	p	p	p	p	p
$Cu(tftm)_2$	p	p	p	p	p
$Cu(tftm)_1(hfac)_1$	p	p	p	p	p
$Cu(hfac)_2$	p	p	p		p
$M(tftm)_1$-^{t}Bu or $M(hfac)_1$-CF_3				p	
$M(tftm)_1$			p	p	
$M(hfac)_1$	p		p	p	
$M(tftm)_1$-2(CF_3)				p	
$M(tftm)_2$-2(^{t}Bu)					p
$M(tftm)_2$-^{t}Bu	p	p	p	p	
$M(hfac)_2$-CF_3 or $M(hfac)_1(tftm)_1$-^{t}Bu	p	p	p	p	
$M(tftm)_2$	p	p	p	p	p
$M(tftm)_1(hfac)_1$	p	p	p	p	p
$M(hfac)_2$	p	p	p	p	
$M(tftm)_3$		p			
$M(tftm)_2(hfac)$		p			

Table 4.33 Positive identification of species present in the reaction of $Cu(tftm)_2$ with various $M(hfac)_n$ complexes. Note M = the other metal involved in the reaction

Table 4.33 shows a summary of the products observed during the reaction of $Cu(tftm)_2$ with various metal-hexafluoroacetylacetonate complexes. The mixed ligand species $[Cu(tftm)_1(hfac)_1]^+$ is observed for all reactions. While $[Cu(hfac)_1]^+$ is not observed, $[Cu(hfac)_2]^+$ is present for all reactions other than with $Ni(hfac)_2$.

Every other metal involved in the reaction forms the mixed ligand complex $[M(tftm)_1(hfac)_1]^+$. A higher order heteroleptic species is only observed for the reaction with $Fe(hfac)_2$.

The species present in that reaction is $[Fe(tftm)_2(hfac)_1]^+$, and its fully substituted form $[Fe(tftm)_3]^+$ is also present. No other reactions yielded more than two exchanges.

The substituted fragment $[M(tftm)_1]^+$ is seen only for reactions with $Co(hfac)_2$ and $Ni(hfac)_2$, though the fully substituted form $[M(tftm)_2]^+$ is observed for all reactions.

4.1.4.3.4 $Zn(tftm)_2$ with $M(hfac)_n$

Species Present	$Fe(hfac)_2$	$Co(hfac)_2$	$Ni(hfac)_2$	$Cu(hfac)_2$	$Al(hfac)_3$
$Zn(tftm)_1$-^{t}Bu or $Zn(hfac)_1$-CF_3			p	p	
$Zn(tftm)_1$	p	p	p	p	p
$Zn(hfac)_1$	p		p	p	
$Zn(tftm)_2$-2(^{t}Bu)				p	
$Zn(tftm)_2$-^{t}Bu	p	p	p	p	p
$Zn(hfac)_2$-CF_3 or $Zn(hfac)_1(tftm)_1$-^{t}Bu	p	p	p	p	p
$Zn(tftm)_2$	p	p	p	p	p
$Zn(tftm)_1(hfac)_1$	p	p	p	p	
$Zn(hfac)_2$			p	p	
M				p	
$M(tftm)_1$-CF_3				p	
$M(tftm)_1$-^{t}Bu or $M(hfac)_1$-CF_3				p	
$M(tftm)_1$	p	p	p	p	
$M(hfac)_1$			p		
$M(tftm)_2$-2(^{t}Bu)		p		p	
$M(tftm)_2$-2(CF_3)				p	
$M(tftm)_2$-^{t}Bu	p	p	p	p	
$M(hfac)_2$-CF_3 or $M(hfac)_1(tftm)_1$-^{t}Bu	p	p	p	p	
$M(tftm)_2$	p	p	p	p	p
$M(tftm)_1(hfac)_1$	p	p	p	p	p
$M(hfac)_2$	p			p	
$M(tftm)_3$					p

Table 4.34 Positive identification of species present in the reaction of $Zn(tftm)_2$ with various $M(hfac)_n$ complexes. Note M = the other metal involved in the reaction

Table 4.34 represents a summary of the products during the reactions of $Zn(tftm)_2$ with various $M(hfac)_n$ complexes. The mixed ligand species $[Zn(tftm)_1(hfac)_1]^+$ is present for all reactions except with $Al(hfac)_3$.

The fragment $[Zn(hfac)_1]^+$ is present for all reactions except with $Co(hfac)_2$ and $Al(hfac)_3$, and the fully substituted form $[Zn(hfac)_2]^+$ is present only for reactions with $Ni(hfac)_2$ and $Cu(hfac)_2$.

The other metal in the reaction shows the mixed ligand species $[M(tftm)_1(hfac)_1]^+$ for all reactions. The partially substituted fragment $[M(tftm)_1]^+$ is observed for all reactions except for with $Al(hfac)_3$, yet the doubly substituted form $[M(tftm)_2]^+$ is present for all reactions. The only tris-species present is $[Al(tftm)_3]^+$, this fully substituted homoleptic ion shows no heteroleptic precursors.

4.1.4.3.5 $Al(tftm)_3$ with $M(hfac)_n$

Species Present	$Mn(hfac)_2$	$Co(hfac)_2$	$Ni(hfac)_2$	$Cu(hfac)_2$
$Al(tftm)_2$	p	p	p	p
$Al(tftm)_1(hfac)_1$	p	p	p	p
$Al(hfac)_2$	p*	p*	p*	p*
$Al(tftm)_3$	p	p	p*	p
$Al(tftm)_2(hfac)_1$	p*	p*	p*	
$M(tftm)_1$-^{t}Bu or $M(hfac)_1$-CF_3			p	p
$M(tftm)_1$		p*		
$M(hfac)_1$	p*	p	p	
$M(tftm)_2$-2(^{t}Bu)				p
$M(tftm)_2$-CF_3				
$M(tftm)_2$-^{t}Bu		p*	p*	p
$M(hfac)_2$-CF_3 or $M(hfac)_1(tftm)_1$-^{t}Bu	p	p	p	p
$M(tftm)_2$				p*
$M(tftm)_1(hfac)_1$	p	p	p	p*
$M(hfac)_2$	p	p	p	
$M_2(hfac)_1(tftm)_2$		p*		

Table 4.35 Positive identification of species present in the reaction of $Al(tftm)_3$ with various $M(hfac)_n$ complexes. Note M = the other metal involved in the reaction. *denotes nominal mass assurance only

Table 4.35 above gives a summary of the products observed during the reaction of $Al(tftm)_3$ with various metal-hexafluoroacetylacetonates. Much like the reactions between $Al(tftm)_3$ and various $M(acac)_n$ complexes, many of these reactions also had low intensities, making isotope ratio validation unavailable.

Nominal mass validation, coupled with common trends in formation and fragmentation of these compounds, was used to determine identities of these species.

The mixed ligand species $[Al(tftm)_1(hfac)_1]^+$ is present for all reactions and a tris-chelate of the heteroleptic species $[Al(tftm)_2(hfac)_1]^+$ is present in all reactions other than with $Cu(hfac)_2$.

$[Al(hfac)_2]^+$ is the only example of a substituted homoleptic aluminum complex, and it is present for all reactions.

The other metal involved in the reactions exhibit the mixed ligand species $[M(tftm)_1(hfac)_1]^+$ for all reactions. The fragment $[M(tftm)_1]^+$ is observed during the reaction with $Co(hfac)_2$. The fragment $[M(tftm)_1\text{-}^t Bu]^+$ is isobaric with $[M(hfac)_1\text{-}CF_3]^+$, so a fragment of the $[M(tftm)_1]^+$ may be present, but this cannot be determined without hi-resolution data.

4.1.5 Conclusions and Future Work

From the data shown above it is very clear that ligand exchange reactions readily occur in the gas phase. It is observed for nearly every metal and ligand combination. Unfortunately, due to the high abundance of these ligand exchange reactions observed for the various reactants, we do not observe many trends, though the trends observed, such as prevalent loss channels, provide insight for further experimentation.

It has been observed that the valency of the metal is quite important for these reactions. The metal center for which a tris-chelated rearrangement was observed was initially a tris-chelated reactant, meaning a metal center with an initial 3+ oxidation state could yield products with either a 3+ oxidation state.

A 2+ species would not yield a 3+ species, except in the case of the reaction $Cu(tftm)_2$ with $Zn(acac)_2$, though this result is highly unexpected. This finding helps us to re-affirm the fact that the environment created in the ionization chamber is highly reducing, and especially so with all of the reactants being present in the chamber.

Other than the generation of tris-chelates, we cannot conclude anything else about the oxidation state and the reactivity of these complexes.

Much more work can be done in this field. Of particular interest would be more investigations into the mechanisms of formation of these complexes, specifically through metastable ion analyses. If the mechanisms we propose are true, then metastable ions ought to be present. Analyses of these could help validate our findings, or propose a secondary mechanism by which these rearrangements may be occurring.

An interesting experiment would be to isotopically label one compound, and react it with its non-labeled counterpart. This would lend insight into the fragmentation of these complexes, specifically if the ion-neutral reactions we stated earlier, occur even without varying ligand or metal composition. A series of these reactions with different metals and varying substituents on the ligands could lend insight into mechanisms.

Attempting to create these products from the reaction of one metal β-diketonate complex with another β-diketone ligand in the gas phase would also help determine some mechanistic implications.

As stated earlier, residence time should play an important role in the amount of exchange. A series of reactions with varying residence time should help gain clarity on this subject.

Chapter 5: Results and Discussion of Non Gas-Phase Reactions

5.1 Results of Synthetic Reactions

The results of the aqueous, solvent, heteroleptic and heterometallic syntheses are presented herein. Formulae determined by mass spectrometry data has been validated by comparing observed with calculated isotope ratios unless otherwise stated.

5.1.1 Results of Aqueous Synthesis Reactions

The products of the aqueous synthesis outlined by Watson and Lin[51] are presented.

5.1.1.1 $Mn(tftm)_2$

The isolated compound $Mn(tftm)_2$ was analyzed and verified using mass spectrometry.

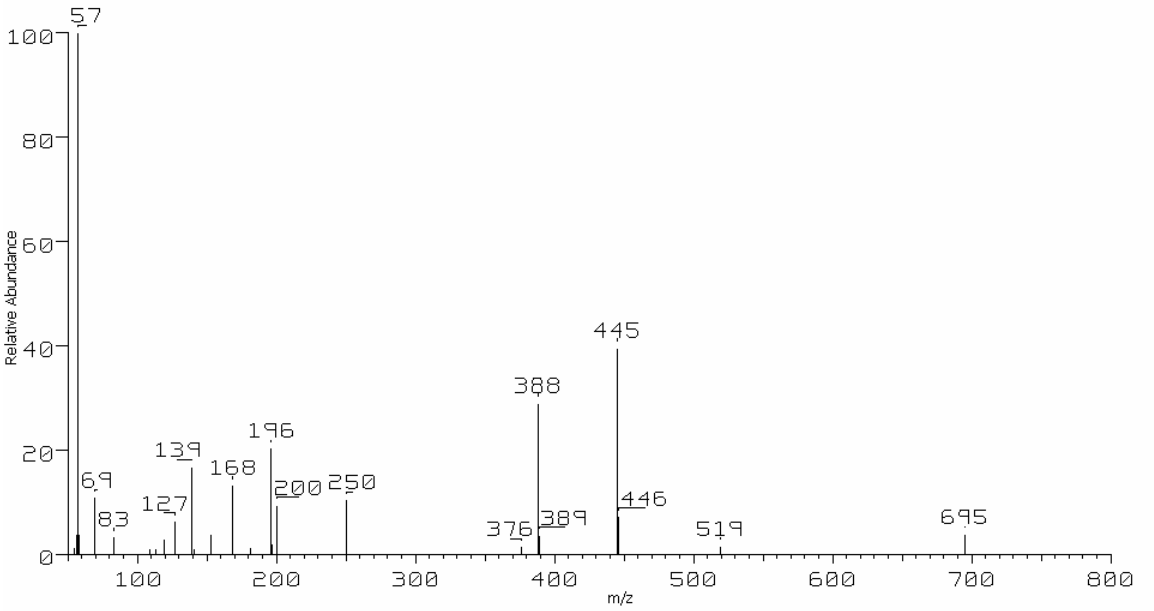

Fig. 5.1 The 70 eV positive EI mass spectrum of the $Mn(tftm)_2$ product.

As evident by the mass spectrum in Fig. 5.1, $Mn(tftm)_2$ is the end product of this reaction. The peak at m/z 445 is the molecular ion, the peak at m/z 388 represents the loss of a ^{t}Bu group from the molecular ion and the fragment $Mn(tftm)_1$ is visible at m/z 250. These fragments are quite common compared to the other $M(tftm)_2$ compounds, as outlined in section 4.1.1.

m/z	Species	Rel. Ab.
250	$Mn(tftm)_1$	26
376	$Mn(tftm)_2$-CF_3	4
388	$Mn(tftm)_2$-^{t}Bu	73
445	$Mn(tftm)_2$	100
519	$Mn_2F(tftm)_2$*	4
695	$Mn_2(tftm)_3$*	10

Table 5.1 The relative abundances of the Mn species present for the positive EI spectrum of $Mn(tftm)_2$.
Note: the relative abundances were normalized to the molecular ion.
*denotes nominal mass assurance only

Clustered compounds are visible at m/z 519 and 697. The peak at m/z 519 may represent the species $Mn_2F(tftm)_2$, but that was determined simply by addition of nominal masses, and the degree of confidence of that assignment is not too high, since species of this kind haven't been observed with the previous compounds. The species at m/z 695 was also determined nominally, but compounds of the form M_xL_y have been observed readily, and this assignment is very reasonable.

5.1.1.2 $Co(tftm)_2$

The species $Co(tftm)_2$ was analyzed with mass spectrometry, which can be seen in section 4.1.1.1. The complete single crystal data set available in Appendix section B.1, though, a short summary is provided below. The structure of this compound has not been reported previously, and was published by this group in Acta Crystallographica Section E[58].

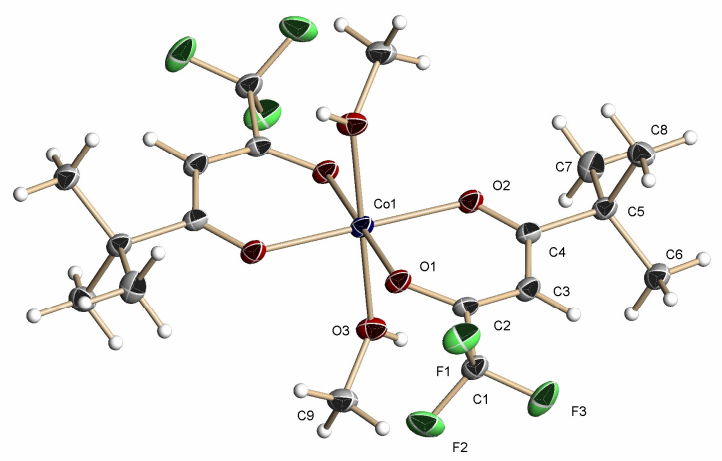

$Co(C_8O_2H_{10}F_3)_2(CH_3OH)_2$	
Formula Weight	513.33 g/mol
Crystal System	Triclinic
Space Group	P_{1bar}
a	5.4390(7) Å
b	8.7181(11) Å
c	12.0169(15) Å
α	78.835(2) ˚
β	80.571(2) ˚
γ	87.946(2) ˚

Table 5.2 Crystallographic information regarding the structure of $Co(tftm)_2(CH_3OH)_2$

Fig. 5.2 The crystal structure of the $Co(tftm)_2$ product.

The product of this synthesis is coordinated to two MeOH molecules giving the formula $Co(C_8O_2H_{10}F_3)_2(CH_3OH)_2$. Though, it was shown earlier that under conditions in the mass spectrometer it should only exist as $Co(tftm)_2$ as the MeOH molecules will de-coordinate from the complex upon sublimation and ionization. A H-bonding network exists for this compound also, and can be seen in the crystallographic information present in the Appendix.

5.1.1.3 $Ni(tftm)_2$

This product was determined to be $Ni(tftm)_2$ through mass spectral analysis as outlined in section 4.1.1.2. Single crystal analysis was also performed to show the product was actually a dimer of two complexes, with each associated to two MeOH molecules, much like the $Co(tftm)_2$ product, though the arrangement of these MeOH molecules are *cis* with respect to each other, as opposed to the *trans* arrangement observed in the cobalt complex.

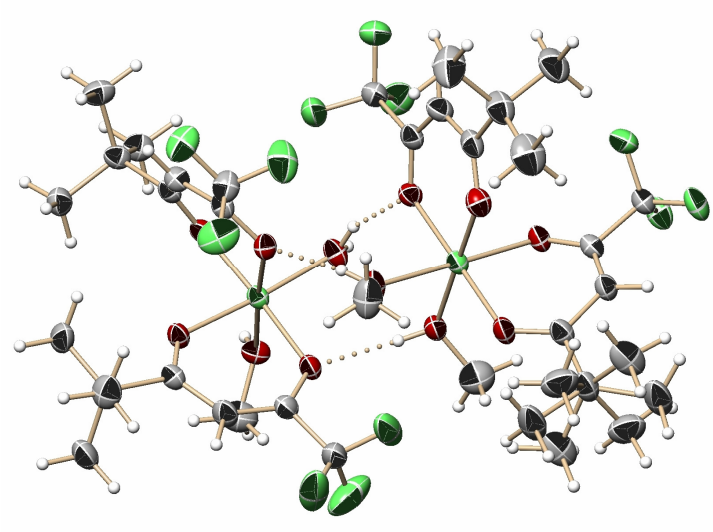

$(Ni(C_8O_2H_{10}F_3)_2(CH_3OH)_2)_2$	
Formula Wieght	1012.16
Crystal System	Triclinic
Space Group	P_{1bar}
a	11.402(2) Å
b	14.813(3)Å
c	15.521(3)Å
α	100.935(3)˚
β	105.216(3)˚
γ	108.009(3)˚

Table 5.3 Crystallographic information regarding the structure of $(Ni(tftm)_2(CH_3OH)_2)_2$

Fig. 5.3 The crystal structure obtained for $Ni(tftm)_2(CH_3OH)_2$

An extensive H-bonding network exists in the structure, and is summarized in the Appendix in section B.2 along with the rest of the crystallographic information. One problem with the refinement of this structure was the disorder of a ^{t}Bu group, due to a fixed rotation of the ^{t}Bu group. The ratio of disorder is 0.856(4) to 0.144(4). More results regarding the treatment of this disorder, and for the rest of the refinement, can be found in the Appendix section B.2.

5.1.1.4 $Cu(tftm)_2$

This product was determined to be $Cu(tftm)_2$ through mass spectrometry as outlined in section 4.1.1.3, though single crystal X-ray analysis shows the product is actually coordinated to one MeOH molecule also as shown below.

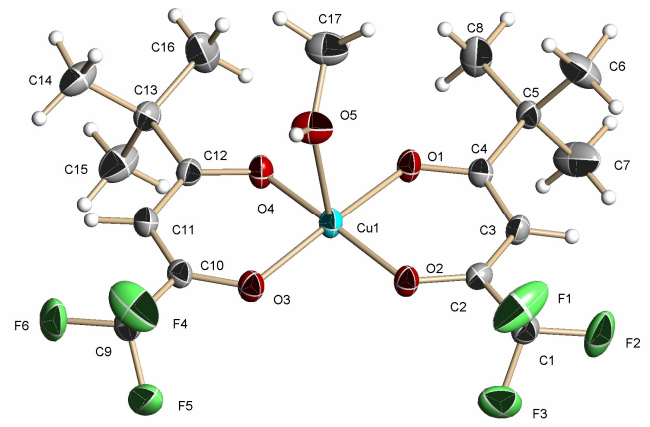

Fig. 5.4 The crystal structure found for $Cu(tftm)_2(MeOH)_1$

$Cu(C_8O_2H_{10}F_3)_2(CH_3OH)_1$	
Formula Wieght	485.90
Crystal System	Triclinic
Space Group	P_{1bar}
a	9.3307(9) Å
b	10.6833(10) Å
c	11.9202(11) Å
α	106.231(2)˚
β	104.166(2)˚
γ	99.418(2)˚

Table 5.4 Crystallographic information regarding the structure of $Cu(tftm)_2(CH_3OH)_1$

H-bonding is present between the hydroxyl group and a nearby oxygen atom of the tftm ligand on a neighboring molecule, as described by the crystallographic information given in Appendix section B.3.

5.1.1.5 $Zn(tftm)_2$

Mass spectral analysis was the only tool used for the structural determination of the $Zn(tftm)_2$ product, shown in secton 4.1.1.4. Since mass spectrometry was the only tool used to investigate this product, it is unknown to what extent it may be coordinated to water, or another solvent such as methanol.

5.1.1.6 $Al(acac)_3$

PXRD was the only technique used to study this particular compound. The powder pattern can be seen in Appendix section C.1. This pattern makes it evident that the product is slightly amorphous, as evident by some peak broadening, though the individual peaks are still quite distinguishable. This powder pattern could not be matched to any rational compounds. Even though this result is inconclusive, this pattern is important for later comparisons with heteroleptic aluminum complexes.

5.1.1.7 $Al(tftm)_3$

Only PXRD analysis was used to analyze this sample, where the powder pattern is shown in Appendix section C.2. As evident by the powder pattern this compound is quite amorphous. The only reliable peaks are the two which are present early on, whereas any other peaks present are lost in the background. Much like the product described in 5.1.1.6, this pattern does not have any logical matches, however, it will be used later in the investigations of the heterometallic aluminum complex.

5.1.1.8 $Ni(acac)_2$

The product synthesized in the $Ni(acac)_2$ reaction, as well as the product after subsequent recrystallization from MeOH, was investigated using PXRD. A powder pattern comparing the two can be seen in Appendix section C.3. As seen in the pattern, recrystallization from MeOH causes a phase change. It is believed that MeOH is replacing the coordinate H_2O, which was initially coordinated during the aqueous synthesis. Also, the recrystallized form seems to have better crystallinity, as evident by its sharper peaks. These powder patterns will be useful for comparisons with later heteroleptic products.

5.1.1.9 $Cu(acac)_2$

The product synthesized in the $Cu(acac)_2$ synthetic reaction was examined using PXRD, as was its MeOH recrystallized analog, both of which can be seen in Appendix section C.4. As evident by the powder pattern, no phase change is observed for the MeOH recrystallized compound, leading us to believe that no MeOH is associating to this compound, unlike the nickel species previously described. These findings will aid us in further comparison with heteroleptic and heterometallic compounds.

5.1.2 Non-Aqueous Synthesis Reaction

5.1.2.1 $Al(tftm)_3$

The product of these reactions has been investigated through mass spectrometry as outlined in 4.1.15. Multiple recrystallization steps were taken in an attempt to define an exact structure through single crystal X-ray analysis, but no suitable crystals were able to be formed.

5.2 Synthetic Approach to Heteroleptic Complexes

5.2.1 $Ni(acac)_1(tftm)_1$

The product of this reaction was determined by PXRD, and can be seen in Appendix section C.5, where it is plotted against the powder pattern for the $Ni(tftm)_2$ synthetic product. As evident by the powder pattern, this reaction consists primarily of $Ni(tftm)_2$, and the lack of unassigned peaks leads us to believe that no other phases besides $Ni(tftm)_2$ are present.

This powder pattern also shows the product as being slightly amorphous, evident by the broadened peaks, which is also consistent with the data collected for the $Ni(tftm)_2$ product. If the free $tftm^{-1}$ ligand chelated much quicker than the free $acac^{-1}$ ligand, one would still expect the leftover acac to chelate to the remainder of the free Ni^{2+}. Why no $Ni(acac)_2$ is present remains unknown. Perhaps more time (greater than one hour) was necessary for the free $acac^{-1}$ to chelate, or perhaps if any $Ni(acac)_2$ is present, it is completely amorphous, and unable to diffract.

5.2.2 $Cu(acac)_1(tftm)_1$

Much like the Ni reaction of this type, only the $Cu(tftm)_2$ product is present by PXRD, as shown in Appendix section C.6. The $Cu(acac)_1(tftm)_1$ synthetic product is of lower crystalline quality, as compared to the $Cu(tftm)_2$ product, however the most intense peaks in the beginning of the powder pattern are matches between the two patterns.

As was the case with the Ni species, the free $tftm^{-1}$ appears to chelate much quicker to the free metal in solution. Again, more time may be necessary in order to form the secondary $Cu(acac)_2$ byproduct.

5.2.3 $Al(acac)_x(tftm)_{3-x}$

The powder patterns of the 1:1:2, and 1:2:1 products compared to the $Al(acac)_3$ and $Al(tftm)_3$ products can be seen in Appendix sections C.7 and C.8, respectively.

Both reactions have very poor crystalline character, which makes it very hard to conclude anything from them, however it can be seen that the $Al(acac)_3$ product matches a few of the most intense peaks from both reactions. Unfortunately, the $Al(acac)_3$ product has quite a few peaks that are not present in either the 1:1:2 or 1:2:1 reactions. Due to such poor data, the results of this reaction are inconclusive.

5.3 Synthetic Approach to Hetero-Metal β-diketonate Complexes

Many of these β-diketonate complexes exist as dimers. The following three experiments were done to determine if a dimeric, or oligomeric, complex could be formed with differing metal centers. The synthetic approach used by Watson & Lin was again used for these reactions[57].

5.3.1 Ni + Cu + Hacac + acid synthesis

This product was analyzed using PXRD, which can be seen in Appendix section C.9. As evident by the powder pattern, the metal-chlorides from the starting materials are the only two crystalline products. This should have been expected though, since the protonated form of the ligand chelates to the metal much slower than in basic medium. The base deprotonates the ligand and drives the reaction towards the chelated products. The presence of a strong acid, and also the chloride ion, is going to inhibit the reactivity of the free ligand and drive the reaction towards the metal chloride starting materials.

5.3.2 Ni + Cu + Hacac + base synthesis

The products in this reaction heavily favored the formation of $Cu(acac)_2$ as can be seen in the powder patterns shown in Appendix sections C.10 and C.11. This leads us to believe that the ligand has a much higher affinity for the copper ion than the nickel ion. In the case of the 1:1:2 ratio, the lack of any phases containing nickel is understandable since most of the copper was chelated by the free ligand, in the form of the $Cu(acac)_2$ precipitate. Any nickel that was not chelated would remain in solution.

As for the 1:1:4 reaction, the reason for no nickel phases present remains unclear. Assuming most of the copper is chelated by the Hacac present in the reaction, there should still be two equivalents of protonated ligand left in the reaction. One reason could be the lack of free ligand available since the amount of base is present in the amount of 2/3 of the ligand. The high amount of chloride, and the lack of free ligand in solution may drive the reaction, in the case of nickel, towards the reactants, thus creating no $Ni(acac)_2$, or analogs thereof, though it appears that regardless of the amount of base or ligand present, the ligand chelates too quickly to copper to form any heterometal species.

5.3.3 Ni + Al + Hacac + base synthesis

The products of the 1:1:3 and 1:1:5 reactions were analyzed using PXRD, and can be seen plotted together in Appendix section C.12. By this plot it is evident that these reactions yielded the same product. These products are, as can be seen in the powder patterns shows in Appendix section C.13, nickel chloride and sodium chloride. The powder patterns of these reactions were compared to the powder patterns from the $Ni(acac)_2$ and $Al(acac)_3$ syntheses, and no positive identification could be made. It is unknown why neither metal was chelated by the free ligand.

5.4 Solution Ligand Exchange Reactions

5.4.1 $Ni(acac)_2$ with $Ni(hfac)_2$

The product of this reaction was a green powder. A total of four fractions were collected from the product.

The four fractions were recrystallized by methods stated earlier, though only three yielded single crystals suitable for X-ray analysis. More data regarding these structures can be found in the Appendix in sections B.4-6.

Fraction one yielded a mixed monomeric mixed ligand product: $Ni(acac)_1(hfac)_1 \bullet H_2O$ shown below in Fig. 5.5.

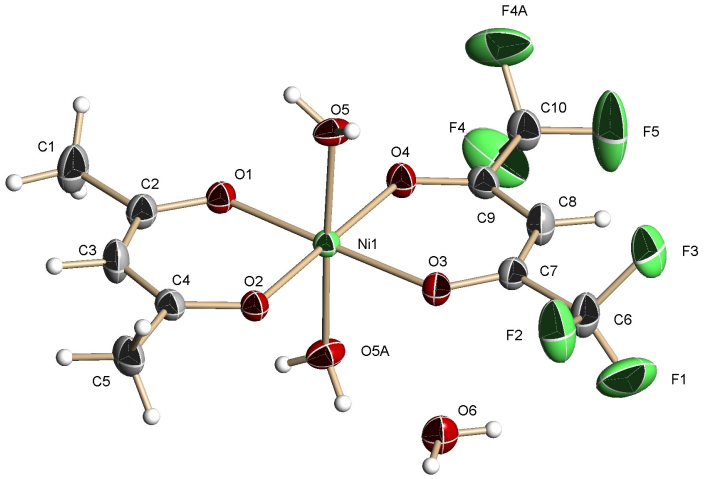

$Ni(acac)_1(hfac)_1(H_2O)_2•H_2O$	
Formula Wieght	419.92 g/mol
Crystal System	Monoclinic
Space Group	$P2_1/m$
a	9.265(2) Å
b	7.5750(17) Å
c	11.471(3) Å
α	90˚
β	106.539(3)˚
γ	90˚

Table 5.5 Crystallographic information regarding the structure of $Ni(acac)_1(hfac)_1•H_2O$

Fig. 5.5 The crystal structure obtained for the product of the 1st fraction $Ni(acac)_1(hfac)_1(H_2O)_2•H_2O$

Fraction two yielded two distinct products. The first of which, a minor species, is shown below in Fig. 5.6. The major component of this fraction is also the product of fraction three, shown in Fig. 5.7. These products share the same molecular formula, as they are molecularly the same. The difference between the two lies in the packing arrangement. The minor contribution of fraction two, summarized in Table 5.6, has an orthorhombic spacegroup, while the major contributor, summarized in Table 5.7 has a triclinic spacegroup.

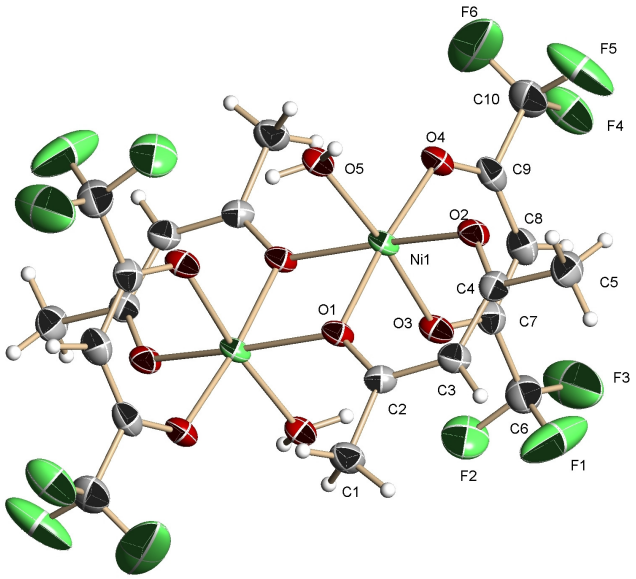

$(Ni(acac)_1(hfac)_1H_2O)_2$	
Formula Wieght	765.74 g/mol
Crystal System	Orthorhombic
Space Group	Pbcn
a	18.5920(16) Å
b	10.5397(9) Å
c	14.7123(12) Å
α	90˚
β	90˚
γ	90˚

Table 5.6 Crystallographic information regarding the structure of $(Ni(acac)_1(hfac)_1H_2O)_2$

Fig 5.6 The crystal structure obtained for the minor product in fraction 3: $(Ni(acac)_1(hfac)_1H_2O)_2$

Fraction three was comprised of the dimer that also happened to be the major contributor to the product of fraction two. Its structure, which is shared with the major product of fraction two, is shown in Fig. 5.7, and basic crystallographic information is summarized in Table 5.7.

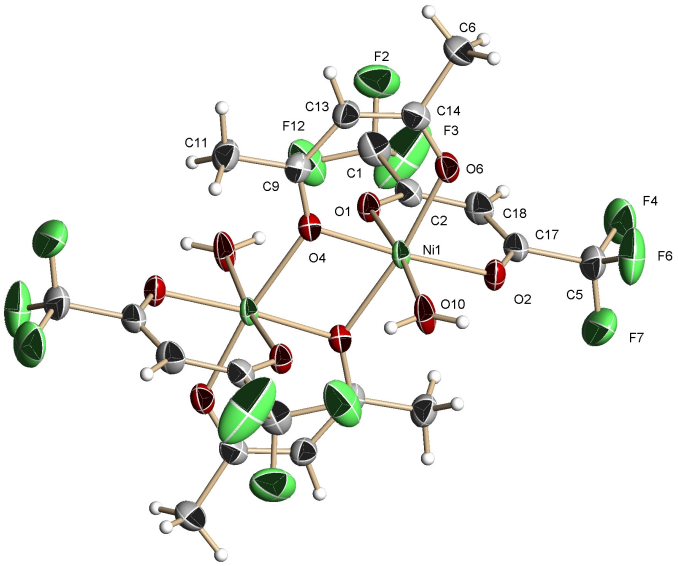

Fig 5.7 The crystal structure obtained for the 3rd fraction: $(Ni(acac)_1(hfac)_1H_2O)_2$

$(Ni(acac)_1(hfac)_1H_2O)_2$	
Formula Wieght	765.78 g/mol
Crystal System	Triclinic
Space Group	P_{1bar}
a	7.511(4) Å
b	9.510(5) Å
c	9.824(5) Å
α	96.247(11)˚
β	93.655(11)˚
γ	93.811(9)˚

Table 5.7 Crystallographic information regarding the structure of $(Ni(acac)_1(hfac)_1H_2O)_2$

Fraction four yielded no suitable crystals for analysis. This experiment confirms that $Ni(acac)_1(hfac)_1$ complexes are quite stable complexes. It is not surprising that these heteroleptic compounds are observed as both hydrated monomers and dimers, as many other homoleptic species share these traits in the solid phase.

One may ask if these products are solely the result of solution-phase ligand exchange, and we believe it so. As stated previously, other groups have shown that solution phase ligand exchange readily occurs, and if it had not occurred, we would expect to see starting materials only. Upon sublimation, we would not expect to see mixed ligand species, since the increased volatility of the hfac complexes would cause them to sublimate before the acac complexes.

5.4.2. $Ni(tftm)_2$ with $Ni(acac)_2$

Given time constraints no further analyses were taken on this sample.

5.4.3 $Ni(hfac)_2$ with $Ni(tftm)_2$

Given time constraints no further analyses were taken on this sample.

5.5 Conclusions and Future Work

Based on the work done in this chapter, it appears that the best method of creating heteroleptic complexes is through ligand exchange in solution since none of the other methods outlined in the prior sections yielded any confirmatory results.

As evident by the multiple heteroleptic species observed for the reaction outlined in section 5.4.1 much more work can with the solution reactions. The metal center identity may also be changed to yield interesting results. The dimeric nature of some of the products outlined in 5.4.1 may lead to the generation of some mixed-metal compounds, with potentially homoleptic and heteroleptic ligand systems.

Varying the polarity of the solvent may have an important role. One may also consider observing the reaction *in situ* with some form of spectroscopy with the hopes of gaining some kinetic data regarding these exchange reactions.

References

1. Kowalski, B. R., Isenhour, T. L., Sievers, R. E. *Analytical Chemistry* **1969** 41(8), 998-1003
2. Burtoloso, A. C. *Synlett* **2005** 18, 2859-2860
3. Condorelli, G. G., Malandrino, G., Fragalà, I. L. *Coordination Chemistry Reviews* **2007** 251, 1931-1950
4. Bessergenev, V. *Journal of Physics: Condensed Matter* **2004** 16, S531-s552
5. Croxtall, B., Fawcett, J., Hope, E. G., Stuart, A. M. *Journal of Fluorine Chemistry* **2003** 119, 65-73
6. Jones, M. M. *Journal of the American Chemical Society* **1959** 8, 3188-3189
7. Reid, J. C., Calvin, M. *Journal of the American Chemical Society* **1950** 72, 2948-2952
8. Skopenko, V. V., Amirkhanov, V. M., Yu Sliva, T., Vasilchenko, I. S., Anpilova, E. L., Garnoskii, A. D. *Russian Chemical Reviews* **2004** 73(8) 737-752
9. Fahlman, B. D., Barron, A. R. *Advanced Materials for Optics and Electronics* **2000** 10, 223-232
10. Allen, G., Dwek, R. A. *Journal of the Chemical Society (B)* **1966** 2, 161-163
11. Ogoshi, H., Nakamoto, K. *Journal of Chemical Physics* **1966** 45(8), 3113-3120
12. Egan, W., Gunnarson, G., Bull, T. E., Forsén, S. *Journa of the American Chemical Society* **1977** 99(14), 4568-4572
13. Wallen, S. L., Yonker, C. R., Phelps, C. L., Wai, C. M. *Journal of the Chemical Society, Faraday Transactions* **1997** 93(14), 2391-2394
14. Grushow, A., Zielinski, T. J. *Journal of Chemical Education* **2002** 79(6), 707-714
15. Sloop, J. C., Baumgardner, C. L., Washington, G., Loehle, W. D., Sankar, S. S., Lewis, A. B. *Journal of Fluorine Chemistry* **2006** 127, 780-786
16. Shi, S., Dongge, M., Peng, J. *Semiconductor Science Tehcnology* **2007** 22, 249-252
17. Pollard, K. D., Jenkins, H. A., Puddephat, R. J. *Chemistry of Materials* **2002** 12, 701-710
18. Liu, Z., Bian, Z., Ming, L., Ding, F., Shen, H., Nie, D., Huang, C. *Organic Electronics* **2008** 9, 171-182
19. Bessergenev, V. *Journal of Physics: Condensed Matter* **2004** 16, S531-s552
20. Macdonald, C. G., Shannon, J. S. *Australian Journal of Chemistry* 1966 19, 1454-1566
21. Sharpe, P., Richardson, D. E. *Journal of the American Chemical Society* **1991** 113, 8339-8346
22. Sharpe, P., Eyler, J. R., Richardson. D. E. *Inorganic Chemistry* **1990** 29, 2779-2787
23. Clobes, A. L., Morris, M. L., Koob, R. D. *Organic Mass Spectrometry* 1971 5, 633-649\
24. Rubesch, M., Clobes, A. L., Morris, M. L., Koob, R. D. *Organic Mass Spectrometry* 1971 5, 237-248
25. Koob, R. D., Morris, M. L., Clobes, A. L. *Chemical Communications* **1969** 20, 1177-1178
26. Westmore, J. B. *Chemical Reviews* 1976 6, 695-715

27. Holtzclaw Jr., H. F., Lintvedt, R. L., Baumgarten, H. E., Parker, R. G., Bursey, M. M., Rogerson, P. F. *Journal of the American Chemical Society* 1969 91(14), 3774-3778
28. Bancroft, G. M., Reichert, C., Westmore, J. B. *Inorganic Chemistry* 1968 7(5), 870-874
29. Bancroft, G. M., Reichert, C., Westmore, J. B., Gesser, H. D. *Inorganic Chemistry* 1969 8(3), 474-480
30. Reichert, C., Westmore, J. B. *Inorganic Chemistry* 1969 8(4), 1012-1014
31. Lacey, M. J., Shannon, J. S. *Organic Mass Spectrometry* 1972 6, 931-937
32. Majer, J. R., Perry, R. *Chemical Communications* **1969** 9, 454-455
33. Schildcrout, S. M. *The Journal of Physical Chemistry* 1976 80(26), 2834-2838
34. Dean, L. K. L., DiDonato, G. C., Wood, T. D., Busch, K. L. *Inorganic Chemistry* 1988 27, 4622-4627
35. Morris, M. L., Koob, R. D. *Inorganic Chemistry* 1981 20, 2737-2738
36. Schildcrout, S. M., Pearson, R. G., Stafford, F. E. *Journal of the American Chemical Society* 1968 90(15), 4006-4010
37. Kuska, H. A., Beebe, D. H. *Inorganic Chemistry* 1978 17(1), 198-200
38. Pierce, J. L., Busch, K. L., Graham Cooks, R., Walton, R. A. Inorganic Chemistry 1982 21, 2597-2602
39. Bartlett, M. G., Bruce, D. A., Busch, K. L. *Applied Spectroscopy* 1997 51(11), 1757-1760
40. Saraswathi M., Miller, J. M. Rapid Comm. in Mass Spectrometry 1995 9, 1101-1105
41. Wyatt, M. F., Havard, S., Stien, B. K., Brenton, A. G. *Rapid Communications in Mass Spectrometry* **2008** 22, 11-18
42. Matsumoto, K., Ajiro, H., Habaue, S., Okamoto, Y. *Rapid Communications in Mass Spectrometry* **2002** 16, 730-732
43. Brabander, H. F., Le Bizec, B., Pinel, G., Antignac, J.-P., Verheyden, K., Mortier, v., Courtheyn, D., Noppe, H. *Journal of Mass Spectrometry* **2007** 42, 983-998
44. Maurer, H. H. *Analytical and Bioanalytical Chemistry* **2007** 338, 1315-1325
45. Flamani, R., Panighel, A. *Mass Spectrometry Reviews* **2006** 25, 741-774
46. Flamani, R. *Mass Spectrometry Reviews* **2003** 22, 218-250
47. Hilchenbach, H. *International Journal of Mass Spectrometry* **2002** 215, 113-129
48. Downard, K. *Mass Spectrometry: A Foundations Course* Royal Society of Chemistry: Cambridge, UK 2007; pp 22-65
49. Barker, J., Davis, R., Frearson, M. J. *Mass Spectrometry: Analytical Chemistry By Open Learning 2nd ed.* Ando, D.: John Wiley & Sons Ltd.; West Sussex, England, 1999; pp 19-90
50. March, R. E. *Journal of Mass Spectrometry***1997** 32, 351-369
51. Watson Jr, W. H., Lin, C. *Inorganic Chemistry* **1966** 5(6), 1074-1077
52. Zheng, B. Goldberg, C., Eisenbraun, E. T., Liu, J., Kaloyeros, A. E., Toscano, P. J., Murarka, S. P., Loan, J. F., Sullivan, J. *Materials Chemistry and Physics* **1995** 41, 173-181
53. Fay, R. C., Piper, T. S. *Inorganic Chemistry* **1963** 85, 500-504
54. Pinnavaia, T. J., Sebeson II, J. M., Case, D. A. *Inorganic Chemistry* **1969** 8(3), 644-648

55. Pinnavaia, T. J., Fay, R. C. *Inorganic Chemistry* **1966** 5(2), 233-239
56. Dikarev, E. V., Zhang, H., Li, B. *Journal of the American Chemical Society* **2005** 127, 6156-6157
57. Mains, D. G. Gas Phase Association Reactions of Mixed-Metal Acetylacetonate Complexes M.S. Thesis, Youngstown State University, August 2008.
58. Lerach. J. O., Leskiw, B. D. *Acta Crystallographica Section E* **2008** E63, m2369

Appendix A: Mass Spectra

A.1 $Co(tftm)_2$ Reactions

A.1.1 The 70 eV positive EI mass spectrum obtained during the reaction between $Co(tftm)_2$ with $Cr(acac)_3$

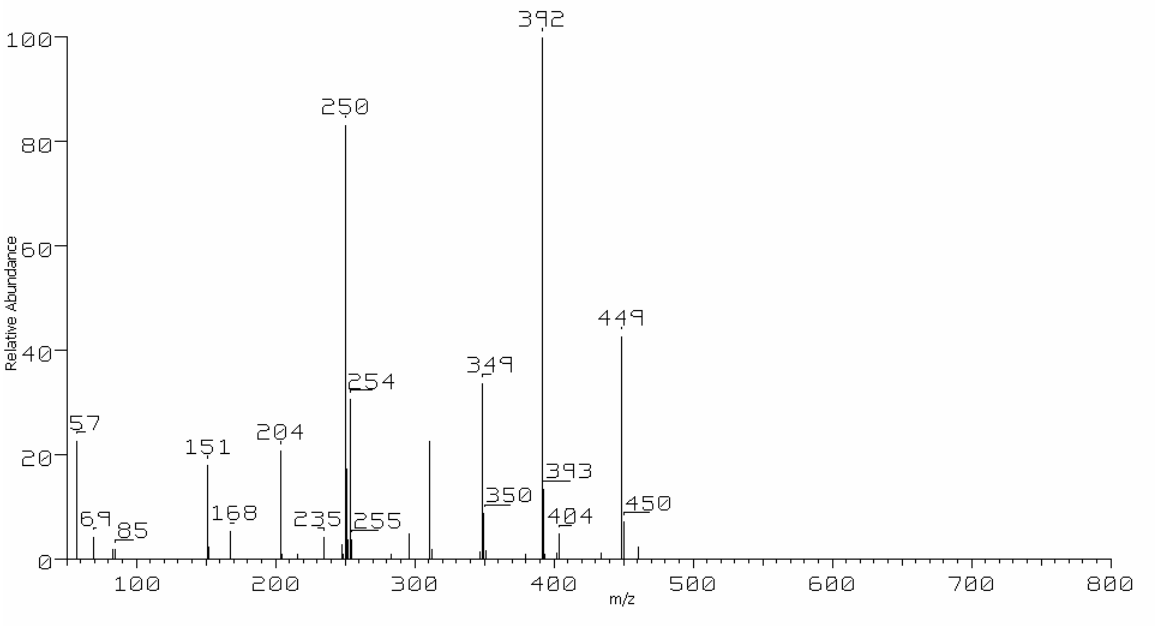

A.1.2 The 70 eV positive EI mass spectrum obtained during the reaction between $Co(tftm)_2$ with $Mn(acac)_2$

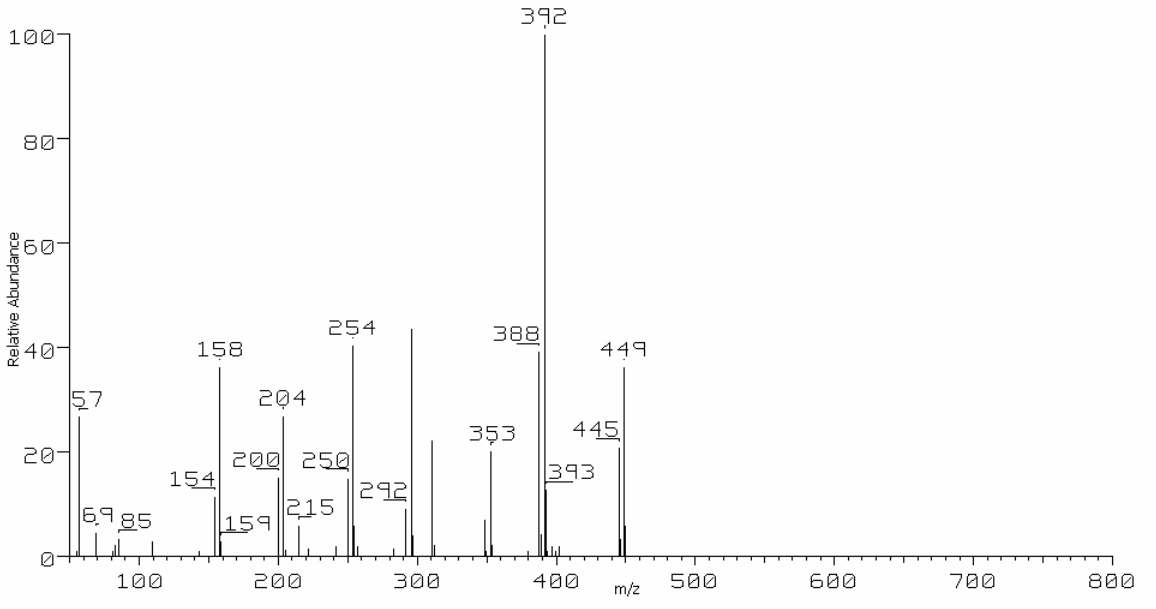

A.1.3 The 70 eV positive EI mass spectrum obtained during the reaction between $Co(tftm)_2$ with $Mn(hfac)_2$

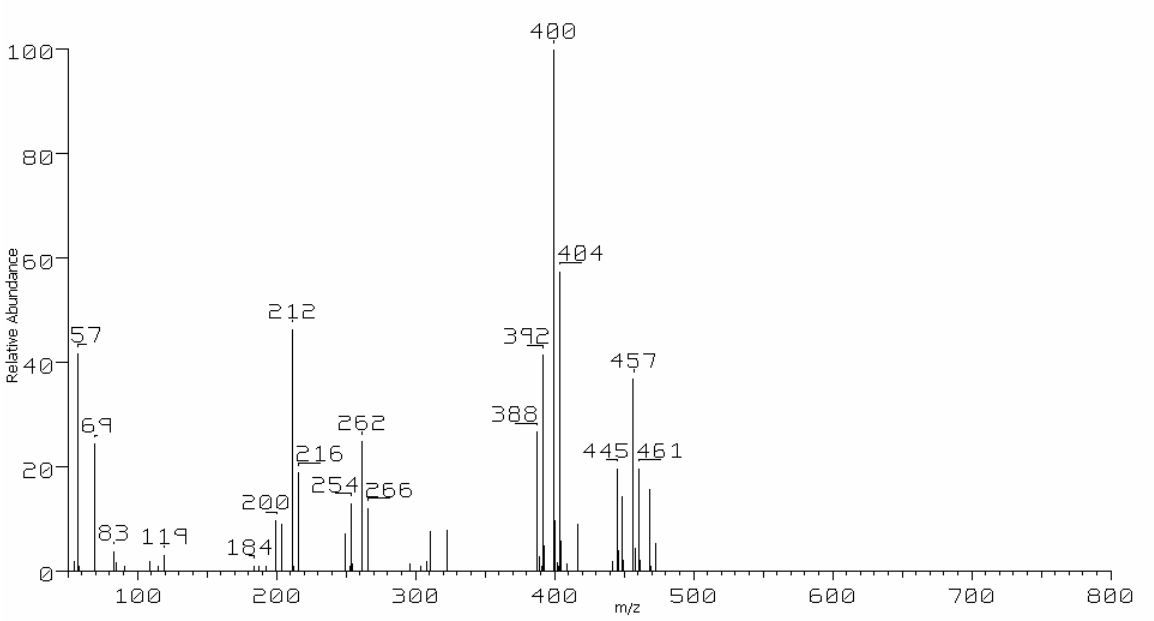

A.1.4 The 70 eV positive EI mass spectrum obtained during the reaction between $Co(tftm)_2$ with $Fe(acac)_3$

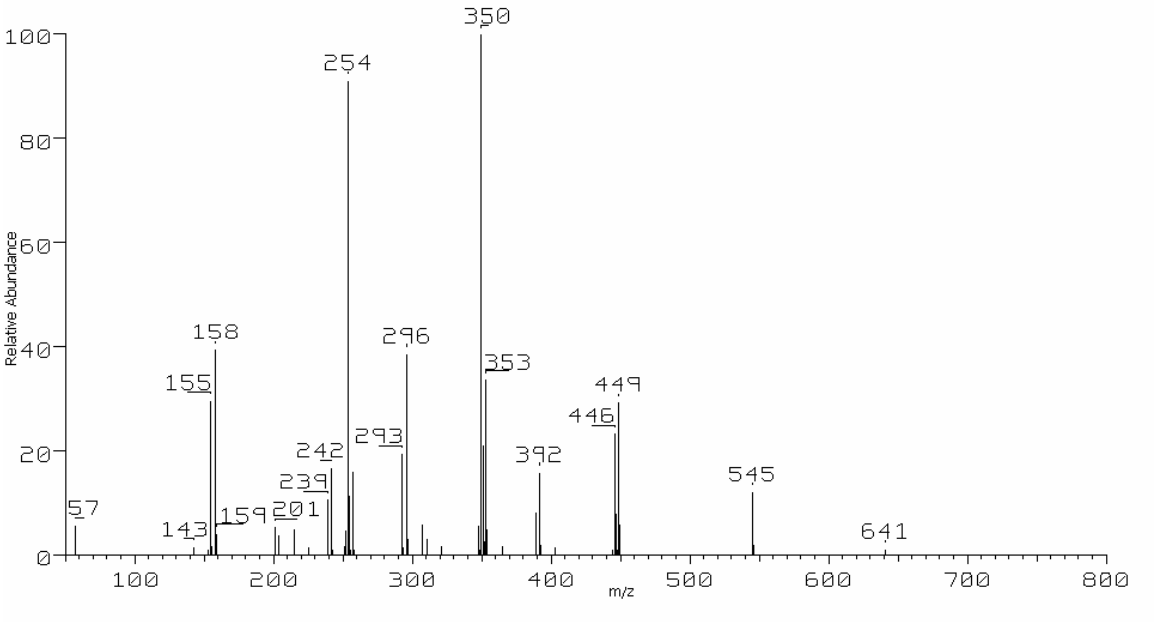

A.1.5 The 70 eV positive EI mass spectrum obtained during the reaction between $Co(tftm)_2$ with $Fe(hfac)_2$

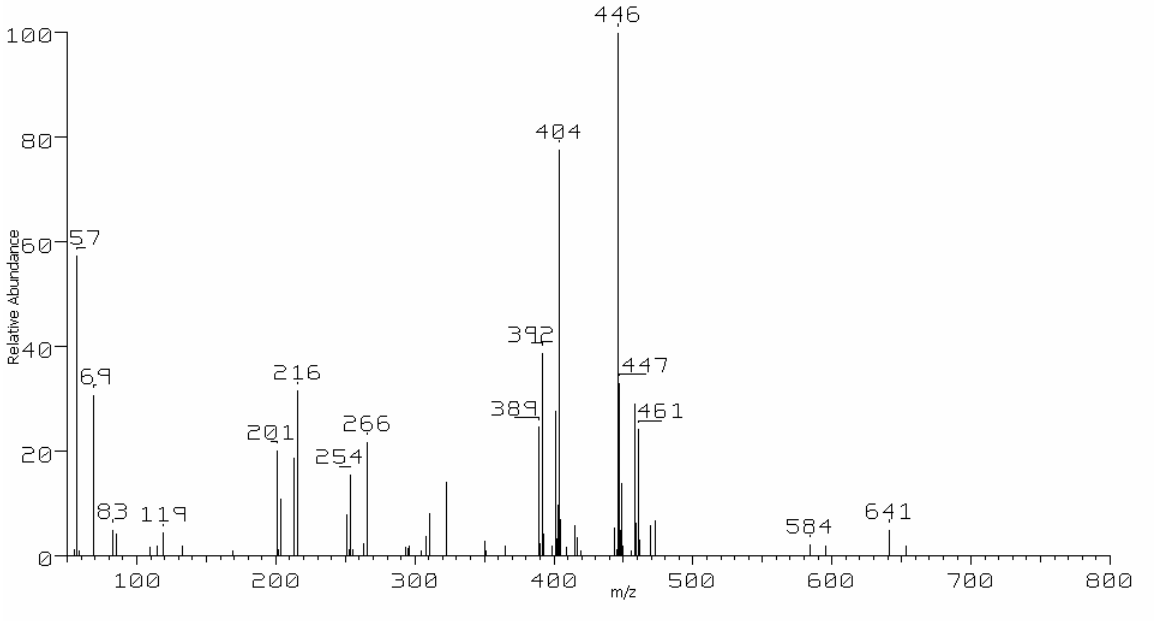

A.1.6 The 70 eV positive EI mass spectrum obtained during the reaction between $Co(tftm)_2$ with $Ni(acac)_2$

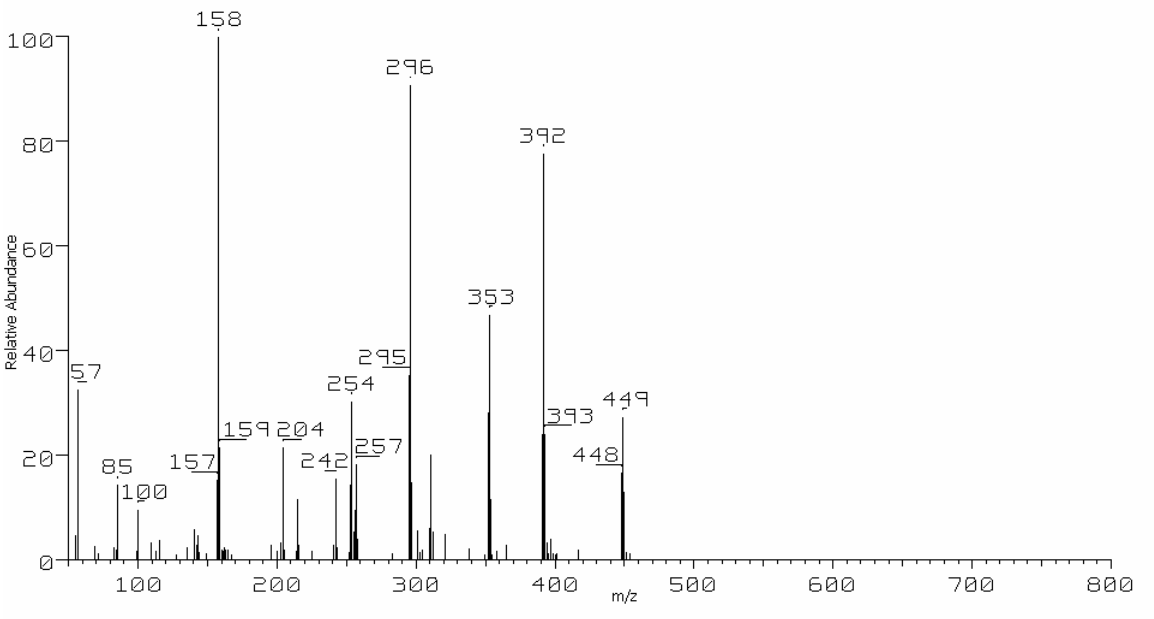

A.1.7 The 70 eV positive EI mass spectrum obtained during the reaction between $Co(tftm)_2$ with $Ni(hfac)_2$

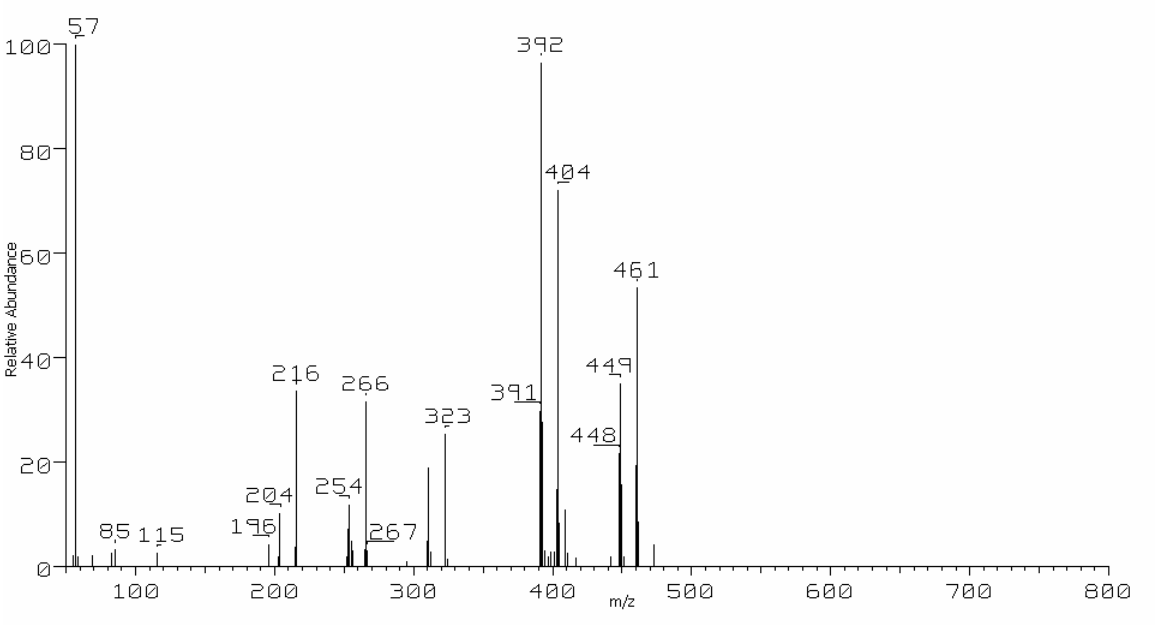

A.1.8. The 70 eV positive EI mass spectrum obtained during the reaction between $Co(tftm)_2$ with $Cu(hfac)_2$

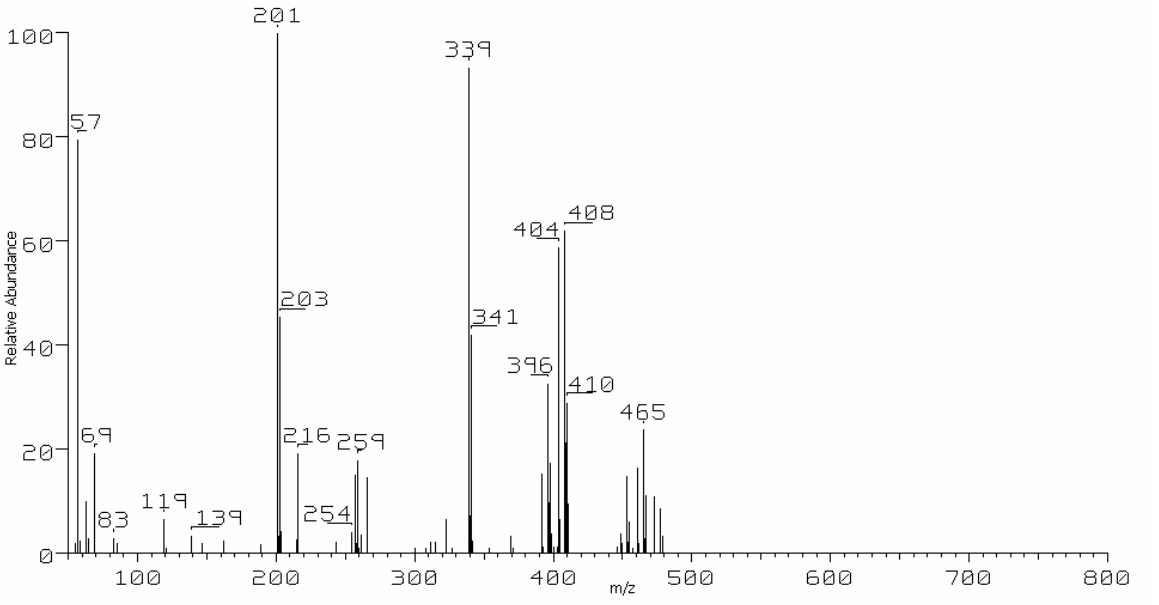

A.1.9 The 70 eV positive EI mass spectrum obtained during the reaction between $Co(tftm)_2$ with $Zn(acac)_2$

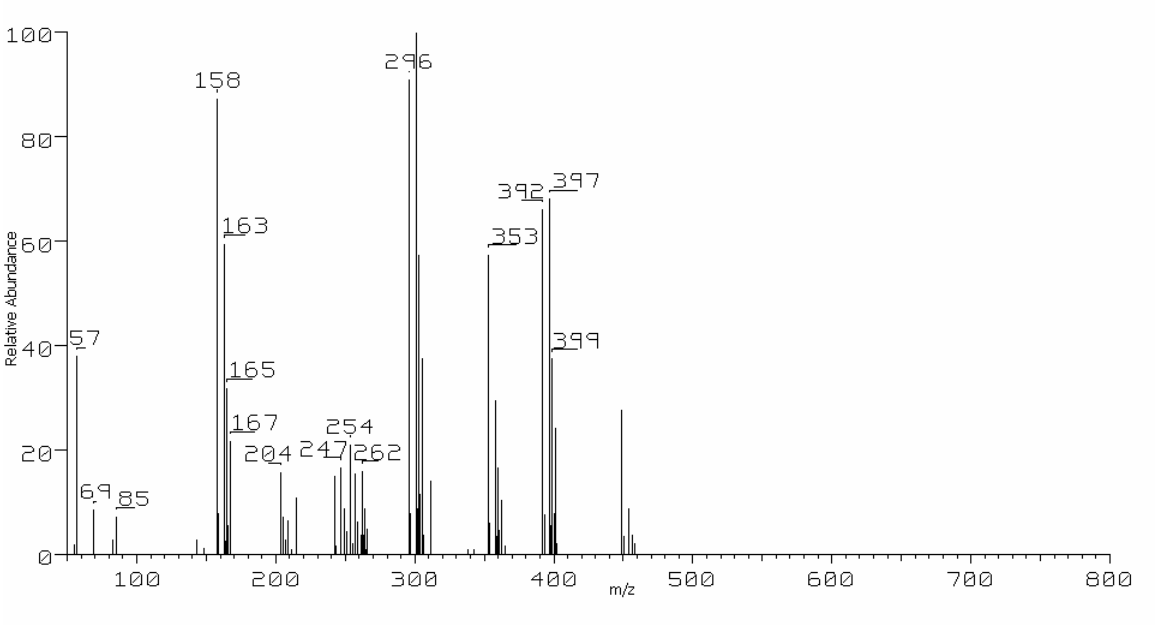

A.1.10 The 70 eV positive EI mass spectrum obtained during the reaction between $Co(tftm)_2$ with $Al(acac)_3$

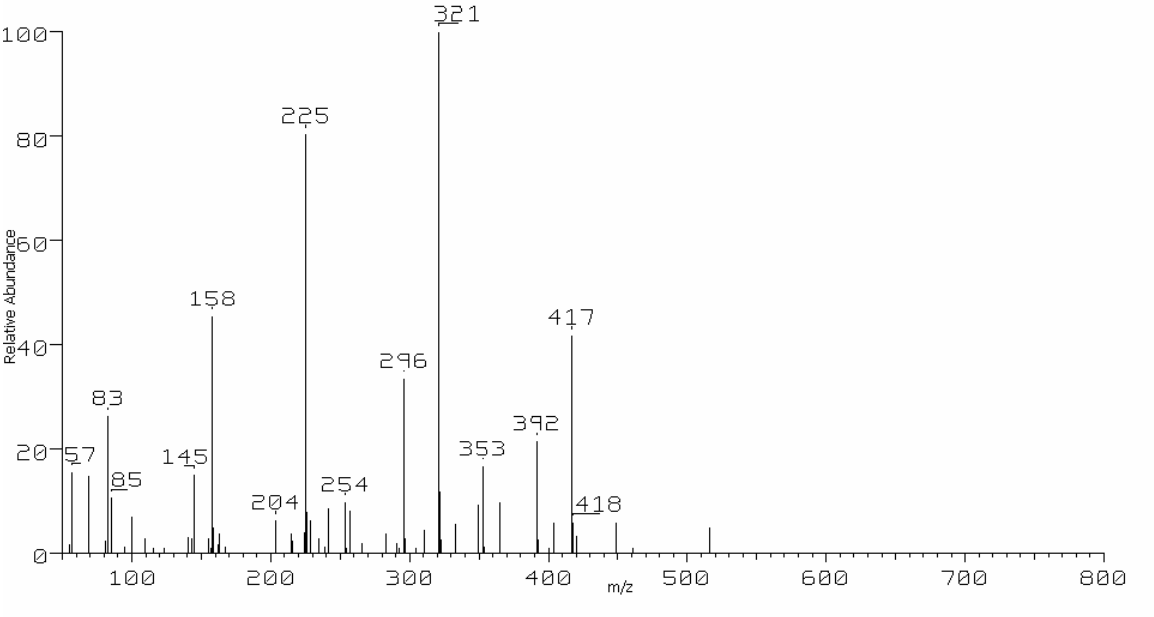

A.1.11 The 70 eV positive EI mass spectrum obtained during the reaction between $Co(tftm)_2$ with $Al(hfac)_3$

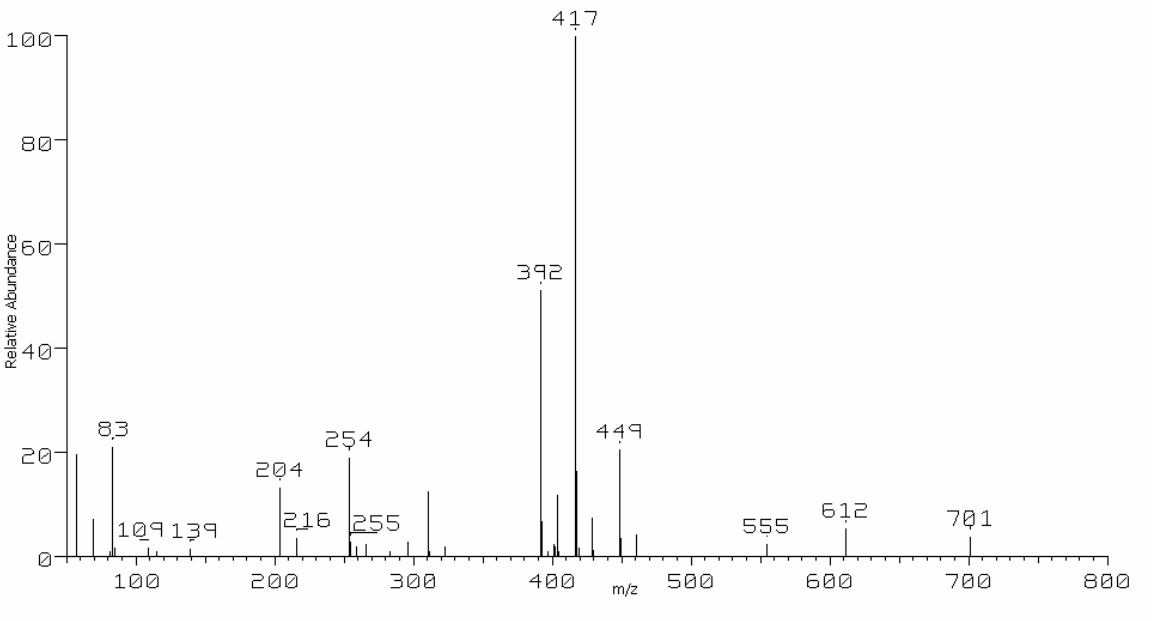

A.2 $Ni(tftm)_2$ Reactions

A.2.1 The 70 eV positive EI mass spectrum obtained during the reaction between $Ni(tftm)_2$ and $Cr(acac)_3$

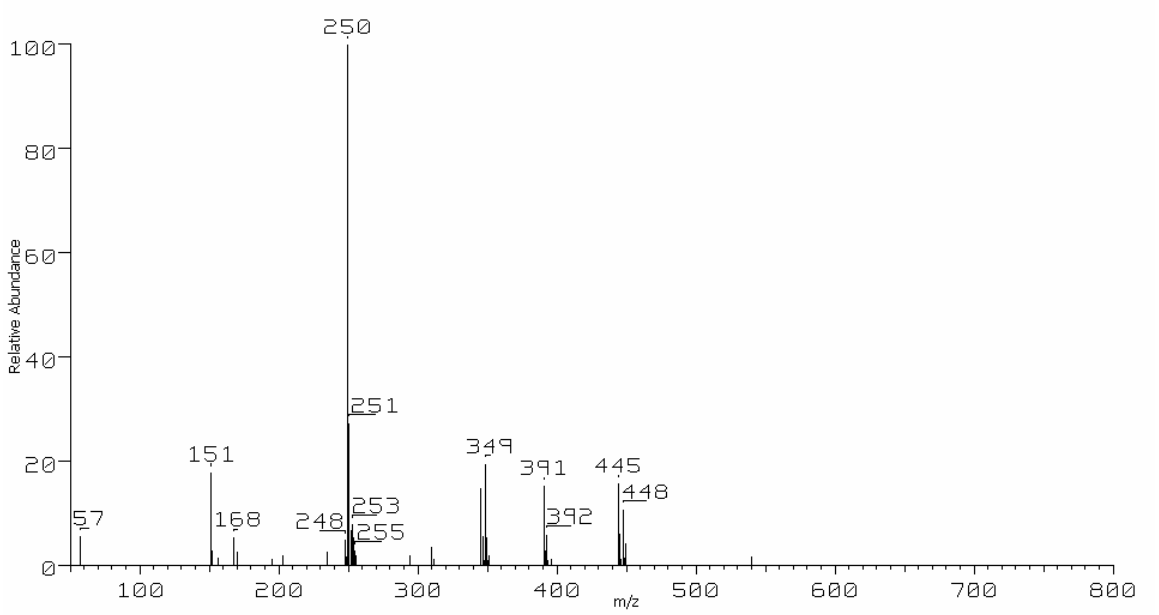

A.2.2 The 70 eV positive EI mass spectrum obtained during the reaction between $Ni(tftm)_2$ and $Mn(acac)_2$

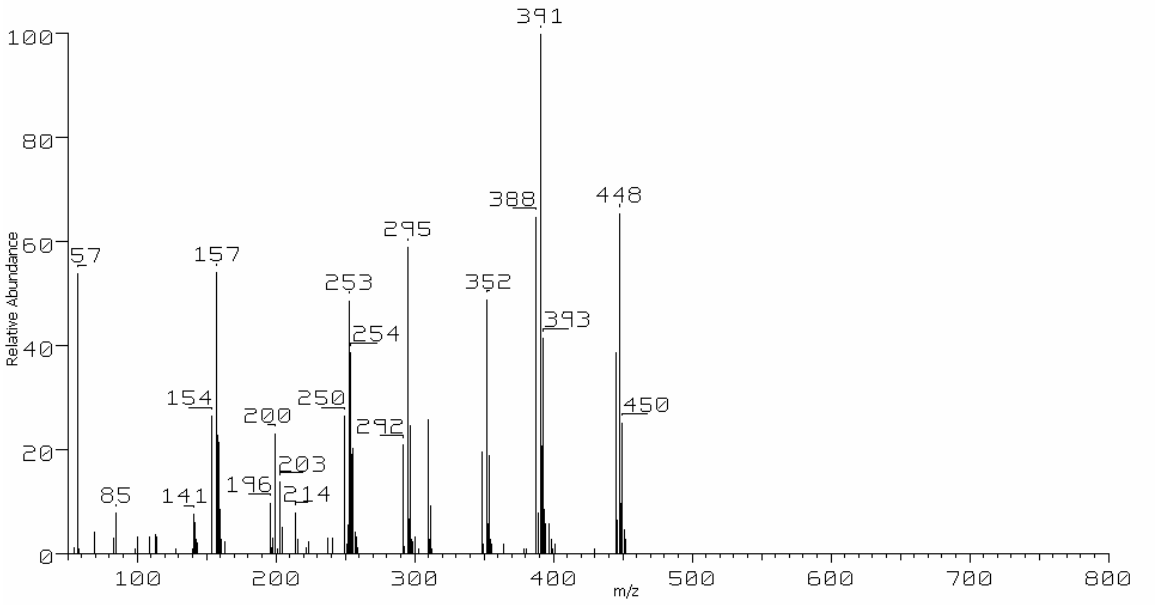

A.2.3 The 70 eV positive EI mass spectrum obtained during the reaction between $Ni(tftm)_2$ and $Mn(hfac)_2$

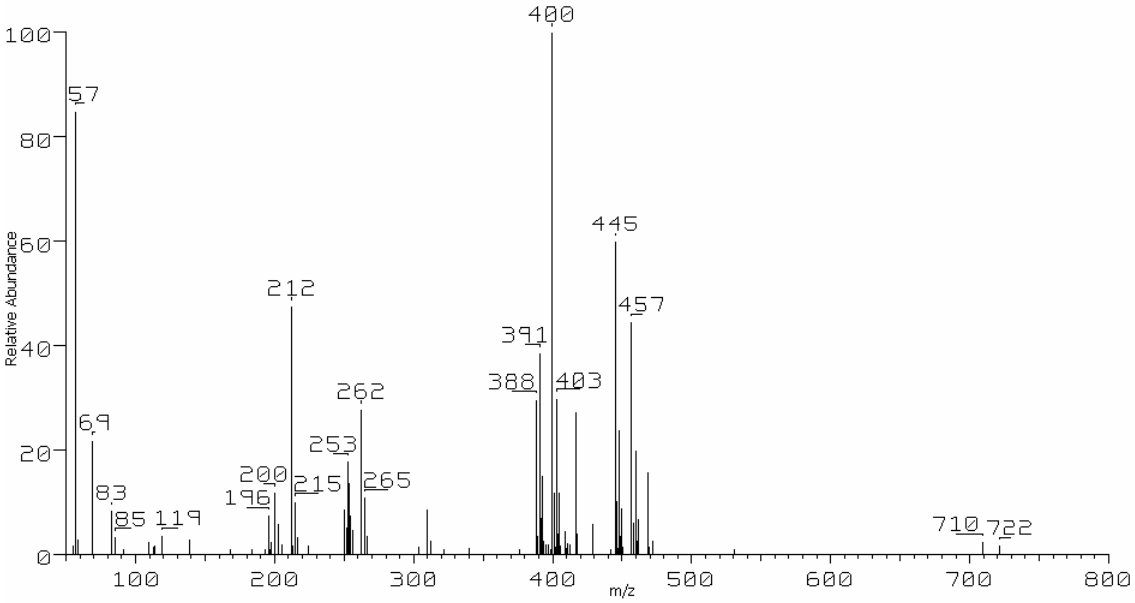

A.2.4 The 70 eV positive EI mass spectrum obtained during the reaction between $Ni(tftm)_2$ and $Fe(acac)_3$

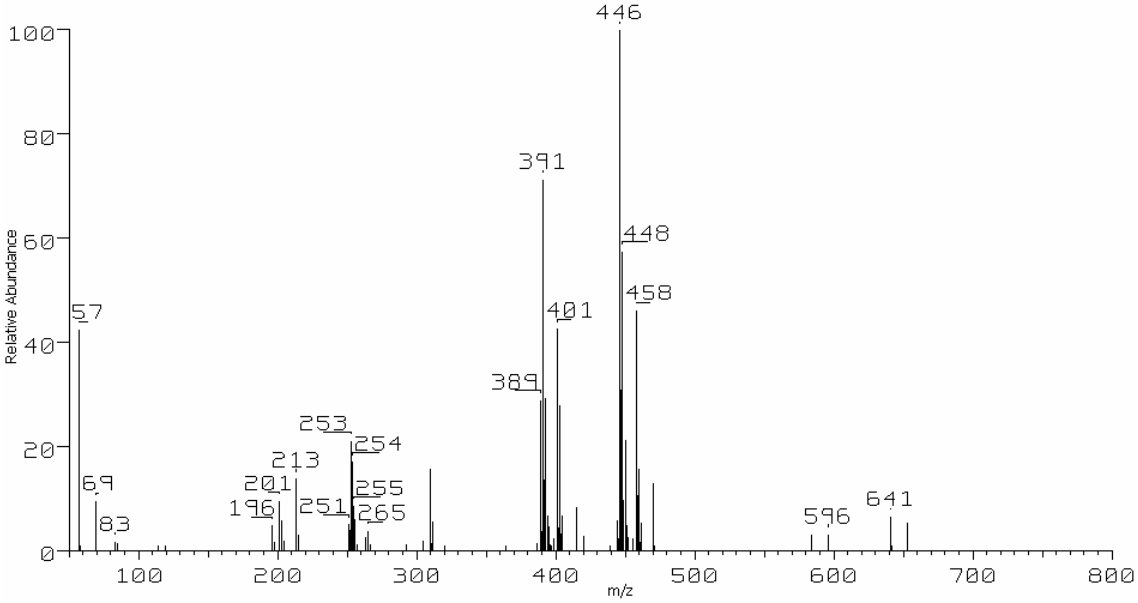

A.2.5 The 70 eV positive EI mass spectrum obtained during the reaction between $Ni(tftm)_2$ and $Co(acac)_3$

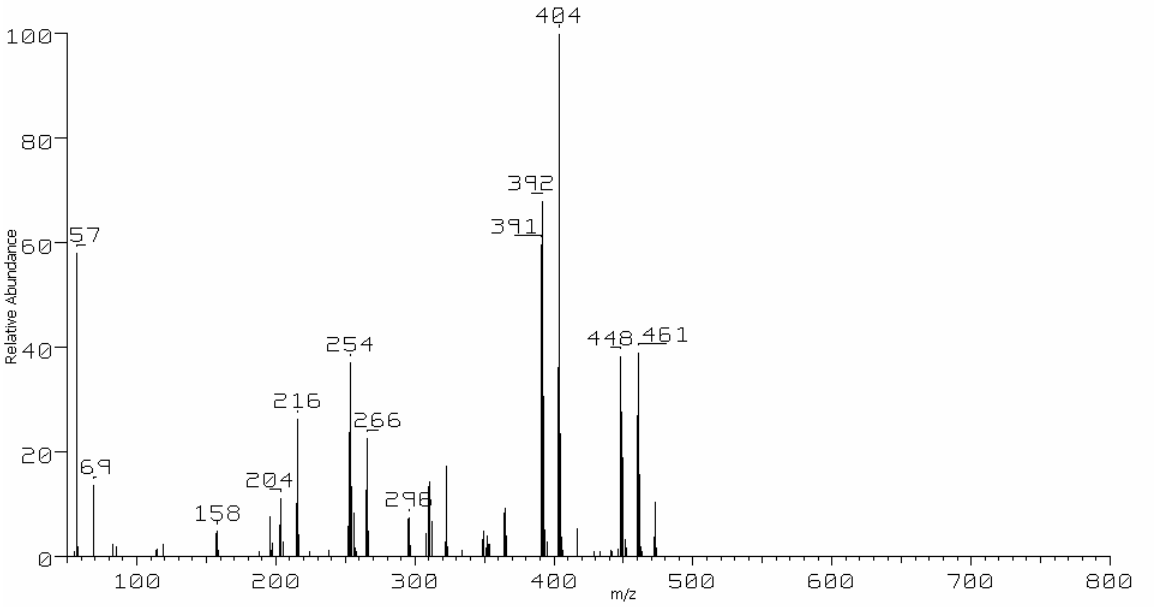

A.2.6 The 70 eV positive EI mass spectrum obtained during the reaction between $Ni(tftm)_2$ and $Co(hfac)_2$

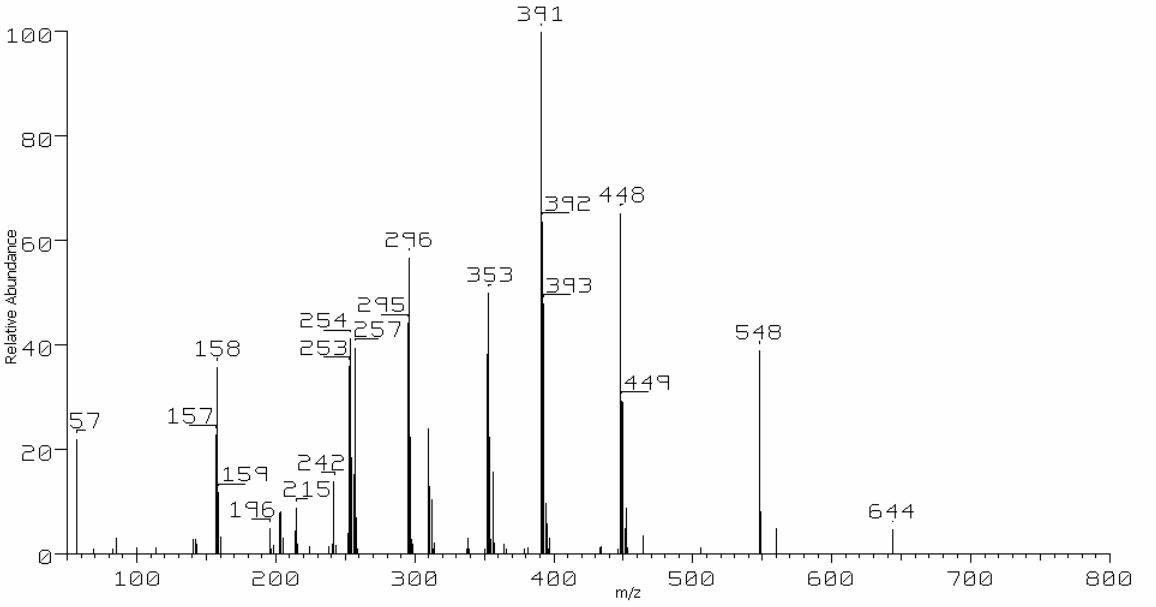

A.2.7 The 70 eV positive EI mass spectrum obtained during the reaction between $Ni(tftm)_2$ and $Cu(hfac)_2$

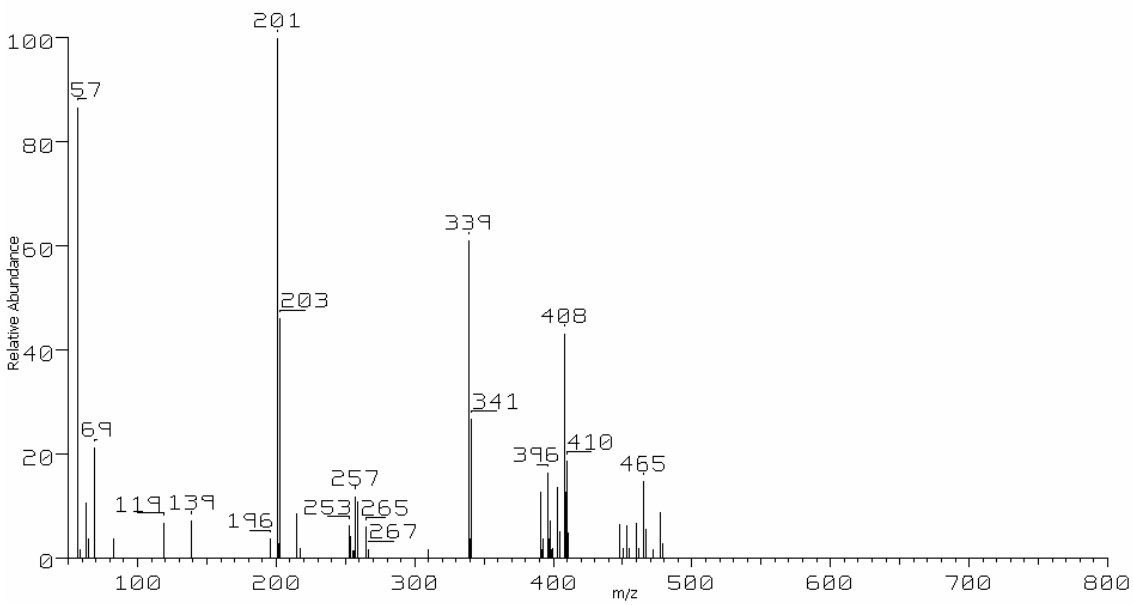

A.2.8 The 70 eV positive EI mass spectrum obtained during the reaction between $Ni(tftm)_2$ and $Zn(acac)_2$

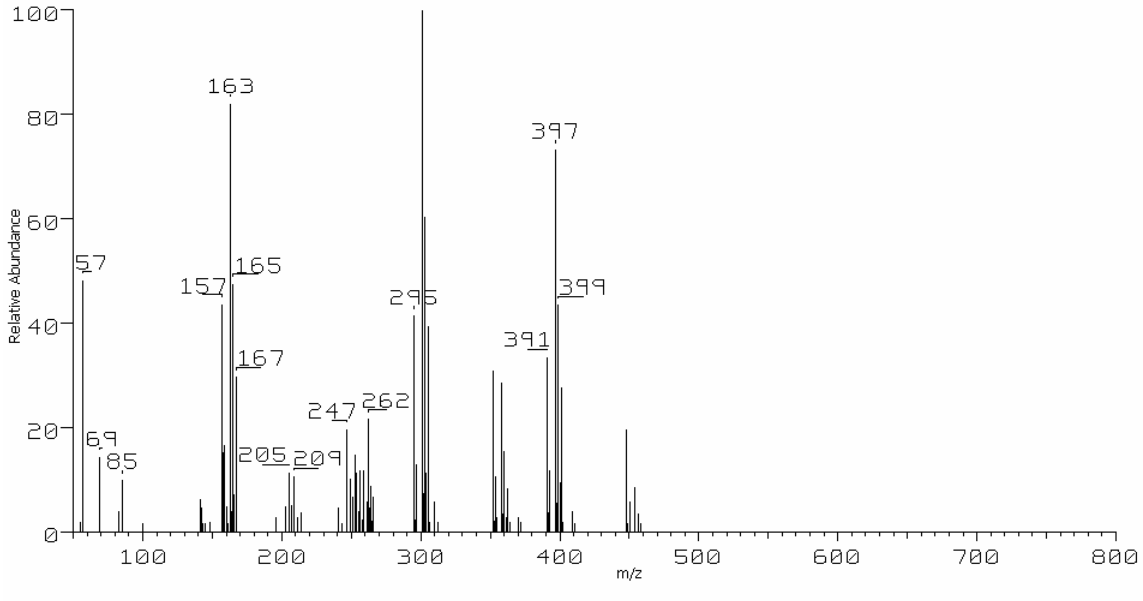

A.2.9 The 70 eV positive EI mass spectrum obtained during the reaction between $Ni(tftm)_2$ and $Al(acac)_3$

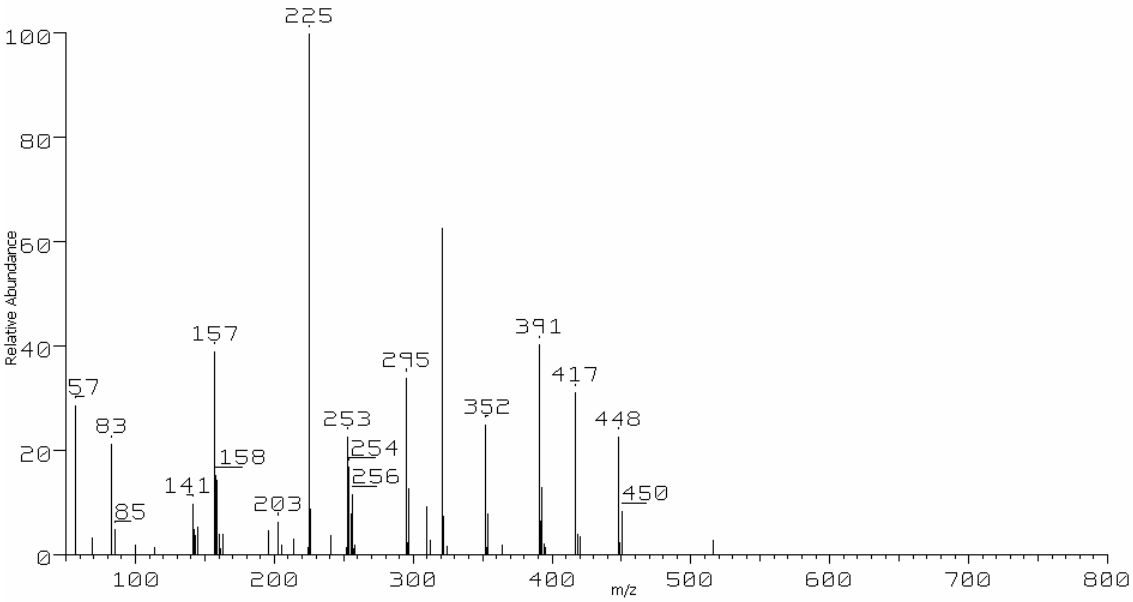

A.2.10 The 70 eV positive EI mass spectrum obtained during the reaction between $Ni(tftm)_2$ and $Al(hfac)_3$

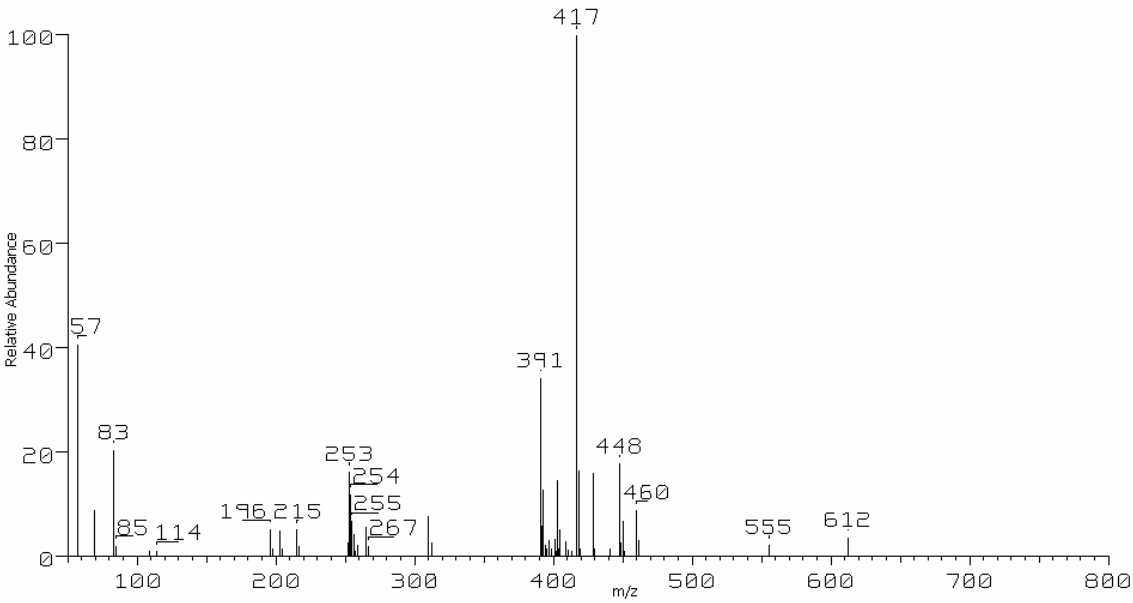

A.3 $Cu(tftm)_2$ Reactions

A.3.1 The 70 eV positive EI mass spectrum obtained during the reaction between $Cu(tftm)_2$ and $Cr(acac)_3$

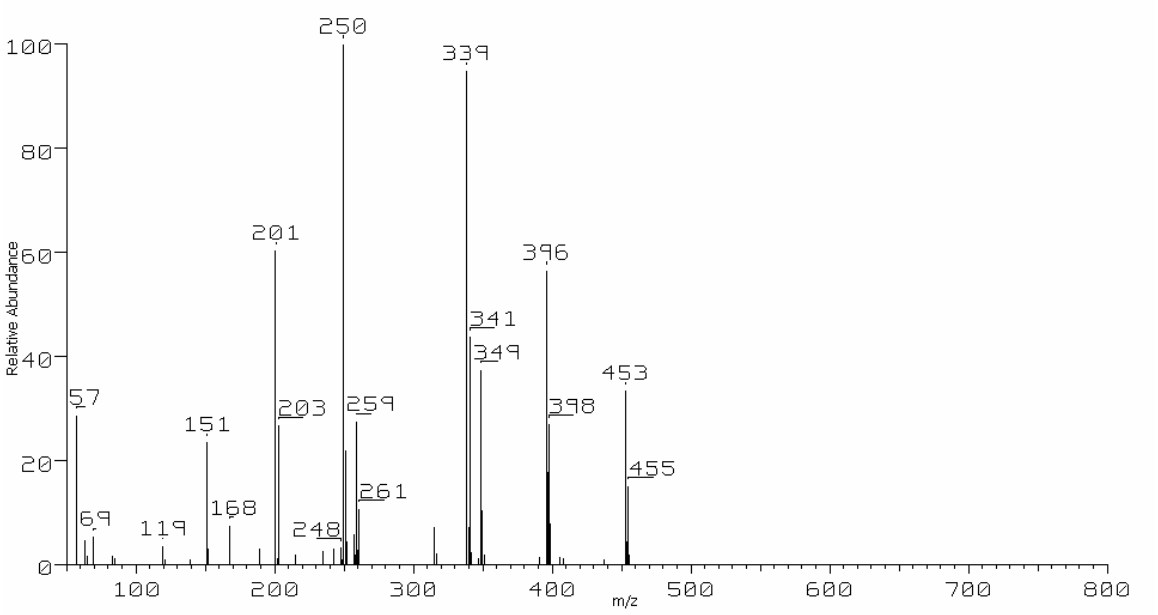

A.3.2 The 70 eV positive EI mass spectrum obtained during the reaction between $Cu(tftm)_2$ and $Mn(hfac)_2$

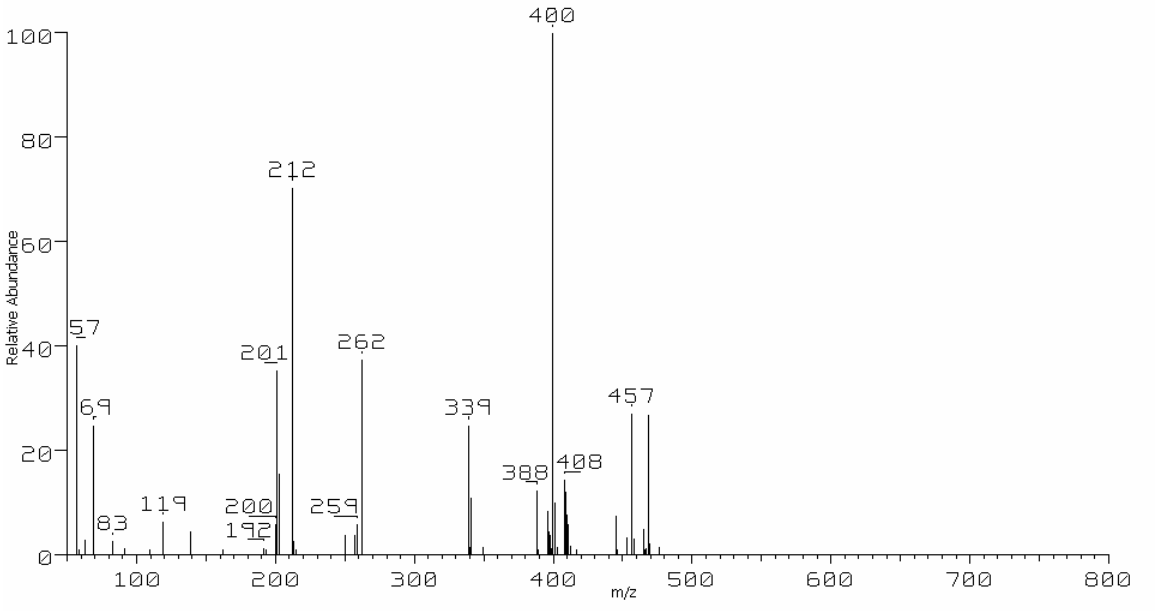

A.3.3 The 70 eV positive EI mass spectrum obtained during the reaction between $Cu(tftm)_2$ and $Fe(acac)_3$

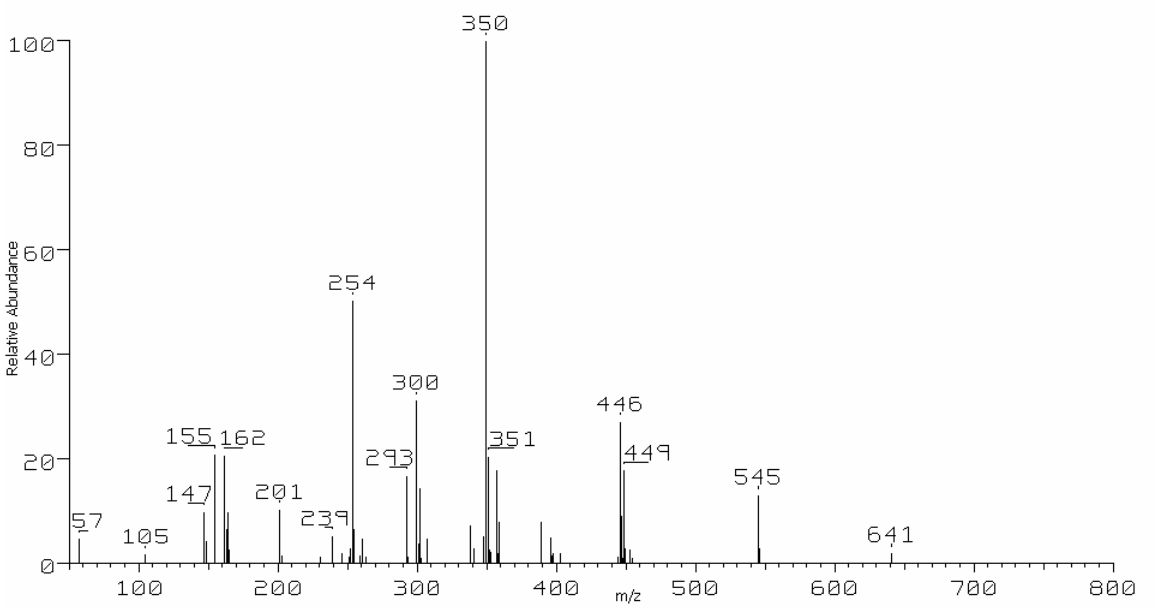

A.3.4 The 70 eV positive EI mass spectrum obtained during the reaction between $Cu(tftm)_2$ and $Fe(hfac)_2$

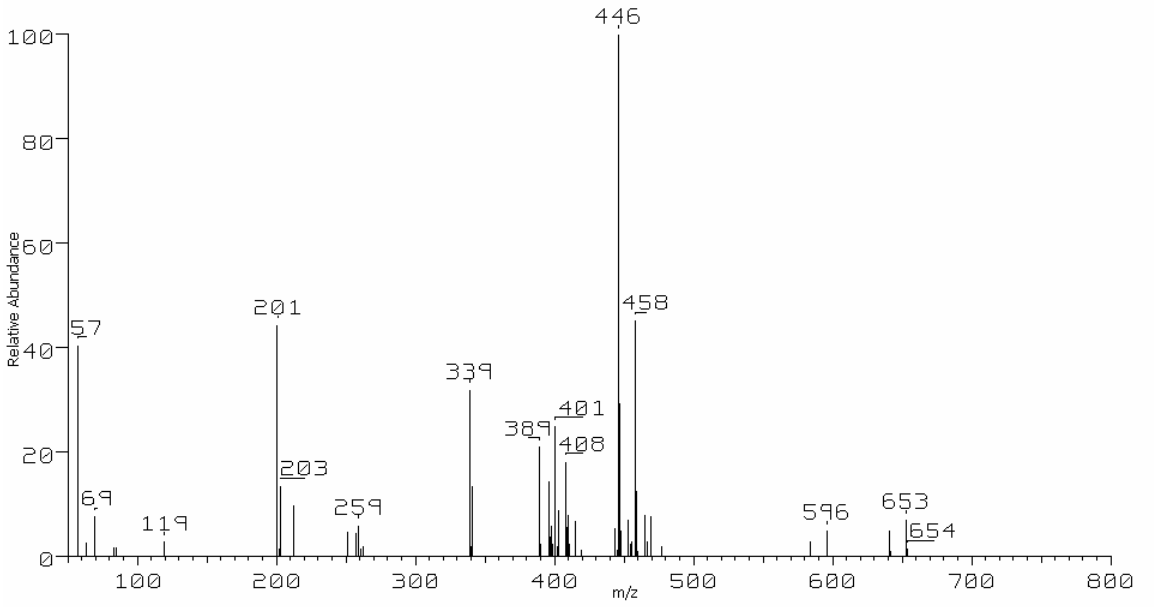

A.3.5 The 70 eV positive EI mass spectrum obtained during the reaction between $Cu(tftm)_2$ and $Co(acac)_2$

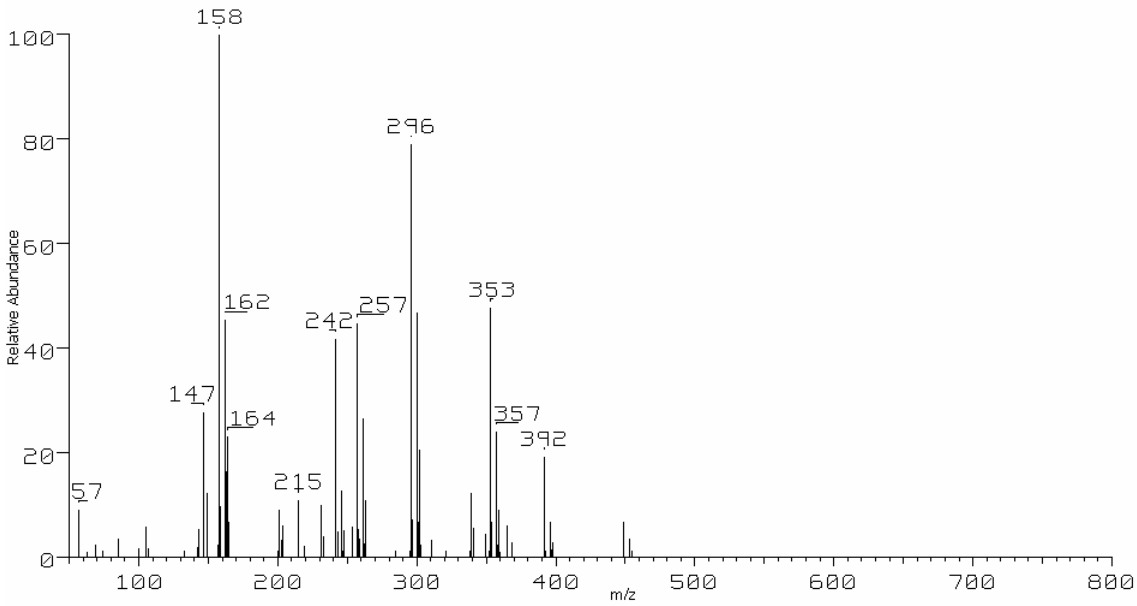

A.3.6 The 70 eV positive EI mass spectrum obtained during the reaction between $Cu(tftm)_2$ and $Co(acac)_3$

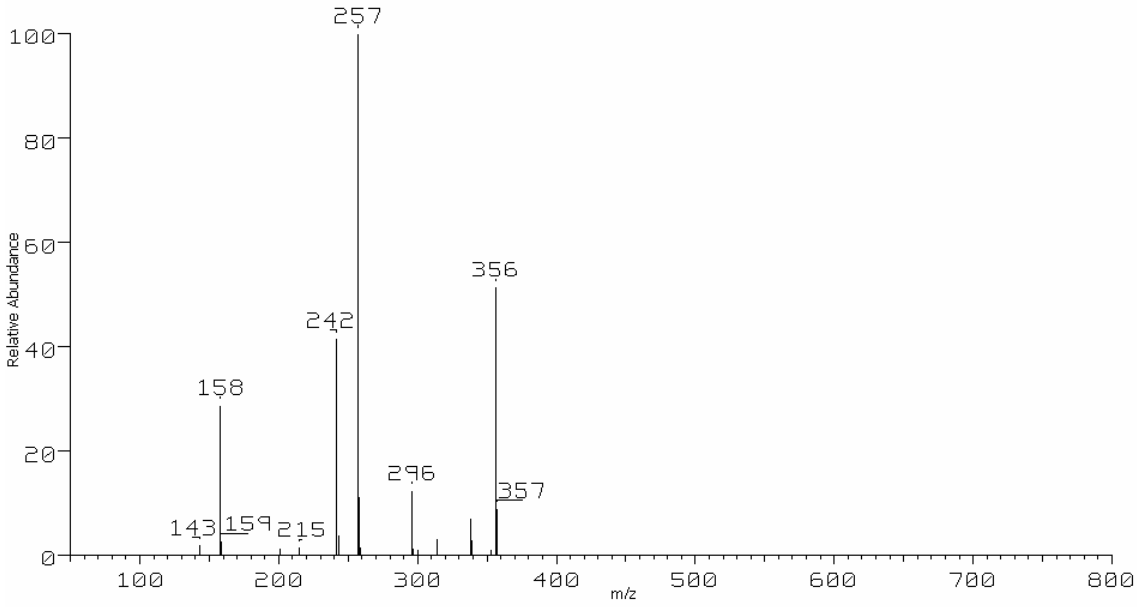

A.3.7 The 70 eV positive EI mass spectrum obtained during the reaction between $Cu(tftm)_2$ and $Co(hfac)_2$

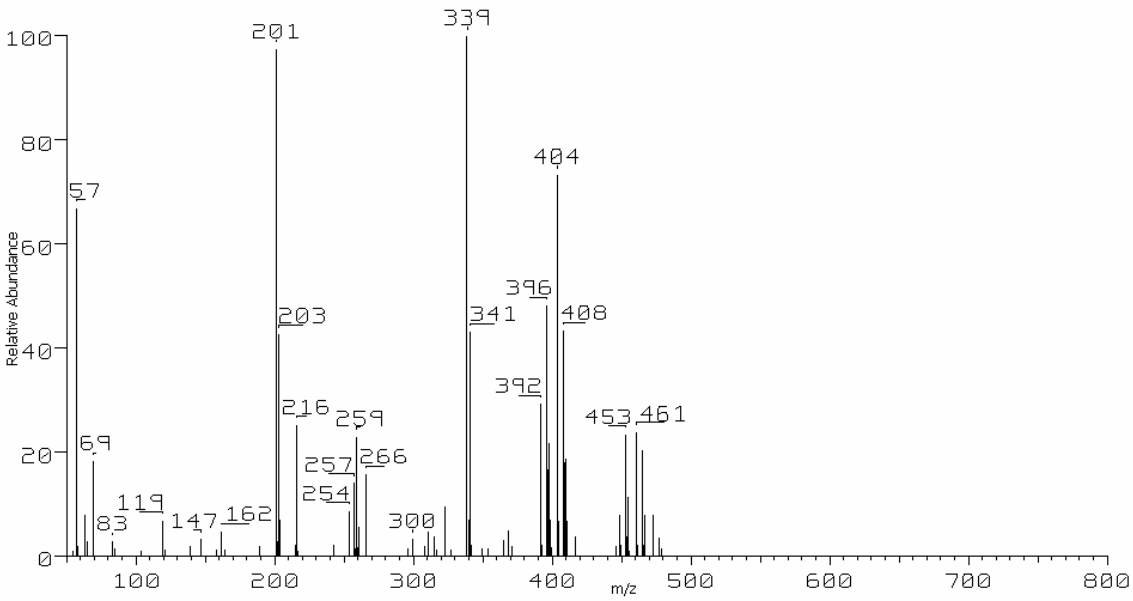

A.3.8 The 70 eV positive EI mass spectrum obtained during the reaction between $Cu(tftm)_2$ and $Zn(acac)_2$

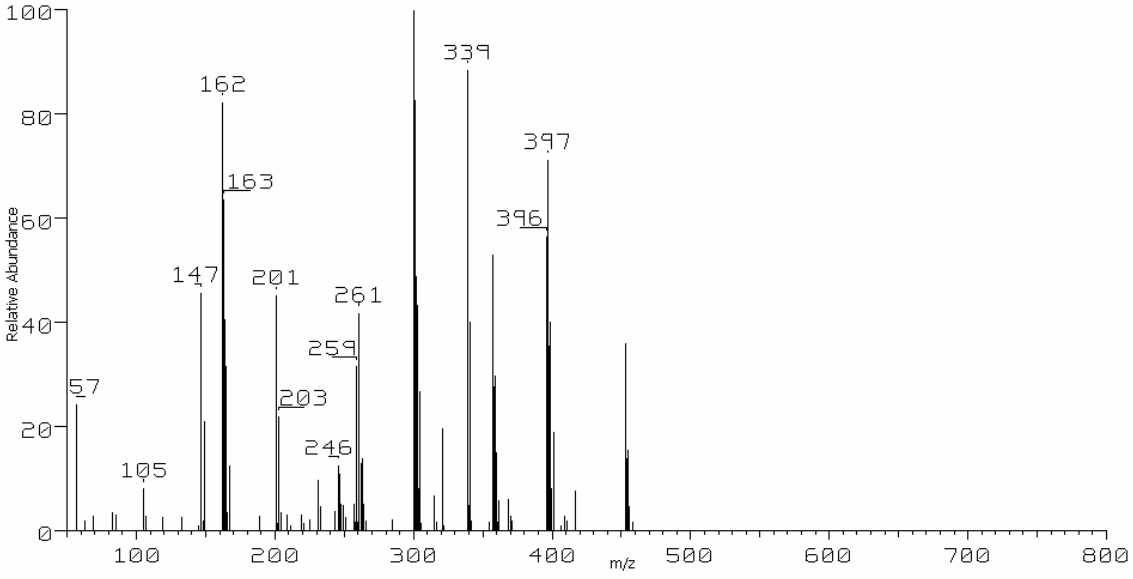

A.3.9 The 70 eV positive EI mass spectrum obtained during the reaction between $Cu(tftm)_2$ and $Al(acac)_3$

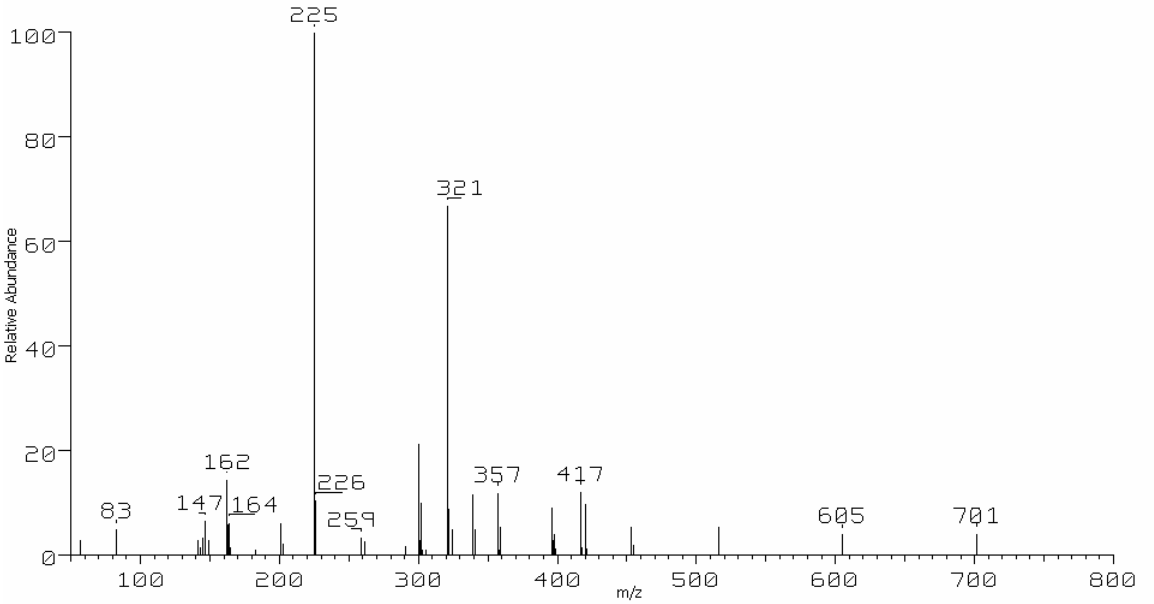

A.3.10 The 70 eV positive EI mass spectrum obtained during the reaction between $Cu(tftm)_2$ and $Al(hfac)_3$

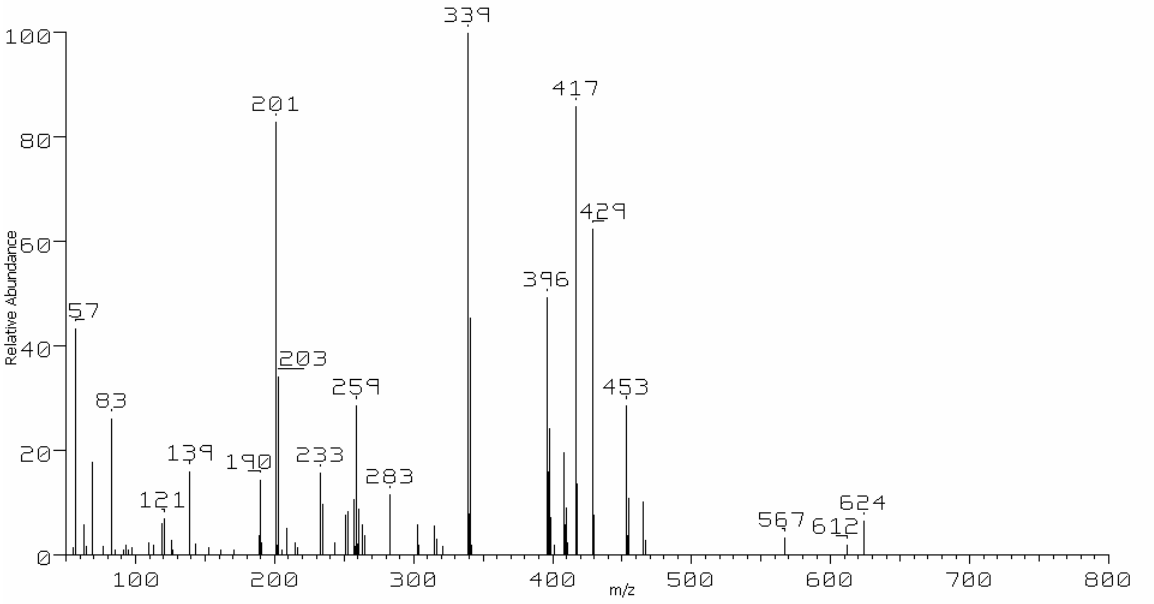

A.4 $Zn(tftm)_2$ Reactions

A.4.1 The 70 eV positive EI mass spectrum obtained during the reaction between $Zn(tftm)_2$ with $Al(acac)_3$

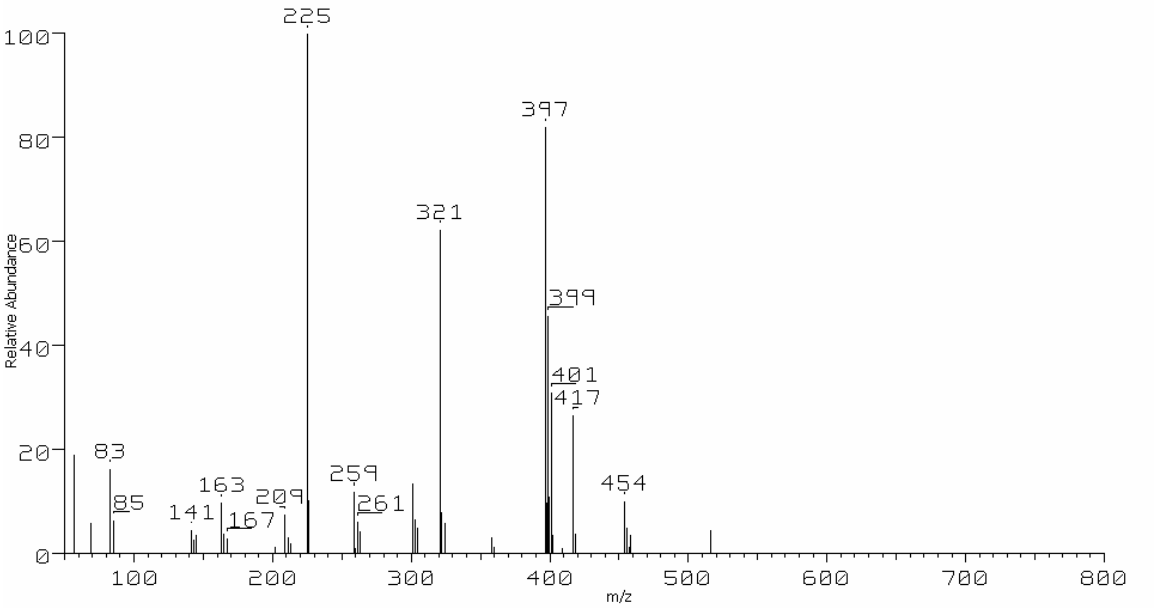

A.4.2 The 70 eV positive EI mass spectrum obtained during the reaction between $Zn(tftm)_2$ with $Al(hfac)_3$

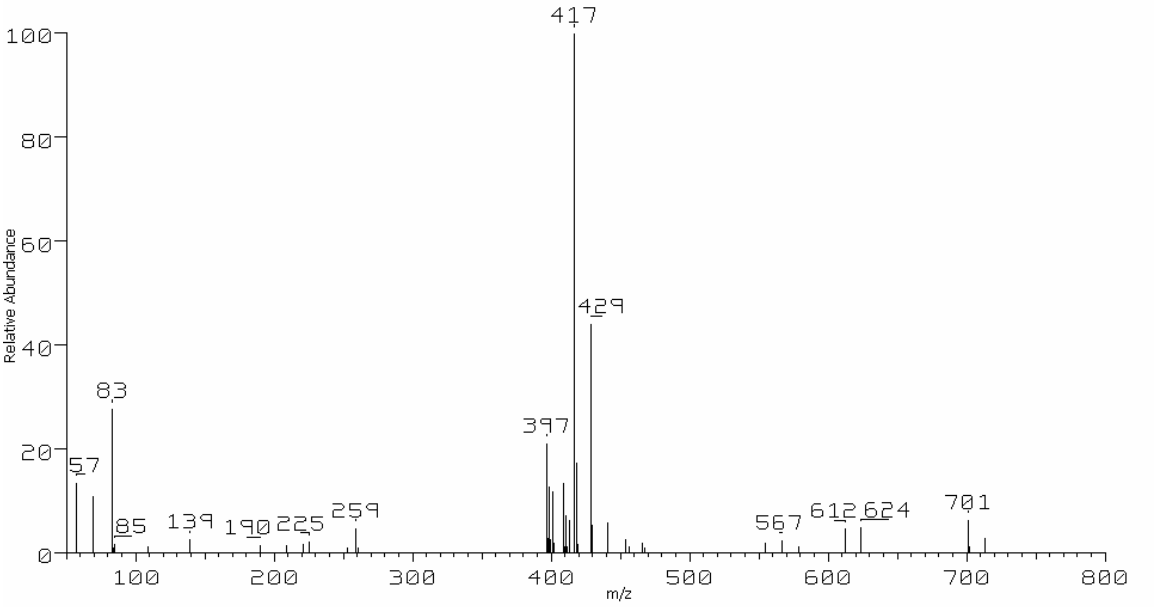

A.4.3 The 70 eV positive EI mass spectrum obtained during the reaction between $Zn(tftm)_2$ with $Ni(hfac)_3$

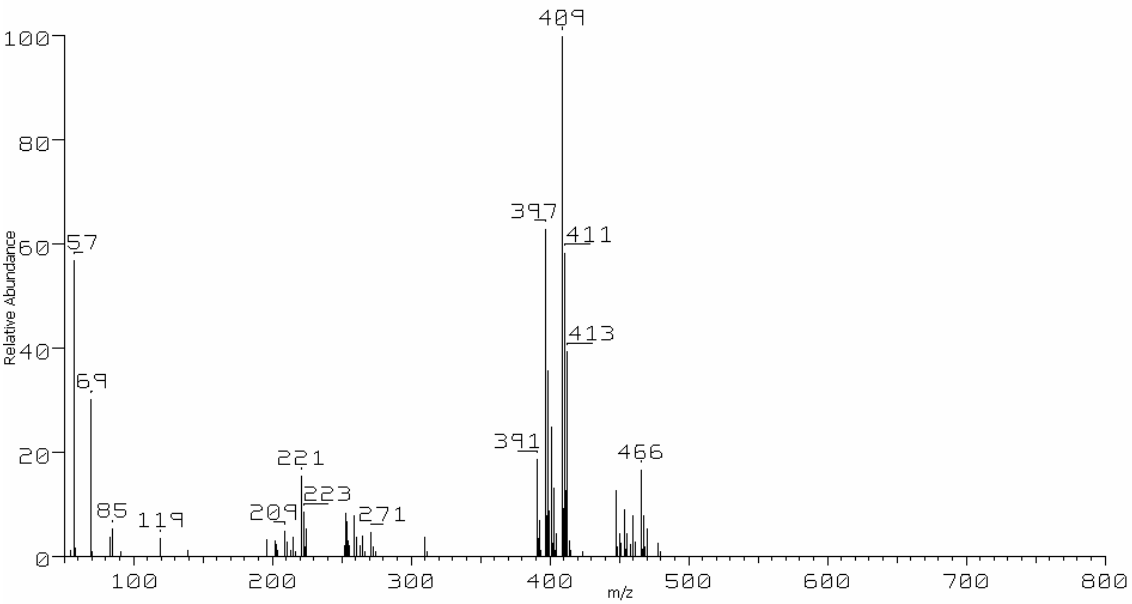

A.4.4. The 70 eV positive EI mass spectrum obtained during the reaction between $Zn(tftm)_2$ with $Mn(acac)_2$

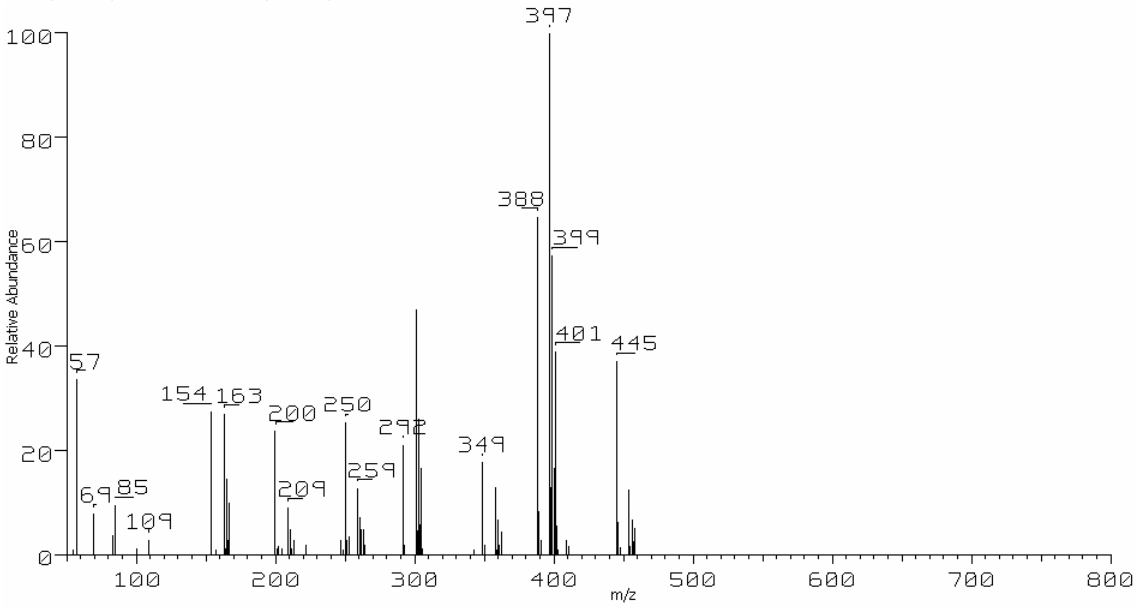

A.4.5 The 70 eV positive EI mass spectrum obtained during the reaction between $Zn(tftm)_2$ with $Fe(acac)_3$

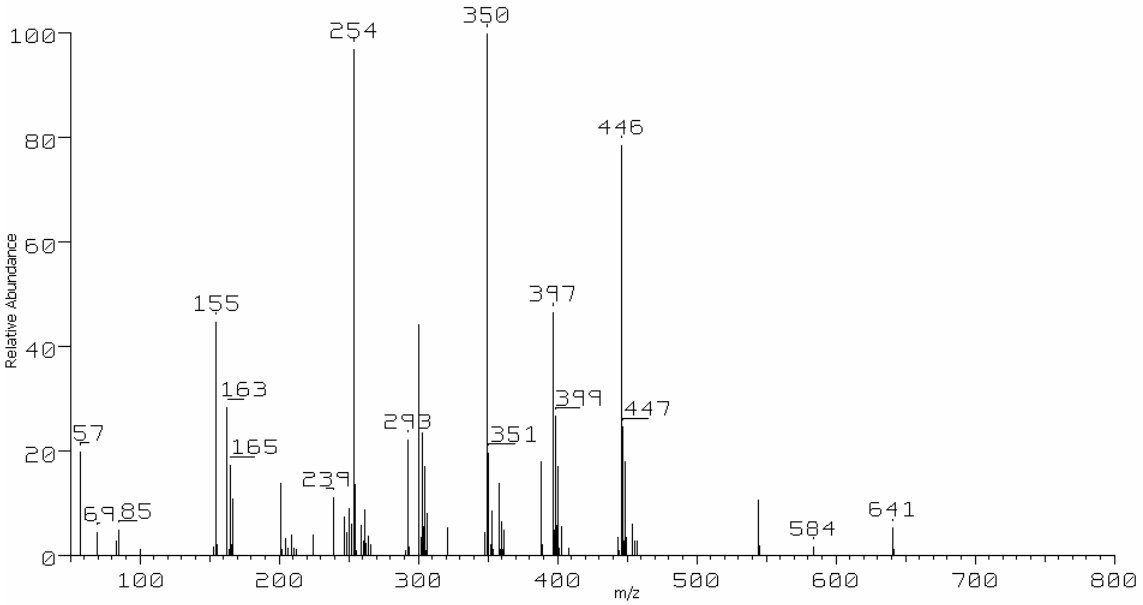

A.4.6 The 70 eV positive EI mass spectrum obtained during the reaction between $Zn(tftm)_2$ with $Fe(hfac)_2$

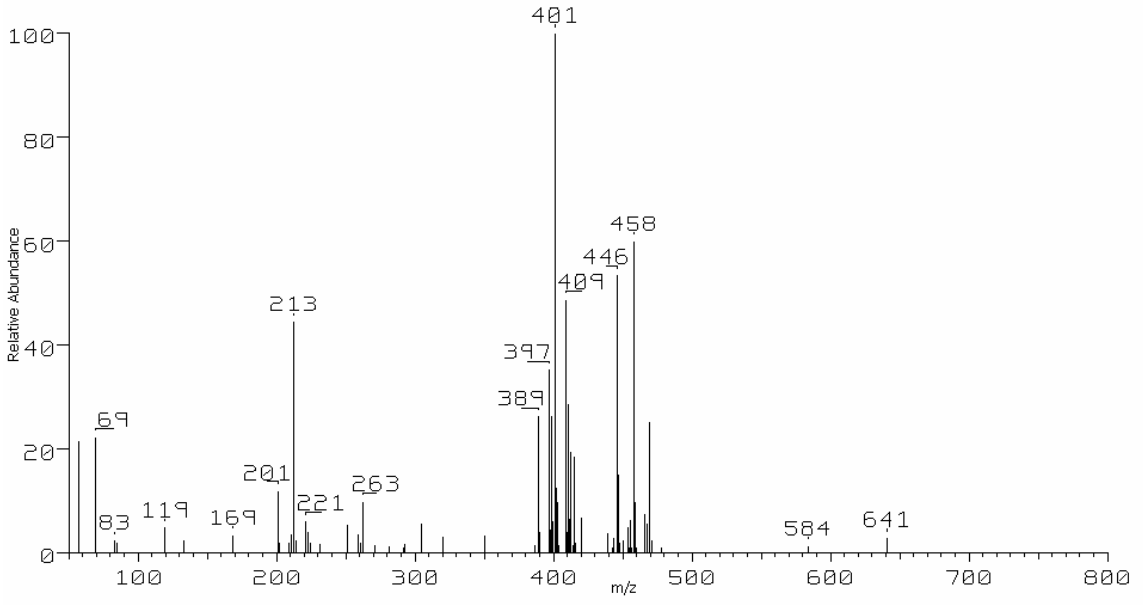

A.4.7 The 70 eV positive EI mass spectrum obtained during the reaction between $Zn(tftm)_2$ with $Ni(acac)_2$

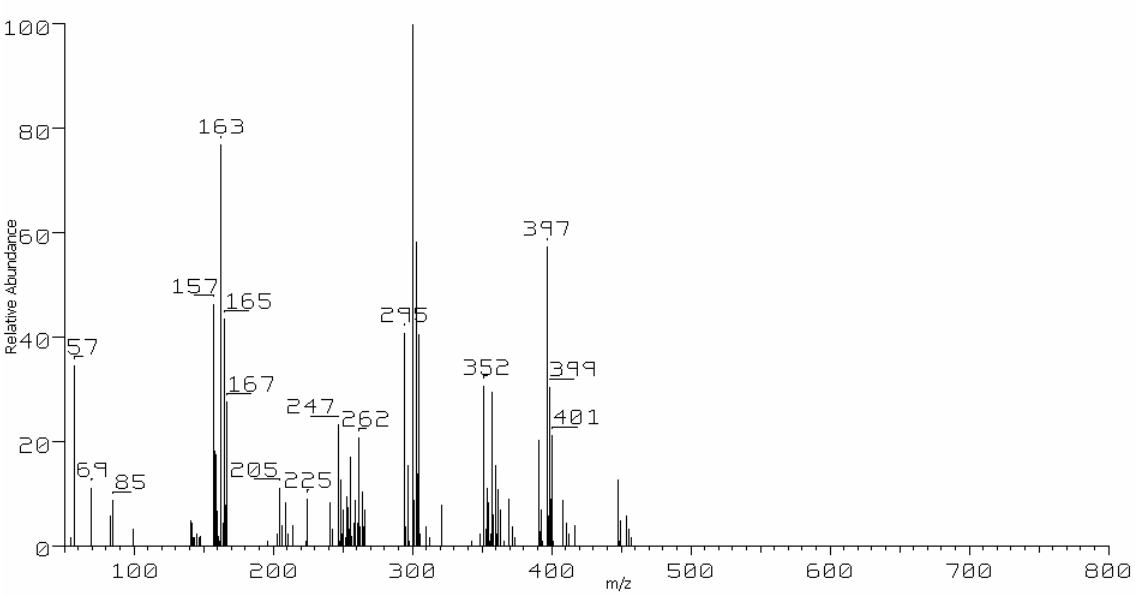

A.4.8 The 70 eV positive EI mass spectrum obtained during the reaction between $Zn(tftm)_2$ with $Co(hfac)_2$

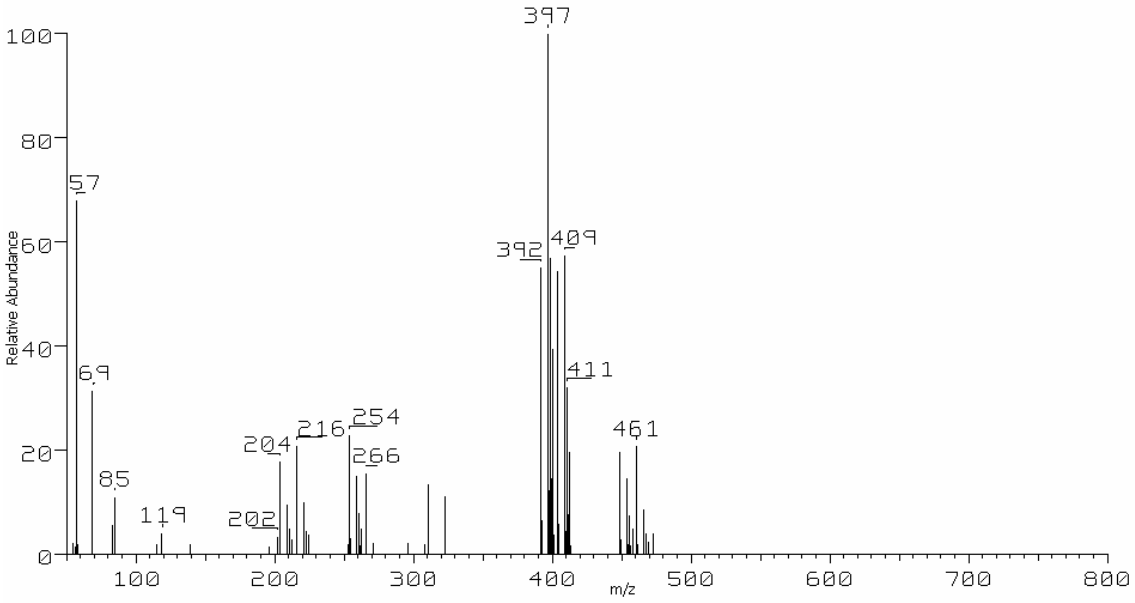

A.4.9 The 70 eV positive EI mass spectrum obtained during the reaction between $Zn(tftm)_2$ with $Co(acac)_2$

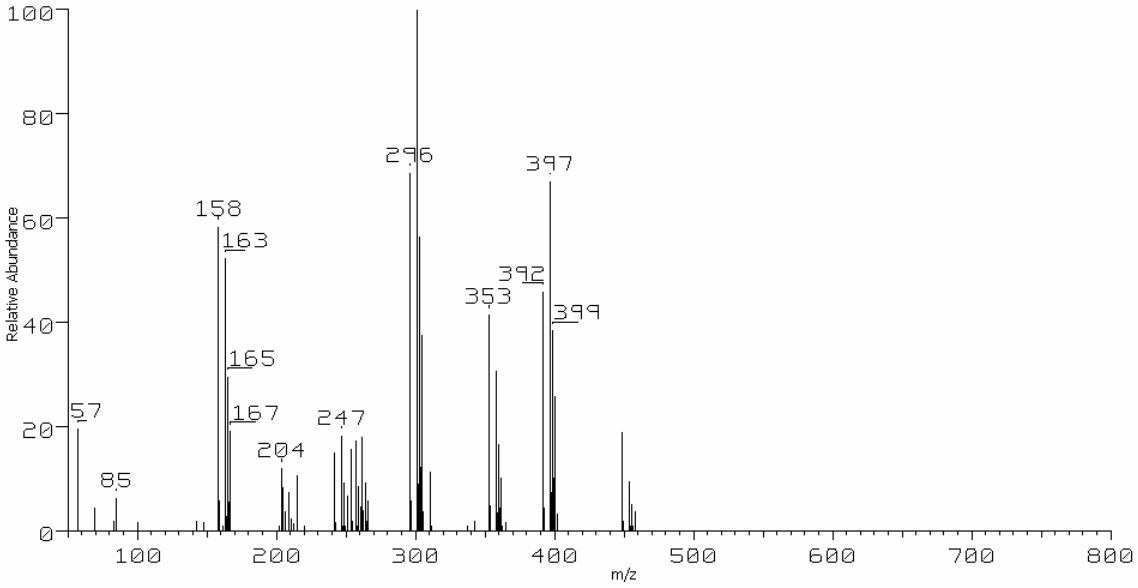

A.4.10The 70 eV positive EI mass spectrum obtained during the reaction between $Zn(tftm)_2$ with $Co(acac)_3$

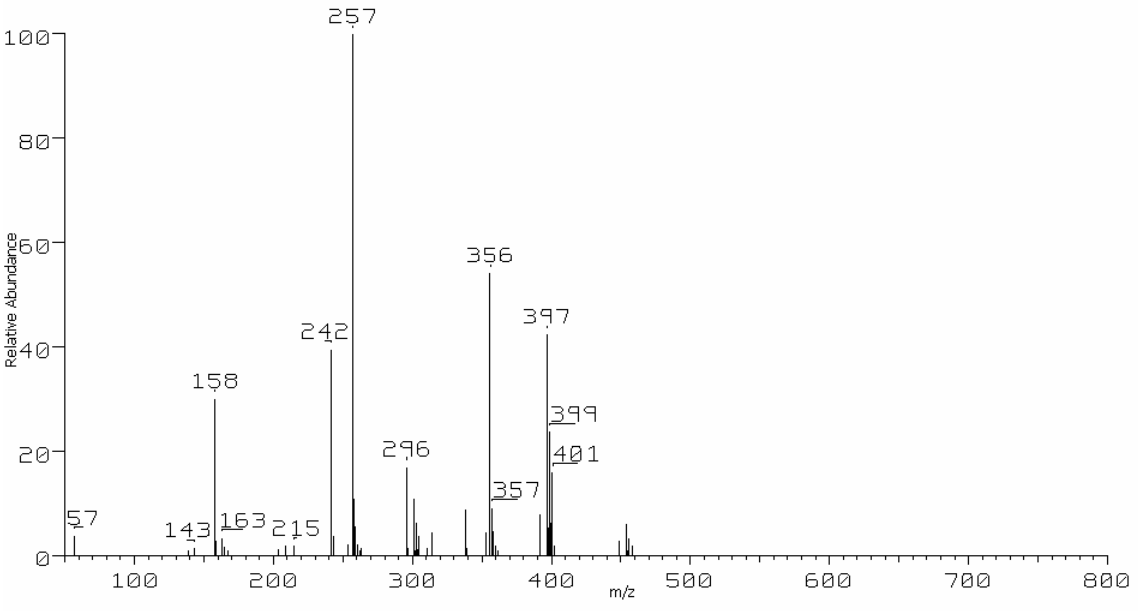

A.4.11 The 70 eV positive EI mass spectrum obtained during the reaction between $Zn(tftm)_2$ with $Cu(hfac)_2$

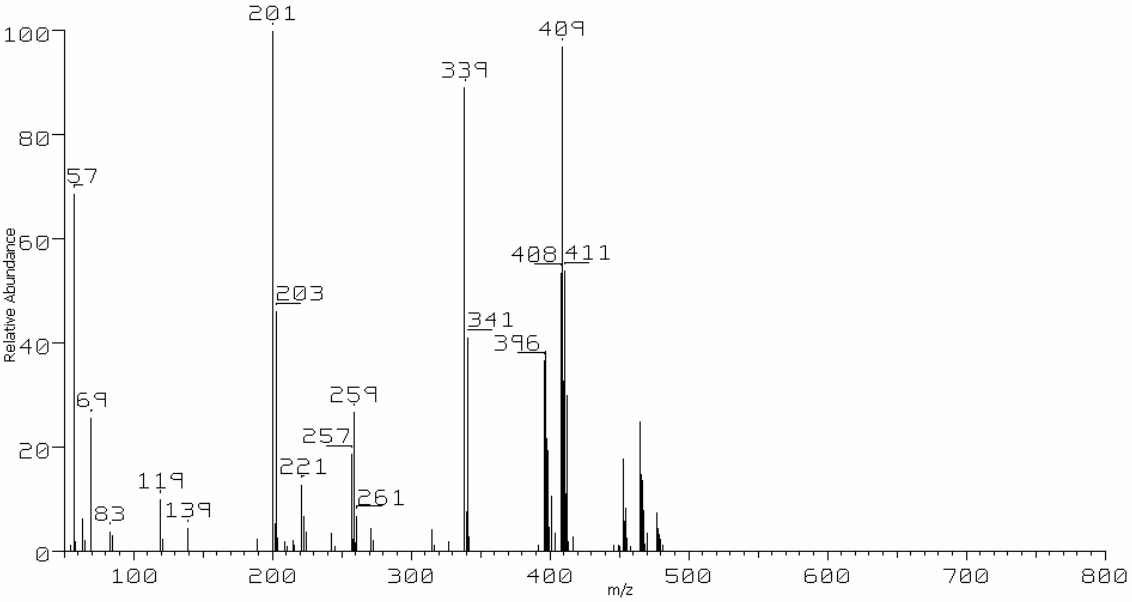

A.4.12 The 70 eV positive EI mass spectrum obtained during the reaction between $Zn(tftm)_2$ with $Cr(acac)_3$

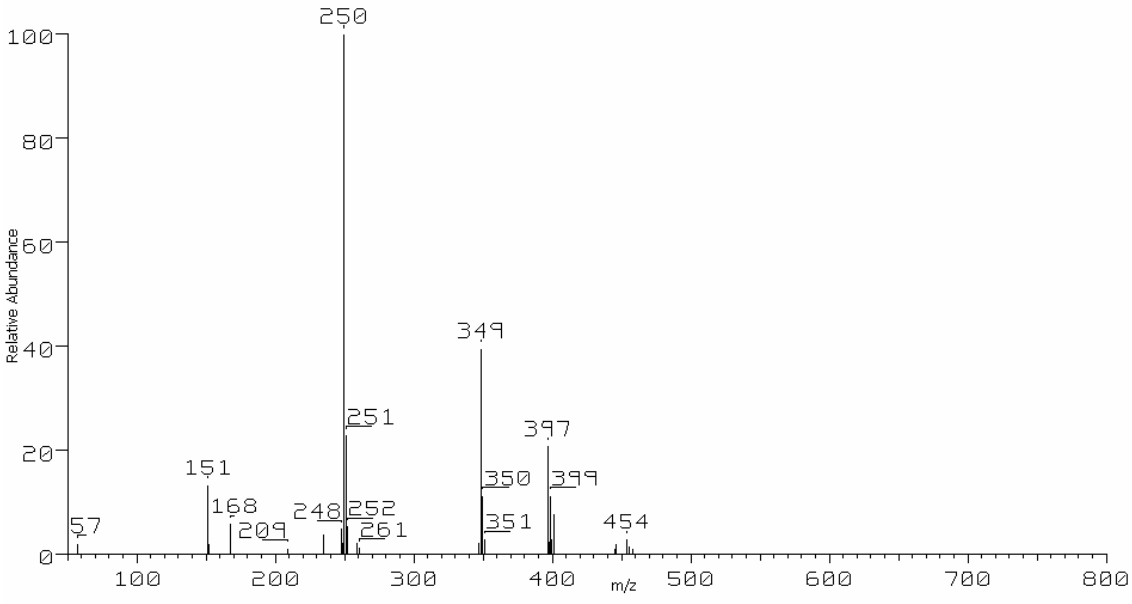

A.5 $Al(tftm)_3$ Reactions

A.5.1 The 70 eV positive EI mass spectrum obtained during the reaction between $Al(tftm)_3$ & $Cr(acac)_3$

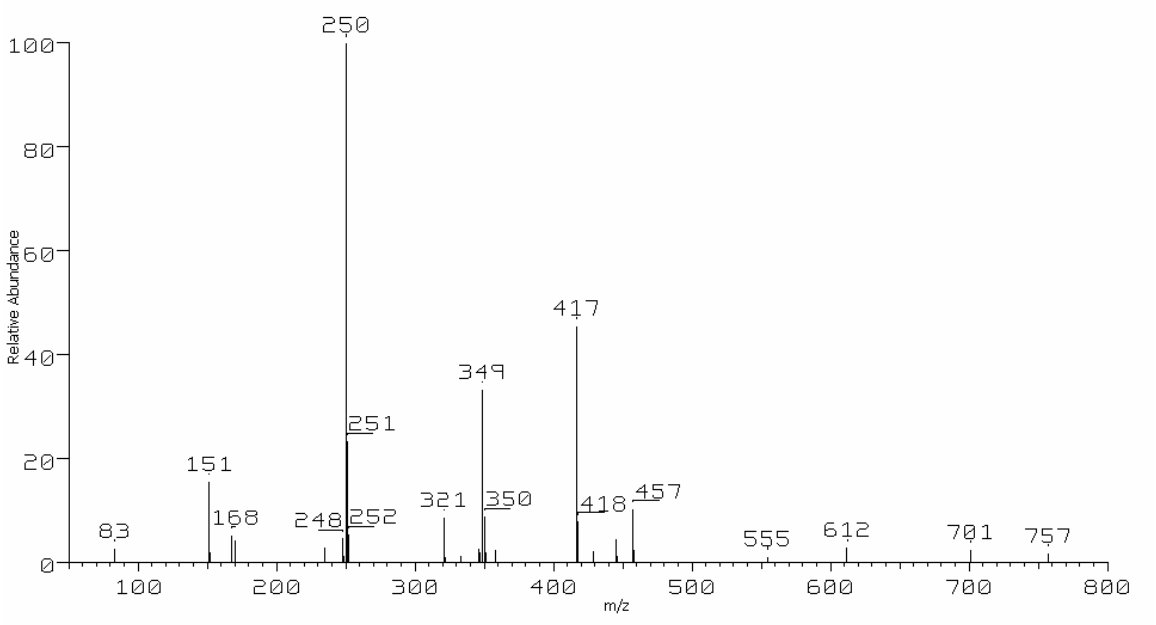

A.5.2 The 70 eV positive EI mass spectrum obtained during the reaction between $Al(tftm)_3$ & $Mn(acac)_2$

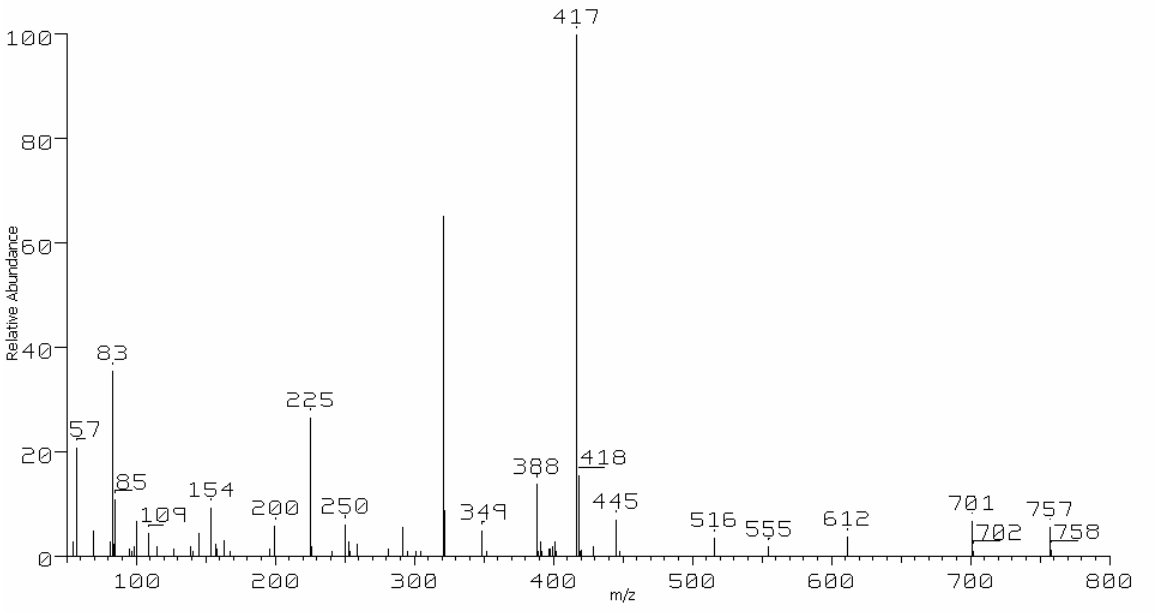

A.5.3 The 70 eV positive EI mass spectrum obtained during the reaction between $Al(tftm)_3$ & $Mn(hfac)_2$

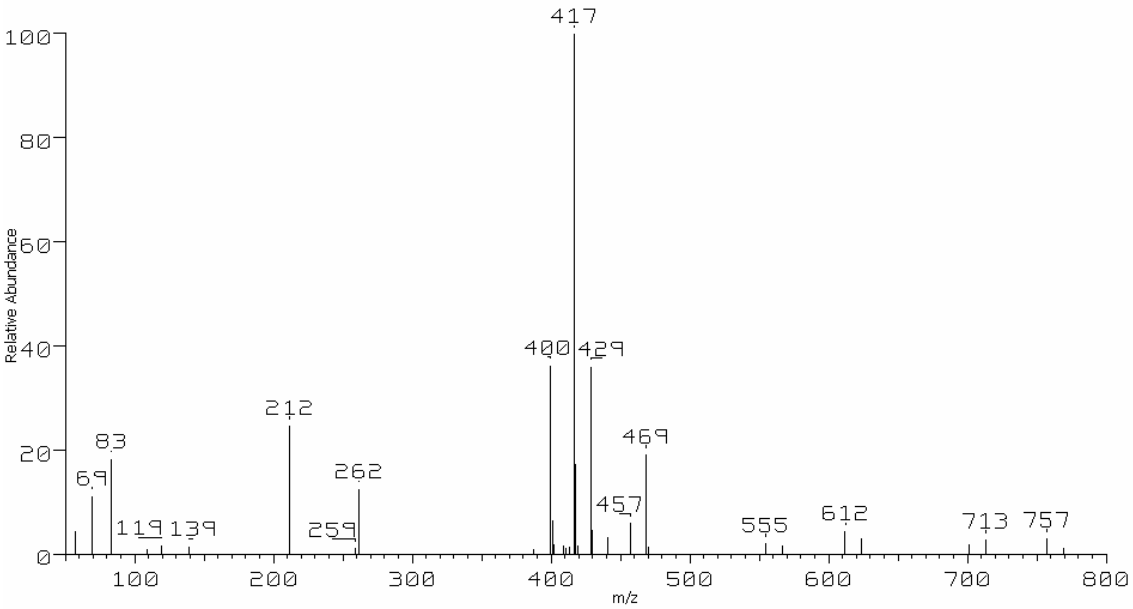

A.5.4 The 70 eV positive EI mass spectrum obtained during the reaction between $Al(tftm)_3$ & $Co(acac)_2$

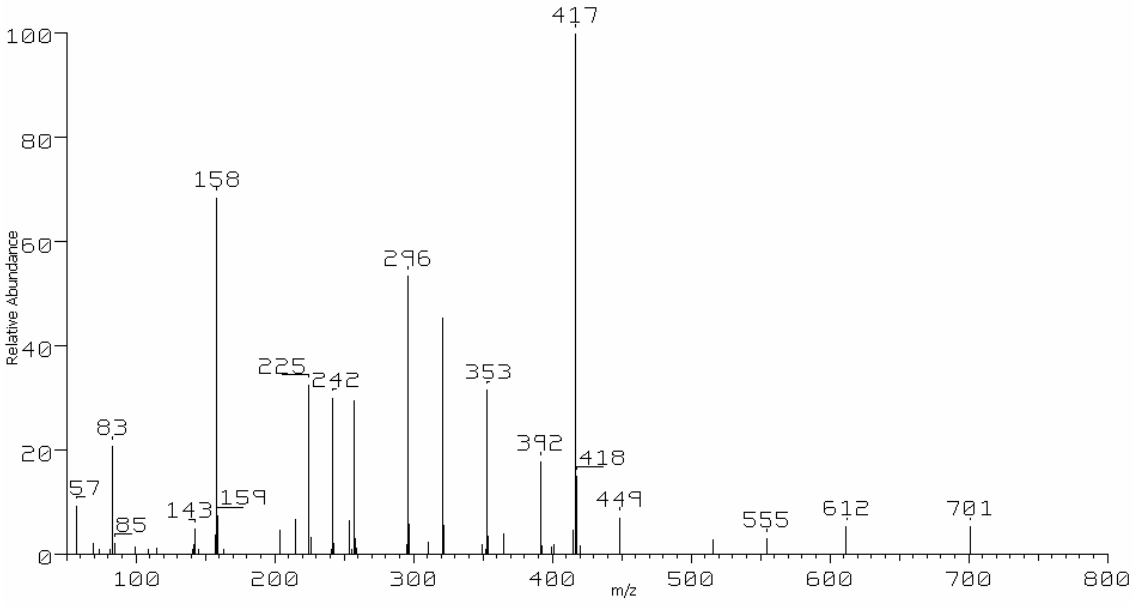

A.5.6 The 70 eV positive EI mass spectrum obtained during the reaction between $Al(tftm)_3$ & $Co(hfac)_2$

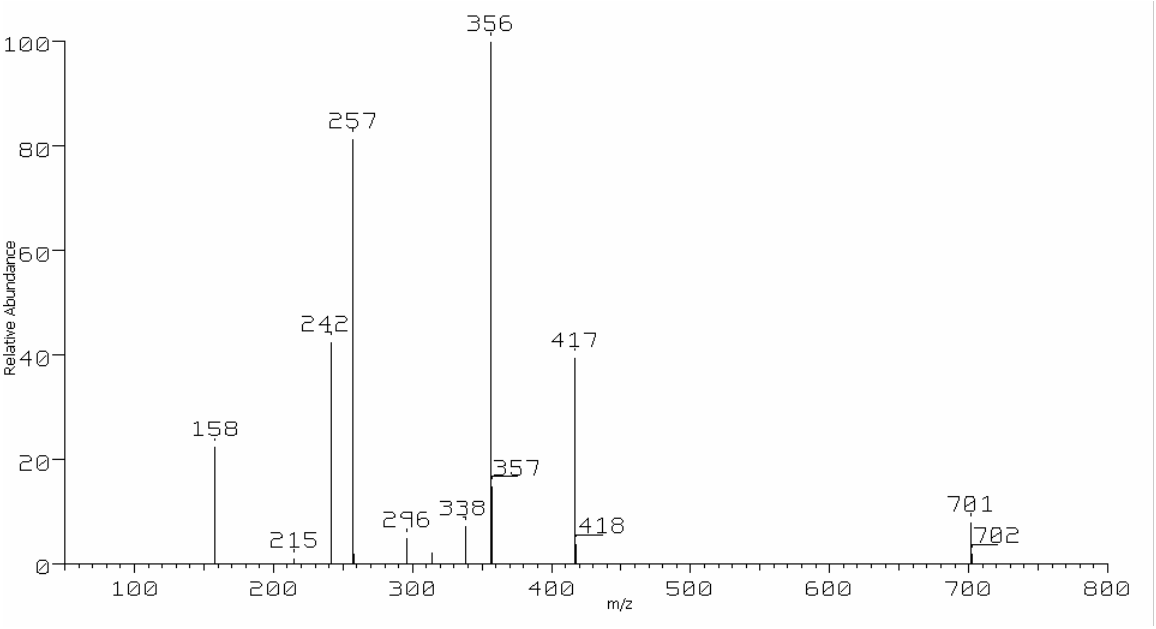

A.5.7 The 70 eV positive EI mass spectrum obtained during the reaction between $Al(tftm)_3$ & $Co(acac)_3$

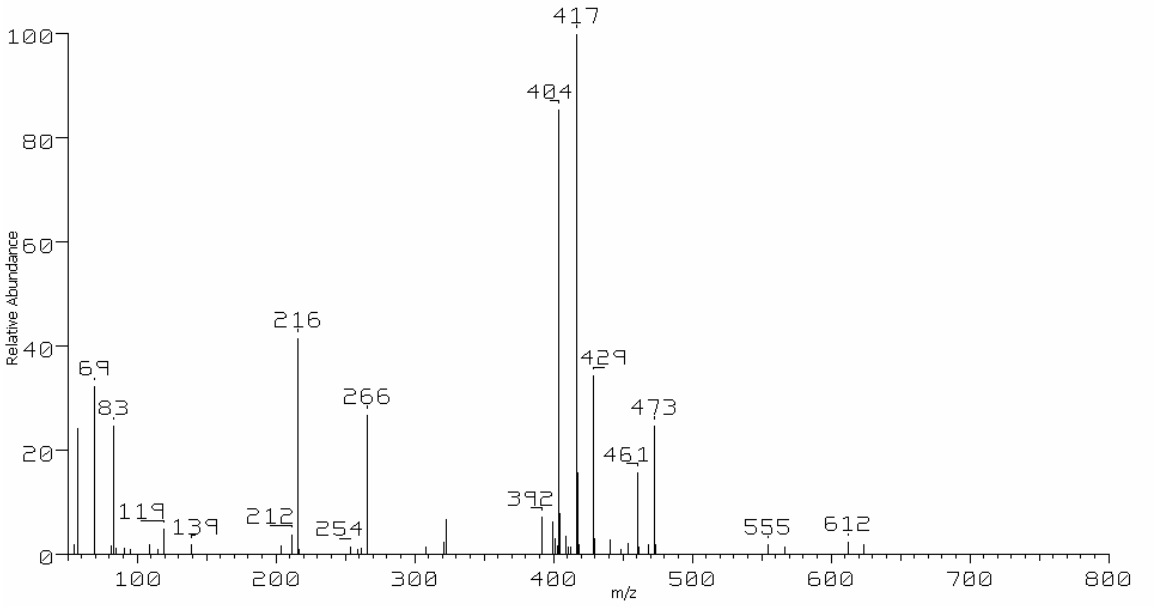

A.5.8 The 70 eV positive EI mass spectrum obtained during the reaction between $Al(tftm)_3$ & $Ni(acac)_2$

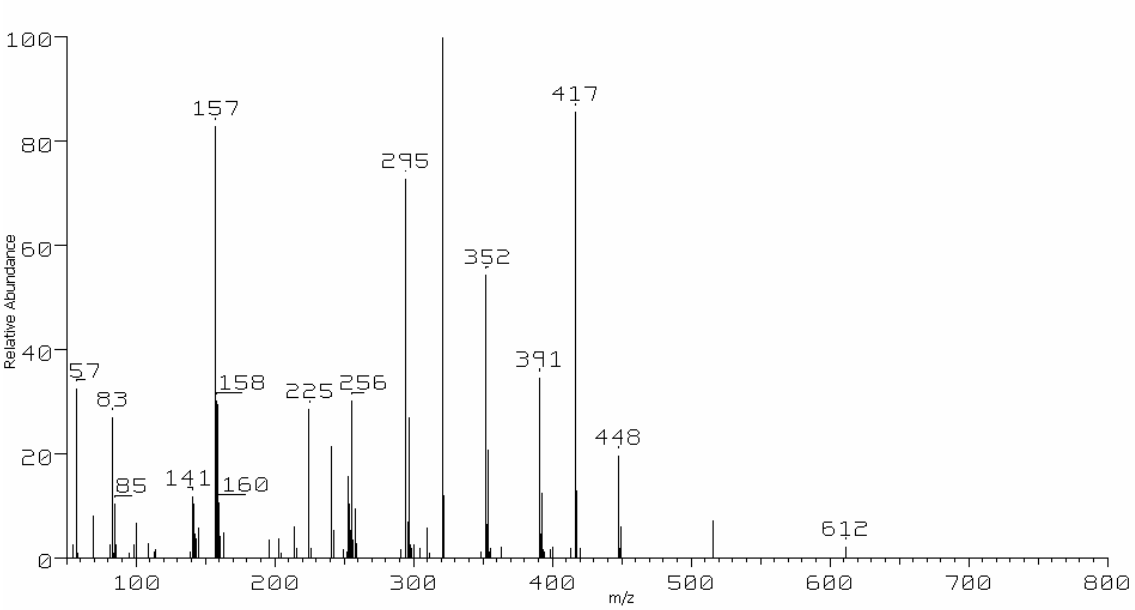

A.5.9 The 70 eV positive EI mass spectrum obtained during the reaction between $Al(tftm)_3$ & $Ni(hfac)_2$

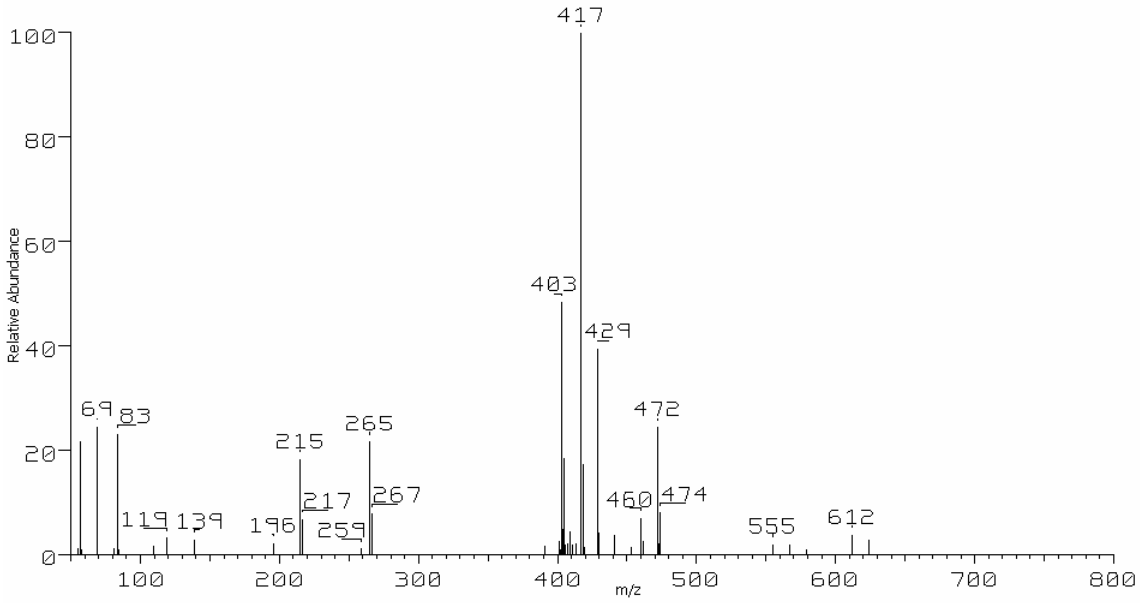

A.5.10 The 70 eV positive EI mass spectrum obtained during the reaction between $Al(tftm)_3$ & $Cu(hfac)_2$

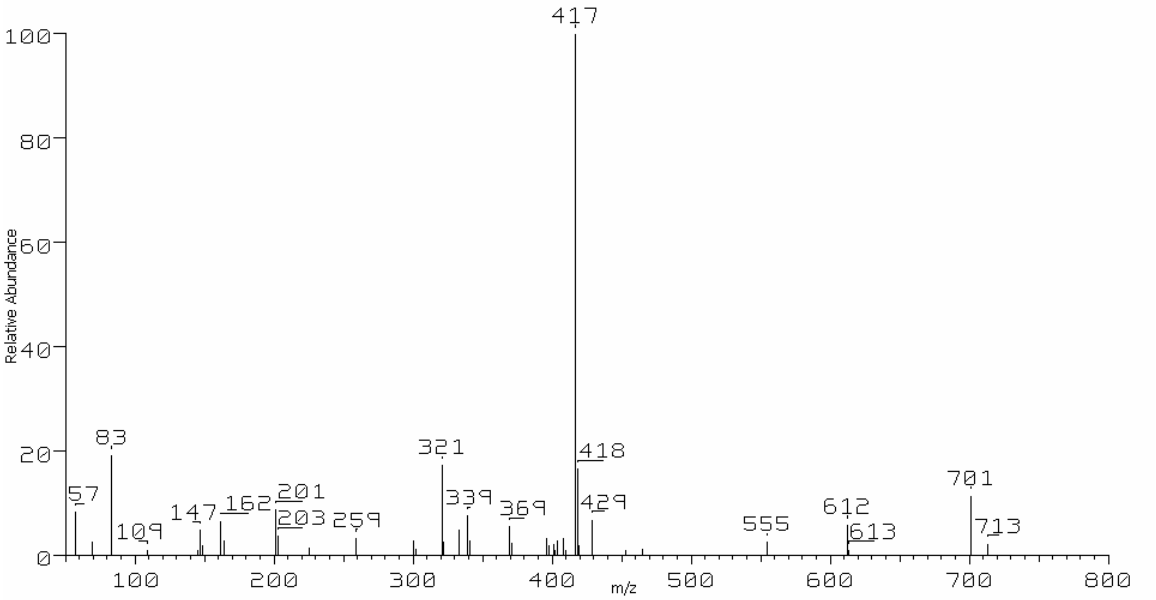

A.5.11 The 70 eV positive EI mass spectrum obtained during the reaction between $Al(tftm)_3$ & $Zn(acac)_2$

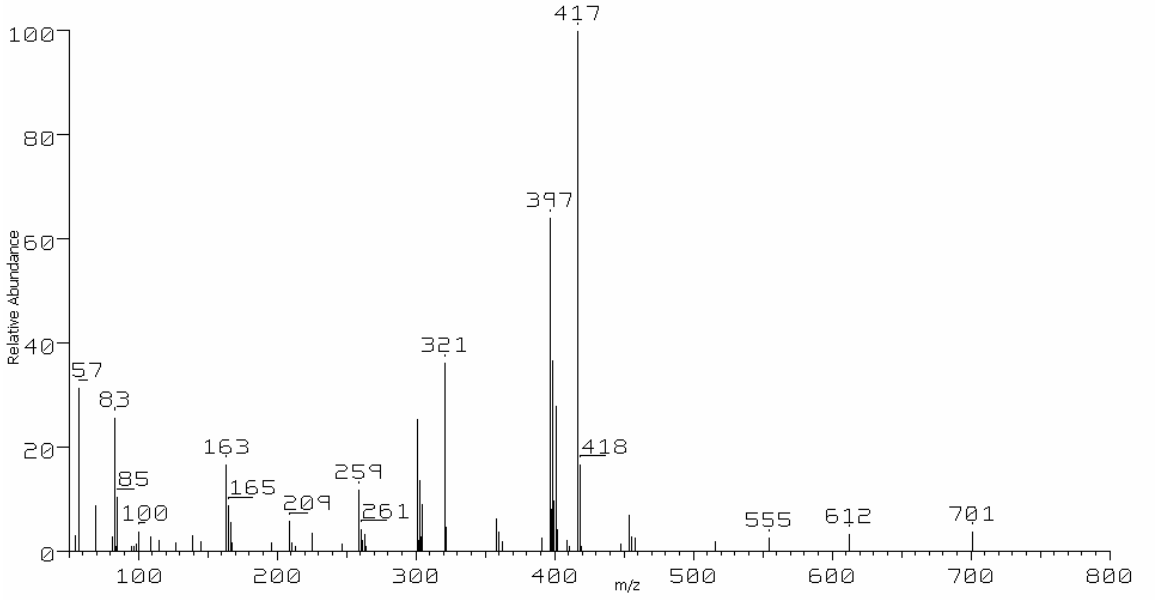

Appendix B: Single Crystal X-Ray Data

B.1 $Co(tftm)_2$

Table 1. Crystal data and structure refinement for 07mz269m:

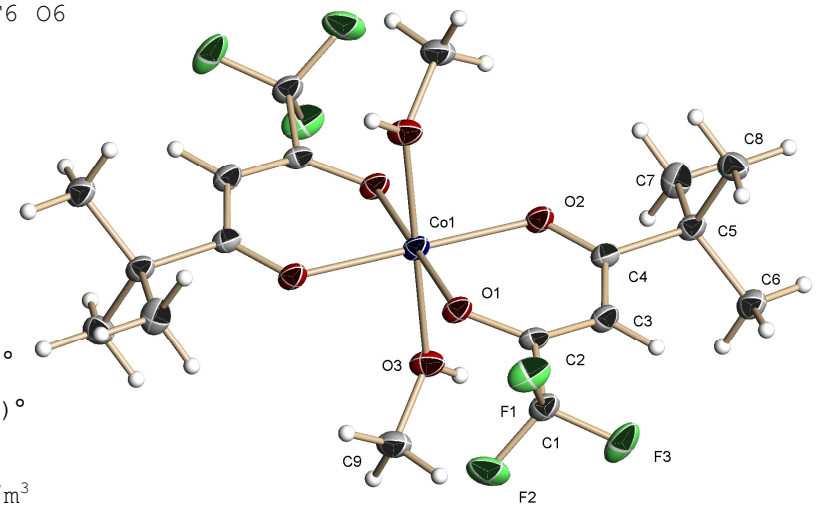

Identification code: 07mz269m

Empirical formula: C18 H28 Co F6 O6

Formula weight: 513.33

Temperature: 100(2) K

Wavelength: 0.71073 Å

Crystal system: Triclinic

Space group: P-1

Unit cell dimensions:

a = 5.4390(7) Å, α = 78.835(2)°

b = 8.7181(11) Å, β = 80.571(2)°

c = 12.0169(15) Å, γ = 87.946(2)°

Volume, Z: 551.47(12) $Å^3$, 1

Density (calculated): 1.546 Mg/m^3

Absorption coefficient: 0.859 mm^{-1}

F(000): 265

Crystal size: 0.49 × 0.23 × 0.08 mm

Crystal shape, colour: plate, orange

θ range for data collection: 1.75 to 28.27°

Limiting indices: $-7 \le h \le 7$, $-11 \le k \le 11$, $-15 \le l \le 15$

Reflections collected: 4542

Independent reflections: 2637 (R(int) = 0.0211)

Completeness to θ = 28.27°: 96.3 %

Absorption correction: multi-scan

Max. and min. transmission: 0.934 and 0.572

Refinement method: Full-matrix least-squares on F^2

Data / restraints / parameters: 2637 / 1 / 149

Goodness-of-fit on F^2: 1.068

Final R indices [$I>2\sigma(I)$]: R1 = 0.0431, wR2 = 0.1093

R indices (all data): R1 = 0.0479, wR2 = 0.1140

Largest diff. peak and hole: 0.890 and −0.787 e × $Å^{-3}$

Refinement of F^2 against ALL reflections. The weighted R-factor wR and goodness of fit are based on F^2, conventional R-factors R are based on F, with F set to zero for negative F^2. The threshold expression of

$F^2 > 2\sigma(F^2)$ is used only for calculating R-factors

Treatment of hydrogen atoms:
The hydroxyl H atom was located in the difference density Fourier map and its O-H distance was restrained to be 0.84 Å within a standard deviation of 0.02 Å. All other hydrogen atoms were placed in calculated positions and all hydrogen atoms were refined with an isotropic displacement parameter 1.5 (methyl, hydroxyl) or 1.2 times (all others) that of the adjacent carbon or oxygen atom.

Table 2. Atomic coordinates [× 10^4] and equivalent isotropic displacement parameters [$Å^2$ × 10^3] for 07mz269m. U(eq) is defined as one third of the trace of the orthogonalized U_{ij} tensor.

	x	y	z	U(eq)
C(1)	6715(4)	12223(2)	2639(2)	22(1)
C(2)	5746(3)	10953(2)	2103(2)	19(1)
C(3)	4063(4)	9910(2)	2792(2)	21(1)
C(4)	3002(3)	8652(2)	2421(2)	19(1)
C(5)	1482(3)	7401(2)	3324(2)	20(1)
C(6)	-258(4)	8130(2)	4224(2)	25(1)
C(7)	-22(4)	6457(3)	2725(2)	28(1)
C(8)	3351(4)	6316(2)	3924(2)	26(1)
C(9)	2186(4)	13202(2)	62(2)	28(1)
Co(1)	5000	10000	0	18(1)
F(1)	9170(2)	12084(2)	2630(1)	33(1)
F(2)	6323(3)	13644(2)	2040(1)	37(1)
F(3)	5676(3)	12205(2)	3725(1)	38(1)
O(1)	6700(2)	11055(2)	1042(1)	20(1)
O(2)	3314(3)	8484(2)	1399(1)	21(1)
O(3)	1904(3)	11548(2)	185(1)	24(1)

All esds (except the esd in the dihedral angle between two l.s. planes)
are estimated using the full covariance matrix. The cell esds are taken
into account individually in the estimation of esds in distances, angles
and torsion angles; correlations between esds in cell parameters are only

used when they are defined by crystal symmetry. An approximate (isotropic)
treatment of cell esds is used for estimating esds involving l.s. planes.

Table 3. Bond lengths [Å] and angles [deg] for 07mz269m.

C(1)-F(3)	1.332(2)	O(1)-C(2)-C(1)	112.25(16)
C(1)-F(1)	1.335(2)	C(3)-C(2)-C(1)	117.60(17)
C(1)-F(2)	1.336(2)	C(2)-C(3)-C(4)	124.26(18)
C(1)-C(2)	1.532(3)	C(2)-C(3)-H(3)	117.9
C(2)-O(1)	1.282(2)	C(4)-C(3)-H(3)	117.9
C(2)-C(3)	1.368(3)	O(2)-C(4)-C(3)	123.37(17)
C(3)-C(4)	1.432(3)	O(2)-C(4)-C(5)	117.62(16)
C(3)-H(3)	0.9500	C(3)-C(4)-C(5)	118.97(17)
C(4)-O(2)	1.248(2)	C(7)-C(5)-C(8)	109.26(17)
C(4)-C(5)	1.537(3)	C(7)-C(5)-C(6)	110.21(16)
C(5)-C(7)	1.528(3)	C(8)-C(5)-C(6)	109.09(17)
C(5)-C(8)	1.535(3)	C(7)-C(5)-C(4)	109.43(16)
C(5)-C(6)	1.535(3)	C(8)-C(5)-C(4)	107.12(15)
C(6)-H(6A)	0.9800	C(6)-C(5)-C(4)	111.66(15)
C(6)-H(6B)	0.9800	C(5)-C(6)-H(6A)	109.5
C(6)-H(6C)	0.9800	C(5)-C(6)-H(6B)	109.5
C(7)-H(7A)	0.9800	H(6A)-C(6)-H(6B)	109.5
C(7)-H(7B)	0.9800	C(5)-C(6)-H(6C)	109.5
C(7)-H(7C)	0.9800	H(6A)-C(6)-H(6C)	109.5
C(8)-H(8A)	0.9800	H(6B)-C(6)-H(6C)	109.5
C(8)-H(8B)	0.9800	C(5)-C(7)-H(7A)	109.5
C(8)-H(8C)	0.9800	C(5)-C(7)-H(7B)	109.5
C(9)-O(3)	1.432(2)	H(7A)-C(7)-H(7B)	109.5
C(9)-H(9A)	0.9800	C(5)-C(7)-H(7C)	109.5
C(9)-H(9B)	0.9800	H(7A)-C(7)-H(7C)	109.5
C(9)-H(9C)	0.9800	H(7B)-C(7)-H(7C)	109.5
Co(1)-O(2)	2.0338(14)	C(5)-C(8)-H(8A)	109.5
Co(1)-O(2)#1	2.0339(14)	C(5)-C(8)-H(8B)	109.5
Co(1)-O(1)#1	2.0388(13)	H(8A)-C(8)-H(8B)	109.5
Co(1)-O(1)	2.0388(13)	C(5)-C(8)-H(8C)	109.5
Co(1)-O(3)	2.1301(15)	H(8A)-C(8)-H(8C)	109.5
Co(1)-O(3)#1	2.1302(15)	H(8B)-C(8)-H(8C)	109.5
O(3)-H(3A)	0.840(17)	O(3)-C(9)-H(9A)	109.5
		O(3)-C(9)-H(9B)	109.5
F(3)-C(1)-F(1)	106.65(17)	H(9A)-C(9)-H(9B)	109.5
F(3)-C(1)-F(2)	107.19(17)	O(3)-C(9)-H(9C)	109.5
F(1)-C(1)-F(2)	106.60(16)	H(9A)-C(9)-H(9C)	109.5
F(3)-C(1)-C(2)	114.14(16)	H(9B)-C(9)-H(9C)	109.5
F(1)-C(1)-C(2)	111.10(16)	O(2)-Co(1)-O(2)#1	180.00(6)
F(2)-C(1)-C(2)	110.78(16)	O(2)-Co(1)-O(1)#1	90.18(5)
O(1)-C(2)-C(3)	130.15(17)	O(2)#1-Co(1)-O(1)#1	89.82(5)

O(2)-Co(1)-O(1)	89.82(5)
O(2)#1-Co(1)-O(1)	90.18(5)
O(1)#1-Co(1)-O(1)	180.00(6)
O(2)-Co(1)-O(3)	89.28(6)
O(2)#1-Co(1)-O(3)	90.72(6)
O(1)#1-Co(1)-O(3)	90.09(6)
O(1)-Co(1)-O(3)	89.91(6)
O(2)-Co(1)-O(3)#1	90.72(6)
O(2)#1-Co(1)-O(3)#1	89.28(6)
O(1)#1-Co(1)-O(3)#1	89.91(6)
O(1)-Co(1)-O(3)#1	90.09(6)
O(3)-Co(1)-O(3)#1	179.999(1)
C(2)-O(1)-Co(1)	119.97(12)
C(4)-O(2)-Co(1)	127.11(13)
C(9)-O(3)-Co(1)	122.65(12)
C(9)-O(3)-H(3A)	107(2)
Co(1)-O(3)-H(3A)	129(2)

Symmetry transformations used to generate equivalent atoms:

#1 -x+1,-y+2,-z

Table 4. Anisotropic displacement parameters [Å^2 × 10^3] for 07mz269m. The anisotropic displacement factor exponent takes the form: -2 π2 [(h a*)^2 U11 + ... + 2 h k a* b* U12]

	U11	U22	U33	U23	U13	U12
C(1)	23(1)	22(1)	24(1)	-11(1)	-1(1)	-4(1)
C(2)	19(1)	17(1)	22(1)	-9(1)	-3(1)	0(1)
C(3)	21(1)	23(1)	20(1)	-9(1)	-1(1)	-2(1)
C(4)	17(1)	18(1)	22(1)	-7(1)	-1(1)	0(1)
C(5)	19(1)	19(1)	22(1)	-8(1)	0(1)	-3(1)
C(6)	22(1)	25(1)	25(1)	-6(1)	4(1)	-2(1)
C(7)	26(1)	32(1)	26(1)	-8(1)	-1(1)	-13(1)
C(8)	24(1)	22(1)	29(1)	-4(1)	-1(1)	-2(1)
C(9)	32(1)	19(1)	34(1)	-9(1)	-2(1)	1(1)
Co(1)	19(1)	17(1)	19(1)	-8(1)	-1(1)	-3(1)
F(1)	24(1)	39(1)	43(1)	-22(1)	-7(1)	-6(1)
F(2)	54(1)	18(1)	46(1)	-13(1)	-18(1)	-1(1)
F(3)	44(1)	44(1)	29(1)	-24(1)	8(1)	-18(1)
O(1)	20(1)	20(1)	22(1)	-10(1)	0(1)	-4(1)
O(2)	23(1)	19(1)	21(1)	-9(1)	0(1)	-4(1)
O(3)	20(1)	20(1)	34(1)	-10(1)	0(1)	-2(1)

Table 5. Hydrogen coordinates (× 10^4) and isotropic displacement parameters (Å^2 × 10^3) for 07mz269m.

	x	y	z	U(eq)
H(3)	3564	10027	3566	25
H(6A)	-1322	8919	3836	37
H(6B)	738	8624	4666	37
H(6C)	-1302	7313	4744	37
H(7A)	1114	5960	2178	42
H(7B)	-1169	7155	2314	42
H(7C)	-977	5652	3300	42
H(8A)	2446	5499	4508	38
H(8B)	4352	6923	4290	38
H(8C)	4449	5832	3355	38
H(9A)	2177	13465	820	42
H(9B)	805	13743	-284	42
H(9C)	3768	13530	-433	42
H(3A)	420(40)	11340(30)	490(20)	37

Table 6. Torsion angles [deg] for 07mz242m.

F(3)-C(1)-C(2)-O(1)	176.81(17)
F(1)-C(1)-C(2)-O(1)	-62.6(2)
F(2)-C(1)-C(2)-O(1)	55.7(2)
F(3)-C(1)-C(2)-C(3)	-3.3(3)
F(1)-C(1)-C(2)-C(3)	117.3(2)
F(2)-C(1)-C(2)-C(3)	-124.4(2)
O(1)-C(2)-C(3)-C(4)	0.3(3)
C(1)-C(2)-C(3)-C(4)	-179.48(18)
C(2)-C(3)-C(4)-O(2)	-7.8(3)
C(2)-C(3)-C(4)-C(5)	169.72(18)
O(2)-C(4)-C(5)-C(7)	-17.5(2)
C(3)-C(4)-C(5)-C(7)	164.78(18)
O(2)-C(4)-C(5)-C(8)	100.8(2)
C(3)-C(4)-C(5)-C(8)	-76.9(2)
O(2)-C(4)-C(5)-C(6)	-139.84(19)
C(3)-C(4)-C(5)-C(6)	42.5(2)
C(3)-C(2)-O(1)-Co(1)	19.4(3)
C(1)-C(2)-O(1)-Co(1)	-160.77(12)
O(2)-Co(1)-O(1)-C(2)	-23.55(14)
O(2)#1-Co(1)-O(1)-C(2)	156.45(14)
O(3)-Co(1)-O(1)-C(2)	65.73(14)
O(3)#1-Co(1)-O(1)-C(2)	-114.27(14)
C(3)-C(4)-O(2)-Co(1)	-7.2(3)
C(5)-C(4)-O(2)-Co(1)	175.20(12)
O(1)#1-Co(1)-O(2)-C(4)	-160.79(16)
O(1)-Co(1)-O(2)-C(4)	19.21(16)
O(3)-Co(1)-O(2)-C(4)	-70.70(16)
O(3)#1-Co(1)-O(2)-C(4)	109.30(16)
O(2)-Co(1)-O(3)-C(9)	137.10(16)
O(2)#1-Co(1)-O(3)-C(9)	-42.90(16)
O(1)#1-Co(1)-O(3)-C(9)	-132.72(16)
O(1)-Co(1)-O(3)-C(9)	47.28(16)

Symmetry transformations used to generate equivalent atoms:

#1 -x+1,-y+1,-z+1 #2 -x+1,y,-z+1/2

Table 7. Hydrogen bonds for 07mz269m [Å and deg].

D-H...A	d(D-H)	d(H...A)	d(D...A)	<(DHA)
O(3)-H(3A)...O(1)#2	0.840(17)	2.032(18)	2.867(2)	172(3)

Symmetry transformations used to generate equivalent atoms:

#1 -x+1,-y+2,-z #2 x-1,y,z

B.2 $Ni(tftm)_2$

Table 1. Crystal data and structure refinement for 07mz225m:

Identification code: 07mz225m

Empirical formula: C35 H54 F12 Ni2 O12

Moiety formula: C18 H28 F6 Ni O6, C17 H26 F6 Ni O6

Formula weight: 1012.16

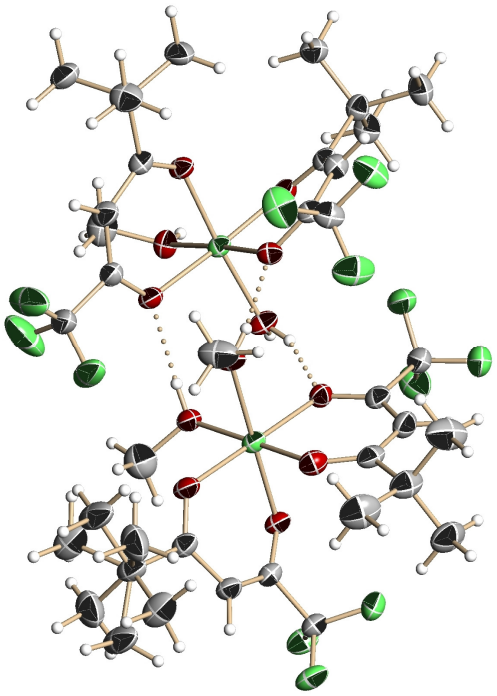

Temperature: 100(2) K

Wavelength: 0.71073 Å

Crystal system: Triclinic

Space group: P-1

Unit cell dimensions:

a = 11.402(2) Å, α = 100.935(3)°

b = 14.813(3) Å, β = 105.216(3)°

c = 15.521(3) Å, γ = 108.009(3)°

Volume, *Z*: 2298.5(7) $Å^3$, 2

Density (calculated): 1.462 g/m^3

Absorption coefficient: 0.921 mm^{-1}

F(000): 1048

Crystal size: 0.42 × 0.38 × 0.31

Crystal shape, colour: block, blue

θ range for data collection: 1.42 to 28.28°

Limiting indices: −15 ≤ h ≤ 15, −19 ≤ *k* ≤ 19, −20 ≤ *l* ≤ 20

Reflections collected: 23068

Independent reflections: 11347 (*R*(int) = 0.0230)

Completeness to θ = 28.28°: 96.8 %

Absorption correction: multi-scan

Max. and min. transmission: 0.752 and 0.542

Refinement method: Full-matrix least-squares on F^2

Data / restraints / parameters: 11347 / 23 / 597

Goodness-of-fit on F^2: 1.060

Final *R* indices [$I>2\sigma(I)$]: R1 = 0.0493, wR2 = 0.1228

R indices (all data): 0.0757, wR2 = 0.1416

Largest diff. peak and hole: 1.209 and −0.643 e × $Å^{-3}$

Refinement of F^2 against ALL reflections. The weighted R-factor wR and goodness of fit are based on F^2, conventional R-factors R are based on F, with F set to zero for negative F^2. The threshold expression of $F^2 > 2\sigma(F^2)$ is used only for calculating R-factors

Comments:
One tert-butyl group is disordered over two positions with an occupancy ratio of 0.856(4) to 0.144(4). The C-C bonds in both moieties were restrained to be the same, and the methyl-methyl distances in the minor component were restrained to be equal, all within a standard deviation of 0.02 Å. The ADPs of the methyl carbon atoms were set to be the same as that of the other moieties on the opposite side of the tert-butyl group.

Treatment of hydrogen atoms:

Water and hydroxyl H atoms were located in the difference density Fourier map and the O-H distances were restrained to be 0.84 Å within a standard deviation of 0.02Å. All other hydrogen atoms were placed in calculated positions and all H atoms were refined with an isotropic displacement parameter 1.5 (methyl, hydroxyl) or 1.2 times (all others) that of the adjacent carbon or oxygen atom. Methyl H atoms were allowed to rotate to best fit the experimental electron density.

Table 2. Atomic coordinates [$\times 10^4$] and equivalent isotropic displacement parameters [$Å^2 \times 10^3$] for 07mz225m. U(eq) is defined as one third of the trace of the orthogonalized U_{ij} tensor.

	x	y	z	U(eq)
C(1)	10396(3)	1549(3)	6080(2)	45(1)
C(2)	9624(3)	1809(2)	6700(2)	32(1)
C(3)	10336(3)	2402(2)	7602(2)	36(1)
C(4)	9782(3)	2631(2)	8302(2)	29(1)
C(5)	10700(3)	3292(2)	9291(2)	34(1)
C(6)	11412(3)	2685(3)	9755(2)	45(1)
C(7)	11708(3)	4241(3)	9250(2)	47(1)
C(8)	9889(3)	3589(3)	9850(2)	43(1)
C(9)	7858(3)	4633(2)	7081(2)	38(1)
C(10)	7229(3)	3619(2)	7214(2)	29(1)
C(11)	6591(3)	3566(2)	7853(2)	30(1)
C(12)	5915(3)	2663(2)	8025(2)	27(1)
C(13)	5210(3)	2697(2)	8744(2)	31(1)
C(14)	4021(3)	1721(2)	8455(2)	38(1)
C(15)	6210(3)	2794(2)	9682(2)	38(1)
C(16)	4750(3)	3567(2)	8868(2)	41(1)
C(17)	7871(4)	-76(3)	7512(3)	58(1)
C(18)	3732(3)	2406(2)	4798(2)	38(1)

C(19)	4754(3)	2521(2)	4309(2)	31(1)
C(20)	4884(3)	3197(2)	3812(2)	36(1)
C(21)	5866(3)	3436(2)	3379(2)	34(1)
C(22)	5925(4)	4218(2)	2859(2)	45(1)
C(23)	7101(5)	4397(3)	2517(3)	63(1)
C(24)	4657(4)	3816(3)	2000(3)	58(1)
C(25)	6037(5)	5188(3)	3504(3)	65(1)
C(26)	4285(3)	633(2)	1046(2)	32(1)
C(27)	5553(3)	980(2)	1882(2)	28(1)
C(28)	6726(3)	1265(2)	1729(2)	31(1)
C(29)	7981(3)	1594(2)	2456(2)	32(1)
C(30)	9197(3)	1666(3)	2179(2)	39(1)
C(31)	9030(5)	617(4)	1699(4)	59(1)
C(32)	9270(4)	2296(4)	1489(3)	55(1)
C(33)	10433(4)	2163(4)	3035(3)	61(1)
C(31B)	8950(20)	1161(17)	1154(10)	61(1)
C(32B)	10180(20)	2703(12)	2526(17)	59(1)
C(33B)	9830(20)	1025(16)	2733(15)	55(1)
C(34)	9282(4)	3662(3)	5204(3)	56(1)
C(35)	7219(4)	-30(3)	3879(3)	60(1)
F(1)	9938(2)	1608(2)	5231(1)	67(1)
F(2)	10270(4)	605(2)	5971(2)	94(1)
F(3)	11666(2)	2086(2)	6421(2)	81(1)
F(4)	7354(3)	4623(2)	6193(2)	61(1)
F(5)	9148(2)	4877(2)	7272(2)	58(1)
F(6)	7716(2)	5385(1)	7620(2)	51(1)
F(7)	2871(2)	1461(2)	4513(2)	52(1)
F(8)	4311(2)	2640(2)	5726(1)	50(1)
F(9)	3034(2)	2976(2)	4654(1)	51(1)
F(10)	3558(2)	-325(1)	875(1)	40(1)
F(11)	4476(2)	742(2)	251(1)	43(1)
F(12)	3546(2)	1146(2)	1211(1)	45(1)
Ni(1)	7099(1)	1595(1)	6940(1)	25(1)
Ni(2)	6750(1)	1876(1)	3881(1)	27(1)
O(1)	8377(2)	1391(1)	6289(1)	29(1)
O(2)	8583(2)	2300(1)	8164(1)	28(1)
O(3)	7393(2)	2931(1)	6680(1)	28(1)
O(4)	5906(2)	1829(1)	7646(1)	27(1)
O(5)	6833(2)	220(2)	7130(2)	32(1)
O(6)	5515(2)	922(2)	5730(1)	32(1)
O(7)	5380(2)	1954(1)	4459(1)	29(1)
O(8)	6685(2)	3039(2)	3407(1)	35(1)
O(9)	5340(2)	955(1)	2653(1)	29(1)
O(10)	8124(2)	1798(2)	3308(1)	33(1)
O(11)	6887(2)	674(2)	4384(1)	31(1)
O(12)	8180(2)	2823(2)	5127(1)	35(1)

All esds (except the esd in the dihedral angle between two l.s. planes) are estimated using the full covariance matrix. The cell esds are taken into account individually in the estimation of esds in distances, angles and torsion angles; correlations between esds in cell parameters are only used when they are defined by crystal symmetry. An approximate (isotropic) treatment of cell esds is used for estimating esds involving l.s. planes.

Table 3. Bond lengths [Å] and angles [deg] for 07mz225m.

C(1)-F(1)	1.316(4)	C(18)-F(7)	1.344(4)
C(1)-F(3)	1.317(4)	C(18)-C(19)	1.534(4)
C(1)-F(2)	1.333(5)	C(19)-O(7)	1.276(3)
C(1)-C(2)	1.538(4)	C(19)-C(20)	1.371(4)
C(2)-O(1)	1.281(3)	C(20)-C(21)	1.439(4)
C(2)-C(3)	1.374(4)	C(20)-H(20)	0.9500
C(3)-C(4)	1.430(4)	C(21)-O(8)	1.245(4)
C(3)-H(3)	0.9500	C(21)-C(22)	1.527(4)
C(4)-O(2)	1.244(3)	C(22)-C(23)	1.535(6)
C(4)-C(5)	1.538(4)	C(22)-C(25)	1.535(5)
C(5)-C(8)	1.526(4)	C(22)-C(24)	1.542(5)
C(5)-C(6)	1.541(4)	C(23)-H(23A)	0.9800
C(5)-C(7)	1.541(4)	C(23)-H(23B)	0.9800
C(6)-H(6D)	0.9800	C(23)-H(23C)	0.9800
C(6)-H(6E)	0.9800	C(24)-H(24A)	0.9800
C(6)-H(6C)	0.9800	C(24)-H(24B)	0.9800
C(7)-H(7A)	0.9800	C(24)-H(24C)	0.9800
C(7)-H(7B)	0.9800	C(25)-H(25A)	0.9800
C(7)-H(7C)	0.9800	C(25)-H(25B)	0.9800
C(8)-H(8A)	0.9800	C(25)-H(25C)	0.9800
C(8)-H(8B)	0.9800	C(26)-F(10)	1.336(3)
C(8)-H(8C)	0.9800	C(26)-F(12)	1.338(3)
C(9)-F(5)	1.336(4)	C(26)-F(11)	1.338(3)
C(9)-F(6)	1.340(4)	C(26)-C(27)	1.529(4)
C(9)-F(4)	1.343(4)	C(27)-O(9)	1.287(3)
C(9)-C(10)	1.530(4)	C(27)-C(28)	1.371(4)
C(10)-O(3)	1.280(3)	C(28)-C(29)	1.439(4)
C(10)-C(11)	1.377(4)	C(28)-H(28)	0.9500
C(11)-C(12)	1.436(4)	C(29)-O(10)	1.254(3)
C(11)-H(11)	0.9500	C(29)-C(30)	1.534(4)
C(12)-O(4)	1.259(3)	C(30)-C(32B)	1.485(14)
C(12)-C(13)	1.538(4)	C(30)-C(33)	1.516(5)
C(13)-C(16)	1.534(4)	C(30)-C(31)	1.520(5)
C(13)-C(14)	1.534(4)	C(30)-C(31B)	1.534(14)
C(13)-C(15)	1.546(4)	C(30)-C(32)	1.551(5)
C(14)-H(14A)	0.9800	C(30)-C(33B)	1.604(14)
C(14)-H(14B)	0.9800	C(31)-H(31A)	0.9800
C(14)-H(14C)	0.9800	C(31)-H(31B)	0.9800
C(15)-H(15A)	0.9800	C(31)-H(31C)	0.9800
C(15)-H(15B)	0.9800	C(32)-H(32A)	0.9800
C(15)-H(15C)	0.9800	C(32)-H(32B)	0.9800
C(16)-H(16A)	0.9800	C(32)-H(32C)	0.9800
C(16)-H(16B)	0.9800	C(33)-H(33A)	0.9800
C(16)-H(16C)	0.9800	C(33)-H(33B)	0.9800
C(17)-O(5)	1.414(4)	C(33)-H(33C)	0.9800
C(17)-H(17A)	0.9800	C(31B)-H(31D)	0.9800
C(17)-H(17B)	0.9800	C(31B)-H(31E)	0.9800
C(17)-H(17C)	0.9800	C(31B)-H(31F)	0.9800
C(18)-F(9)	1.337(4)	C(32B)-H(32D)	0.9800
C(18)-F(8)	1.342(3)	C(32B)-H(32E)	0.9800

C(32B)-H(32F)	0.9800	C(5)-C(6)-H(6C)	109.5
C(33B)-H(33D)	0.9800	H(6D)-C(6)-H(6C)	109.5
C(33B)-H(33E)	0.9800	H(6E)-C(6)-H(6C)	109.5
C(33B)-H(33F)	0.9800	C(5)-C(7)-H(7A)	109.5
C(34)-O(12)	1.427(4)	C(5)-C(7)-H(7B)	109.5
C(34)-H(34A)	0.9800	H(7A)-C(7)-H(7B)	109.5
C(34)-H(34B)	0.9800	C(5)-C(7)-H(7C)	109.5
C(34)-H(34C)	0.9800	H(7A)-C(7)-H(7C)	109.5
C(35)-O(11)	1.390(4)	H(7B)-C(7)-H(7C)	109.5
C(35)-H(35A)	0.9800	C(5)-C(8)-H(8A)	109.5
C(35)-H(35B)	0.9800	C(5)-C(8)-H(8B)	109.5
C(35)-H(35C)	0.9800	H(8A)-C(8)-H(8B)	109.5
Ni(1)-O(2)	2.0083(18)	C(5)-C(8)-H(8C)	109.5
Ni(1)-O(4)	2.0247(19)	H(8A)-C(8)-H(8C)	109.5
Ni(1)-O(3)	2.0382(19)	H(8B)-C(8)-H(8C)	109.5
Ni(1)-O(1)	2.0401(19)	F(5)-C(9)-F(6)	106.4(3)
Ni(1)-O(6)	2.044(2)	F(5)-C(9)-F(4)	106.7(3)
Ni(1)-O(5)	2.054(2)	F(6)-C(9)-F(4)	106.8(3)
Ni(2)-O(8)	2.011(2)	F(5)-C(9)-C(10)	110.9(3)
Ni(2)-O(10)	2.016(2)	F(6)-C(9)-C(10)	114.6(2)
Ni(2)-O(7)	2.0166(19)	F(4)-C(9)-C(10)	111.1(2)
Ni(2)-O(9)	2.0318(19)	O(3)-C(10)-C(11)	129.9(3)
Ni(2)-O(12)	2.066(2)	O(3)-C(10)-C(9)	111.7(2)
Ni(2)-O(11)	2.108(2)	C(11)-C(10)-C(9)	118.4(3)
O(5)-H(5A)	0.832(18)	C(10)-C(11)-C(12)	124.5(3)
O(6)-H(6A)	0.824(18)	C(10)-C(11)-H(11)	117.8
O(6)-H(6B)	0.842(19)	C(12)-C(11)-H(11)	117.8
O(11)-H(11A)	0.832(19)	O(4)-C(12)-C(11)	123.6(3)
O(12)-H(12A)	0.812(17)	O(4)-C(12)-C(13)	116.8(2)
		C(11)-C(12)-C(13)	119.6(2)
F(1)-C(1)-F(3)	107.8(3)	C(16)-C(13)-C(14)	108.9(2)
F(1)-C(1)-F(2)	105.4(3)	C(16)-C(13)-C(12)	113.7(2)
F(3)-C(1)-F(2)	106.5(3)	C(14)-C(13)-C(12)	109.6(2)
F(1)-C(1)-C(2)	112.7(3)	C(16)-C(13)-C(15)	109.3(3)
F(3)-C(1)-C(2)	114.6(3)	C(14)-C(13)-C(15)	109.0(2)
F(2)-C(1)-C(2)	109.2(3)	C(12)-C(13)-C(15)	106.2(2)
O(1)-C(2)-C(3)	129.6(3)	C(13)-C(14)-H(14A)	109.5
O(1)-C(2)-C(1)	113.1(2)	C(13)-C(14)-H(14B)	109.5
C(3)-C(2)-C(1)	117.3(3)	H(14A)-C(14)-H(14B)	109.5
C(2)-C(3)-C(4)	124.8(3)	C(13)-C(14)-H(14C)	109.5
C(2)-C(3)-H(3)	117.6	H(14A)-C(14)-H(14C)	109.5
C(4)-C(3)-H(3)	117.6	H(14B)-C(14)-H(14C)	109.5
O(2)-C(4)-C(3)	123.5(3)	C(13)-C(15)-H(15A)	109.5
O(2)-C(4)-C(5)	117.2(2)	C(13)-C(15)-H(15B)	109.5
C(3)-C(4)-C(5)	119.3(2)	H(15A)-C(15)-H(15B)	109.5
C(8)-C(5)-C(4)	109.4(2)	C(13)-C(15)-H(15C)	109.5
C(8)-C(5)-C(6)	110.2(3)	H(15A)-C(15)-H(15C)	109.5
C(4)-C(5)-C(6)	107.8(3)	H(15B)-C(15)-H(15C)	109.5
C(8)-C(5)-C(7)	108.8(3)	C(13)-C(16)-H(16A)	109.5
C(4)-C(5)-C(7)	110.6(2)	C(13)-C(16)-H(16B)	109.5
C(6)-C(5)-C(7)	110.1(3)	H(16A)-C(16)-H(16B)	109.5
C(5)-C(6)-H(6D)	109.5	C(13)-C(16)-H(16C)	109.5
C(5)-C(6)-H(6E)	109.5	H(16A)-C(16)-H(16C)	109.5
H(6D)-C(6)-H(6E)	109.5	H(16B)-C(16)-H(16C)	109.5

O(5)-C(17)-H(17A)	109.5	C(27)-C(28)-C(29)	123.5(3)
O(5)-C(17)-H(17B)	109.5	C(27)-C(28)-H(28)	118.3
H(17A)-C(17)-H(17B)	109.5	C(29)-C(28)-H(28)	118.3
O(5)-C(17)-H(17C)	109.5	O(10)-C(29)-C(28)	123.0(3)
H(17A)-C(17)-H(17C)	109.5	O(10)-C(29)-C(30)	118.2(2)
H(17B)-C(17)-H(17C)	109.5	C(28)-C(29)-C(30)	118.7(2)
F(9)-C(18)-F(8)	106.7(2)	C(32B)-C(30)-C(33)	50.1(9)
F(9)-C(18)-F(7)	107.0(3)	C(32B)-C(30)-C(31)	140.9(10)
F(8)-C(18)-F(7)	106.8(3)	C(33)-C(30)-C(31)	111.5(4)
F(9)-C(18)-C(19)	114.1(3)	C(32B)-C(30)-C(31B)	112.7(10)
F(8)-C(18)-C(19)	110.8(2)	C(33)-C(30)-C(31B)	132.5(9)
F(7)-C(18)-C(19)	111.0(2)	C(31)-C(30)-C(31B)	49.5(9)
O(7)-C(19)-C(20)	130.2(3)	C(32B)-C(30)-C(29)	111.3(10)
O(7)-C(19)-C(18)	111.5(2)	C(33)-C(30)-C(29)	110.3(3)
C(20)-C(19)-C(18)	118.3(3)	C(31)-C(30)-C(29)	107.5(3)
C(19)-C(20)-C(21)	124.2(3)	C(31B)-C(30)-C(29)	117.0(9)
C(19)-C(20)-H(20)	117.9	C(32B)-C(30)-C(32)	61.2(9)
C(21)-C(20)-H(20)	117.9	C(33)-C(30)-C(32)	108.9(3)
O(8)-C(21)-C(20)	123.3(3)	C(31)-C(30)-C(32)	109.7(3)
O(8)-C(21)-C(22)	117.5(3)	C(31B)-C(30)-C(32)	60.6(9)
C(20)-C(21)-C(22)	119.2(3)	C(29)-C(30)-C(32)	108.9(3)
C(21)-C(22)-C(23)	109.7(3)	C(32B)-C(30)-C(33B)	107.4(10)
C(21)-C(22)-C(25)	109.9(3)	C(33)-C(30)-C(33B)	58.7(8)
C(23)-C(22)-C(25)	110.5(3)	C(31)-C(30)-C(33B)	58.0(9)
C(21)-C(22)-C(24)	108.2(3)	C(31B)-C(30)-C(33B)	103.5(10)
C(23)-C(22)-C(24)	108.5(3)	C(29)-C(30)-C(33B)	103.8(9)
C(25)-C(22)-C(24)	110.0(3)	C(32)-C(30)-C(33B)	147.3(9)
C(22)-C(23)-H(23A)	109.5	C(30)-C(31)-H(31A)	109.5
C(22)-C(23)-H(23B)	109.5	C(30)-C(31)-H(31B)	109.5
H(23A)-C(23)-H(23B)	109.5	C(30)-C(31)-H(31C)	109.5
C(22)-C(23)-H(23C)	109.5	C(30)-C(32)-H(32A)	109.5
H(23A)-C(23)-H(23C)	109.5	C(30)-C(32)-H(32B)	109.5
H(23B)-C(23)-H(23C)	109.5	C(30)-C(32)-H(32C)	109.5
C(22)-C(24)-H(24A)	109.5	C(30)-C(33)-H(33A)	109.5
C(22)-C(24)-H(24B)	109.5	C(30)-C(33)-H(33B)	109.5
H(24A)-C(24)-H(24B)	109.5	C(30)-C(33)-H(33C)	109.5
C(22)-C(24)-H(24C)	109.5	C(30)-C(31B)-H(31D)	109.5
H(24A)-C(24)-H(24C)	109.5	C(30)-C(31B)-H(31E)	109.5
H(24B)-C(24)-H(24C)	109.5	H(31D)-C(31B)-H(31E)	109.5
C(22)-C(25)-H(25A)	109.5	C(30)-C(31B)-H(31F)	109.5
C(22)-C(25)-H(25B)	109.5	H(31D)-C(31B)-H(31F)	109.5
H(25A)-C(25)-H(25B)	109.5	H(31E)-C(31B)-H(31F)	109.5
C(22)-C(25)-H(25C)	109.5	C(30)-C(32B)-H(32D)	109.5
H(25A)-C(25)-H(25C)	109.5	C(30)-C(32B)-H(32E)	109.5
H(25B)-C(25)-H(25C)	109.5	H(32D)-C(32B)-H(32E)	109.5
F(10)-C(26)-F(12)	106.8(2)	C(30)-C(32B)-H(32F)	109.5
F(10)-C(26)-F(11)	107.0(2)	H(32D)-C(32B)-H(32F)	109.5
F(12)-C(26)-F(11)	106.3(2)	H(32E)-C(32B)-H(32F)	109.5
F(10)-C(26)-C(27)	111.5(2)	C(30)-C(33B)-H(33D)	109.5
F(12)-C(26)-C(27)	110.7(2)	C(30)-C(33B)-H(33E)	109.5
F(11)-C(26)-C(27)	114.1(2)	H(33D)-C(33B)-H(33E)	109.5
O(9)-C(27)-C(28)	129.0(2)	C(30)-C(33B)-H(33F)	109.5
O(9)-C(27)-C(26)	112.6(2)	H(33D)-C(33B)-H(33F)	109.5
C(28)-C(27)-C(26)	118.3(2)	H(33E)-C(33B)-H(33F)	109.5

O(12)-C(34)-H(34A)	109.5	C(27)-O(9)-Ni(2)	119.36(17)
O(12)-C(34)-H(34B)	109.5	C(29)-O(10)-Ni(2)	127.03(18)
H(34A)-C(34)-H(34B)	109.5	C(35)-O(11)-Ni(2)	118.7(2)
O(12)-C(34)-H(34C)	109.5	C(35)-O(11)-H(11A)	112(3)
H(34A)-C(34)-H(34C)	109.5	Ni(2)-O(11)-H(11A)	112(3)
H(34B)-C(34)-H(34C)	109.5	C(34)-O(12)-Ni(2)	124.58(19)
O(11)-C(35)-H(35A)	109.5	C(34)-O(12)-H(12A)	107(2)
O(11)-C(35)-H(35B)	109.5	Ni(2)-O(12)-H(12A)	119(2)
H(35A)-C(35)-H(35B)	109.5		
O(11)-C(35)-H(35C)	109.5		
H(35A)-C(35)-H(35C)	109.5		
H(35B)-C(35)-H(35C)	109.5		
O(2)-Ni(1)-O(4)	86.48(8)		
O(2)-Ni(1)-O(3)	88.57(8)		
O(4)-Ni(1)-O(3)	90.55(7)		
O(2)-Ni(1)-O(1)	90.69(8)		
O(4)-Ni(1)-O(1)	177.17(7)		
O(3)-Ni(1)-O(1)	89.50(8)		
O(2)-Ni(1)-O(6)	176.15(8)		
O(4)-Ni(1)-O(6)	89.90(8)		
O(3)-Ni(1)-O(6)	90.14(8)		
O(1)-Ni(1)-O(6)	92.93(8)		
O(2)-Ni(1)-O(5)	93.05(8)		
O(4)-Ni(1)-O(5)	92.74(8)		
O(3)-Ni(1)-O(5)	176.41(8)		
O(1)-Ni(1)-O(5)	87.28(8)		
O(6)-Ni(1)-O(5)	88.44(8)		
O(8)-Ni(2)-O(10)	89.11(9)		
O(8)-Ni(2)-O(7)	91.08(8)		
O(10)-Ni(2)-O(7)	179.73(8)		
O(8)-Ni(2)-O(9)	88.85(8)		
O(10)-Ni(2)-O(9)	88.96(8)		
O(7)-Ni(2)-O(9)	91.23(8)		
O(8)-Ni(2)-O(12)	90.67(9)		
O(10)-Ni(2)-O(12)	91.17(8)		
O(7)-Ni(2)-O(12)	88.63(8)		
O(9)-Ni(2)-O(12)	179.49(9)		
O(8)-Ni(2)-O(11)	178.01(8)		
O(10)-Ni(2)-O(11)	89.22(8)		
O(7)-Ni(2)-O(11)	90.59(8)		
O(9)-Ni(2)-O(11)	92.20(8)		
O(12)-Ni(2)-O(11)	88.29(8)		
C(2)-O(1)-Ni(1)	121.94(17)		
C(4)-O(2)-Ni(1)	127.99(18)		
C(10)-O(3)-Ni(1)	119.98(17)		
C(12)-O(4)-Ni(1)	125.78(17)		
C(17)-O(5)-Ni(1)	124.0(2)		
C(17)-O(5)-H(5A)	107(3)		
Ni(1)-O(5)-H(5A)	121(3)		
Ni(1)-O(6)-H(6A)	119(3)		
Ni(1)-O(6)-H(6B)	132(3)		
H(6A)-O(6)-H(6B)	105(4)		
C(19)-O(7)-Ni(2)	122.09(18)		
C(21)-O(8)-Ni(2)	128.0(2)		

Table 4. Anisotropic displacement parameters [$Å^2 \times 10^3$] for 07mz225m. The anisotropic displacement factor exponent takes the form: $-2\pi^2 [(h\ a^*)^2\ U11 + ... + 2\ h\ k\ a^*\ b^*\ U12]$

	U11	U22	U33	U23	U13	U12
C(1)	38(2)	68(2)	31(2)	9(2)	10(1)	29(2)
C(2)	29(1)	40(2)	28(1)	12(1)	10(1)	16(1)
C(3)	23(1)	47(2)	31(1)	9(1)	6(1)	9(1)
C(4)	26(1)	31(1)	27(1)	9(1)	5(1)	8(1)
C(5)	24(1)	42(2)	28(1)	6(1)	5(1)	8(1)
C(6)	35(2)	64(2)	32(2)	14(2)	5(1)	19(2)
C(7)	36(2)	44(2)	44(2)	4(2)	10(1)	3(1)
C(8)	35(2)	52(2)	30(2)	-1(1)	5(1)	14(1)
C(9)	46(2)	31(2)	37(2)	12(1)	18(1)	9(1)
C(10)	26(1)	29(1)	25(1)	8(1)	5(1)	6(1)
C(11)	29(1)	28(1)	31(1)	9(1)	9(1)	9(1)
C(12)	21(1)	33(1)	25(1)	10(1)	4(1)	9(1)
C(13)	26(1)	33(1)	35(1)	15(1)	12(1)	12(1)
C(14)	32(2)	39(2)	45(2)	17(1)	17(1)	11(1)
C(15)	38(2)	45(2)	31(2)	11(1)	12(1)	16(1)
C(16)	39(2)	43(2)	53(2)	21(2)	25(2)	21(1)
C(17)	52(2)	58(2)	70(3)	25(2)	19(2)	25(2)
C(18)	33(2)	47(2)	33(2)	9(1)	8(1)	19(1)
C(19)	26(1)	33(1)	26(1)	4(1)	2(1)	8(1)
C(20)	38(2)	37(2)	34(2)	12(1)	7(1)	19(1)
C(21)	37(2)	30(1)	25(1)	5(1)	1(1)	10(1)
C(22)	58(2)	33(2)	39(2)	17(1)	9(2)	14(2)
C(23)	78(3)	54(2)	58(2)	34(2)	23(2)	15(2)
C(24)	78(3)	52(2)	43(2)	22(2)	8(2)	31(2)
C(25)	104(4)	35(2)	53(2)	13(2)	23(2)	24(2)
C(26)	32(1)	36(2)	27(1)	11(1)	6(1)	13(1)
C(27)	26(1)	29(1)	26(1)	10(1)	4(1)	9(1)
C(28)	29(1)	38(2)	24(1)	11(1)	8(1)	11(1)
C(29)	25(1)	40(2)	28(1)	13(1)	7(1)	9(1)
C(30)	27(1)	56(2)	28(1)	12(1)	8(1)	10(1)
C(31)	44(2)	68(3)	71(3)	14(2)	25(2)	28(2)
C(32)	35(2)	80(3)	56(3)	38(2)	20(2)	14(2)
C(33)	28(2)	109(4)	37(2)	16(2)	8(2)	20(2)
C(31B)	28(2)	109(4)	37(2)	16(2)	8(2)	20(2)
C(32B)	44(2)	68(3)	71(3)	14(2)	25(2)	28(2)
C(33B)	35(2)	80(3)	56(3)	38(2)	20(2)	14(2)
C(34)	43(2)	58(2)	44(2)	4(2)	17(2)	-5(2)
C(35)	62(3)	59(2)	63(2)	18(2)	22(2)	25(2)
F(1)	51(1)	138(2)	35(1)	34(1)	23(1)	53(1)
F(2)	148(3)	94(2)	100(2)	38(2)	87(2)	81(2)
F(3)	32(1)	139(2)	47(1)	-9(1)	14(1)	23(1)
F(4)	94(2)	45(1)	44(1)	25(1)	24(1)	19(1)

F(5)	43(1)	41(1)	89(2)	19(1)	33(1)	3(1)
F(6)	67(1)	31(1)	59(1)	14(1)	34(1)	14(1)
F(7)	40(1)	53(1)	62(1)	15(1)	24(1)	12(1)
F(8)	45(1)	79(1)	31(1)	14(1)	12(1)	32(1)
F(9)	44(1)	68(1)	49(1)	16(1)	14(1)	35(1)
F(10)	36(1)	34(1)	35(1)	9(1)	1(1)	2(1)
F(11)	36(1)	59(1)	27(1)	19(1)	5(1)	11(1)
F(12)	38(1)	55(1)	40(1)	10(1)	3(1)	26(1)
Ni(1)	21(1)	28(1)	24(1)	7(1)	5(1)	7(1)
Ni(2)	24(1)	32(1)	23(1)	9(1)	6(1)	9(1)
O(1)	25(1)	36(1)	23(1)	9(1)	6(1)	10(1)
O(2)	21(1)	36(1)	23(1)	8(1)	6(1)	7(1)
O(3)	29(1)	29(1)	25(1)	8(1)	9(1)	8(1)
O(4)	24(1)	28(1)	29(1)	12(1)	8(1)	9(1)
O(5)	28(1)	33(1)	40(1)	16(1)	13(1)	11(1)
O(6)	26(1)	34(1)	26(1)	11(1)	3(1)	2(1)
O(7)	29(1)	32(1)	27(1)	13(1)	10(1)	14(1)
O(8)	36(1)	34(1)	31(1)	13(1)	10(1)	9(1)
O(9)	24(1)	36(1)	23(1)	11(1)	6(1)	7(1)
O(10)	27(1)	48(1)	22(1)	12(1)	7(1)	13(1)
O(11)	30(1)	39(1)	24(1)	9(1)	8(1)	14(1)
O(12)	31(1)	41(1)	23(1)	6(1)	9(1)	2(1)

Table 5. Hydrogen coordinates ($\times 10^4$) and isotropic displacement parameters ($Å^2 \times 10^3$) for 07mz225m.

	x	y	z	U(eq)
H(3)	11265	2680	7774	43
H(6D)	11998	3087	10390	67
H(6E)	11927	2497	9389	67
H(6C)	10762	2084	9779	67
H(7A)	11245	4597	8914	70
H(7B)	12268	4061	8923	70
H(7C)	12253	4670	9886	70
H(8A)	9419	3956	9538	64
H(8B)	10473	4011	10481	64
H(8C)	9255	2991	9890	64
H(11)	6598	4168	8205	36
H(14A)	3589	1735	8923	57
H(14B)	4313	1163	8409	57
H(14C)	3400	1640	7847	57
H(15A)	5802	2806	10165	56
H(15B)	6980	3411	9866	56
H(15C)	6483	2226	9612	56
H(16A)	4167	3535	8264	61
H(16B)	5513	4195	9109	61
H(16C)	4275	3526	9311	61
H(17A)	8505	66	7186	87

H(17B)	7520	-790	7438	87
H(17C)	8310	290	8178	87
H(20)	4288	3528	3749	43
H(23A)	7915	4642	3055	95
H(23B)	7128	4892	2175	95
H(23C)	7012	3773	2103	95
H(24A)	4588	3193	1596	86
H(24B)	4681	4304	1652	86
H(24C)	3896	3694	2207	86
H(25A)	5250	5072	3680	98
H(25B)	6118	5696	3176	98
H(25C)	6815	5416	4067	98
H(28)	6710	1243	1110	37
H(31A)	9762	641	1473	89
H(31B)	8201	303	1170	89
H(31C)	9021	229	2145	89
H(32A)	9257	2942	1770	83
H(32B)	8516	1949	908	83
H(32C)	10085	2397	1352	83
H(33A)	10399	1764	3472	91
H(33B)	10496	2828	3340	91
H(33C)	11202	2217	2848	91
H(31D)	8466	1454	750	91
H(31E)	8442	449	996	91
H(31F)	9797	1259	1062	91
H(32D)	10402	2953	3203	89
H(32E)	9802	3122	2220	89
H(32F)	10967	2717	2383	89
H(33D)	10603	1007	2576	83
H(33E)	9183	347	2556	83
H(33F)	10094	1330	3407	83
H(34A)	9633	3489	4711	83
H(34B)	9963	3855	5816	83
H(34C)	9007	4217	5137	83
H(35A)	6518	-385	3271	90
H(35B)	7329	-503	4226	90
H(35C)	8042	303	3783	90
H(5A)	6210(30)	-80(20)	7280(30)	46(10)
H(6A)	5310(40)	1260(20)	5400(20)	48
H(6B)	4840(30)	400(20)	5560(30)	77(15)
H(11A)	7330(40)	860(30)	4951(15)	67(13)
H(12A)	7970(30)	2970(20)	5581(16)	20(7)

Table 6. Torsion angles [deg] for 07mz225m.

F(1)-C(1)-C(2)-O(1)	45.7(4)
F(3)-C(1)-C(2)-O(1)	169.5(3)
F(2)-C(1)-C(2)-O(1)	-71.1(3)
F(1)-C(1)-C(2)-C(3)	-137.0(3)
F(3)-C(1)-C(2)-C(3)	-13.2(5)
F(2)-C(1)-C(2)-C(3)	106.2(4)
O(1)-C(2)-C(3)-C(4)	3.6(5)

C(1)-C(2)-C(3)-C(4)	-173.1(3)
C(2)-C(3)-C(4)-O(2)	1.1(5)
C(2)-C(3)-C(4)-C(5)	178.9(3)
O(2)-C(4)-C(5)-C(8)	-12.7(4)
C(3)-C(4)-C(5)-C(8)	169.4(3)
O(2)-C(4)-C(5)-C(6)	107.0(3)
C(3)-C(4)-C(5)-C(6)	-70.9(3)
O(2)-C(4)-C(5)-C(7)	-132.5(3)
C(3)-C(4)-C(5)-C(7)	49.6(4)
F(5)-C(9)-C(10)-O(3)	-59.7(3)
F(6)-C(9)-C(10)-O(3)	179.8(3)
F(4)-C(9)-C(10)-O(3)	58.7(3)
F(5)-C(9)-C(10)-C(11)	120.5(3)
F(6)-C(9)-C(10)-C(11)	0.1(4)
F(4)-C(9)-C(10)-C(11)	-121.0(3)
O(3)-C(10)-C(11)-C(12)	-2.2(5)
C(9)-C(10)-C(11)-C(12)	177.5(3)
C(10)-C(11)-C(12)-O(4)	4.6(4)
C(10)-C(11)-C(12)-C(13)	-178.6(3)
O(4)-C(12)-C(13)-C(16)	-155.7(3)
C(11)-C(12)-C(13)-C(16)	27.3(4)
O(4)-C(12)-C(13)-C(14)	-33.5(3)
C(11)-C(12)-C(13)-C(14)	149.4(3)
O(4)-C(12)-C(13)-C(15)	84.1(3)
C(11)-C(12)-C(13)-C(15)	-92.9(3)
F(9)-C(18)-C(19)-O(7)	-179.2(2)
F(8)-C(18)-C(19)-O(7)	60.3(3)
F(7)-C(18)-C(19)-O(7)	-58.1(3)
F(9)-C(18)-C(19)-C(20)	2.0(4)
F(8)-C(18)-C(19)-C(20)	-118.5(3)
F(7)-C(18)-C(19)-C(20)	123.0(3)
O(7)-C(19)-C(20)-C(21)	-3.4(5)
C(18)-C(19)-C(20)-C(21)	175.1(3)
C(19)-C(20)-C(21)-O(8)	0.9(5)
C(19)-C(20)-C(21)-C(22)	-178.8(3)
O(8)-C(21)-C(22)-C(23)	-3.6(4)
C(20)-C(21)-C(22)-C(23)	176.1(3)
O(8)-C(21)-C(22)-C(25)	-125.3(3)
C(20)-C(21)-C(22)-C(25)	54.4(4)
O(8)-C(21)-C(22)-C(24)	114.6(3)
C(20)-C(21)-C(22)-C(24)	-65.7(4)
F(10)-C(26)-C(27)-O(9)	-64.9(3)
F(12)-C(26)-C(27)-O(9)	53.9(3)
F(11)-C(26)-C(27)-O(9)	173.7(2)
F(10)-C(26)-C(27)-C(28)	115.0(3)
F(12)-C(26)-C(27)-C(28)	-126.2(3)
F(11)-C(26)-C(27)-C(28)	-6.4(4)
O(9)-C(27)-C(28)-C(29)	0.6(5)
C(26)-C(27)-C(28)-C(29)	-179.3(3)
C(27)-C(28)-C(29)-O(10)	-11.6(5)
C(27)-C(28)-C(29)-C(30)	166.2(3)
O(10)-C(29)-C(30)-C(32B)	-64.0(11)
C(28)-C(29)-C(30)-C(32B)	118.1(10)
O(10)-C(29)-C(30)-C(33)	-10.2(4)
C(28)-C(29)-C(30)-C(33)	171.9(3)
O(10)-C(29)-C(30)-C(31)	111.5(3)
C(28)-C(29)-C(30)-C(31)	-66.4(4)

O(10)-C(29)-C(30)-C(31B)	164.4(11)
C(28)-C(29)-C(30)-C(31B)	-13.5(11)
O(10)-C(29)-C(30)-C(32)	-129.7(3)
C(28)-C(29)-C(30)-C(32)	52.4(4)
O(10)-C(29)-C(30)-C(33B)	51.2(9)
C(28)-C(29)-C(30)-C(33B)	-126.7(9)
C(3)-C(2)-O(1)-Ni(1)	3.0(4)
C(1)-C(2)-O(1)-Ni(1)	179.8(2)
O(2)-Ni(1)-O(1)-C(2)	-9.0(2)
O(3)-Ni(1)-O(1)-C(2)	79.6(2)
O(6)-Ni(1)-O(1)-C(2)	169.7(2)
O(5)-Ni(1)-O(1)-C(2)	-102.0(2)
C(3)-C(4)-O(2)-Ni(1)	-12.1(4)
C(5)-C(4)-O(2)-Ni(1)	170.06(18)
O(4)-Ni(1)-O(2)-C(4)	-166.1(2)
O(3)-Ni(1)-O(2)-C(4)	-75.5(2)
O(1)-Ni(1)-O(2)-C(4)	14.0(2)
O(5)-Ni(1)-O(2)-C(4)	101.3(2)
C(11)-C(10)-O(3)-Ni(1)	-16.4(4)
C(9)-C(10)-O(3)-Ni(1)	163.82(18)
O(2)-Ni(1)-O(3)-C(10)	-63.0(2)
O(4)-Ni(1)-O(3)-C(10)	23.5(2)
O(1)-Ni(1)-O(3)-C(10)	-153.7(2)
O(6)-Ni(1)-O(3)-C(10)	113.4(2)
C(11)-C(12)-O(4)-Ni(1)	13.3(4)
C(13)-C(12)-O(4)-Ni(1)	-163.60(17)
O(2)-Ni(1)-O(4)-C(12)	65.3(2)
O(3)-Ni(1)-O(4)-C(12)	-23.3(2)
O(6)-Ni(1)-O(4)-C(12)	-113.4(2)
O(5)-Ni(1)-O(4)-C(12)	158.2(2)
O(2)-Ni(1)-O(5)-C(17)	-40.3(3)
O(4)-Ni(1)-O(5)-C(17)	-126.9(3)
O(1)-Ni(1)-O(5)-C(17)	50.2(3)
O(6)-Ni(1)-O(5)-C(17)	143.2(3)
C(20)-C(19)-O(7)-Ni(2)	-3.8(4)
C(18)-C(19)-O(7)-Ni(2)	177.60(17)
O(8)-Ni(2)-O(7)-C(19)	8.8(2)
O(9)-Ni(2)-O(7)-C(19)	-80.1(2)
O(12)-Ni(2)-O(7)-C(19)	99.5(2)
O(11)-Ni(2)-O(7)-C(19)	-172.3(2)
C(20)-C(21)-O(8)-Ni(2)	8.7(4)
C(22)-C(21)-O(8)-Ni(2)	-171.59(19)
O(10)-Ni(2)-O(8)-C(21)	168.4(2)
O(7)-Ni(2)-O(8)-C(21)	-11.8(2)
O(9)-Ni(2)-O(8)-C(21)	79.5(2)
O(12)-Ni(2)-O(8)-C(21)	-100.4(2)
C(28)-C(27)-O(9)-Ni(2)	25.7(4)
C(26)-C(27)-O(9)-Ni(2)	-154.37(18)
O(8)-Ni(2)-O(9)-C(27)	58.1(2)
O(10)-Ni(2)-O(9)-C(27)	-31.0(2)
O(7)-Ni(2)-O(9)-C(27)	149.2(2)
O(11)-Ni(2)-O(9)-C(27)	-120.2(2)
C(28)-C(29)-O(10)-Ni(2)	-7.5(4)
C(30)-C(29)-O(10)-Ni(2)	174.7(2)
O(8)-Ni(2)-O(10)-C(29)	-64.9(3)
O(9)-Ni(2)-O(10)-C(29)	24.0(3)
O(12)-Ni(2)-O(10)-C(29)	-155.5(3)

O(11)-Ni(2)-O(10)-C(29)	116.2(3)
O(10)-Ni(2)-O(11)-C(35)	-30.1(3)
O(7)-Ni(2)-O(11)-C(35)	150.1(2)
O(9)-Ni(2)-O(11)-C(35)	58.9(3)
O(12)-Ni(2)-O(11)-C(35)	-121.3(3)
O(8)-Ni(2)-O(12)-C(34)	-43.4(3)
O(10)-Ni(2)-O(12)-C(34)	45.7(3)
O(7)-Ni(2)-O(12)-C(34)	-134.4(3)
O(11)-Ni(2)-O(12)-C(34)	134.9(3)

Table 7. Hydrogen bonds for 07mz225m [Å and deg].

D-H...A	d(D-H)	d(H...A)	d(D...A)	<(DHA)
O(12)-H(12A)...O(3)	0.812(17)	1.988(19)	2.778(3)	164(3)
O(11)-H(11A)...O(1)	0.832(19)	1.965(19)	2.796(3)	176(4)
O(6)-H(6B)...O(6)#1	0.842(19)	2.37(4)	2.872(4)	119(4)
O(6)-H(6B)...O(11)#1	0.842(19)	2.15(2)	2.950(3)	159(4)
O(6)-H(6A)...O(7)	0.824(18)	1.94(2)	2.716(3)	157(4)
O(5)-H(5A)...O(9)#1	0.832(18)	1.88(2)	2.698(3)	167(4)

Symmetry transformations used to generate equivalent atoms:
#1 -x+1,-y,-z+1

B.3 $Cu(tftm)_2$

Table 1. Crystal data and structure refinement for 07mz384m:

Identification code: 07mz384m
Empirical formula: C17 H24 Cu F6 O5
Formula weight: 485.90
Temperature: 100(2) K
Wavelength: 0.71073 Å
Crystal system: Triclinic
Space group: P-1
Unit cell dimensions:
a = 9.3307(9) Å, α = 106.231(2)°
b = 10.6833(10) Å, β = 104.166(2)°
c = 11.9202(11) Å, γ = 99.418(2)°
Volume, *Z*: 1071.27(17) $Å^3$, 2
Density (calculated): 1.506 Mg/m^3
Absorption coefficient: 1.094 mm^{-1}
F(000): 498
Crystal size: 0.40 × 0.18 × 0.12 mm
Crystal shape, colour: needle, blue
θ range for data collection: 1.87 to 28.28°
Limiting indices: $-12 \le h \le 12$, $-14 \le k \le 13$, $-15 \le l \le 15$
Reflections collected: 11033
Independent reflections: 5304 (*R*(int) = 0.0310)
Completeness to θ = 28.28°: 99.6 %
Absorption correction: multi-scan
Max. and min. transmission: 0.8622 and 0.7500
Refinement method: Full-matrix least-squares on F^2
Data / restraints / parameters: 5304 / 1 / 272
Goodness-of-fit on F^2: 1.039
Final *R* indices [$I>2\sigma(I)$]: R1 = 0.0436, wR2 = 0.1127
R indices (all data): R1 = 0.0498, wR2 = 0.1174
Largest diff. peak and hole: 0.734 and -0.501 e × $Å^{-3}$

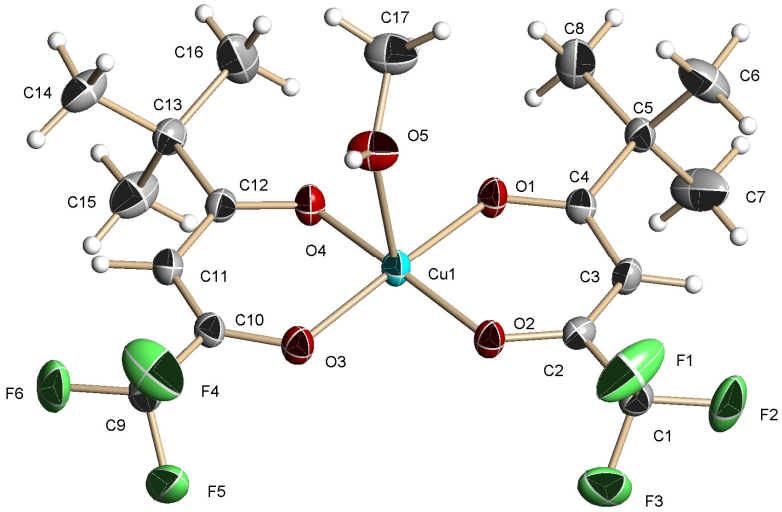

Refinement of F^2 against ALL reflections. The weighted R-factor wR and goodness of fit are based on F^2, conventional R-factors R are based on *F*, with *F* set to zero for negative F^2. The threshold expression of $F^2 > 2\sigma(F^2)$ is used only for calculating R-factors

Treatment of hydrogen atoms:
The hydroxyl H atom was located in a difference density Fourier map and the O-H distance was restrained to 0.84(2) Å. All other hydrogen atoms were placed in calculated positions and all H atoms were refined with an isotropic displacement parameter 1.5 (methyl, hydroxyl) or 1.2 times (all others) that of the adjacent carbon or oxygen atom.

Table 2. Atomic coordinates [$\times 10^4$] and equivalent isotropic displacement parameters [$Å^2 \times 10^3$] for 07mz384m. U(eq) is defined as one third of the trace of the orthogonalized U_{ij} tensor.

	x	y	z	U(eq)
C(1)	7953(3)	10932(2)	3024(2)	28(1)
C(2)	7964(2)	9928(2)	3723(2)	24(1)
C(3)	8308(3)	8734(2)	3235(2)	26(1)
C(4)	8184(2)	7672(2)	3745(2)	23(1)
C(5)	8344(2)	6288(2)	3046(2)	25(1)
C(6)	7124(4)	5751(3)	1788(3)	49(1)
C(7)	9931(3)	6450(3)	2894(4)	56(1)
C(8)	8095(4)	5311(3)	3742(3)	48(1)
C(9)	6857(3)	12216(2)	8742(2)	32(1)
C(10)	7170(2)	10906(2)	8040(2)	24(1)
C(11)	7189(3)	9901(2)	8551(2)	27(1)
C(12)	7457(2)	8642(2)	7970(2)	23(1)
C(13)	7469(3)	7573(2)	8596(2)	29(1)
C(14)	6158(3)	7497(3)	9173(3)	42(1)
C(15)	9003(3)	7996(3)	9610(3)	45(1)
C(16)	7273(5)	6203(3)	7653(3)	55(1)
C(17)	4298(3)	7048(3)	4659(3)	45(1)
Cu(1)	7522(1)	9348(1)	5827(1)	24(1)
F(1)	6566(2)	11035(2)	2585(2)	71(1)
F(2)	8531(3)	10612(2)	2094(2)	60(1)
F(3)	8787(2)	12152(2)	3744(2)	57(1)
F(4)	5530(2)	12361(2)	8161(2)	65(1)
F(5)	7925(2)	13290(1)	8882(2)	47(1)
F(6)	6843(2)	12291(2)	9883(2)	55(1)
O(1)	7904(2)	7808(2)	4744(1)	27(1)
O(2)	7595(2)	10353(2)	4708(1)	26(1)
O(3)	7361(2)	10920(2)	7015(1)	28(1)
O(4)	7724(2)	8356(2)	6957(1)	27(1)
O(5)	4961(2)	8450(2)	5150(2)	39(1)

All esds (except the esd in the dihedral angle between two l.s. planes) are estimated using the full covariance matrix. The cell esds are taken

into account individually in the estimation of esds in distances, angles and torsion angles; correlations between esds in cell parameters are only used when they are defined by crystal symmetry. An approximate (isotropic) treatment of cell esds is used for estimating esds involving l.s. planes.

Table 3. Bond lengths [Å] and angles [deg] for 07mz384m.

C(1)-F(1)	1.307(3)	C(17)-O(5)	1.414(3)
C(1)-F(3)	1.325(3)	C(17)-H(17A)	0.9800
C(1)-F(2)	1.334(3)	C(17)-H(17B)	0.9800
C(1)-C(2)	1.532(3)	C(17)-H(17C)	0.9800
C(2)-O(2)	1.286(3)	Cu(1)-O(3)	1.9252(15)
C(2)-C(3)	1.370(3)	Cu(1)-O(4)	1.9274(15)
C(3)-C(4)	1.431(3)	Cu(1)-O(1)	1.9322(15)
C(3)-H(3)	0.9500	Cu(1)-O(2)	1.9381(15)
C(4)-O(1)	1.255(3)	Cu(1)-O(5)	2.2698(18)
C(4)-C(5)	1.533(3)	O(5)-H(5A)	0.800(18)
C(5)-C(7)	1.523(3)		
C(5)-C(8)	1.527(3)	F(1)-C(1)-F(3)	107.3(2)
C(5)-C(6)	1.531(3)	F(1)-C(1)-F(2)	107.9(2)
C(6)-H(6A)	0.9800	F(3)-C(1)-F(2)	105.2(2)
C(6)-H(6B)	0.9800	F(1)-C(1)-C(2)	110.87(19)
C(6)-H(6C)	0.9800	F(3)-C(1)-C(2)	111.60(19)
C(7)-H(7A)	0.9800	F(2)-C(1)-C(2)	113.58(19)
C(7)-H(7B)	0.9800	O(2)-C(2)-C(3)	129.4(2)
C(7)-H(7C)	0.9800	O(2)-C(2)-C(1)	112.05(18)
C(8)-H(8A)	0.9800	C(3)-C(2)-C(1)	118.55(19)
C(8)-H(8B)	0.9800	C(2)-C(3)-C(4)	122.69(19)
C(8)-H(8C)	0.9800	C(2)-C(3)-H(3)	118.7
C(9)-F(4)	1.318(3)	C(4)-C(3)-H(3)	118.7
C(9)-F(5)	1.333(3)	O(1)-C(4)-C(3)	122.70(19)
C(9)-F(6)	1.343(3)	O(1)-C(4)-C(5)	117.32(18)
C(9)-C(10)	1.531(3)	C(3)-C(4)-C(5)	119.95(18)
C(10)-O(3)	1.281(3)	C(7)-C(5)-C(8)	110.7(2)
C(10)-C(11)	1.375(3)	C(7)-C(5)-C(6)	110.2(2)
C(11)-C(12)	1.423(3)	C(8)-C(5)-C(6)	108.9(2)
C(11)-H(11)	0.9500	C(7)-C(5)-C(4)	108.60(19)
C(12)-O(4)	1.257(3)	C(8)-C(5)-C(4)	110.19(18)
C(12)-C(13)	1.529(3)	C(6)-C(5)-C(4)	108.25(18)
C(13)-C(16)	1.526(3)	C(5)-C(6)-H(6A)	109.5
C(13)-C(15)	1.534(3)	C(5)-C(6)-H(6B)	109.5
C(13)-C(14)	1.545(3)	H(6A)-C(6)-H(6B)	109.5
C(14)-H(14A)	0.9800	C(5)-C(6)-H(6C)	109.5
C(14)-H(14B)	0.9800	H(6A)-C(6)-H(6C)	109.5
C(14)-H(14C)	0.9800	H(6B)-C(6)-H(6C)	109.5
C(15)-H(15A)	0.9800	C(5)-C(7)-H(7A)	109.5
C(15)-H(15B)	0.9800	C(5)-C(7)-H(7B)	109.5
C(15)-H(15C)	0.9800	H(7A)-C(7)-H(7B)	109.5
C(16)-H(16A)	0.9800	C(5)-C(7)-H(7C)	109.5
C(16)-H(16B)	0.9800	H(7A)-C(7)-H(7C)	109.5
C(16)-H(16C)	0.9800	H(7B)-C(7)-H(7C)	109.5

C(5)-C(8)-H(8A)	109.5	O(3)-Cu(1)-O(2)	89.39(6)
C(5)-C(8)-H(8B)	109.5	O(4)-Cu(1)-O(2)	172.55(6)
H(8A)-C(8)-H(8B)	109.5	O(1)-Cu(1)-O(2)	92.36(6)
C(5)-C(8)-H(8C)	109.5	O(3)-Cu(1)-O(5)	92.68(7)
H(8A)-C(8)-H(8C)	109.5	O(4)-Cu(1)-O(5)	89.44(7)
H(8B)-C(8)-H(8C)	109.5	O(1)-Cu(1)-O(5)	92.90(7)
F(4)-C(9)-F(5)	107.5(2)	O(2)-Cu(1)-O(5)	97.42(7)
F(4)-C(9)-F(6)	107.4(2)	C(4)-O(1)-Cu(1)	129.22(14)
F(5)-C(9)-F(6)	105.4(2)	C(2)-O(2)-Cu(1)	123.07(13)
F(4)-C(9)-C(10)	111.2(2)	C(10)-O(3)-Cu(1)	122.33(14)
F(5)-C(9)-C(10)	111.77(18)	C(12)-O(4)-Cu(1)	127.40(14)
F(6)-C(9)-C(10)	113.2(2)	C(17)-O(5)-Cu(1)	122.96(15)
O(3)-C(10)-C(11)	129.4(2)	C(17)-O(5)-H(5A)	113(3)
O(3)-C(10)-C(9)	112.23(19)	Cu(1)-O(5)-H(5A)	124(3)
C(11)-C(10)-C(9)	118.39(19)		
C(10)-C(11)-C(12)	122.8(2)		
C(10)-C(11)-H(11)	118.6		
C(12)-C(11)-H(11)	118.6		
O(4)-C(12)-C(11)	123.3(2)		
O(4)-C(12)-C(13)	116.72(19)		
C(11)-C(12)-C(13)	119.99(19)		
C(16)-C(13)-C(12)	109.62(19)		
C(16)-C(13)-C(15)	111.0(2)		
C(12)-C(13)-C(15)	107.24(19)		
C(16)-C(13)-C(14)	109.2(2)		
C(12)-C(13)-C(14)	110.35(19)		
C(15)-C(13)-C(14)	109.4(2)		
C(13)-C(14)-H(14A)	109.5		
C(13)-C(14)-H(14B)	109.5		
H(14A)-C(14)-H(14B)	109.5		
C(13)-C(14)-H(14C)	109.5		
H(14A)-C(14)-H(14C)	109.5		
H(14B)-C(14)-H(14C)	109.5		
C(13)-C(15)-H(15A)	109.5		
C(13)-C(15)-H(15B)	109.5		
H(15A)-C(15)-H(15B)	109.5		
C(13)-C(15)-H(15C)	109.5		
H(15A)-C(15)-H(15C)	109.5		
H(15B)-C(15)-H(15C)	109.5		
C(13)-C(16)-H(16A)	109.5		
C(13)-C(16)-H(16B)	109.5		
H(16A)-C(16)-H(16B)	109.5		
C(13)-C(16)-H(16C)	109.5		
H(16A)-C(16)-H(16C)	109.5		
H(16B)-C(16)-H(16C)	109.5		
O(5)-C(17)-H(17A)	109.5		
O(5)-C(17)-H(17B)	109.5		
H(17A)-C(17)-H(17B)	109.5		
O(5)-C(17)-H(17C)	109.5		
H(17A)-C(17)-H(17C)	109.5		
H(17B)-C(17)-H(17C)	109.5		
O(3)-Cu(1)-O(4)	93.21(7)		
O(3)-Cu(1)-O(1)	173.89(7)		
O(4)-Cu(1)-O(1)	84.37(6)		

Table 4. Anisotropic displacement parameters [$Å^2 \times 10^3$] for 07mz384m. The anisotropic displacement factor exponent takes the form: $-2\pi^2$ [$(h\ a^*)^2$ U11 + ... + 2 h k a* b* U12]

	U11	U22	U33	U23	U13	U12
C(1)	32(1)	27(1)	29(1)	13(1)	13(1)	7(1)
C(2)	24(1)	24(1)	26(1)	10(1)	9(1)	6(1)
C(3)	34(1)	27(1)	26(1)	11(1)	16(1)	10(1)
C(4)	23(1)	25(1)	23(1)	8(1)	10(1)	8(1)
C(5)	31(1)	22(1)	26(1)	7(1)	15(1)	10(1)
C(6)	62(2)	30(1)	40(2)	2(1)	1(1)	12(1)
C(7)	38(1)	37(1)	93(3)	5(2)	37(2)	11(1)
C(8)	86(2)	31(1)	47(2)	20(1)	37(2)	28(1)
C(9)	36(1)	30(1)	36(1)	7(1)	20(1)	11(1)
C(10)	22(1)	27(1)	24(1)	5(1)	10(1)	7(1)
C(11)	29(1)	30(1)	25(1)	8(1)	13(1)	8(1)
C(12)	23(1)	26(1)	21(1)	9(1)	7(1)	5(1)
C(13)	34(1)	29(1)	25(1)	12(1)	9(1)	7(1)
C(14)	35(1)	50(2)	50(2)	30(1)	16(1)	6(1)
C(15)	35(1)	58(2)	49(2)	34(1)	8(1)	9(1)
C(16)	102(3)	33(1)	39(2)	18(1)	26(2)	21(2)
C(17)	37(1)	34(1)	60(2)	12(1)	12(1)	11(1)
Cu(1)	32(1)	25(1)	23(1)	10(1)	14(1)	13(1)
F(1)	38(1)	109(2)	102(2)	88(2)	18(1)	25(1)
F(2)	105(2)	50(1)	62(1)	37(1)	60(1)	35(1)
F(3)	87(1)	29(1)	48(1)	19(1)	9(1)	0(1)
F(4)	50(1)	62(1)	74(1)	3(1)	11(1)	39(1)
F(5)	64(1)	25(1)	57(1)	6(1)	37(1)	8(1)
F(6)	93(1)	40(1)	49(1)	13(1)	50(1)	25(1)
O(1)	40(1)	26(1)	27(1)	13(1)	19(1)	16(1)
O(2)	34(1)	25(1)	26(1)	11(1)	15(1)	14(1)
O(3)	35(1)	26(1)	28(1)	10(1)	16(1)	13(1)
O(4)	37(1)	29(1)	24(1)	12(1)	14(1)	16(1)
O(5)	28(1)	31(1)	57(1)	13(1)	11(1)	13(1)

Table 5. Hydrogen coordinates ($\times 10^4$) and isotropic displacement parameters ($Å^2 \times 10^3$) for 07mz384m.

	x	y	z	U(eq)
H(3)	8641	8607	2529	32
H(6A)	6112	5712	1898	73
H(6B)	7177	4847	1341	73
H(6C)	7301	6352	1320	73
H(7A)	10084	7104	2472	84
H(7B)	10030	5580	2408	84
H(7C)	10701	6770	3704	84
H(8A)	8868	5649	4551	72
H(8B)	8179	4426	3279	72
H(8C)	7076	5232	3843	72
H(11)	7016	10053	9326	33
H(14A)	5191	7378	8552	63
H(14B)	6355	8332	9857	63
H(14C)	6096	6733	9477	63
H(15A)	9112	8886	10191	67
H(15B)	9836	8033	9244	67
H(15C)	9043	7340	10043	67
H(16A)	7251	5515	8051	82
H(16B)	8129	6235	7313	82
H(16C)	6314	5980	6991	82
H(17A)	5106	6565	4706	67
H(17B)	3685	6810	3800	67
H(17C)	3643	6798	5131	67
H(5A)	4340(30)	8890(30)	5170(30)	58

Table 6. Torsion angles [deg] for 07mz384m

F(1)-C(1)-C(2)-O(2)	-67.1(3)
F(3)-C(1)-C(2)-O(2)	52.5(3)
F(2)-C(1)-C(2)-O(2)	171.3(2)
F(1)-C(1)-C(2)-C(3)	111.2(3)
F(3)-C(1)-C(2)-C(3)	-129.2(2)
F(2)-C(1)-C(2)-C(3)	-10.4(3)
O(2)-C(2)-C(3)-C(4)	5.1(4)
C(1)-C(2)-C(3)-C(4)	-172.9(2)
C(2)-C(3)-C(4)-O(1)	-7.5(3)
C(2)-C(3)-C(4)-C(5)	170.5(2)
O(1)-C(4)-C(5)-C(7)	-120.5(2)

C(3)-C(4)-C(5)-C(7)	61.3(3)
O(1)-C(4)-C(5)-C(8)	0.8(3)
C(3)-C(4)-C(5)-C(8)	-177.3(2)
O(1)-C(4)-C(5)-C(6)	119.8(2)
C(3)-C(4)-C(5)-C(6)	-58.4(3)
F(4)-C(9)-C(10)-O(3)	66.9(3)
F(5)-C(9)-C(10)-O(3)	-53.3(3)
F(6)-C(9)-C(10)-O(3)	-172.1(2)
F(4)-C(9)-C(10)-C(11)	-112.2(2)
F(5)-C(9)-C(10)-C(11)	127.6(2)
F(6)-C(9)-C(10)-C(11)	8.8(3)
O(3)-C(10)-C(11)-C(12)	0.6(4)
C(9)-C(10)-C(11)-C(12)	179.5(2)
C(10)-C(11)-C(12)-O(4)	1.3(3)
C(10)-C(11)-C(12)-C(13)	179.7(2)
O(4)-C(12)-C(13)-C(16)	-19.2(3)
C(11)-C(12)-C(13)-C(16)	162.3(2)
O(4)-C(12)-C(13)-C(15)	101.4(2)
C(11)-C(12)-C(13)-C(15)	-77.1(3)
O(4)-C(12)-C(13)-C(14)	-139.5(2)
C(11)-C(12)-C(13)-C(14)	41.9(3)
C(3)-C(4)-O(1)-Cu(1)	1.7(3)
C(5)-C(4)-O(1)-Cu(1)	-176.35(14)
O(4)-Cu(1)-O(1)-C(4)	-169.20(19)
O(2)-Cu(1)-O(1)-C(4)	4.10(19)
O(5)-Cu(1)-O(1)-C(4)	101.65(19)
C(3)-C(2)-O(2)-Cu(1)	2.8(3)
C(1)-C(2)-O(2)-Cu(1)	-179.07(13)
O(3)-Cu(1)-O(2)-C(2)	168.02(17)
O(1)-Cu(1)-O(2)-C(2)	-6.12(17)
O(5)-Cu(1)-O(2)-C(2)	-99.35(17)
C(11)-C(10)-O(3)-Cu(1)	6.9(3)
C(9)-C(10)-O(3)-Cu(1)	-172.11(14)
O(4)-Cu(1)-O(3)-C(10)	-11.26(17)
O(2)-Cu(1)-O(3)-C(10)	175.73(17)
O(5)-Cu(1)-O(3)-C(10)	78.33(17)
C(11)-C(12)-O(4)-Cu(1)	-10.8(3)
C(13)-C(12)-O(4)-Cu(1)	170.72(14)
O(3)-Cu(1)-O(4)-C(12)	13.86(19)
O(1)-Cu(1)-O(4)-C(12)	-171.76(19)
O(5)-Cu(1)-O(4)-C(12)	-78.80(18)
O(3)-Cu(1)-O(5)-C(17)	-150.6(2)
O(4)-Cu(1)-O(5)-C(17)	-57.5(2)
O(1)-Cu(1)-O(5)-C(17)	26.9(2)
O(2)-Cu(1)-O(5)-C(17)	119.6(2)

Table 7. Hydrogen bonds for 07mz384m [Å and deg].

D-H...A	d(D-H)	d(H...A)	d(D...A)	<(DHA)
O(5)-H(5A)...O(2)#1	0.800(18)	2.118(19)	2.902(2)	167(3)

Symmetry transformations used to generate equivalent atoms:

#1 -x+1,-y+2,-z+1

B.4 $Ni(acac)_2$ & $Ni(hfac)_2$ Sublimation Product: Fraction 1

Table 1. Crystal data and structure refinement for 08mz253_0m:

Identification code: 08mz253_0m
Empirical formula: C10 H14 F6 Ni O7
Moiety formula: C10 H12 F6 Ni O6, H2 O
Formula weight: 418.92
Temperature: 140(2) K
Wavelength: 0.71073 Å
Crystal system: Monoclinic
Space group: $P2_1/m$
Unit cell dimensions:
a = 9.265(2) Å, α = 90°
b = 7.5750(17) Å, β = 106.539(3)°
c = 11.471(3) Å, γ = 90°
Volume, *Z*: 771.8(3) $Å^3$, 2
Density (calculated): 1.803 Mg/m^3
Absorption coefficient: 1.355 mm^{-1}
F(000): 424
Crystal size: 0.30 × 0.20 × 0.08 mm
Crystal shape, colour: plate, green
θ range for data collection: 1.85 to 28.28°
Limiting indices: $-12 \le h \le 12$, $-6 \le k \le 10$, $-14 \le l \le 15$
Reflections collected: 5733
Independent reflections: 2052 (*R*(int) = 0.0383)
Completeness to θ = 28.28°: 99.8 %
Absorption correction: multi-scan
Max. and min. transmission: 0.897 and 0.673
Refinement method: Full-matrix least-squares on F^2
Data / restraints / parameters: 2052 / 109 / 190
Goodness-of-fit on F^2: 1.058
Final *R* indices [$I>2\sigma(I)$]: R1 = 0.0446, wR2 = 0.0988
R indices (all data): R1 = 0.0603, wR2 = 0.1069
Largest diff. peak and hole: 0.501 and −0.755 e × $Å^{-3}$

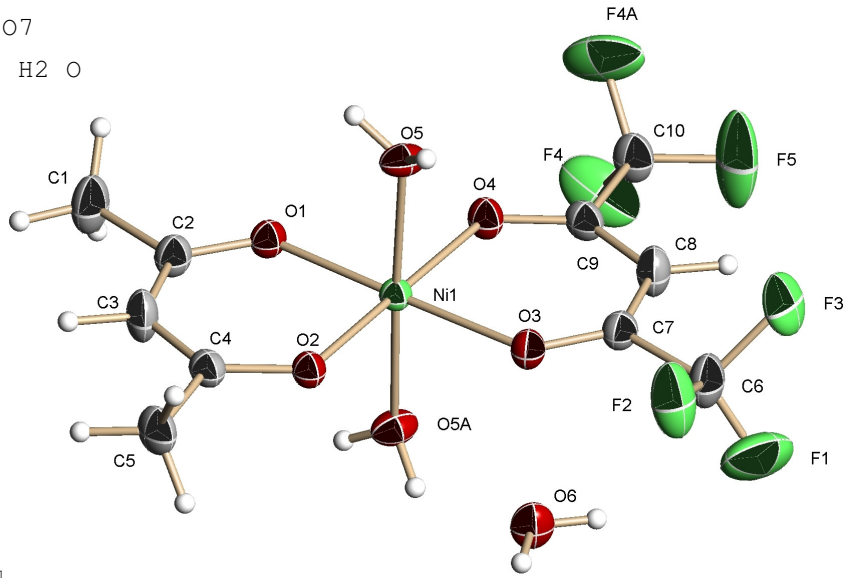

Refinement of F^2 against ALL reflections. The weighted R-factor wR and goodness of fit are based on F^2, conventional R-factors R are based on *F*, with *F* set to zero for negative F^2. The threshold expression of

$F^2 > 2\sigma(F^2)$ is used only for calculating R-factors

Comments:

The complex is located on a mirror plane and the F atoms of the CF3 groups are disordered across this plane. They were refined as disordered over two positions with occupancies for the major components of 0.82(2) and 0.81(1) for each CF3 group.

The remainder was refined as each occupied by a moiety obeying the mirror plane. All C-F distances and F...F distances were each restrained to be the same (standard deviation 0.02 Angstrom) and F atoms were restrained to be isotropic within a standard deviation of 0.02 Angstrom squared.

Treatment of hydrogen atoms:

All hydrogen atoms were placed in calculated positions and were refined with an isotropic displacement parameter 1.5 (methyl, hydroxyl) or 1.2 times (all others) that of the adjacent carbon or oxygen atom.

Table 2. Atomic coordinates [$\times 10^4$] and equivalent isotropic displacement parameters [$Å^2 \times 10^3$] for 08mz253_0m. U(eq) is defined as one third of the trace of the orthogonalized U_{ij} tensor.

	x	y	z	U(eq)
C(1)	9256(5)	7500	2702(5)	43(1)
C(2)	7993(5)	7500	3298(4)	28(1)
C(3)	6508(5)	7500	2583(4)	36(1)
C(4)	5223(5)	7500	2977(4)	25(1)
C(5)	3695(5)	7500	2042(4)	34(1)
C(6)	4988(5)	7500	8418(4)	38(1)
C(7)	6209(5)	7500	7769(4)	25(1)
C(8)	7684(5)	7500	8511(4)	34(1)
C(9)	8926(5)	7500	8062(4)	27(1)
C(10)	10486(5)	7500	8993(4)	35(1)
F(1)	4835(13)	6100(15)	8957(12)	77(5)
F(2)	3698(8)	8164(14)	7715(7)	60(4)
F(3)	5350(10)	8771(15)	9333(8)	47(3)
F(4)	11299(4)	6138(5)	8846(4)	75(2)
F(5)	10467(5)	7500	10126(4)	96(4)
F(1B)	4037(18)	8880(20)	8036(15)	44(7)
F(2B)	5350(30)	7500	9590(12)	68(10)
F(4B)	10598(16)	6110(20)	9678(16)	80(9)
F(5B)	11560(20)	7500	8490(20)	91(10)
Ni(1)	7070(1)	7500	5516(1)	19(1)
O(1)	8424(3)	7500	4453(3)	24(1)

O(2)	5203(3)	7500	4091(2)	22(1)
O(3)	5733(3)	7500	6636(3)	24(1)
O(4)	8965(3)	7500	6983(3)	26(1)
O(5)	7097(2)	10225(3)	5557(2)	28(1)
O(6)	1408(3)	7500	5598(3)	33(1)

All esds (except the esd in the dihedral angle between two l.s. planes) are estimated using the full covariance matrix. The cell esds are taken into account individually in the estimation of esds in distances, angles and torsion angles; correlations between esds in cell parameters are only used when they are defined by crystal symmetry. An approximate (isotropic) treatment of cell esds is used for estimating esds involving l.s. planes.

Table 3. Bond lengths [Å] and angles [deg] for 08mz253_0m.

C(1)-C(2)	1.514(6)	C(10)-F(4)	1.316(4)
C(1)-H(1A)	0.9800	Ni(1)-O(1)	1.983(3)
C(1)-H(1B)	0.9800	Ni(1)-O(2)	2.013(3)
C(1)-H(1C)	0.9800	Ni(1)-O(3)	2.023(3)
C(2)-O(1)	1.271(5)	Ni(1)-O(4)	2.057(3)
C(2)-C(3)	1.387(6)	Ni(1)-O(5)	2.065(2)
C(3)-C(4)	1.389(6)	Ni(1)-O(5)#1	2.065(2)
C(3)-H(3)	0.9500	O(5)-H(5D)	0.83(2)
C(4)-O(2)	1.283(5)	O(5)-H(5E)	0.84(2)
C(4)-C(5)	1.514(6)	O(6)-H(6A)	0.83(2)
C(5)-H(5A)	0.9800	O(6)-H(6B)	0.83(2)
C(5)-H(5B)	0.9800		
C(5)-H(5C)	0.9800	C(2)-C(1)-H(1A)	109.5
C(6)-F(1)#1	1.256(10)	C(2)-C(1)-H(1B)	109.5
C(6)-F(1)	1.256(10)	H(1A)-C(1)-H(1B)	109.5
C(6)-F(2B)	1.290(13)	C(2)-C(1)-H(1C)	109.5
C(6)-F(2)#1	1.335(8)	H(1A)-C(1)-H(1C)	109.5
C(6)-F(2)	1.335(8)	H(1B)-C(1)-H(1C)	109.5
C(6)-F(1B)	1.359(11)	O(1)-C(2)-C(3)	125.5(4)
C(6)-F(1B)#1	1.359(11)	O(1)-C(2)-C(1)	114.7(4)
C(6)-F(3)	1.394(9)	C(3)-C(2)-C(1)	119.8(4)
C(6)-F(3)#1	1.394(8)	C(2)-C(3)-C(4)	127.2(4)
C(6)-C(7)	1.521(6)	C(2)-C(3)-H(3)	116.4
C(7)-O(3)	1.248(5)	C(4)-C(3)-H(3)	116.4
C(7)-C(8)	1.389(6)	O(2)-C(4)-C(3)	125.5(4)
C(8)-C(9)	1.388(6)	O(2)-C(4)-C(5)	115.5(4)
C(8)-H(8)	0.9500	C(3)-C(4)-C(5)	119.0(4)
C(9)-O(4)	1.249(5)	C(4)-C(5)-H(5A)	109.5
C(9)-C(10)	1.533(6)	C(4)-C(5)-H(5B)	109.5
C(10)-F(5B)	1.288(14)	H(5A)-C(5)-H(5B)	109.5
C(10)-F(4B)#1	1.302(11)	C(4)-C(5)-H(5C)	109.5
C(10)-F(4B)	1.302(11)	H(5A)-C(5)-H(5C)	109.5
C(10)-F(5)	1.305(6)	H(5B)-C(5)-H(5C)	109.5
C(10)-F(4)#1	1.316(4)	F(1)#1-C(6)-F(1)	115.2(14)

F(1)#1-C(6)-F(2)#1	114.1(7)	C(2)-O(1)-Ni(1)	125.2(3)
F(1)-C(6)-F(2)	114.1(7)	C(4)-O(2)-Ni(1)	123.8(3)
F(2B)-C(6)-F(1B)	106.8(9)	C(7)-O(3)-Ni(1)	124.2(3)
F(2B)-C(6)-F(1B)#1	106.8(9)	C(9)-O(4)-Ni(1)	123.5(3)
F(1B)-C(6)-F(1B)#1	101.0(17)	Ni(1)-O(5)-H(5D)	124(3)
F(1)-C(6)-F(3)	104.4(6)	Ni(1)-O(5)-H(5E)	122(3)
F(2)-C(6)-F(3)	100.2(5)	H(5D)-O(5)-H(5E)	104(4)
F(1)#1-C(6)-F(3)#1	104.4(6)	H(6A)-O(6)-H(6B)	112(6)
F(2)#1-C(6)-F(3)#1	100.2(5)		
F(1)#1-C(6)-C(7)	116.4(7)		
F(1)-C(6)-C(7)	116.4(7)		
F(2B)-C(6)-C(7)	119.9(12)		
F(2)#1-C(6)-C(7)	111.6(5)		
F(2)-C(6)-C(7)	111.6(5)		
F(1B)-C(6)-C(7)	110.3(8)		
F(1B)#1-C(6)-C(7)	110.3(8)		
F(3)-C(6)-C(7)	108.4(6)		
F(3)#1-C(6)-C(7)	108.4(6)		
O(3)-C(7)-C(8)	129.2(4)		
O(3)-C(7)-C(6)	114.7(4)		
C(8)-C(7)-C(6)	116.1(4)		
C(9)-C(8)-C(7)	123.2(4)		
C(9)-C(8)-H(8)	118.4		
C(7)-C(8)-H(8)	118.4		
O(4)-C(9)-C(8)	128.9(4)		
O(4)-C(9)-C(10)	113.8(4)		
C(8)-C(9)-C(10)	117.3(4)		
F(5B)-C(10)-F(4B)#1	109.3(9)		
F(5B)-C(10)-F(4B)	109.3(9)		
F(4B)#1-C(10)-F(4B)	108(2)		
F(5)-C(10)-F(4)#1	107.4(3)		
F(5)-C(10)-F(4)	107.4(3)		
F(4)#1-C(10)-F(4)	103.2(5)		
F(5B)-C(10)-C(9)	112.6(12)		
F(4B)#1-C(10)-C(9)	108.6(7)		
F(4B)-C(10)-C(9)	108.6(7)		
F(5)-C(10)-C(9)	114.6(4)		
F(4)#1-C(10)-C(9)	111.8(3)		
F(4)-C(10)-C(9)	111.8(3)		
O(1)-Ni(1)-O(2)	92.76(12)		
O(1)-Ni(1)-O(3)	178.61(11)		
O(2)-Ni(1)-O(3)	88.63(11)		
O(1)-Ni(1)-O(4)	87.75(12)		
O(2)-Ni(1)-O(4)	179.49(12)		
O(3)-Ni(1)-O(4)	90.86(12)		
O(1)-Ni(1)-O(5)	90.45(7)		
O(2)-Ni(1)-O(5)	91.17(7)		
O(3)-Ni(1)-O(5)	89.52(7)		
O(4)-Ni(1)-O(5)	88.83(7)		
O(1)-Ni(1)-O(5)#1	90.45(7)		
O(2)-Ni(1)-O(5)#1	91.17(7)		
O(3)-Ni(1)-O(5)#1	89.52(7)		
O(4)-Ni(1)-O(5)#1	88.83(7)		
O(5)-Ni(1)-O(5)#1	177.45(14)		

Symmetry transformations used to generate equivalent atoms:
#1 x,-y+3/2,z

Table 4. Anisotropic displacement parameters [Å^2 × 10^3] for 08mz253_0m. The anisotropic displacement factor exponent takes the form: -2 π2 [(h a*)^2 U11 + ... + 2 h k a* b* U12]

	U11	U22	U33	U23	U13	U12
C(1)	32(2)	73(4)	30(2)	0	15(2)	0
C(2)	25(2)	35(3)	25(2)	0	10(2)	0
C(3)	32(2)	57(4)	18(2)	0	7(2)	0
C(4)	28(2)	23(2)	21(2)	0	5(2)	0
C(5)	29(2)	47(3)	20(2)	0	-1(2)	0
C(6)	32(2)	59(4)	26(2)	0	14(2)	0
C(7)	27(2)	27(3)	24(2)	0	10(2)	0
C(8)	29(2)	52(3)	20(2)	0	8(2)	0
C(9)	25(2)	30(3)	22(2)	0	2(2)	0
C(10)	25(2)	51(3)	26(2)	0	3(2)	0
F(1)	73(9)	66(6)	112(13)	-14(7)	59(8)	-30(6)
F(2)	29(3)	115(12)	36(3)	-10(4)	11(2)	11(4)
F(3)	35(4)	72(7)	39(4)	-14(4)	21(3)	10(4)
F(4)	42(2)	72(3)	87(3)	-14(2)	-18(2)	27(2)
F(5)	33(2)	225(11)	26(2)	0	1(2)	0
F(1B)	44(12)	30(9)	72(16)	10(9)	37(11)	24(8)
F(2B)	70(14)	100(20)	31(10)	0	15(9)	0
F(4B)	43(8)	78(13)	99(16)	48(11)	-9(9)	0(8)
F(5B)	60(13)	120(20)	80(15)	0	2(11)	0
Ni(1)	18(1)	19(1)	19(1)	0	6(1)	0
O(1)	21(1)	28(2)	24(2)	0	8(1)	0
O(2)	21(1)	24(2)	19(1)	0	5(1)	0
O(3)	21(1)	32(2)	20(1)	0	6(1)	0
O(4)	22(1)	35(2)	21(1)	0	5(1)	0
O(5)	27(1)	19(1)	42(1)	-2(1)	15(1)	-2(1)
O(6)	20(1)	45(2)	33(2)	0	8(1)	0

Table 5. Hydrogen coordinates (× 10^4) and isotropic displacement parameters (Å^2 × 10^3) for 08mz253_0m.

	x	y	z	U(eq)
H(1A)	8831	7501	1816	65

H(1B)	9878	6443	2952	65
H(1C)	9879	8556	2953	65
H(3)	6352	7500	1728	43
H(5A)	3089	6524	2210	51
H(5B)	3822	7354	1228	51
H(5C)	3184	8622	2082	51
H(8)	7851	7500	9367	40
H(5D)	6380(30)	10850(50)	5620(30)	42
H(5E)	7480(40)	10810(50)	5110(30)	42
H(6A)	490(30)	7500	5250(50)	49
H(6B)	1580(70)	7500	6350(20)	49

Table 6. Torsion angles [deg] for 08mz253_0m.

O(1)-C(2)-C(3)-C(4)	0.000(1)
C(1)-C(2)-C(3)-C(4)	180.0
C(2)-C(3)-C(4)-O(2)	0.0
C(2)-C(3)-C(4)-C(5)	180.0
F(1)#1-C(6)-C(7)-O(3)	-109.5(7)
F(1)-C(6)-C(7)-O(3)	109.5(7)
F(2B)-C(6)-C(7)-O(3)	180.000(2)
F(2)#1-C(6)-C(7)-O(3)	23.9(5)
F(2)-C(6)-C(7)-O(3)	-23.9(5)
F(1B)-C(6)-C(7)-O(3)	-55.3(9)
F(1B)#1-C(6)-C(7)-O(3)	55.3(9)
F(3)-C(6)-C(7)-O(3)	-133.3(5)
F(3)#1-C(6)-C(7)-O(3)	133.3(5)
F(1)#1-C(6)-C(7)-C(8)	70.5(7)
F(1)-C(6)-C(7)-C(8)	-70.5(7)
F(2B)-C(6)-C(7)-C(8)	0.000(3)
F(2)#1-C(6)-C(7)-C(8)	-156.1(5)
F(2)-C(6)-C(7)-C(8)	156.1(5)
F(1B)-C(6)-C(7)-C(8)	124.7(9)
F(1B)#1-C(6)-C(7)-C(8)	-124.7(9)
F(3)-C(6)-C(7)-C(8)	46.7(5)
F(3)#1-C(6)-C(7)-C(8)	-46.7(5)
O(3)-C(7)-C(8)-C(9)	0.000(3)
C(6)-C(7)-C(8)-C(9)	180.000(2)
C(7)-C(8)-C(9)-O(4)	0.000(3)
C(7)-C(8)-C(9)-C(10)	180.000(2)
O(4)-C(9)-C(10)-F(5B)	0.000(8)
C(8)-C(9)-C(10)-F(5B)	180.000(8)
O(4)-C(9)-C(10)-F(4B)#1	121.2(11)
C(8)-C(9)-C(10)-F(4B)#1	-58.8(11)
O(4)-C(9)-C(10)-F(4B)	-121.2(11)
C(8)-C(9)-C(10)-F(4B)	58.8(11)
O(4)-C(9)-C(10)-F(5)	180.000(2)
C(8)-C(9)-C(10)-F(5)	0.000(2)
O(4)-C(9)-C(10)-F(4)#1	57.5(4)
C(8)-C(9)-C(10)-F(4)#1	-122.5(4)

O(4)-C(9)-C(10)-F(4)	-57.5(4)
C(8)-C(9)-C(10)-F(4)	122.5(4)
C(3)-C(2)-O(1)-Ni(1)	0.0
C(1)-C(2)-O(1)-Ni(1)	180.0
O(2)-Ni(1)-O(1)-C(2)	0.0
O(4)-Ni(1)-O(1)-C(2)	180.0
O(5)-Ni(1)-O(1)-C(2)	-91.19(7)
O(5)#1-Ni(1)-O(1)-C(2)	91.19(7)
C(3)-C(4)-O(2)-Ni(1)	0.0
C(5)-C(4)-O(2)-Ni(1)	180.0
O(1)-Ni(1)-O(2)-C(4)	0.0
O(3)-Ni(1)-O(2)-C(4)	180.0
O(5)-Ni(1)-O(2)-C(4)	90.51(7)
O(5)#1-Ni(1)-O(2)-C(4)	-90.51(7)
C(8)-C(7)-O(3)-Ni(1)	0.000(2)
C(6)-C(7)-O(3)-Ni(1)	180.000(1)
O(2)-Ni(1)-O(3)-C(7)	180.000(2)
O(4)-Ni(1)-O(3)-C(7)	0.000(2)
O(5)-Ni(1)-O(3)-C(7)	-88.82(7)
O(5)#1-Ni(1)-O(3)-C(7)	88.82(7)
C(8)-C(9)-O(4)-Ni(1)	0.000(3)
C(10)-C(9)-O(4)-Ni(1)	180.000(1)
O(1)-Ni(1)-O(4)-C(9)	180.000(2)
O(3)-Ni(1)-O(4)-C(9)	0.000(1)
O(5)-Ni(1)-O(4)-C(9)	89.50(7)
O(5)#1-Ni(1)-O(4)-C(9)	-89.50(7)

Symmetry transformations used to generate equivalent atoms:
#1 x,-y+3/2,z

Table 7. Hydrogen bonds for 08mz253_0m [Å and deg].

D-H...A	d(D-H)	d(H...A)	d(D...A)	<(DHA)
O(6)-H(6B)...F(2)#1	0.83(2)	2.20(5)	2.778(7)	128(5)
O(6)-H(6B)...F(2)	0.83(2)	2.20(5)	2.778(7)	128(5)
O(6)-H(6A)...O(1)#2	0.83(2)	1.87(2)	2.702(4)	180(6)
O(5)-H(5E)...O(6)#3	0.84(2)	1.95(2)	2.773(3)	167(4)
O(5)-H(5D)...O(2)#3	0.83(2)	2.03(2)	2.857(3)	174(4)

Symmetry transformations used to generate equivalent atoms:

#1 x,-y+3/2,z #2 x-1,y,z #3 -x+1,-y+2,-z+1

B.5 $Ni(acac)_2$ & $Ni(hfac)_2$ Sublimation Product: Fraction 2, Minor Product

Table 1. Crystal data and structure refinement for 08mz256_0m:

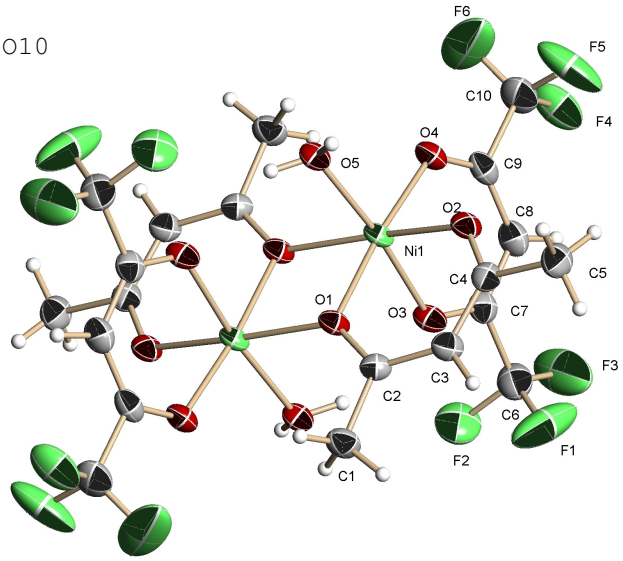

Identification code: 08mz256_0m
Empirical formula: C20 H20 F12 Ni2 O10
Formula weight: 765.74
Temperature: 140(2) K
Wavelength: 0.71073 Å
Crystal system: Orthorhombic
Space group: Pbcn
Unit cell dimensions:
a = 18.5920(16) Å, α = 90°
b = 10.5397(9) Å, β = 90°
c = 14.7123(12) Å, γ = 90°
Volume, *Z*: 2882.9(4) $Å^3$, 4
Density (calculated): 1.764 Mg/m^3
Absorption coefficient: 1.433 mm^{-1}
F(000): 1536
Crystal size: 0.40 × 0.16 × 0.11 mm
Crystal shape, colour: block, green
θ range for data collection: 2.19 to 28.28°
Limiting indices: $-24 \le h \le 22$, $-14 \le k \le 13$, $-19 \le l \le 17$
Reflections collected: 15918
Independent reflections: 3579 (*R*(int) = 0.0391)
Completeness to θ = 28.28°: 99.9 %
Absorption correction: multi-scan
Max. and min. transmission: 0.854 and 0.7563
Refinement method: Full-matrix least-squares on F^2
Data / restraints / parameters: 3579 / 2 / 207
Goodness-of-fit on F^2: 1.038
Final *R* indices [$I>2\sigma(I)$]: R1 = 0.0452, wR2 = 0.1120
R indices (all data): R1 = 0.0607, wR2 = 0.1238
Largest diff. peak and hole: 1.119 and −0.606 e × $Å^{-3}$

Refinement of F^2 against ALL reflections. The weighted R-factor wR and goodness of fit are based on F^2, conventional R-factors R are based on *F*, with *F* set to zero for negative F^2. The threshold expression of $F^2 > 2\sigma(F^2)$ is used only for calculating R-factors

Treatment of hydrogen atoms:

All hydrogen atoms were placed in calculated positions and were refined with an isotropic displacement parameter 1.5 (methyl, hydroxyl) or 1.2 times (all others) that of the adjacent carbon or oxygen atom.

Table 2. Atomic coordinates [$\times 10^4$] and equivalent isotropic displacement parameters [$Å^2 \times 10^3$] for 08mz256_0m. U(eq) is defined as one third of the trace of the orthogonalized U_{ij} tensor.

	x	y	z	U(eq)
C(1)	4834(2)	3318(3)	-419(2)	37(1)
C(2)	4699(2)	2376(3)	320(2)	26(1)
C(3)	4326(2)	2761(3)	1097(2)	31(1)
C(4)	4163(2)	2014(3)	1865(2)	29(1)
C(5)	3865(2)	2666(4)	2699(2)	40(1)
C(6)	2474(2)	-109(4)	-331(2)	44(1)
C(7)	3080(2)	-565(3)	298(2)	30(1)
C(8)	2924(2)	-1489(3)	941(2)	36(1)
C(9)	3461(2)	-2016(3)	1494(2)	32(1)
C(10)	3237(2)	-3083(4)	2152(3)	47(1)
F(1)	2358(2)	1112(3)	-231(2)	99(1)
F(2)	2674(1)	-217(3)	-1196(2)	63(1)
F(3)	1879(2)	-733(4)	-258(2)	117(2)
F(4)	2620(1)	-3632(2)	1935(2)	64(1)
F(5)	3136(2)	-2603(3)	2975(2)	93(1)
F(6)	3724(2)	-3947(3)	2212(3)	136(2)
Ni(1)	4586(1)	-285(1)	893(1)	24(1)
O(1)	4961(1)	1247(2)	210(1)	25(1)
O(2)	4255(1)	824(2)	1920(1)	29(1)
O(3)	3673(1)	-32(2)	142(1)	30(1)
O(4)	4110(1)	-1751(2)	1536(1)	32(1)
O(5)	5565(1)	-578(2)	1508(1)	29(1)

All esds (except the esd in the dihedral angle between two l.s. planes) are estimated using the full covariance matrix. The cell esds are taken into account individually in the estimation of esds in distances, angles and torsion angles; correlations between esds in cell parameters are only used when they are defined by crystal symmetry. An approximate (isotropic) treatment of cell esds is used for estimating esds involving l.s. planes.

Table 3. Bond lengths [Å] and angles [deg] for 08mz256_0m.

C(1)-C(2)	1.493(4)	C(4)-C(5)-H(5A)	109.5
C(1)-H(1A)	0.9800	C(4)-C(5)-H(5B)	109.5
C(1)-H(1B)	0.9800	H(5A)-C(5)-H(5B)	109.5
C(1)-H(1C)	0.9800	C(4)-C(5)-H(5C)	109.5
C(2)-O(1)	1.296(3)	H(5A)-C(5)-H(5C)	109.5
C(2)-C(3)	1.397(4)	H(5B)-C(5)-H(5C)	109.5
C(3)-C(4)	1.410(4)	F(3)-C(6)-F(1)	110.5(4)
C(3)-H(3)	0.9500	F(3)-C(6)-F(2)	106.0(3)
C(4)-O(2)	1.268(4)	F(1)-C(6)-F(2)	103.7(3)
C(4)-C(5)	1.511(4)	F(3)-C(6)-C(7)	114.7(3)
C(5)-H(5A)	0.9800	F(1)-C(6)-C(7)	111.1(3)
C(5)-H(5B)	0.9800	F(2)-C(6)-C(7)	110.2(3)
C(5)-H(5C)	0.9800	O(3)-C(7)-C(8)	128.3(3)
C(6)-F(3)	1.292(5)	O(3)-C(7)-C(6)	113.1(3)
C(6)-F(1)	1.313(5)	C(8)-C(7)-C(6)	118.6(3)
C(6)-F(2)	1.331(4)	C(7)-C(8)-C(9)	121.7(3)
C(6)-C(7)	1.536(5)	C(7)-C(8)-H(8)	119.2
C(7)-O(3)	1.260(4)	C(9)-C(8)-H(8)	119.2
C(7)-C(8)	1.388(4)	O(4)-C(9)-C(8)	129.2(3)
C(8)-C(9)	1.402(5)	O(4)-C(9)-C(10)	113.3(3)
C(8)-H(8)	0.9500	C(8)-C(9)-C(10)	117.5(3)
C(9)-O(4)	1.240(4)	F(6)-C(10)-F(4)	108.5(4)
C(9)-C(10)	1.541(4)	F(6)-C(10)-F(5)	107.9(4)
C(10)-F(6)	1.287(5)	F(4)-C(10)-F(5)	105.4(3)
C(10)-F(4)	1.325(4)	F(6)-C(10)-C(9)	111.6(3)
C(10)-F(5)	1.326(5)	F(4)-C(10)-C(9)	113.7(3)
Ni(1)-O(2)	2.007(2)	F(5)-C(10)-C(9)	109.5(3)
Ni(1)-O(4)	2.016(2)	O(2)-Ni(1)-O(4)	87.66(8)
Ni(1)-O(1)	2.0265(19)	O(2)-Ni(1)-O(1)	90.83(8)
Ni(1)-O(3)	2.044(2)	O(4)-Ni(1)-O(1)	174.06(9)
Ni(1)-O(5)	2.055(2)	O(2)-Ni(1)-O(3)	94.38(8)
Ni(1)-O(1)#1	2.0904(19)	O(4)-Ni(1)-O(3)	89.38(9)
O(1)-Ni(1)#1	2.0905(19)	O(1)-Ni(1)-O(3)	85.00(8)
O(5)-H(5D)	0.841(19)	O(2)-Ni(1)-O(5)	91.58(8)
O(5)-H(5E)	0.824(19)	O(4)-Ni(1)-O(5)	93.86(9)
		O(1)-Ni(1)-O(5)	91.92(8)
C(2)-C(1)-H(1A)	109.5	O(3)-Ni(1)-O(5)	173.33(8)
C(2)-C(1)-H(1B)	109.5	O(2)-Ni(1)-O(1)#1	172.02(8)
H(1A)-C(1)-H(1B)	109.5	O(4)-Ni(1)-O(1)#1	99.73(8)
C(2)-C(1)-H(1C)	109.5	O(1)-Ni(1)-O(1)#1	82.12(8)
H(1A)-C(1)-H(1C)	109.5	O(3)-Ni(1)-O(1)#1	88.75(8)
H(1B)-C(1)-H(1C)	109.5	O(5)-Ni(1)-O(1)#1	84.96(8)
O(1)-C(2)-C(3)	123.8(3)	C(2)-O(1)-Ni(1)	122.71(18)
O(1)-C(2)-C(1)	117.1(3)	C(2)-O(1)-Ni(1)#1	133.95(18)
C(3)-C(2)-C(1)	119.1(3)	Ni(1)-O(1)-Ni(1)#1	97.89(8)
C(2)-C(3)-C(4)	126.9(3)	C(4)-O(2)-Ni(1)	124.72(18)
C(2)-C(3)-H(3)	116.6	C(7)-O(3)-Ni(1)	124.77(19)
C(4)-C(3)-H(3)	116.6	C(9)-O(4)-Ni(1)	125.2(2)
O(2)-C(4)-C(3)	125.0(3)	Ni(1)-O(5)-H(5D)	115(3)
O(2)-C(4)-C(5)	116.6(3)	Ni(1)-O(5)-H(5E)	117(3)
C(3)-C(4)-C(5)	118.4(3)	H(5D)-O(5)-H(5E)	100(4)

Symmetry transformations used to generate equivalent atoms:
#1 -x+1,-y,-z

Table 4. Anisotropic displacement parameters [$Å^2 \times 10^3$] for 08mz256_0m. The anisotropic displacement factor exponent takes the form: $-2\pi^2 [(h\ a^*)^2\ U11 + ... + 2\ h\ k\ a^*\ b^*\ U12]$

	U11	U22	U33	U23	U13	U12
C(1)	49(2)	26(2)	35(2)	5(1)	6(1)	1(1)
C(2)	31(1)	24(1)	24(1)	-1(1)	-5(1)	-2(1)
C(3)	39(2)	26(2)	28(1)	-1(1)	-1(1)	2(1)
C(4)	29(1)	34(2)	23(1)	-5(1)	-4(1)	2(1)
C(5)	43(2)	49(2)	27(2)	-8(1)	1(1)	10(2)
C(6)	36(2)	59(2)	38(2)	-2(2)	-4(1)	-1(2)
C(7)	32(2)	33(2)	24(1)	-6(1)	2(1)	0(1)
C(8)	33(2)	38(2)	37(2)	0(1)	7(1)	-8(1)
C(9)	43(2)	25(1)	27(1)	-3(1)	12(1)	-5(1)
C(10)	49(2)	37(2)	55(2)	12(2)	11(2)	-9(2)
F(1)	133(3)	78(2)	87(2)	-32(2)	-57(2)	62(2)
F(2)	65(2)	88(2)	37(1)	-8(1)	-16(1)	2(1)
F(3)	41(2)	195(4)	113(3)	80(3)	-20(2)	-36(2)
F(4)	82(2)	56(2)	53(1)	5(1)	9(1)	-38(1)
F(5)	144(3)	100(2)	35(1)	14(1)	4(2)	-69(2)
F(6)	87(2)	75(2)	247(5)	105(3)	61(3)	22(2)
Ni(1)	32(1)	25(1)	14(1)	2(1)	-1(1)	-4(1)
O(1)	37(1)	21(1)	18(1)	0(1)	-1(1)	-3(1)
O(2)	36(1)	33(1)	18(1)	0(1)	-2(1)	1(1)
O(3)	36(1)	34(1)	21(1)	2(1)	-5(1)	-6(1)
O(4)	39(1)	31(1)	25(1)	6(1)	5(1)	-4(1)
O(5)	35(1)	34(1)	17(1)	-1(1)	-2(1)	-2(1)

Table 5. Hydrogen coordinates ($\times 10^4$) and isotropic displacement parameters ($Å^2 \times 10^3$) for 08mz256_0m.

	x	y	z	U(eq)
H(1A)	5345	3541	-429	55
H(1B)	4547	4082	-308	55
H(1C)	4697	2947	-1005	55
H(3)	4165	3616	1109	37
H(5A)	3514	2109	2995	60

H(5B)	3630	3459	2520	60
H(5C)	4258	2851	3122	60
H(8)	2442	-1771	1009	43
H(5D)	5924(15)	-420(40)	1180(20)	43
H(5E)	5660(20)	-130(30)	1950(20)	43

Table 6. Torsion angles [deg] for 08mz256_0m.

O(1)-C(2)-C(3)-C(4)	-1.0(5)
C(1)-C(2)-C(3)-C(4)	-178.7(3)
C(2)-C(3)-C(4)-O(2)	-9.2(5)
C(2)-C(3)-C(4)-C(5)	169.8(3)
F(3)-C(6)-C(7)-O(3)	172.7(3)
F(1)-C(6)-C(7)-O(3)	-61.1(4)
F(2)-C(6)-C(7)-O(3)	53.2(4)
F(3)-C(6)-C(7)-C(8)	-6.6(5)
F(1)-C(6)-C(7)-C(8)	119.6(4)
F(2)-C(6)-C(7)-C(8)	-126.1(3)
O(3)-C(7)-C(8)-C(9)	-3.8(5)
C(6)-C(7)-C(8)-C(9)	175.3(3)
C(7)-C(8)-C(9)-O(4)	2.8(5)
C(7)-C(8)-C(9)-C(10)	-177.0(3)
O(4)-C(9)-C(10)-F(6)	-37.7(5)
C(8)-C(9)-C(10)-F(6)	142.1(4)
O(4)-C(9)-C(10)-F(4)	-160.8(3)
C(8)-C(9)-C(10)-F(4)	19.0(5)
O(4)-C(9)-C(10)-F(5)	81.7(4)
C(8)-C(9)-C(10)-F(5)	-98.6(4)
C(3)-C(2)-O(1)-Ni(1)	22.6(4)
C(1)-C(2)-O(1)-Ni(1)	-159.7(2)
C(3)-C(2)-O(1)-Ni(1)#1	170.3(2)
C(1)-C(2)-O(1)-Ni(1)#1	-12.0(4)
O(2)-Ni(1)-O(1)-C(2)	-26.6(2)
O(3)-Ni(1)-O(1)-C(2)	67.8(2)
O(5)-Ni(1)-O(1)-C(2)	-118.2(2)
O(1)#1-Ni(1)-O(1)-C(2)	157.2(2)
O(2)-Ni(1)-O(1)-Ni(1)#1	176.25(9)
O(3)-Ni(1)-O(1)-Ni(1)#1	-89.42(9)
O(5)-Ni(1)-O(1)-Ni(1)#1	84.64(9)
O(1)#1-Ni(1)-O(1)-Ni(1)#1	0.0
C(3)-C(4)-O(2)-Ni(1)	-4.8(4)
C(5)-C(4)-O(2)-Ni(1)	176.17(19)
O(4)-Ni(1)-O(2)-C(4)	-156.2(2)
O(1)-Ni(1)-O(2)-C(4)	18.1(2)
O(3)-Ni(1)-O(2)-C(4)	-67.0(2)
O(5)-Ni(1)-O(2)-C(4)	110.0(2)
C(8)-C(7)-O(3)-Ni(1)	-5.6(5)
C(6)-C(7)-O(3)-Ni(1)	175.2(2)
O(2)-Ni(1)-O(3)-C(7)	-76.6(2)
O(4)-Ni(1)-O(3)-C(7)	11.0(2)

O(1)-Ni(1)-O(3)-C(7)	-167.1(2)
O(1)#1-Ni(1)-O(3)-C(7)	110.7(2)
C(8)-C(9)-O(4)-Ni(1)	7.6(5)
C(10)-C(9)-O(4)-Ni(1)	-172.6(2)
O(2)-Ni(1)-O(4)-C(9)	82.5(2)
O(3)-Ni(1)-O(4)-C(9)	-11.9(2)
O(5)-Ni(1)-O(4)-C(9)	173.9(2)
O(1)#1-Ni(1)-O(4)-C(9)	-100.5(2)

Symmetry transformations used to generate equivalent atoms:
#1 -x+1,-y,-z

Table 7. Hydrogen bonds for 08mz256_0m [Å and deg].

D-H...A	d(D-H)	d(H...A)	d(D...A)	<(DHA)
O(5)-H(5E)...O(2)#2	0.824(19)	1.95(2)	2.765(3)	171(4)
O(5)-H(5D)...O(3)#1	0.841(19)	2.14(3)	2.883(3)	148(4)

Symmetry transformations used to generate equivalent atoms:

#1 -x+1,-y,-z #2 -x+1,y,-z+1/2

B.6 $Ni(acac)_2$ & $Ni(hfac)_2$ Sublimation Product: Fractions 2 and 3, Major Product

Table 1. Crystal data and structure refinement for 08mz223_0m:

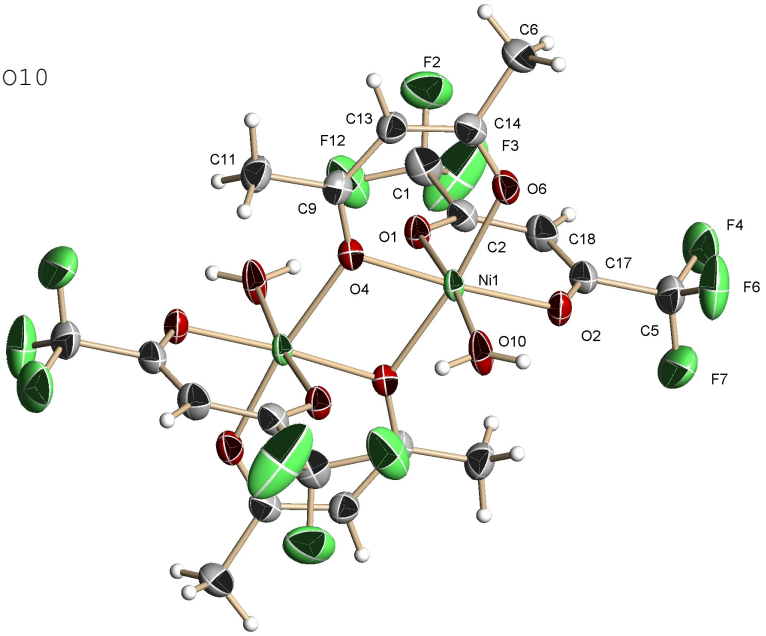

Identification code: 08mz223_0m
Empirical formula: C20 H20 F12 Ni2 O10
Formula weight: 765.78
Temperature: 140(2) K
Wavelength: 0.71073 Å
Crystal system: Triclinic
Space group: P-1
Unit cell dimensions:
a = 7.511(4) Å, α = 96.247(11)°
b = 9.510(5) Å, β = 93.655(11)°
c = 9.824(5) Å, γ = 93.811(9)°
Volume, *Z*: 694.3(6) $Å^3$, 1
Density (calculated): 1.832 Mg/m^3
Absorption coefficient: 1.487 mm^{-1}
F(000): 384
Crystal size: 0.20 × 0.12 × 0.06 mm
Crystal shape, colour: plate, green
θ range for data collection: 2.09 to 28.28°
Limiting indices: $-10 \le h \le 9$, $-12 \le k \le 12$, $0 \le l \le 13$
Reflections collected: 11782
Independent reflections: 3328 (*R*(int) = 0.0397)
Completeness to θ = 28.28°: 96.9 %
Absorption correction: multi-scan
Max. and min. transmission: 0.915 and 0.772
Refinement method: Full-matrix least-squares on F^2
Data / restraints / parameters: 3328 / 2 / 208
Goodness-of-fit on F^2: 1.100
Final *R* indices [$I>2\sigma(I)$]: R1 = 0.0446, wR2 = 0.1048
R indices (all data): R1 = 0.0546, wR2 = 0.1115
Largest diff. peak and hole: 0.690 and -0.520 e × $Å^{-3}$

Refinement of F^2 against ALL reflections. The weighted R-factor wR and goodness of fit are based on F^2, conventional R-factors R are based on *F*, with *F* set to zero for negative F^2. The threshold expression of $F^2 > 2\sigma(F^2)$ is used only for calculating R-factors

Comments:

The crystal under investigation was found to be non-merohedrally twinned. The orientation matrices for the two components were identified using the program Cell_Now, and the two components were integrated using Saint, resulting in a total of 11782 reflections. 3871 reflections (2110 unique ones) involved component 1 only (mean I/sigma = 10.4), 3862 reflections (2104 unique ones) involved component 2 only (mean I/sigma = 5.4), and 4049 reflections (2306 unique ones) involved both components (mean I/sigma = 9.7). The exact twin matrix identified by the integration program was found to be -0.99996 -0.00056 0.00106, 0.00180 -0.99904 0.00737, 0.19046 0.24354 0.99900.

The data were corrected for absorption using twinabs, and the structure was solved using direct methods with only the non-overlapping reflections of component 1. The structure was refined using the hklf 5 routine with all reflections of component 1 (including the overlapping ones) below a d-spacing threshold of 0.75, resulting in a BASF value of 0.238(1).

The Rint value given is for all reflections before the cutoff at d = 0.75 and is based on agreement between observed single and composite intensities and those calculated from refined unique intensities and twin fractions (TWINABS (Sheldrick, 2007)).

Treatment of hydrogen atoms:

All hydrogen atoms were placed in calculated positions and were refined with an isotropic displacement parameter 1.5 (methyl, hydroxyl) or 1.2 times (all others) that of the adjacent carbon or oxygen atom.

Table 2. Atomic coordinates [$\times 10^4$] and equivalent isotropic displacement parameters [$Å^2 \times 10^3$] for 08mz223_0m. U(eq) is defined as one third of the trace of the orthogonalized U_{ij} tensor.

	x	y	z	U(eq)
C(1)	9762(6)	316(5)	2699(5)	41(1)
C(2)	8707(5)	1634(4)	2881(4)	30(1)
C(5)	4464(6)	2726(5)	1070(5)	41(1)
C(6)	5125(6)	1633(5)	6924(5)	46(1)
C(9)	9536(5)	3929(4)	7280(4)	28(1)
C(11)	10989(5)	4180(5)	8403(4)	40(1)
C(13)	8058(5)	3041(4)	7468(4)	33(1)
C(14)	6566(5)	2685(4)	6549(4)	32(1)
C(17)	6099(5)	2799(4)	2094(4)	32(1)

C(18)	7172(5)	1660(4)	2021(4)	35(1)
F(2)	9233(5)	-617(3)	3529(4)	73(1)
F(3)	9599(7)	-334(5)	1478(4)	114(2)
F(4)	3996(4)	1415(3)	476(3)	68(1)
F(6)	3063(4)	3183(4)	1642(4)	75(1)
F(7)	4814(5)	3497(4)	80(4)	80(1)
F(12)	11479(4)	608(3)	3051(4)	75(1)
Ni(1)	8100(1)	4293(1)	4504(1)	23(1)
O(1)	9337(3)	2533(3)	3843(3)	28(1)
O(2)	6308(3)	3939(3)	2863(3)	31(1)
O(4)	9780(3)	4549(3)	6210(2)	25(1)
O(6)	6294(3)	3156(3)	5409(3)	32(1)
O(10)	7154(3)	6215(3)	5035(3)	40(1)

All esds (except the esd in the dihedral angle between two l.s. planes) are estimated using the full covariance matrix. The cell esds are taken into account individually in the estimation of esds in distances, angles and torsion angles; correlations between esds in cell parameters are only used when they are defined by crystal symmetry. An approximate (isotropic) treatment of cell esds is used for estimating esds involving l.s. planes.

Table 3. Bond lengths [Å] and angles [deg] for 08mz223_0m.

C(1)-F(3)	1.283(6)	Ni(1)-O(6)	1.992(3)
C(1)-F(12)	1.317(5)	Ni(1)-O(4)	2.015(3)
C(1)-F(2)	1.327(6)	Ni(1)-O(2)	2.018(3)
C(1)-C(2)	1.527(6)	Ni(1)-O(10)	2.033(3)
C(2)-O(1)	1.250(5)	Ni(1)-O(1)	2.033(3)
C(2)-C(18)	1.388(5)	Ni(1)-O(4)#1	2.079(3)
C(5)-F(6)	1.301(6)	O(4)-Ni(1)#1	2.079(3)
C(5)-F(7)	1.310(5)	O(10)-H(10A)	0.83(2)
C(5)-F(4)	1.332(5)	O(10)-H(10B)	0.838(19)
C(5)-C(17)	1.530(5)		
C(6)-C(14)	1.515(5)	F(3)-C(1)-F(12)	108.2(4)
C(6)-H(6A)	0.9800	F(3)-C(1)-F(2)	106.7(4)
C(6)-H(6B)	0.9800	F(12)-C(1)-F(2)	104.6(4)
C(6)-H(6C)	0.9800	F(3)-C(1)-C(2)	114.1(4)
C(9)-O(4)	1.277(4)	F(12)-C(1)-C(2)	112.1(3)
C(9)-C(13)	1.384(5)	F(2)-C(1)-C(2)	110.6(4)
C(9)-C(11)	1.490(5)	O(1)-C(2)-C(18)	128.8(4)
C(11)-H(11A)	0.9800	O(1)-C(2)-C(1)	113.7(3)
C(11)-H(11B)	0.9800	C(18)-C(2)-C(1)	117.4(3)
C(11)-H(11C)	0.9800	F(6)-C(5)-F(7)	108.3(4)
C(13)-C(14)	1.393(5)	F(6)-C(5)-F(4)	106.8(4)
C(13)-H(13)	0.9500	F(7)-C(5)-F(4)	106.5(4)
C(14)-O(6)	1.260(5)	F(6)-C(5)-C(17)	112.3(4)
C(17)-O(2)	1.247(5)	F(7)-C(5)-C(17)	109.8(4)
C(17)-C(18)	1.391(6)	F(4)-C(5)-C(17)	112.9(4)
C(18)-H(18)	0.9500	C(14)-C(6)-H(6A)	109.5

C(14)-C(6)-H(6B)	109.5
H(6A)-C(6)-H(6B)	109.5
C(14)-C(6)-H(6C)	109.5
H(6A)-C(6)-H(6C)	109.5
H(6B)-C(6)-H(6C)	109.5
O(4)-C(9)-C(13)	125.5(3)
O(4)-C(9)-C(11)	116.5(3)
C(13)-C(9)-C(11)	118.0(4)
C(9)-C(11)-H(11A)	109.5
C(9)-C(11)-H(11B)	109.5
H(11A)-C(11)-H(11B)	109.5
C(9)-C(11)-H(11C)	109.5
H(11A)-C(11)-H(11C)	109.5
H(11B)-C(11)-H(11C)	109.5
C(9)-C(13)-C(14)	126.5(4)
C(9)-C(13)-H(13)	116.7
C(14)-C(13)-H(13)	116.7
O(6)-C(14)-C(13)	125.9(4)
O(6)-C(14)-C(6)	115.9(4)
C(13)-C(14)-C(6)	118.3(4)
O(2)-C(17)-C(18)	128.9(4)
O(2)-C(17)-C(5)	113.0(4)
C(18)-C(17)-C(5)	118.0(4)
C(2)-C(18)-C(17)	122.6(4)
C(2)-C(18)-H(18)	118.7
C(17)-C(18)-H(18)	118.7
O(6)-Ni(1)-O(4)	91.80(11)
O(6)-Ni(1)-O(2)	84.16(12)
O(4)-Ni(1)-O(2)	175.92(11)
O(6)-Ni(1)-O(10)	96.58(13)
O(4)-Ni(1)-O(10)	90.44(11)
O(2)-Ni(1)-O(10)	90.54(11)
O(6)-Ni(1)-O(1)	91.93(12)
O(4)-Ni(1)-O(1)	88.96(10)
O(2)-Ni(1)-O(1)	90.66(11)
O(10)-Ni(1)-O(1)	171.49(12)
O(6)-Ni(1)-O(4)#1	172.22(10)
O(4)-Ni(1)-O(4)#1	80.56(11)
O(2)-Ni(1)-O(4)#1	103.47(11)
O(10)-Ni(1)-O(4)#1	85.03(12)
O(1)-Ni(1)-O(4)#1	86.49(11)
C(2)-O(1)-Ni(1)	123.7(2)
C(17)-O(2)-Ni(1)	123.6(2)
C(9)-O(4)-Ni(1)	124.4(2)
C(9)-O(4)-Ni(1)#1	135.4(2)
Ni(1)-O(4)-Ni(1)#1	99.44(11)
C(14)-O(6)-Ni(1)	124.9(2)
Ni(1)-O(10)-H(10A)	115(4)
Ni(1)-O(10)-H(10B)	133(4)
H(10A)-O(10)-H(10B)	111(5)

Symmetry transformations used to generate equivalent atoms:
#1 -x+2,-y+1,-z+1

Table 4. Anisotropic displacement parameters [$Å^2 \times 10^3$] for 08mz223_0m. The anisotropic displacement factor exponent takes the form: $-2\pi^2 [(h\ a^*)^2\ U11 + ... + 2\ h\ k\ a^*\ b^*\ U12]$

	U11	U22	U33	U23	U13	U12
C(1)	39(2)	31(2)	52(3)	-7(2)	6(2)	6(2)
C(2)	25(2)	26(2)	37(2)	-1(2)	7(2)	3(1)
C(5)	37(2)	43(2)	39(2)	1(2)	-12(2)	-4(2)
C(6)	33(2)	51(3)	58(3)	19(2)	7(2)	-5(2)
C(9)	26(2)	31(2)	28(2)	-1(2)	5(1)	9(1)
C(11)	34(2)	55(3)	31(2)	10(2)	-4(2)	1(2)
C(13)	28(2)	41(2)	32(2)	11(2)	4(2)	4(2)
C(14)	26(2)	29(2)	43(2)	4(2)	10(2)	6(2)
C(17)	30(2)	34(2)	29(2)	3(2)	-5(2)	-4(2)
C(18)	37(2)	29(2)	36(2)	-8(2)	-2(2)	-2(2)
F(2)	63(2)	45(2)	121(3)	32(2)	26(2)	19(2)
F(3)	170(4)	104(3)	65(2)	-36(2)	-23(3)	97(3)
F(4)	66(2)	52(2)	75(2)	-12(2)	-34(2)	-9(2)
F(6)	43(2)	99(3)	74(2)	-18(2)	-25(2)	14(2)
F(7)	80(2)	90(3)	67(2)	37(2)	-38(2)	-19(2)
F(12)	34(2)	43(2)	148(3)	-4(2)	14(2)	11(1)
Ni(1)	13(1)	25(1)	29(1)	-2(1)	-1(1)	3(1)
O(1)	22(1)	25(1)	35(1)	-3(1)	-2(1)	4(1)
O(2)	24(1)	28(1)	39(2)	-1(1)	-9(1)	3(1)
O(4)	21(1)	30(1)	24(1)	0(1)	1(1)	1(1)
O(6)	21(1)	36(2)	39(2)	4(1)	1(1)	1(1)
O(10)	17(1)	33(2)	65(2)	-13(1)	-5(1)	7(1)

Table 5. Hydrogen coordinates ($\times 10^4$) and isotropic displacement parameters ($Å^2 \times 10^3$) for 08mz223_0m.

	x	y	z	U(eq)
H(6A)	4050	2124	7125	69
H(6B)	5555	1204	7734	69
H(6C)	4839	890	6154	69
H(11A)	12120	3908	8045	60
H(11B)	10696	3610	9143	60
H(11C)	11105	5187	8762	60

H(13)	8062	2633	8309	40
H(18)	6842	868	1356	42
H(10A)	7860(60)	6780(50)	5560(50)	59
H(10B)	6130(40)	6520(60)	4970(50)	59

Table 6. Torsion angles [deg] for 08mz223_0m.

F(3)-C(1)-C(2)-O(1)	-154.8(5)
F(12)-C(1)-C(2)-O(1)	-31.4(5)
F(2)-C(1)-C(2)-O(1)	85.0(5)
F(3)-C(1)-C(2)-C(18)	27.8(6)
F(12)-C(1)-C(2)-C(18)	151.1(4)
F(2)-C(1)-C(2)-C(18)	-92.5(5)
O(4)-C(9)-C(13)-C(14)	-1.3(7)
C(11)-C(9)-C(13)-C(14)	179.5(4)
C(9)-C(13)-C(14)-O(6)	-2.6(7)
C(9)-C(13)-C(14)-C(6)	177.0(4)
F(6)-C(5)-C(17)-O(2)	-44.5(5)
F(7)-C(5)-C(17)-O(2)	76.0(5)
F(4)-C(5)-C(17)-O(2)	-165.3(4)
F(6)-C(5)-C(17)-C(18)	138.0(4)
F(7)-C(5)-C(17)-C(18)	-101.5(5)
F(4)-C(5)-C(17)-C(18)	17.2(6)
O(1)-C(2)-C(18)-C(17)	2.7(7)
C(1)-C(2)-C(18)-C(17)	179.7(4)
O(2)-C(17)-C(18)-C(2)	1.6(7)
C(5)-C(17)-C(18)-C(2)	178.6(4)
C(18)-C(2)-O(1)-Ni(1)	4.6(6)
C(1)-C(2)-O(1)-Ni(1)	-172.5(3)
O(6)-Ni(1)-O(1)-C(2)	73.8(3)
O(4)-Ni(1)-O(1)-C(2)	165.6(3)
O(2)-Ni(1)-O(1)-C(2)	-10.4(3)
O(4)#1-Ni(1)-O(1)-C(2)	-113.8(3)
C(18)-C(17)-O(2)-Ni(1)	-12.0(6)
C(5)-C(17)-O(2)-Ni(1)	170.8(3)
O(6)-Ni(1)-O(2)-C(17)	-78.1(3)
O(10)-Ni(1)-O(2)-C(17)	-174.7(3)
O(1)-Ni(1)-O(2)-C(17)	13.7(3)
O(4)#1-Ni(1)-O(2)-C(17)	100.3(3)
C(13)-C(9)-O(4)-Ni(1)	-3.2(5)
C(11)-C(9)-O(4)-Ni(1)	176.1(3)
C(13)-C(9)-O(4)-Ni(1)#1	-170.7(3)
C(11)-C(9)-O(4)-Ni(1)#1	8.5(5)
O(6)-Ni(1)-O(4)-C(9)	7.4(3)
O(10)-Ni(1)-O(4)-C(9)	104.0(3)
O(1)-Ni(1)-O(4)-C(9)	-84.5(3)
O(4)#1-Ni(1)-O(4)-C(9)	-171.1(3)
O(6)-Ni(1)-O(4)-Ni(1)#1	178.51(12)
O(10)-Ni(1)-O(4)-Ni(1)#1	-84.89(13)
O(1)-Ni(1)-O(4)-Ni(1)#1	86.62(12)
O(4)#1-Ni(1)-O(4)-Ni(1)#1	0.0
C(13)-C(14)-O(6)-Ni(1)	10.2(6)
C(6)-C(14)-O(6)-Ni(1)	-169.5(3)

O(4)-Ni(1)-O(6)-C(14)	-10.7(3)
O(2)-Ni(1)-O(6)-C(14)	168.7(3)
O(10)-Ni(1)-O(6)-C(14)	-101.4(3)
O(1)-Ni(1)-O(6)-C(14)	78.3(3)

Symmetry transformations used to generate equivalent atoms:
#1 -x+2,-y+1,-z+1

Table 7. Hydrogen bonds for 08mz223_0m [Å and deg].

D-H...A	d(D-H)	d(H...A)	d(D...A)	<(DHA)
O(10)-H(10A)...O(1)#1	0.83(2)	2.19(4)	2.917(4)	146(5)
O(10)-H(10B)...O(6)#2	0.838(19)	1.89(2)	2.715(4)	168(5)

Symmetry transformations used to generate equivalent atoms:

#1 -x+2,-y+1,-z+1 #2 -x+1,-y+1,-z+1

Appendix C: Powder X-Ray Data

C.1 Powder pattern of the $Al(acac)_3$ aqueous synthetic product

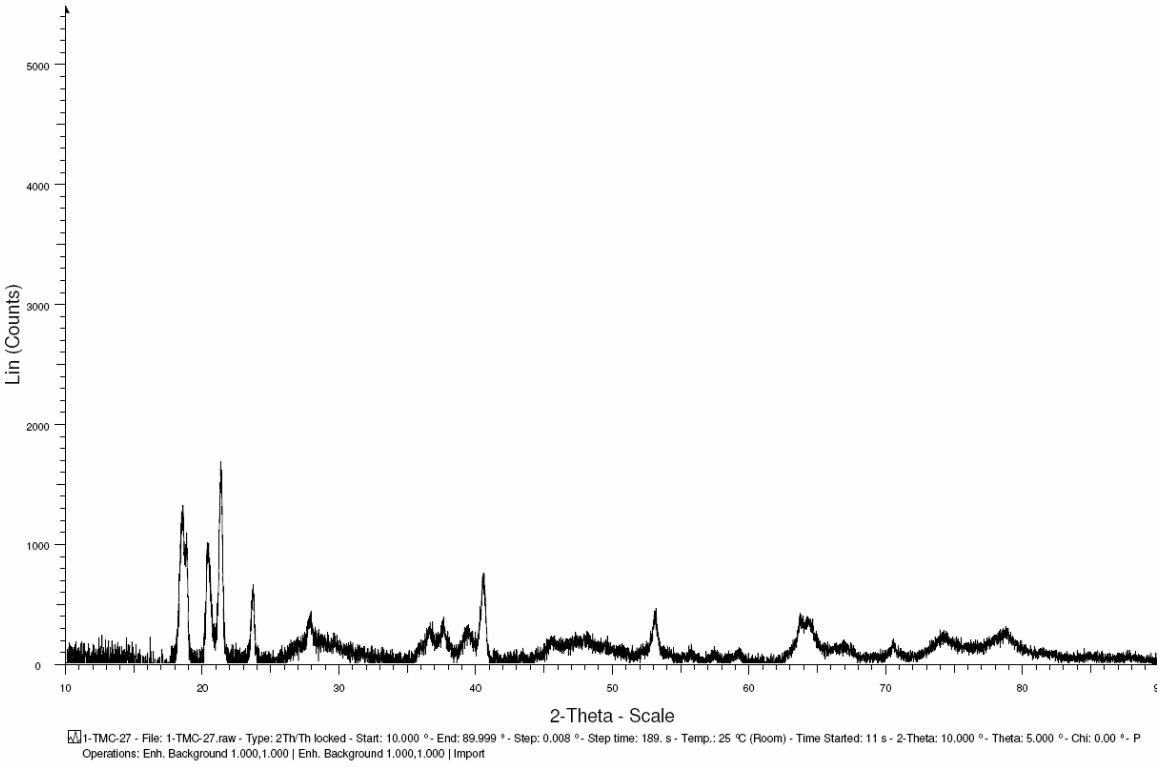

C.2 Powder pattern of the $Al(tftm)_3$ aqueous synthetic product

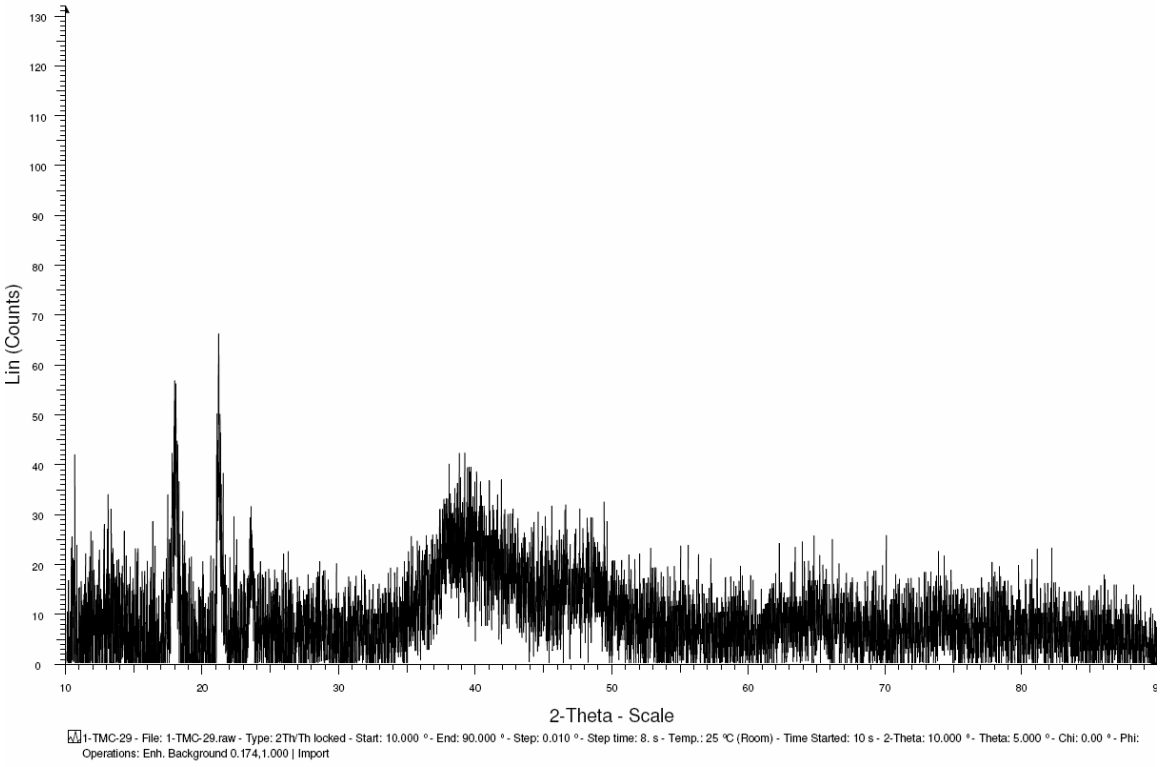

C.3 Powder Pattern of the aqueous $Ni(acac)_2$ product vs. its MeOH recrystallized analog

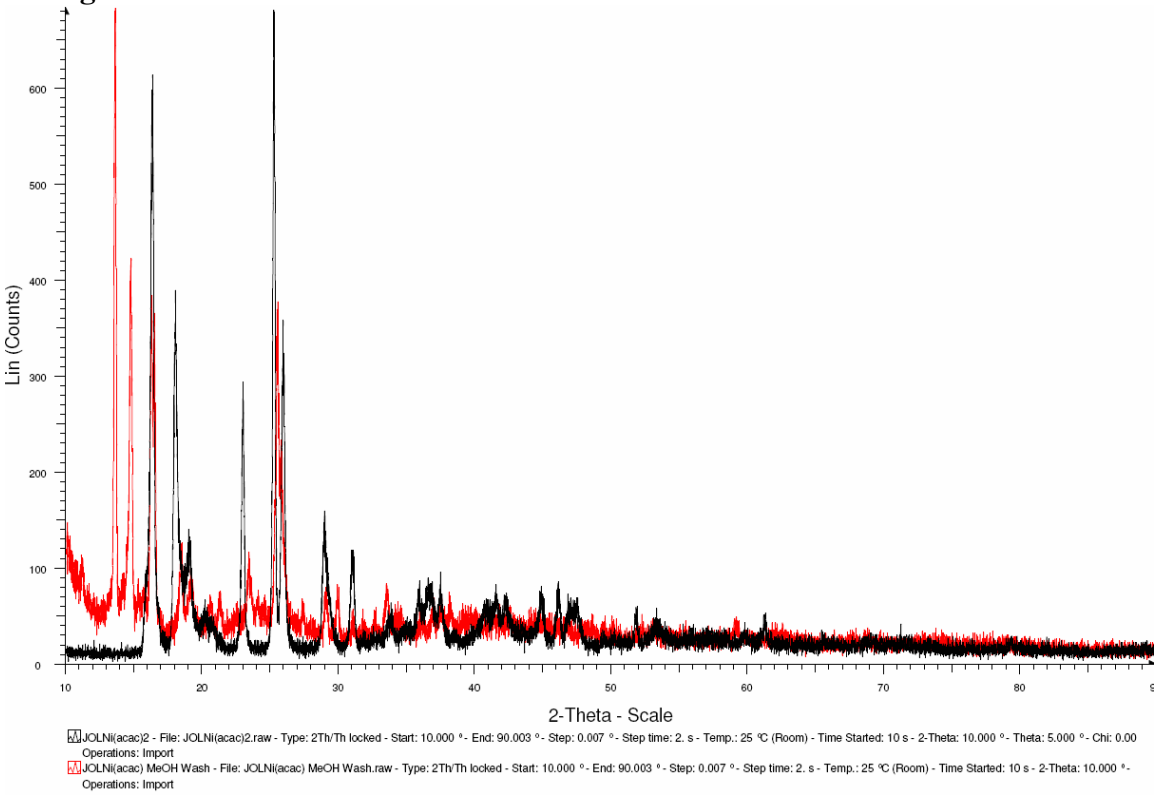

C.4 Powder pattern of the aqueous $Cu(acac)_2$ product vs. its MeOH recrystallized analog

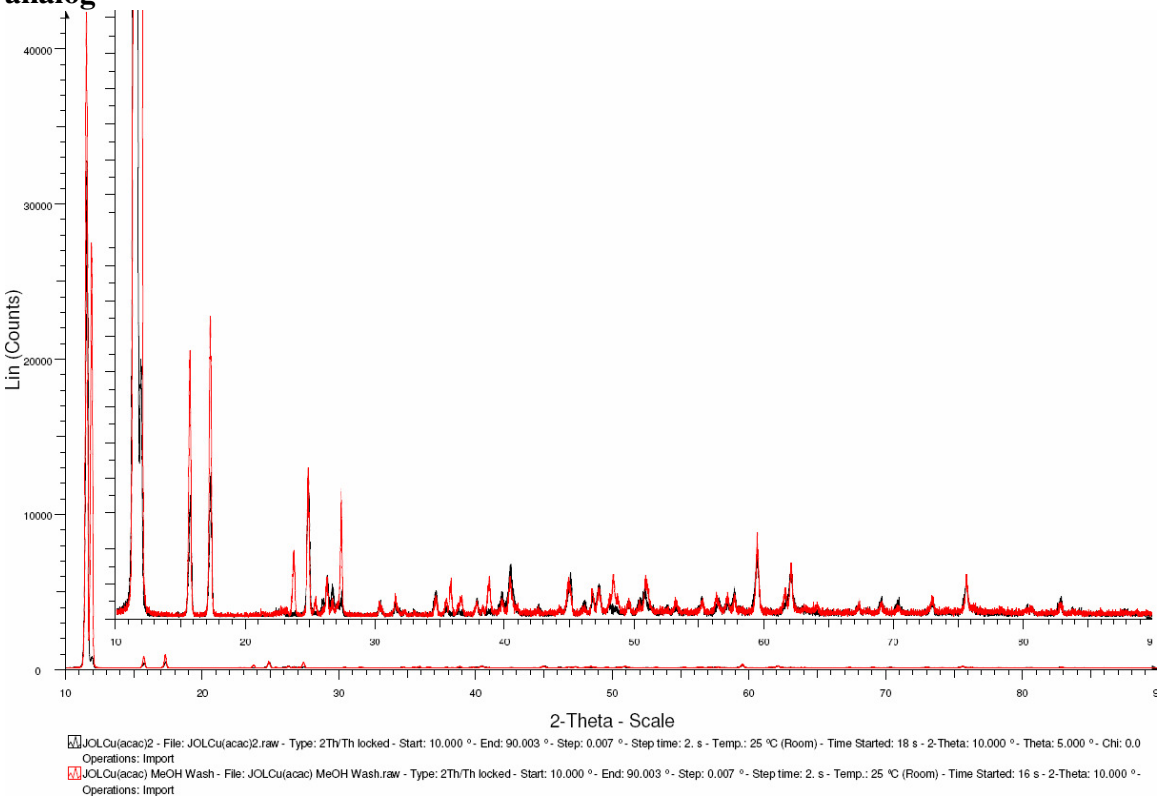

C.5 Powder pattern of the $Ni(acac)_1(tftm)_1$ reactions vs. the $Ni(tftm)_2$ synthetic product

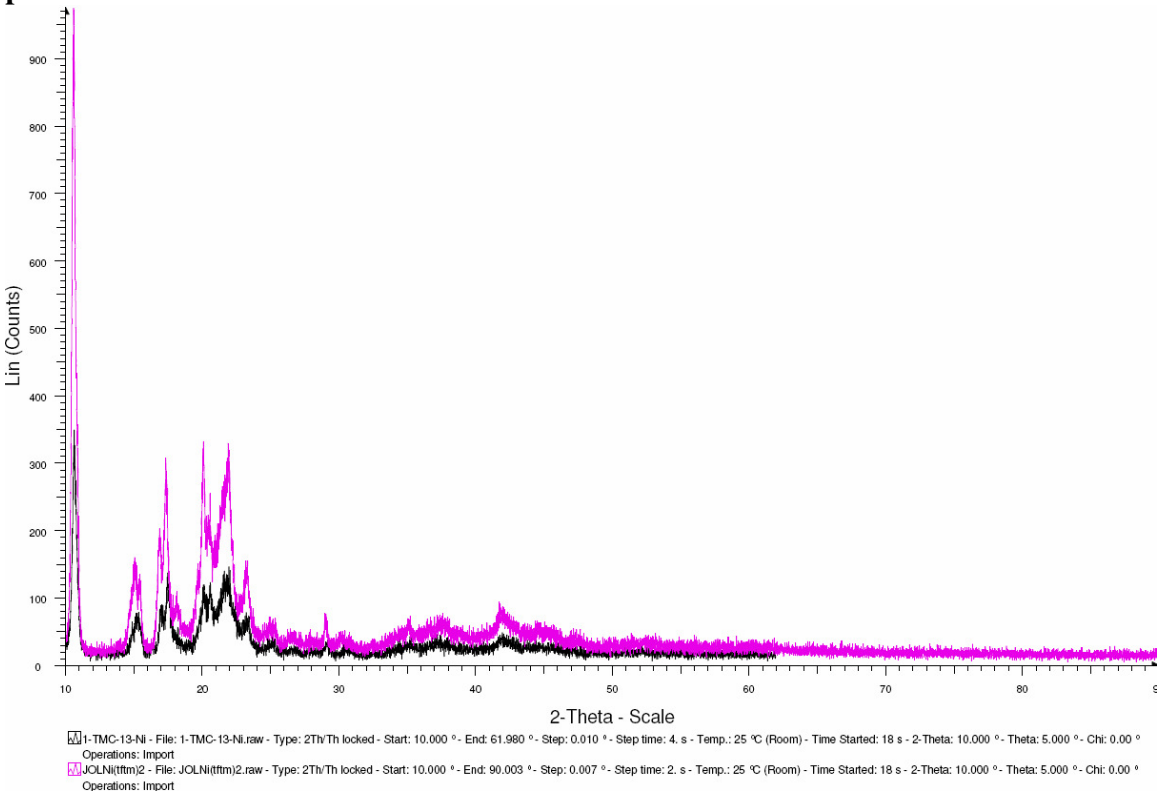

C.6 Powder pattern of the $Cu(acac)_1(tftm)_1$ reaction vs. the $Cu(tftm)_2$ synthetic product

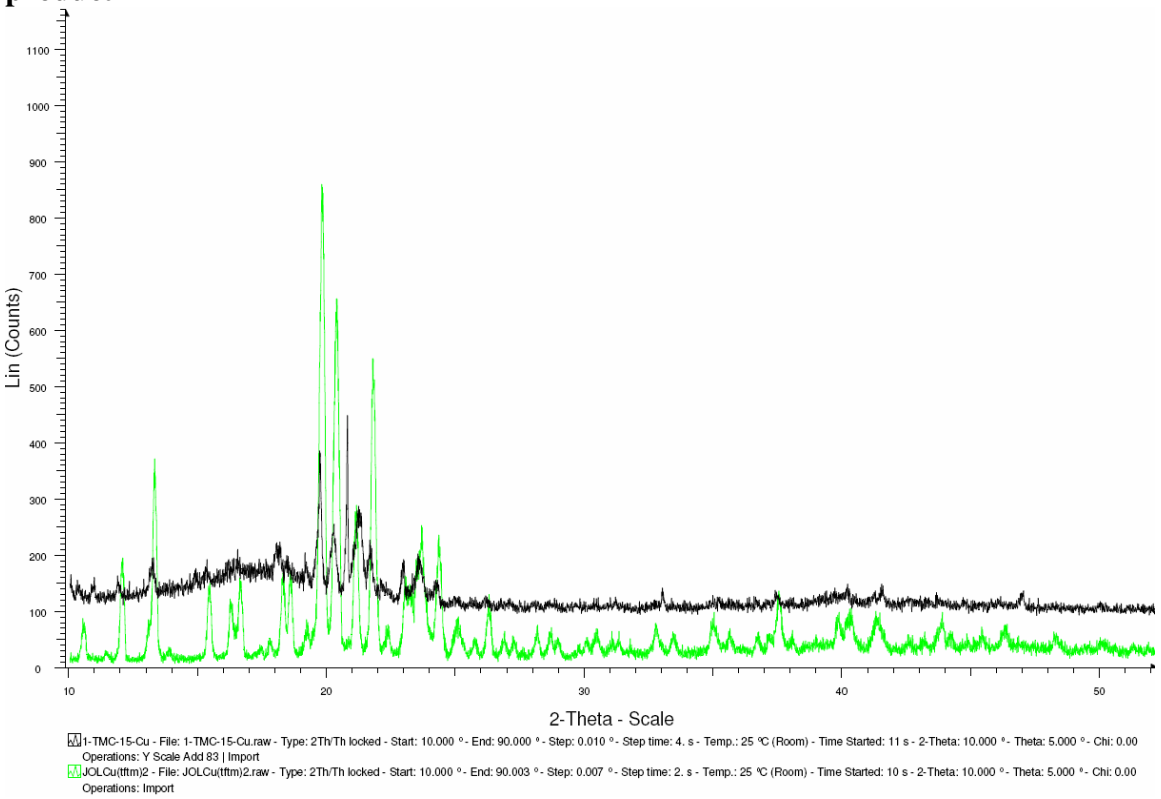

C.7 Powder pattern of the 1:1:2 product of the $Al(acac)_1(tftm)_2$ reaction

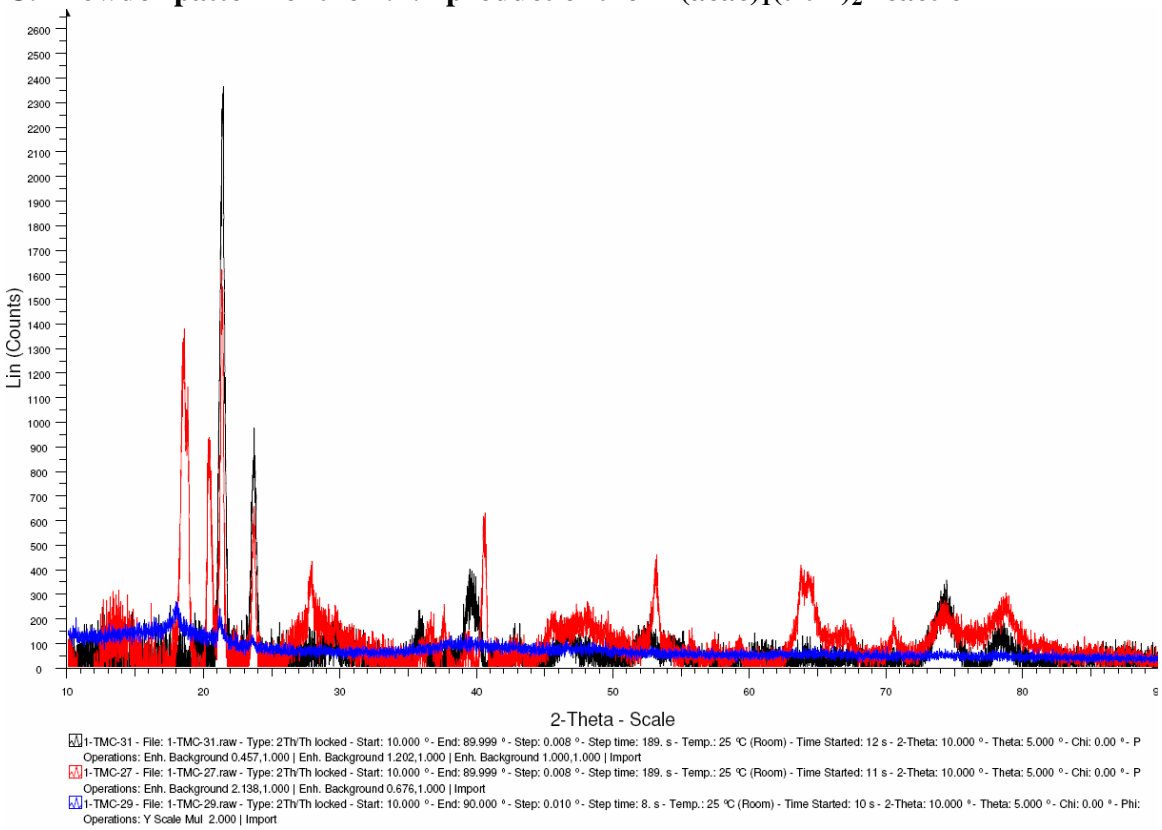

C.8 Powder pattern of the 1:2:1 product of the $Al(acac)_2(tftm)_1$ reaction

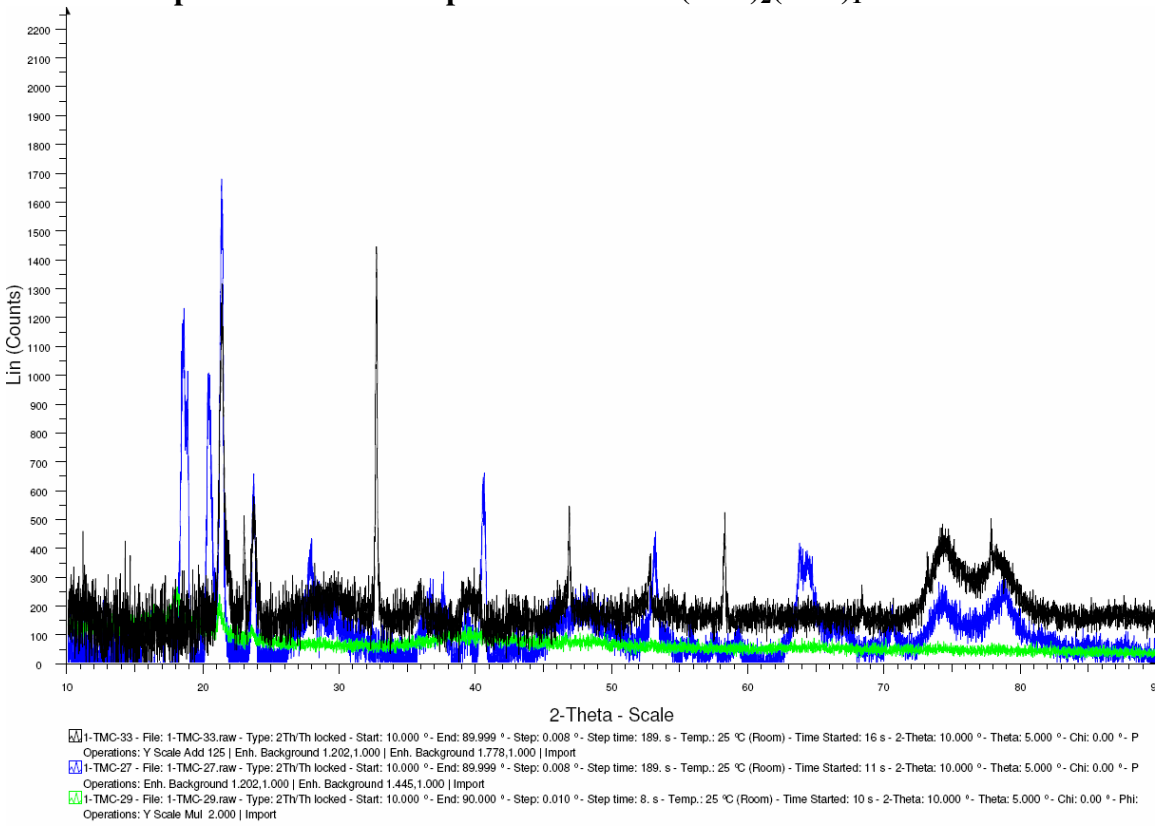

C.9 Powder pattern of the Ni + Cu + Acid synthetic reaction

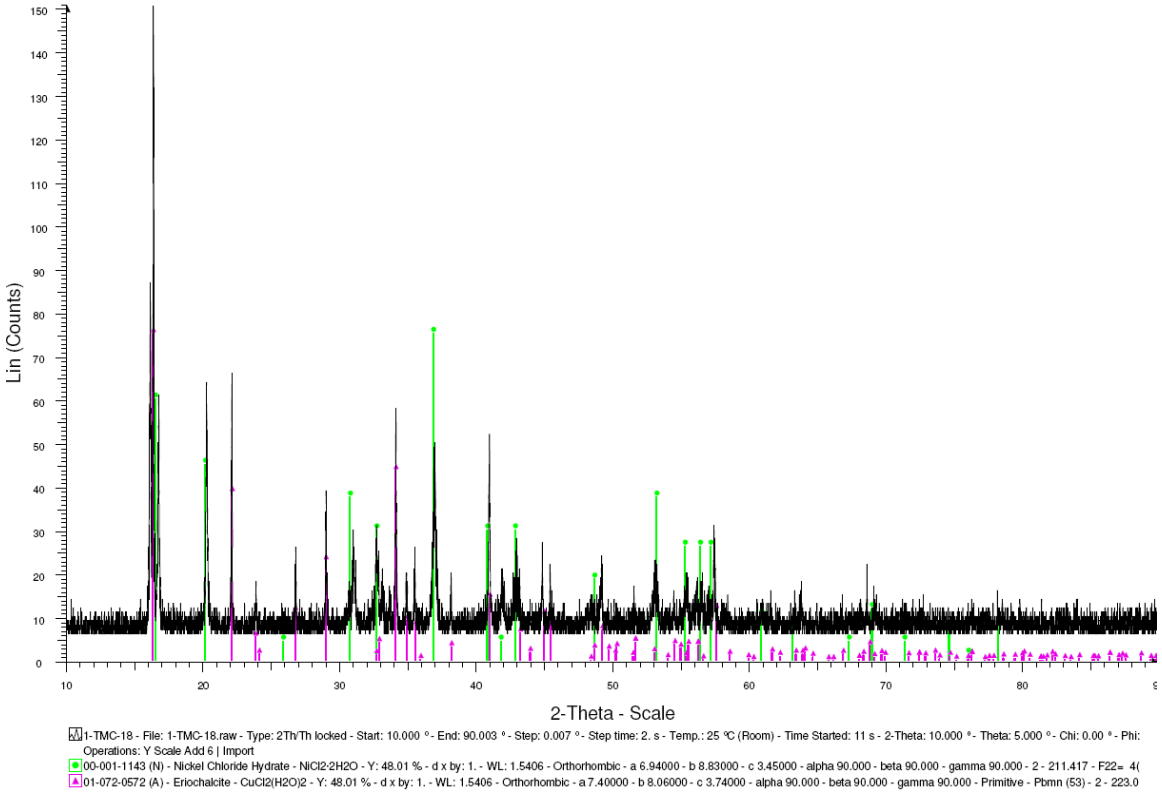

C.10 Powder pattern of the 1:1:2 product of the Ni:Cu:Hacac basic snythesis

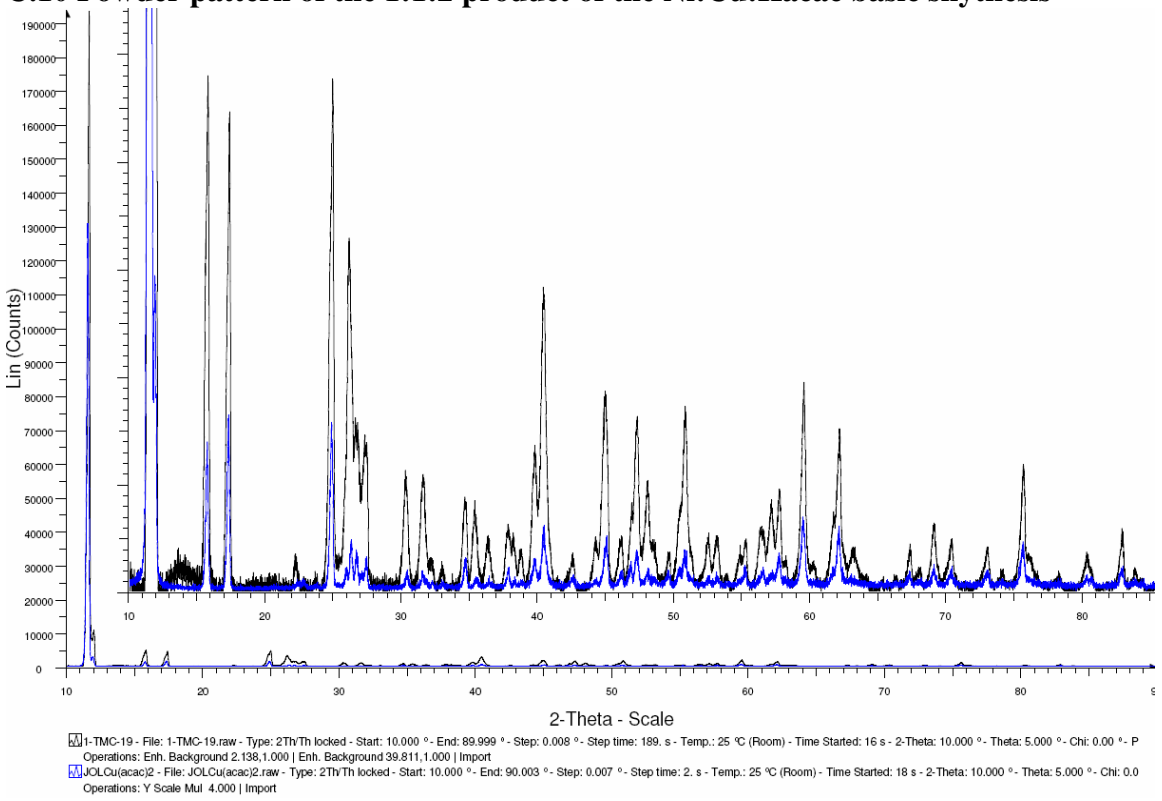

C.11 Powder pattern of the 1:1:2 product of the Ni:Cu:Hacac basic snythesis

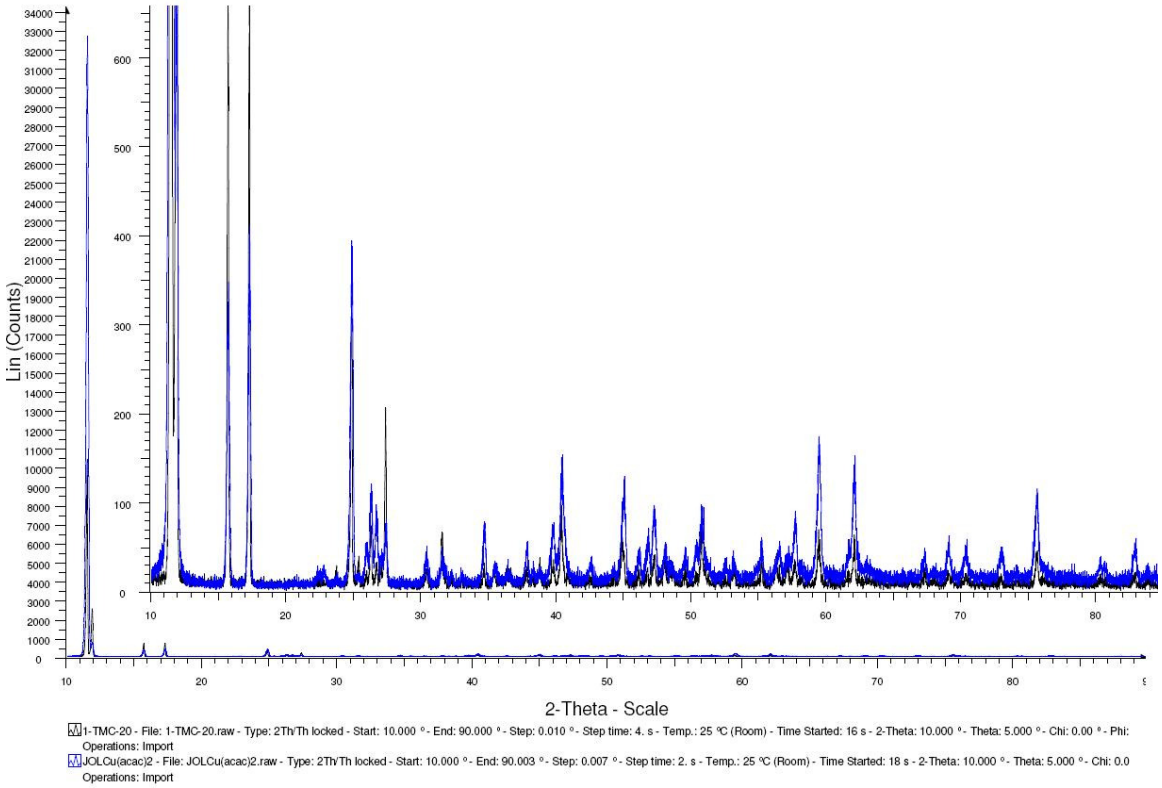

C.12 Powder pattern of the 1:1:3 product vs. the 1:1:5 Ni:Al:Hacac reactions

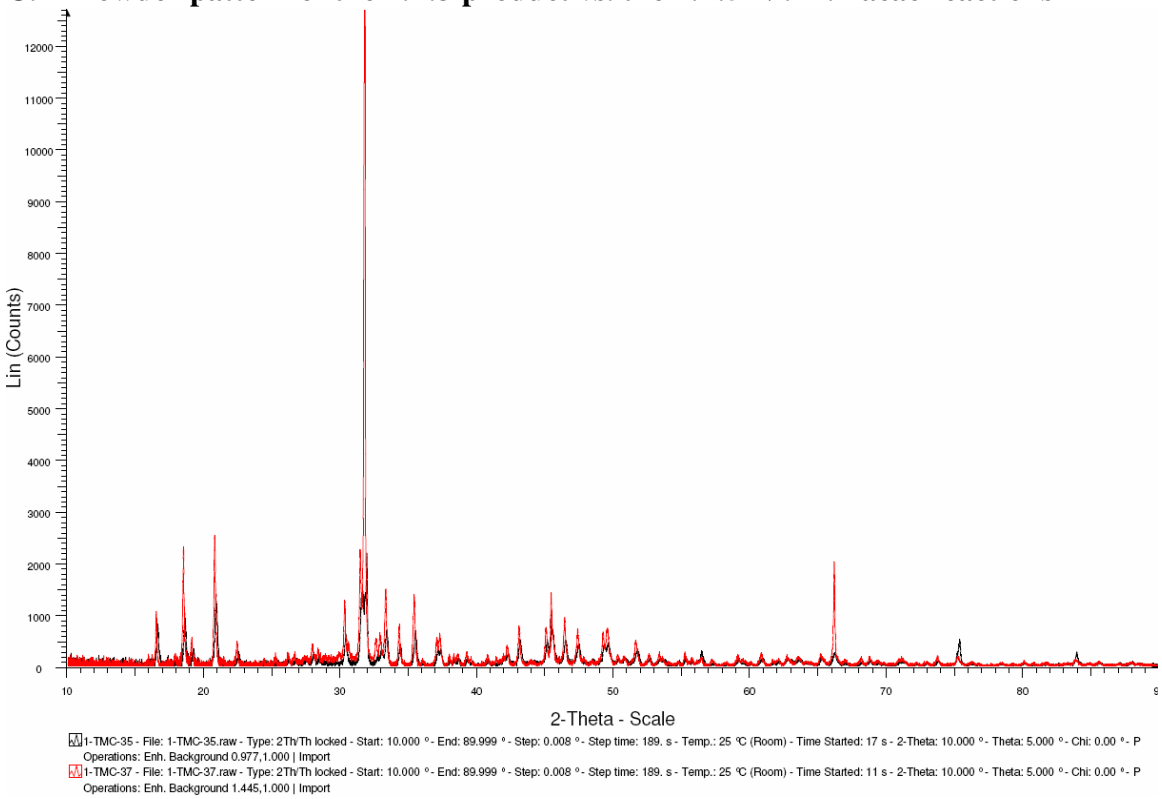

C.13 The 1:1:3 Ni:Al:Hacacac product vs. $NiCl_2 \cdot 4H_2O$ and NaCl

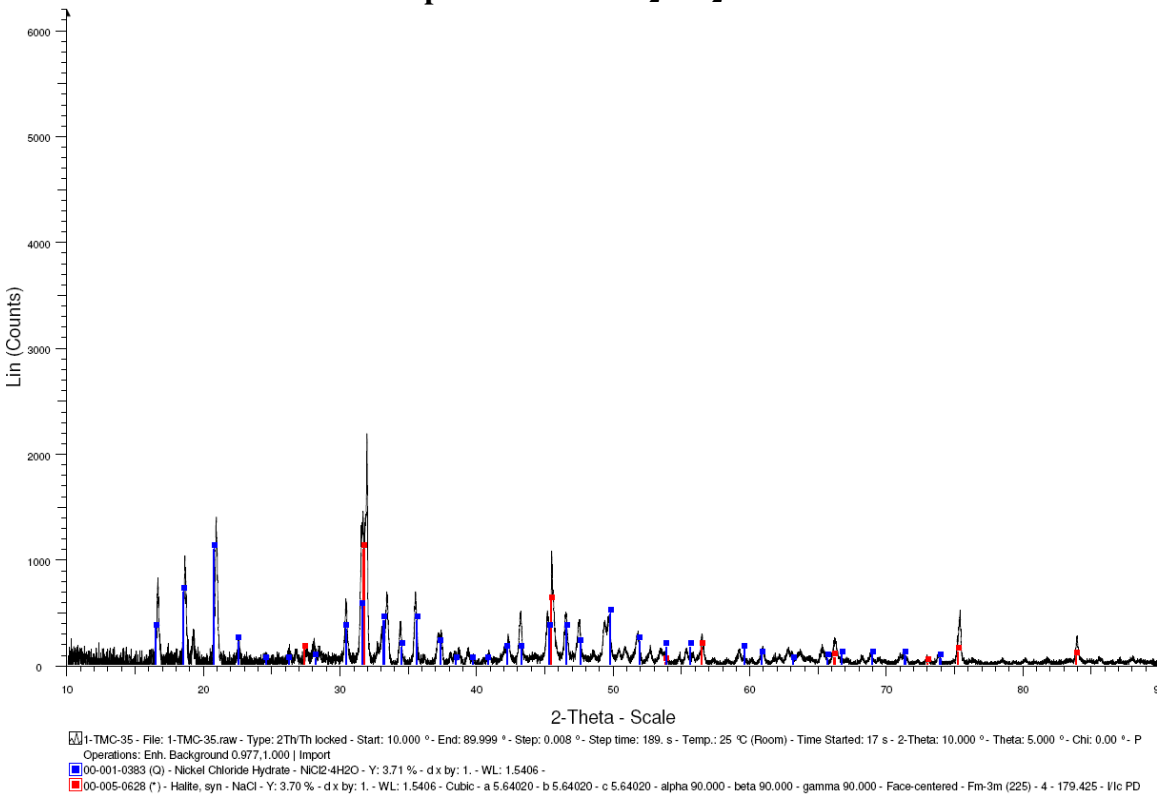

Appendix D: Actual Values Used For Syntheses

D.1 Aqueous Synthetic reactions

D.1.1 $Mn(tftm)_2$

Reaction	$MnCl_2•4H_2O$	Htftm	NH_4OH (1:1 H_2O:NH_4OH)	H_2O	Yield of ppt
1-JoL-62	1.12 mmol	2.49 mmol	3 mL (conc NH_4OH)	40 mL	0.550 g
3-JoL-78	0.557 mmol	1.12 mmol	15 mL	50 mL	0.168 g

D.1.2 $Co(tftm)_2$

Reaction	$CoCl_2•6H_2O$	Htftm	NH_4OH (1:1 H_2O:NH_4OH)	H_2O	Yield
1-JoL-84	0.482 mmol	1.24 mmol	2 mL	?	?

D.1.3 $Ni(tftm)_2$

Reaction	$NiCl_2•6H_2O$	Htftm	NH_4OH (1:1 H_2O:NH_4OH)	H_2O	Yield
1-JoL-25	0.557 mmol	1.37 mmol	8 mL	100 mL	0.245 g
1-TMC-5	1.67 mmol	3.48 mmol	20 mL	100 mL	0.717 g

D.1.4 $Cu(tftm)_2$

Reaction	$CuCl_2$	Htftm	NH_4OH (1:1 H_2O:NH_4OH)	H_2O	Yield
1-JoL-78	0.543 mmol	1.24 mmol	8 mL	50 mL	0.253 g
1-TMC-7	1.67 mmol	3.42 mmol	20 mL	100 mL	0.674 g

D.1.5 $Zn(tftm)_2$

Reaction	$ZnCl_2$	Htftm	NH_4OH (3:1 H_2O:NH_4OH)	H_2O	Yield
1-JoL-48	0.542 mmol	1.24 mmol	25 mL	50 mL	0.126 g
1-JoL-55	1.10 mmol	2.48 mmol	15 mL	50 mL	0.304 g

D.1.6 $Al(tftm)_3$

Reaction	$AlCl_3•6H_2O$	Htftm	Conc. NH_4OH	H_2O	Yield
1-TMC-29	1.25 mmol	3.73 mmol	40 mL	100 mL	0.082 g

D.1.7 $Al(acac)_3$

Reaction	$AlCl_3•6H_2O$	Hacac	NH_4OH (1:1 H_2O:NH_4OH)	H_2O	Yield
1-TMC-27	2.35 mmol	7.21 mmol	45 mL	100 mL	0.236 g

D.1.8 $Ni(acac)_2$

Reaction	$NiCl_2•6H_2O$	Hacac	NH_4OH (1:1 H_2O:NH_4OH)	H_2O	Yield
1-TMC-1	2.94 mmol	5.84 mmol	10 mL	100 mL	0.698 g
1-TMC-11	2.93 mmol	5.84 mmol	10 mL	100 mL	0.725 g

D.1.9 $Cu(acac)_2$

Reaction	$CuCl_2$	Hacac	NH_4OH (1:1 H_2O:NH_4OH)	H_2O	Yield
1-TMC-3	2.87 mmol	5.84 mmol	10 mL	100 mL	0.668 g
1-TMC-12	2.89 mmol	5.84 mmol	10 mL	100 mL	0.670 g

D.2 Non Aqueous Synthetic Reaction

D.2.1 $Al(tftm)_3$

Reaction	$Al(OC_3H_7)_3$	Htftm	Benzene/Toluene	MeOH Washes	Yield
3-JoL-30	1.63 mmol	5.76 mmol	80 mL Toluene	3x	0.1394 g
3-JoL-38	1.63 mmol	5.18 mmol	90 mL Toluene	2x	0.1447 g

D.3 Heteroleptic Snythetic Reactions

D.3.1 $Ni(acac)_1(tftm)_1$

Reaction	$NiCl_2$	Hacac	Htftm	NH_4OH (conc.)	H_2O
1-TMC-13	1.42 mmol	1.66 mmol	1.55 mmol	12 mL	100 mL

D.3.2 $Cu(acac)_1(tftm)_1$

Reaction	$CuCl_2$	Hacac	Htftm	NH_4OH (conc.)	H_2O
1-TMC-15	1.40 mmol	1.46 mmol	1.55 mmol	17 mL	100 mL

D.3.3 $Al(acac)_x(tftm)_{3-x}$

Reaction	$AlCl_3 \cdot 6H_2O$	Htftm	Hacac	NH_4OH (1:1 H_2O:NH_4OH)	H_2O	Yield
1-TMC-31a	1.24 mmol	1.24 mmol	2.43 mmol	20 mL	100	0.010 g
1-TMC-31b	1.01 mmol	1.99 mmol	0.974 mmol	20	100	0.003 g

D.4 Heterometal Synthetic Reactions

D.4.1 Cu + Ni + acac + Acid

Reaction	$CuCl_2$	$NiCl_2$	Hacac	HCl (1:10 HCl:H_2O)	H_2O
1-TMC-18	2.35 mmol	4.69 mmol	4.87 mmol	5.3 mL	100 mL

D.4.2 Cu + Ni + acac + Base

Reaction	$CuCl_2$	$NiCl_2$	Hacac	NaOH	H_2O
1-TMC-19	2.36 mmol	2.35 mmol	4.87 mmol	5.76 mmol	120 mL
1-TMC-20	1.47 mmol	1.45 mmol	5.84 mmol	3.86 mmol	115 mL

D.4.3 Ni + Al + acac + Base

Reaction	$NiCl_2$	$AlCl_3 \cdot 6H_2O$	Hacac	NaOH	H_2O
1-TMC-35	1.96 mmol	1.97 mmol	5.94 mmol	5.04 mmol	120 mL
1-TMC-37	1.30 mmol	1.29 mmol	6.62 mmol	2.84 mmol	115 mL

D.5 Refluxed Ni Synthetic Reactions

D.5.1 Refluxed Ni Reactions

Reaction Title	$Ni(acac)_2$	$Ni(hfac)_2$	$Ni(tftm)_2$	Yield
3-JoL-40	0.694 mmol	0.662 mmol	0.000 mmol	0.303 g
3-JoL-89	0.318 mmol	0.000 mmol	0.317 mmol	0.064 g
3-JoL-90	0.000 mmol	0.302 mmol	0.304 mmol	0.208 g